4.1 SUMMARY DESCRIPTION

This chapter describes: (1) the mechanical components of the reactor and reactor core including the fuel rods and fuel assemblies, (2) the nuclear design, and (3) the thermal-hydraulic design.

The reactor core comprises multiple regions of fuel assemblies which are similar in mechanical design, but different in fuel enrichment. Reload fuel is similar in mechanical design to the initial core; the differences are described in the following sections. The initial core design employed three enrichments in a three-region core, whereas more enrichments may be employed for a particular refueling scheme. Fuel cycle times of six months to over eighteen months are possible, and may be employed with the core described herein.

The core is cooled and moderated by light water at a pressure of 2250 pounds per square inch absolute (psia) in the Reactor Coolant System. The moderator coolant contains boron as a neutron poison. The concentration of boron in the coolant is varied as required to control relatively slow reactivity changes including the effects of fuel burnup. Additional boron, in the form of burnable poison rods, were employed in the initial core to establish the desired initial reactivity. Integral Fuel Burnable Absorbers (IFBA) are employed in reload fuel for this purpose. IFBAs are fuel rods in which a thin zirconium diboride coating is applied directly to the fuel pellets.

Two hundred and sixty four fuel rods are mechanically joined in a square, 17x17 array to form a fuel assembly. The fuel rods are supported at intervals along their length by grid assemblies and intermediate flow mixer (IFM) grids (for the RFA (w IFMs) design) which maintain the lateral spacing between the rods throughout the design life of the assembly. The grid assembly consists of an "egg-crate" arrangement of interlocked straps. The straps contain springs and dimples for fuel rod support as well as coolant mixing vanes. The fuel rods consist of enriched uranium dioxide ceramic cylindrical pellets contained in hermetically sealed zirconium alloy tubing. All fuel rods are pressurized with helium during fabrication to reduce stresses and strains and to increase fatigue life.

The center position in the assembly is reserved for use by the incore instrumentation, while the remaining 24 positions in the array are equipped with guide thimbles joined to the grids and the top and bottom nozzles. The guide thimbles may be used as core locations for Rod Cluster Control Assemblies (RCCAs), neutron source assemblies, or burnable poison rods. Otherwise, the guide thimbles can be fitted with plugging devices to limit bypass flow.

The bottom nozzle is a bottom structural element of the fuel assembly, and admits the coolant flow to the assembly.

The top nozzle assembly is a box-like structure which serves as the upper structural element of the fuel assembly, in addition to providing a partial protective housing for the RCCA or other components.

The RCCAs each consist of a group of individual absorber rods fastened at the top end to a common hub called a spider assembly. These assemblies contain absorber material to control the reactivity of the core, and to control axial power distribution.

The nuclear design analyses and evaluations established physical locations for control rods, burnable poison rods and physical parameters such as fuel enrichments and boron concentration in the coolant. The nuclear design evaluation established that the reactor core has inherent characteristics which, together with corrective actions of the reactor control and protective systems, provide adequate reactivity control even if the highest reactivity worth RCCA is stuck in the fully withdrawn position.

The design also provides for inherent stability against diametral and azimuthal power oscillations and for control of induced axial power oscillation through the use of control rods.

The thermal-hydraulic design analyses and evaluations establish coolant flow parameters which assure that adequate heat transfer is provided between the fuel cladding and the reactor coolant. The thermal design takes into account local variations in dimensions, power generation, flow distribution and mixing. The mixing vanes incorporated in the RFA spacer grid design and the IFMs induce additional flow mixing between the various flow channels within a fuel assembly as well as between adjacent assemblies.

Instrumentation is provided in and out of the core to monitor the nuclear, thermal-hydraulic, and mechanical performance of the reactor and to provide inputs to automatic control functions.

Table 4.1-1 presents a comparison of the principal nuclear, thermal-hydraulic and mechanical design parameters between the Seabrook Station Unit 1 initial case and the W. B. McGuire Nuclear Station Units 1 and 2 (Docket Nos. 50-369 and 50-370).

The analytical techniques employed in the core design are tabulated in Table 4.1-2. The loading conditions considered in general for the core internals and components are tabulated in Table 4.1-3. Specific or limiting loads considered for design purposes of the various components are listed as follows: fuel assemblies in Subsection 4.2.1.5; neutron absorber rods, burnable poison rods, neutron source rods and thimble plug assemblies in Subsection 4.2.1.6. The dynamic analyses, input forcing functions, and response loadings are presented in Section 3.9(N).

4.1.1 References

None

4.2 FUEL SYSTEM DESIGN

The plant design conditions are divided into four categories in accordance with their anticipated frequency of occurrence and risk to the public: Condition I - Normal Operation; Condition II - Incidents of Moderate Frequency; Condition III - Infrequent Incidents; and Condition IV - Limiting Faults. Chapter 15 describes bases and plant operation and events involving each condition.

The reactor is designed so that its components meet the following performance and safety criteria:

a. The mechanical design of the reactor core components and their physical arrangement, together with corrective actions of the reactor control, protection, and emergency cooling systems (when applicable) ensure that:

1. Fuel damage (defined as penetration of the fission product barrier i.e., the fuel rod clad) is not expected during Condition I and Condition II events. It is not possible, however, to preclude a very small number of rod failures. These are within the capability of the plant cleanup system and are consistent with plant design bases.

2. The reactor can be brought to a safe state following a Condition III event with only a small fraction of fuel rods damaged (in any case, the fraction of fuel rods damaged must be limited to meet the dose guidelines of 10 CFR 100) although sufficient fuel damage might occur to preclude immediate resumption of operation.

3. The reactor can be brought to a safe state and the core can be kept subcritical with acceptable heat transfer geometry following transients arising from \Condition IV events.

b. The fuel assemblies are designed to withstand loads induced during shipping, handling, and core loading without exceeding the criteria of Subsection 4.2.1.5.

c. The fuel assemblies are designed to accept control rod insertions to provide the required reactivity control for power operations and reactivity shutdown conditions.

d. All fuel assemblies have provisions for the insertion of incore instrumentation necessary for plant operation.

e. The reactor internals, in conjunction with the fuel assemblies and incore control components, direct reactor coolant through the core. This achieves acceptable flow distribution and restricts bypass flow so that the heat transfer performance requirements can be met for all modes of operation.

4.2.1 Design Bases

The RFA fuel rod and fuel assembly design bases are established to satisfy the general performance and safety criteria presented in Section 4.2.

The fuel rods are designed for a peak rod burnup of approximately 60,000 megawatt days per metric ton of uranium (MWd/Mtu) in the fuel cycle equilibrium condition. Peak rod burnups as high as 62,000 MWd/Mtu can be licensed for Westinghouse fuel in individual fuel cycles using the Westinghouse Fuel Criteria Evaluation Process (References 20 and 22).

Design values for the properties of the materials which comprise the fuel rod, fuel assembly and incore control components are given in Reference 2 for Zircaloy clad in Reference 16 for ZIRLO™ clad fuel. The structural component hydrogen pickup limit has been replaced by structural component stress criterion in Reference 21. Other supplementary fuel design criteria/limits are given in Reference 20.

4.2.1.1 Cladding

a. Material and Mechanical Properties

Zircaloy-4 and ZIRLO™ combine neutron economy (low absorption cross section); high corrosion resistance to coolant, fuel, and fission products; and high strength and ductility at operating temperatures. Reference 1 documents the operating experience with Zircaloy-4 and ZIRLO™ as a clad material. Information on the material chemical and mechanical properties of the cladding is given in Reference 2 and Reference 16 with due consideration of temperature and irradiation effects.

b. Stress-Strain Limits

1. Clad Stress

The von Mises criterion is used to calculate the effective stresses. The cladding stresses under Condition I and II events are less than the Zircaloy 0.2% offset yield stress, with due consideration of temperature and irradiation effects. While the cladding has some capability for accommodating plastic strain, the yield stress has been accepted as a conservative design basis.

2. Clad Tensile Strain

The total tensile creep strain is less than 1 percent from the unirradiated condition. The elastic tensile strain during a transient is less than 1 percent from the pretransient value. These limits are consistent with proven practice.

c. Vibration and Fatigue

1. Strain Fatigue

The cumulative strain fatigue cycles are less than the design strain fatigue life. This basis is consistent with proven practice.

2. Vibration

Potential fretting wear due to vibration is prevented by design of the fuel assembly grid springs and dimples, assuring that the stress-strain limits are not exceeded during design life. Fretting of the clad surface can occur due to flow-induced vibration between the fuel rods and fuel assembly grid springs. Vibration and fretting forces vary during the fuel life due to clad diameter creepdown combined with grid spring relaxation.

d. Chemical Properties

Chemical properties of the cladding are discussed in Reference 2 for Zircaloy-4 and Reference 16 for ZIRLO™.

4.2.1.2 Fuel Material/Integral Fuel Burnable Absorber (IFBA)

a. Thermal-Physical Properties

The thermal-physical properties of UO_2 are described in Reference 2 with due consideration of temperature and irradiation effects.

Fuel pellet temperatures - The center temperature of the hottest pellet is to be below the melting temperature of the UO_2 (melting point of 5080 F (Reference 2) unirradiated and decreasing by 58°F per 10,000 MWd/Mtu). While a limited amount of center melting can be tolerated, the design conservatively precludes center melting. A calculated fuel centerline temperature of 4700 F has been selected as an overpower limit to assure no fuel melting. This provides sufficient margin for uncertainties as described in Subsection 4.4.2.9.

The normal design density of the fuel is approximately 95 percent of theoretical. Additional information on fuel properties is given in Reference 2.

b. Fuel Densification and Fission Product Swelling

The design bases and models used for fuel densification and swelling are provided in References 4 and 17.

c. Chemical Properties

References 2 and 16 provide the basis for justifying that no adverse chemical interactions occur between the fuel and adjacent cladding material.

4.2.1.3 Fuel Rod Performance

The detailed fuel rod design establishes such parameters as pellet size and density, cladding-pellet diameter gap, gas plenum size, and helium prepressurization level. The design also considers effects such as fuel density changes, fission gas release, cladding creep, and other physical properties which vary with burnup. The integrity of the fuel rods is ensured by designing to prevent excessive fuel temperatures, excessive internal rod gas pressures due to fission gas releases, and excessive cladding stresses and strains. This is achieved by designing the fuel rods to satisfy the conservative design basis in the following subsections during Condition I and II events over the fuel lifetime. For each design basis, the performance of the limiting fuel rod must not exceed the limits specified.

a. Fuel Rod Models

The basic fuel rod models and the ability to predict operating characteristics are given in References 16, 17, and 23 and Subsection 4.2.3.

b. Mechanical Design Limits

Fuel rod design methodology described in Reference 18 demonstrates that clad flattening will not occur in Westinghouse fuel designs. The rod internal gas pressure will remain below the value which causes the fuel/clad diametral gap to increase due to outward cladding creep during steady state operation. The maximum rod pressure is also limited so that extensive Departure from Nucleate Boiling (DNB) propagation will not occur during normal operation or any accident event. Reference 7 shows that the DNB propagation criteria is satisfied.

4.2.1.4 Spacer Grids

a. Mechanical Limits and Materials Properties

The grid component strength criteria are based on experimental tests. The limit is established at 0.9 Pc, where Pc is the experimental collapse load. This limit is sufficient to assure that under worst-case combined seismic and blowdown loads the core will maintain a geometry amenable to cooling. As an integral part of the fuel assembly structure, the grids must satisfy the applicable fuel assembly design bases and limits defined in Subsection 4.2.1.5.

The grid material and chemical properties are given in References 2 and 16.

b. Vibration and Fatigue

The grids are designed to provide sufficient fuel rod support to limit fuel rod vibration and maintain clad fretting wear to within acceptable limits.

4.2.1.5 Fuel Assembly

a. Structural Design

As previously discussed in Subsection 4.2.1, the structural integrity of the fuel assemblies is assured by setting design limits on stresses and deformations due to various non-operational, operational and accident loads. These limits are applied to the design and evaluation of the top and bottom nozzles, guide thimbles, grids, and the thimble joints.

The design bases for evaluating the structural integrity of the fuel assemblies are:

1. Non-operational 4g axial and 6g lateral loading with dimensional stability.

2. For the normal operating and upset conditions, the fuel assembly component structural design criteria are established for the two primary material categories, namely austenitic stainless steels and zirconium alloys. The stress categories and strength theory presented in the ASME Boiler and Pressure Vessel Code, Section III, are used as a general guide. The maximum shear-theory (Tresca criterion) for combined stresses is used to determine the stress intensities for the austenitic stainless steel components. The stress intensity is defined as the numerically largest difference between the various principal stresses in a three dimensional field. The design stress intensity, Sm, for austenitic stainless steels such as nickel-chromium-iron alloys, is given by the lowest of the following:

   (a) One-third of the specified minimum tensile strength or two-thirds of the specified minimum yield strength at room temperature

   (b) One-third of the tensile strength or 90 percent of the yield at temperature, but not to exceed two-thirds of the specified minimum yield strength at room temperature. The stress limits for the austenitic stainless steel components are given below. All stress nomenclature is per the ASME Code, Section III.

Stress Intensity Limits

Category	Limit
General Primary Membrane Stress Intensity	Sm
Local Primary Membrane Stress Intensity	1.5 Sm
Primary Membrane plus Bending Stress Intensity	1.5 Sm
Total Primary plus Secondary	3.0 Sm Stress Intensity

The zirconium alloy structural components, which consist of spacer grids, guide thimble and fuel tubes, are in turn subdivided into two categories because of material differences and functional requirements. The fuel tube design criteria are covered separately in Subsection 4.2.1.1. For the guide thimble design, the stress intensities, the design stress intensities and the stress intensity limits are calculated using the same methods as for the austenitic stainless steel structural components. For conservative purposes, the zirconium alloy unirradiated properties are used to define the stress limits.

(c) Abnormal loads during Conditions III or IV - worst cases represented by combined seismic and blowdown loads.

(1) Deflections or failures of components cannot interfere with the reactor shutdown or emergency cooling of the fuel rods.

(2) The fuel assembly structural component stresses under faulted conditions are evaluated using primarily the methods outlined in Appendix F of the ASME Code, Section III. Since the current analytical methods utilize elastic analysis, the stress allowables are defined as the smaller value of 2.4 Sm or 0.70 Su (ultimate strength per ASME nomenclature) for primary membrane and 3.6 Sm or 1.05 Su for primary membrane plus primary bending. For the austenitic steel fuel assembly components, the stress intensity is defined in accordance with the rules described in the previous section for normal operating conditions. For the zirconium alloy components the stress intensity limits are set at two-thirds of the material yield strength, Sy, at reactor operating temperature. This results in zirconium alloy stress limits being the smaller of 1.6 Sy (yield strength per ASME nomenclature) or 0.70 Su for primary membrane and 2.4 Sy or 1.05 Su for primary membrane plus bending. For conservative purposes the zirconium alloy unirradiated properties are used to define the stress limits.

The material and chemical properties of the fuel assembly components are given in References 2 and 16.

b. Thermal-Hydraulic Design

This topic is discussed in Section 4.4.

c. Reconstituted Fuel Assemblies

Those assemblies which contain zirconium alloy or stainless steel filler rods (as discussed in Subsection 4.2.2.1) will be incorporated into core loading plans as normal assemblies. These reconstituted assemblies will typically be grouped with other fuel assemblies with similar exposure histories, and the assemblies in these groups will then be placed in symmetric locations. A single reconstituted assembly may be placed in the center of the core. Appropriate core physics models will be applied to reflect the actual geometry of the reconstituted assemblies in each reload cycle. In the nuclear design analysis for each reload, reconstituted assemblies will be explicitly modeled on a pin-by-pin basis to ensure these assemblies are treated in a conservative manner.

4.2.1.6 Core Components

The core components are subdivided into permanent and temporary devices.

The permanent type components are the Rod Cluster Control Assemblies, secondary neutron source assemblies, and thimble plug assemblies. Thimble plugs may be installed if safety analysis shows the need for them. The temporary components are the burnable poison assemblies and the primary neutron source assemblies, which are normally used only in the initial core. Installation of the secondary sources is optional, provided a sufficient neutron source exists in their absence.

Materials are selected for compatibility in a pressurized water reactor environment, for adequate mechanical properties at room and operating temperature, for resistance to adverse property changes in a radioactive environment, and for compatibility with interfacing components. Materials properties are given in Reference 2.

For Conditions I and II, the stress categories and strength theory presented in the ASME Boiler and Pressure Vessel Code, Section III, Subsection NG-3000 are used as a general guide to establish core component rod cladding stress/strain limits. The code methodology is applied as with fuel assembly structure design, where possible. For Conditions III and IV, code stresses are not limiting.

Additional design bases for each of the mentioned components are given in the following subsections.

a. Control Rods

Design conditions which are considered under Article NB-3000 of the ASME Code, Section III are as follows:

1. External pressure equal to the reactor coolant system operating pressure with appropriate allowance for over-pressure transients

2. Wear allowance equivalent to 1000 reactor trips

3. Bending of the rod due to a misalignment in the guide tube

4. Forces imposed on the rods during rod drop

5. Loads imposed by the accelerations of the control rod drive mechanism

6. Radiation exposure during maximum core life

The stress intensity limit, Sm, for the control rod cladding material is defined at two-thirds of the 0.2 percent offset yield stress.

The absorber material temperature shall not exceed its melting temperature which is 1454°F for Ag-In-Cd absorber material, Reference 8. (The melting point basis is determined by the nominal material melting point minus uncertainty.)

b. Burnable Poison Rods

Failures of burnable poison rods during Conditions I through IV events will not interfere with reactor shutdown or cooling of the fuel rods.

The burnable poison absorber material is nonstructural. The structural elements of the burnable poison rod are designed to maintain the absorber geometry even if the absorber material is fractured. The rods are designed so that the absorber material is below its softening temperature which is 1492^{o}F for Reference 12.5 weight percent boron rods. The absorber material used in burnable poison rods is Borosilicate glass. The softening temperature, as defined in ASTM C338-73, is 720^{o}C.) In addition, the structural elements are designed to prevent excessive slumping.

c. Neutron Source Rods

The neutron source rods are designed to withstand the following:

1. The external pressure equal to the reactor coolant system operating pressure with appropriate allowance for over-pressure transients, and

2. An internal pressure equal to the pressure generated by released gases over the source rod life.

d. Thimble Plug Assembly

The thimble plug assembly may be used to restrict bypass flow through those thimbles not occupied by absorber, source or burnable poison rods.

The thimble plug assemblies satisfy the following criteria:

1. Accommodate the differential thermal expansion between the fuel assembly and the core internals

2. Limit the flow through each occupied thimble

4.2.1.7 Surveillance Program

Subsection 4.2.4.5 and Sections 8 and 23 of Reference 9 discuss the testing and fuel surveillance operational experience program that has, and is, being conducted to verify the adequacy of the fuel performance and design bases. An evaluation of the test program for the IFBA design features is given in Section 2.5 of Reference 14. Fuel surveillance and testing results, as they become available, are used to improve fuel rod design and manufacturing processes and assure that the design bases and safety criteria are satisfied.

4.2.2 Design Description

Each standard fuel assembly consists of 264 fuel rods, 24-guide thimble tubes and one instrumentation thimble tube arranged within a supporting structure.

The instrumentation thimble is located in the center position and provides a channel for insertion of an incore neutron detector, if the fuel assembly is located in an instrumented core position. The guide thimbles provide channels for insertion of either a Rod Cluster Control Assembly, a neutron source assembly, a burnable poison assembly or a thimble plug assembly. Figure 4.2-1 shows a cross section of the fuel assembly array, and Figure 4.2-2A and Figure 4.2-2B show a fuel assembly full length view. The fuel rods are loaded into the fuel assembly structure so that there is clearance between the fuel rod ends and the top and bottom nozzles.

Fuel assemblies are installed vertically in the reactor vessel and stand upright on the lower core plate, which is fitted with alignment pins to locate and orient each assembly. After all fuel assemblies are set in place. The upper support structure is installed. Alignment pins, built into the upper core plate, engage and locate the top nozzle of each fuel assembly. The upper core plate then bears downward against the holddown springs on the top nozzle of each fuel assembly to hold the fuel assemblies in place.

Improper orientation of fuel assemblies within the core is prevented by the use of an indexing hole in one corner of the top nozzle top plate (see Figure 4.2-2A and Figure 4.2-2B). The assembly is oriented with respect to the handling tool and the core by means of a pin which is inserted into this indexing hole. Visual confirmation of proper orientation is also provided by an identification number on the opposite corner clamp.

4.2.2.1 Fuel Rods

The fuel rods consist of fuel pellets contained in hermetically sealed zirconium alloy tubing. The fuel pellets are right circular cylinders consisting of slightly enriched ceramic uranium dioxide which has been sintered to approximately 95% of theoretical density. Some of the pellets may be coated with a thin layer of zirconium di-boride for local reactivity control. Limited substitutions of zirconium alloy or stainless steel filler rods for fuel rods, in accordance with NRC-approved applications of fuel rod configurations, may be used.

Void volume and clearances are provided within the rods to accommodate gases which are released from the fuel pellets during irradiation, differential thermal expansion between the clad and the fuel, and fuel density changes during irradiation. The ends of the fuel pellets may be dished to allow for greater axial expansion at the pellet centerline, and contribute to the void volume available for accommodation of gases. Shifting of the fuel within the clad during handling or shipping prior to core loading is prevented by a spring which bears on top of the fuel.

Some fuel rods may contain annular axial blankets at the top and bottom of the fuel stack. The blankets contain mid-enriched fuel pellets with an annulus through the center and no dish on the ends of the pellet. Mid-enriched annular axial blanket pellets reduce neutron leakage, improve fuel utilization and provide additional void volume to accommodate fission gas release.

With respect to prepressurization, the rods are designed so that (1) the internal gas pressure mechanical design limits given in Subsection 4.2.1.3 are not exceeded, (2) the cladding stress-strain limits (see Subsection 4.2.1.1) are not exceeded for Conditions I and II events, and (3) clad flattening will not occur during the fuel core life.

4.2.2.2 Fuel Assembly Structure

The fuel assembly structure consists of a bottom nozzle, top nozzle, guide thimbles and grids, as shown in Figure 4.2-2A and Figure 4.2-2B.

a. Bottom Nozzle

The bottom nozzle serves as the bottom structural element of the fuel assembly and admits the coolant flow to the assembly. It is fabricated from austenitic stainless steel, and consists of a perforated plate and four angle legs with bearing plates as shown in Figure 4.2-2A and Figure 4.2-2B. The legs form a plenum for the inlet coolant flow to the fuel assembly. The plate also prevents downward ejection of the fuel rods from the fuel assembly. The bottom nozzle is fastened to the fuel assembly guide tubes by screws which penetrate the nozzle and engage threaded plugs in the guide thimbles.

Axial loads (holddown) imposed on the fuel assembly and the weight of the fuel assembly are transmitted through the bottom nozzle to the lower core plate. Indexing and positioning of the fuel assembly are provided by alignment holes in two diagonally opposite bearing plates which mate with locating pins in the lower core plate. Lateral loads on the fuel assembly are transmitted to the lower core plate through the locating pins.

b. Top Nozzle

The top nozzle assembly functions as the upper structural element of the fuel assembly. The top nozzle assembly consists of a box-like structure with holddown springs mounted as shown in Figure 4.2-2A and Figure 4.2-2B. The springs and bolts are made of Inconel, whereas other components are made of austenitic stainless steel.

The square adapter plate is provided with openings to permit the flow of coolant upward through the top nozzle. Other holes are provided to accept the thimble tubes. The ligaments in the plate cover the tops of the fuel rods and prevent their upward ejection from the fuel assembly. The enclosure is a box-like structure which sets the distance between the adapter plate and the top plate. The top plate has a large square hole in the center to permit access for the control rod assembly or other components. Holddown springs are mounted on the top plate and are fastened in place by bolts and clamps located at two diagonally opposite corners. On the other two corners, pads are positioned which contain alignment holes for locating the upper end of the fuel assembly.

c. Guide and Instrument Thimbles

The guide thimbles are structural members which also provide channels for the neutron absorber rods, burnable poison rods, neutron source or thimble plug assemblies. Each thimble is fabricated from zirconium alloy tubing having two different diameters. The tube diameter at the top section provides the annular area necessary to permit rapid control rod insertion during a reactor trip. The lower portion of the guide thimble is of a smaller diameter to reduce diametral clearances and produce a dashpot action near the end of the control rod travel. Holes are provided in the thimble tube above the dashpot to reduce the rod drop time. The dashpot is closed at the bottom by means of an end plug which is provided with a small flow port to avoid fluid stagnation. The top end of the guide thimble is fastened to a tubular sleeve by expansion swages. The sleeve fits into and is fastened to the top nozzle adapter plate. The lower end of the guide thimble is fitted with an end plug which is then fastened to the bottom nozzle by a screw.

Fuel rod support grids are fastened to the guide thimble assemblies to create an integrated structure. A mechanical fastening technique depicted in Figure 4.2-4 and Figure 4.2-5 is used for all but the bottom grids in a fuel assembly.

An expanding tool is inserted into the thimble tube at the elevation of the sleeves that have been attached to the grid assemblies. The four-lobed tool forces the thimble and sleeve outward to a predetermined diameter, thus joining the two components.

The top grid to thimble attachment for the initial core is shown in Figure 4.2-6A. The stainless steel sleeves are brazed into the Inconel grid assembly. The zirconium alloy guide thimbles are fastened to the sleeves by expanding the two members as shown in Figure 4.2-4 and Figure 4.2-5. Finally, the top ends of the sleeves are attached to the top nozzle adapter plate as shown in Figure 4.2-6A and Figure 4.2-6B.

The bottom grid assembly is joined to the skeleton assembly as shown in Figure 4.2-7. The stainless steel insert is attached to the bottom grid and later captured between the guide thimble end plug and the bottom nozzle by a screw fastener.

The described methods of grid fastening are standard and have been used successfully since the introduction of Zircaloy guide thimbles in 1969.

The central instrumentation thimble of each fuel assembly is constrained by seating in counterbores in each nozzle. This tube is a constant diameter and guides the incore neutron detectors. It is expanded at the top and mid-grids in the same manner as the previously discussed expansion of the guide thimbles to the grids.

d. Grid Assemblies

The fuel rods, as shown in Figure 4.2-2A and Figure 4.2-2B, are supported at intervals along their length by grid assemblies which maintain the lateral spacing between the rods. Each fuel rod is supported within each grid by the combination of support dimples and springs.

The grid assembly consists of individual slotted straps interlocked and brazed or welded in an "egg-crate" arrangement to join the straps permanently at their points of intersection. The straps contain springs, support dimples and mixing vanes.

The grid material is Inconel or zirconium alloy, chosen because of its corrosion resistance and strength. The magnitude of the grid restraining force on the fuel rod is set high enough to minimize possible fretting, without overstressing the cladding at the points of contact between the grids and fuel rods. The grid assemblies also allow axial thermal expansion of the fuel rods without imposing restraint sufficient to develop buckling or distortion of the fuel rods.

Nine grids, with mixing vanes projecting from the edges of the straps into the coolant stream, are used in the high heat flux region of the fuel assemblies to promote mixing of the coolant. The top, bottom, and protective grids do not contain mixing vanes on the internal straps. The outside straps on all grids contain mixing vanes which, in addition to their mixing function, aid in guiding the grids and fuel assemblies past projecting surfaces during handling or during loading and unloading of the core.

4.2.2.3 Core Components

Reactivity control is provided by neutron absorbing rods and a soluble chemical neutron absorber (boric acid). The boric acid concentration is varied to control long-term reactivity changes such as:

a. Fuel depletion and fission product buildup

b. Cold to hot, zero power reactivity change

c. Reactivity change produced by intermediate term fission products such as xenon and samarium

d. Burnable poison depletion.

The Chemical and Volume Control System is discussed in Chapter 9.

The Rod Cluster Control Assemblies (RCCAs) provide reactivity control for:

a. Shutdown

b. Reactivity changes resulting from coolant temperature changes in the power range

c. Reactivity changes associated with the power coefficient of reactivity

d. Reactivity changes resulting from void formation.

Figure 4.2-8 illustrates the RCCA and control rod drive mechanism assembly, in addition to the arrangement of these components in the reactor relative to the interfacing fuel assembly and guide tubes. In the following paragraphs, each reactivity control component is described in detail. The control rod drive mechanism assembly is described in Subsection 3.9(N).4.

The neutron source assemblies provide a means of monitoring the core during periods of low neutron level. The thimble plug assemblies may be used to limit bypass flow through those fuel assembly thimbles which do not contain control rods, burnable poison rods, or neutron source rods.

a. (RCCA)

The RCCAs are divided into two categories: control and shutdown. The control groups compensate for reactivity changes associated with variations in operating conditions of the reactor, i.e., power and temperature variations. Two nuclear design criteria have been employed for selection of the control group. First the total reactivity worth must be adequate to meet the nuclear requirements of the reactor. Second, in view of the fact that these rods may be partially inserted at power operation, the total power peaking factor should be low enough to ensure that the power capability is met. Additional shutdown banks are provided which, together with the control banks A, B, C and D, supply reactivity insertion to cover the power defect, plus (a) transient cooldowns below the hot zero power critical state, (b) an NRC requirement for a minimum of 1 percent hot standby shutdown reactivity, (c) the worth of any full length control rod stuck out of the core, and (d) a margin for uncertainty in rod worth and reactivity change calculations. The control and shutdown groups together provide adequate shutdown margin.

The Ag-In-Cd Rod Cluster Control Assembly comprises 24 neutron absorber rods fastened at the top end to a common spider assembly, as illustrated in Figure 4.2-9A and Figure 4.2-9B.

The absorber material used in the control rods is a silver-indium-cadmium alloy which is essentially "black" to thermal neutrons and has sufficient additional resonance absorption to significantly increase its worth. The Ag-In-Cd absorber rod is illustrated in Figure 4.2-10.

The bottom plugs are tapered to reduce the hydraulic drag during reactor trip and to guide the absorber rods smoothly into the dashpot section of the fuel assembly guide thimbles.

The allowable stresses used as a function of temperature are listed in Table 1.1-2 of Section III of the ASME Code. The fatigue strength is based on the S-N curve for austenitic stainless steels in Figure 1.9-2 of Section III.

The spider assembly is in the form of a central hub with radial vanes containing cylindrical fingers from which the absorber rods are suspended. Handling detents and detents for connection to the drive rod assembly are machined into the upper end of the hub. A coil spring inside the spider body absorbs the impact energy at the end of a trip insertion. A center-post which holds the spring and its retainer is threaded into the hub within the skirt and welded to prevent loosening in service. All components of the spider assembly are made from austenitic stainless steel or other corrosion-resistant material such as Inconel.

The absorber rods are fastened securely to the spider. The rods are first threaded into the spider fingers and then pinned to maintain joint tightness. The end plug below the pin position is designed with a reduced section to permit flexing of the rods to correct for small misalignments.

The overall length is such that when the assembly is withdrawn through its full travel, the tips of the absorber rods remain engaged in the guide thimbles so that alignment between rods and thimbles is always maintained. Since the rods are long and slender, they are relatively free to conform to any small misalignments with the guide thimble.

b. Burnable Poison Assembly

Each burnable poison assembly consists of burnable poison rods attached to a holddown assembly. A burnable poison assembly is shown in Figure 4.2-11. When needed for nuclear considerations, burnable poison assemblies are inserted into selected thimbles within fuel assemblies.

The poison rods consist of borosilicate glass tubes contained within austenitic stainless steel tubular cladding which is plugged and seal welded at the ends to encapsulate the glass. The glass is also supported along the length of its inside diameter by a thin wall tubular inner liner. The top end of the liner is open to permit the diffused helium to pass into the void volume, and the liner overhangs the glass. The liner has an outward flange at the bottom end to maintain the position of the liner with the glass. A typical burnable poison rod is shown in longitudinal and transverse cross sections in Figure 4.2-12.

The poison rods in each fuel assembly are grouped and attached together at the top end of the rods to a holddown assembly by a flat perforated retaining plate which fits within the fuel assembly top nozzle and rests on the adaptor plate. The retaining plate and poison rods are held down and restrained against vertical motion through a spring pack which is attached to the plate and is compressed by the upper core plate when the reactor upper internals assembly is lowered into the reactor. This arrangement ensures that the poison rods cannot be ejected from the core by flow forces. Each rod is permanently attached to the base plate by a nut which is lock-welded into place.

The cladding of the burnable poison rods and all other structural materials are austenitic stainless steel except for the springs which are Inconel. The borosilicate glass tube provides sufficient boron content to meet the criteria discussed in Subsection 4.3.1.

c. Neutron-Source Assembly

The purpose of the neutron source assembly is to provide base neutron level to ensure that the neutron detectors are operational and responding to core multiplication neutrons. A neutron source is placed in the reactor to provide a positive neutron count on the source range detectors attributable to core neutrons. The detectors, called source range detectors, are used primarily when the core is subcritical and during special subcritical modes of operations.

The source assembly permits detection of changes in the core multiplication factor during core loading and approach to criticality.

This can be done since the multiplication factor is related to an inverse function of the detector count rate. Changes in the multiplication factor can be detected during addition of fuel assemblies while loading the core, changes in control rod positions, and changes in boron concentration.

Both primary and secondary neutron source rods are used in the initial core. Subsequent cycles do not require a primary source. The primary source rod, containing a radioactive material, spontaneously emits neutrons during initial core loading, reactor startup and initial operation of the first core. After the primary source rod decays beyond the desired neutron flux level, neutrons are then supplied by the secondary source rod. The secondary source rod contains a stable material which is activated during reactor operation. The activation results in the subsequent release of neutrons.

Four source assemblies were installed in the initial reactor core: two primary source assemblies and two secondary source assemblies. Each primary source assembly contains one primary source rod and a number of burnable poison rods. Each secondary source assembly contains a symmetrical grouping of four secondary source rods. Locations not filled with a source rod or burnable poison rod contain a thimble plug rodlet. Two additional secondary source assemblies may be incorporated for future cycles. The source assemblies are shown in Figure 4.2-13, Figure 4.2-14A and Figure 4.2-14B.

The source assemblies are inserted into the rod cluster control guide thimbles in fuel assemblies at selected unrodded locations.

As shown in Figure 4.2-13 and Figure 4.2-14, the source assemblies contain a holddown assembly identical to that of the burnable poison assembly. The additional secondary sources contain a single holddown spring with similar holddown characteristics to that of the original sources.

The primary and secondary source rods have the same cladding as the absorber rods. The secondary source rods contain Sb-Be pellets stacked to a height of approximately 88 inches. The primary source rods contain capsules of californium source material and alumina spacer to position the source material within the cladding. The rods in each assembly are permanently fastened at the top end to a holddown assembly.

The other structural members such as the spider head and vanes are constructed of austenitic stainless steel or Inconel.

d. Thimble Plug Assembly

Thimble plug assemblies may be used to limit bypass flow through the rod cluster control guide thimbles in fuel assemblies which do not contain control rods, source rods, or burnable poison rods.

The thimble plug assemblies consist of a flat base plate with short rods suspended from the bottom surface and a spring pack assembly as shown in Figure 4.2-15. The 24 short rods, called thimble plugs, project into the upper ends of the guide thimbles to reduce the bypass flow. Each thimble plug is permanently attached to the base plate. Similar short rods are also used on the source assemblies and burnable poison assemblies to plug the ends of all vacant fuel assembly guide thimbles. When in the core, the thimble plug assemblies interface with both the upper core plate and with the fuel assembly guide thimbles tubes. The spring pack is compressed by the upper core plate when the upper internals assembly is lowered into place.

All components in the thimble plug assembly, except for the springs, are constructed from austenitic stainless steel or Inconel.

4.2.3 Design Evaluation

The fuel assemblies, fuel rods and incore control components are designed to satisfy the performance and safety criteria of the introduction to Section 4.2, the mechanical design bases of Subsection 4.2.1, and other interfacing nuclear and thermal hydraulic design bases specified in Sections 4.3 and 4.4. Effects of Conditions II, III, IV or Anticipated Transients without Trip on fuel integrity are presented in Chapter 15 or supporting topical reports.

The initial step in fuel rod design evaluation for a region of fuel is to determine the limiting rod(s). Limiting rods are defined as those rod(s) whose predicted performance provides the minimum margin to each of the design criteria. For a number of design criteria, the limiting rod is the lead burnup rod of a fuel region. In other instances it may be the maximum power or the minimum burnup rod. For the most part, no single rod will be limiting with respect to all design criteria.

After identifying the limiting rod(s), a worst-case performance evaluation is made which uses the limiting rod design basis power history and considers the effects of model uncertainties and dimensional variations. Furthermore, to verify adherence to the design criteria, the conservative case evaluation also considers the effects of postulated transient power increases which are achievable during operation consistent with Conditions I and II events. These transient power increases can affect both rod and local power levels. The analytical methods used in the evaluation result in performance parameters which demonstrate the fuel rod behavior. Examples of parameters considered include rod internal pressure, fuel temperature, clad stress, and clad strain. In fuel rod design analyses, these performance parameters provide the basis for comparison between expected fuel rod behavior and the corresponding design criteria limits.

Fuel rod and fuel assembly models used for the various evaluations are documented and maintained under an appropriate control system. Properties of materials used in the design evaluations are given in References 2 and 16.

4.2.3.1 Cladding

a. Vibration and Wear

Fuel rod vibrations are flow induced. The effect of the vibration on the fuel assembly and individual fuel rods is minimal. The cyclic stress range associated with deflections of such small magnitude is insignificant and has no effect on the structural integrity of the fuel rod.

The reaction force on the grid supports due to rod vibration motions is also small and is much less than the spring preload. Firm fuel clad spring contact is maintained. No significant wear of the clad or grid supports is expected during the life of the fuel assembly, based on out-of-pile flow tests performance of similarly designed fuel in operating reactors, and design analysis.

Clad fretting and fuel vibration has been experimentally investigated as shown in Reference 10.

b. Fuel Rod Internal Pressure and Cladding Stresses

The burnup dependent fission gas release model (References 17 and 23) is used in determining the internal gas pressures as a function of irradiation time. The plenum volume of the fuel rod has been established to ensure that the maximum internal pressure of the fuel rod will not exceed the value which would cause (1) the fuel/clad diametral gap to increase during steady state operation and (2) extensive DNB propagation to occur (see Subsection 4.2.1.3b). The clad stresses at a constant local fuel rod power are low. Compressive stresses are created by the pressure differential between the coolant pressure and the rod internal gas pressure.

Stresses due to the temperature gradient are not included in the average effective stress because thermal stresses are, in general, negative at the clad inside diameter and positive at the clad outside diameter and their contribution to the clad volume average stress is small. Furthermore, the thermal stress decreases with time during steady state operation due to stress relaxation. The stress due to pressure differential is highest in the minimum power rod at the beginning-of-life due to low internal gas pressure. The thermal stress is highest in the maximum power rod due to steep temperature gradient.

Tensile stresses could be created once the clad has come in contact with the pellet. These stresses would be induced by the fuel pellet swelling during irradiation. Fuel swelling can result in small clad strains (< 1 percent) for expected discharge burnups but the associated clad stresses are very low because of clad creep (thermal and irradiation-induced creep). The 1 percent strain criterion is extremely conservative for fuel-swelling driven clad strain because the strain rate associated with solid fission products swelling is very slow. A detailed discussion on fuel rod performance is given in Subsection 4.2.3.3.

c. Materials and Chemical Evaluation

Zircaloy-4 and ZIRLO^{TM} clad has a high corrosion resistance to the coolant, fuel and fission products. As shown in Reference 1, there is pressurized water reactor operating experience on the capability of Zircaloy-4 and ZIRLO^{TM} as a clad material. Controls on fuel fabrication specify maximum moisture levels to preclude clad hydriding.

Metallographic examination of irradiated commercial fuel rods have shown occurrences of fuel/clad chemical interaction. Reaction layers of 1 mil in thickness have been observed between fuel and clad at limited points around the circumference. Metallographic data indicate that this interface layer remains very thin even at high burnup. Thus, there is no indication of propagation of the later and eventual clad penetration.

Stress corrosion cracking is another postulated phenomenon related to fuel/clad chemical interaction. Out-of-pile tests have shown that in the presence of high clad tensile stresses, large concentrations of selected fission products (such as iodine) can chemically attack the tubing and can lead to eventual clad cracking. Extensive post-irradiation examination has produced no inpile evidence that this mechanism is operative in Westinghouse produced commercial fuel.

d. Rod Bowing

Reference 11 presents the model used for evaluation of fuel rod bowing. The effects of rod bowing or DNBR are described in Subsection 4.4.2.2e. Also refer to item e in Section 4.2.

e. Consequences of Power-Coolant Mismatch

This subject is discussed in Chapter 15.

f. Creep Collapse and Creepdown

This subject and the associated irradiation stability of cladding have been evaluated using the models described in References 6 and 18. It has been established that the design basis of no clad collapse during planned core life can be satisfied by limiting fuel densification and by having a sufficiently high initial internal rod pressure.

g. Irradiation Stability of the Cladding

As shown in Reference 1, there is PWR operating experience on the capability of Zircaloy and ZIRLO™ as a cladding material. Extensive experience with irradiated Zircaloy-4 is summarized in Reference 2 and Reference 16 for ZIRLO™.

h. Cycling and Fatigue

A comprehensive review of the available strain fatigue models was conducted by Westinghouse as early as 1968. This review included the Langer-O'Donnell model (Reference 12), the Yao-Munse model and the Manson-Halford model. Upon completion of this review and using the results of the Westinghouse experimental programs discussed below, it was concluded that the approach defined by Langer-O'Donnell would be retained and the empirical factors of their correlation modified in order to conservatively bound the results of the Westinghouse testing program.

The Westinghouse testing program was subdivided into the following subprograms:

1. A rotating bend fatigue experiment on unirradiated Zircaloy-4 specimens at room temperature and at 725°F. Both hydrided and non-hydrided Zircaloy-4 cladding were tested.

2. A biaxial fatigue experiment in gas autoclave on unirradiated Zircaloy-4 cladding, both hydrided and non-hydrided.

3. A fatigue test program on irradiated cladding from the CVS and Yankee Core V conducted at Battelle Memorial institute.

The results of these test programs provided information on different cladding conditions including the effects of irradiation, of hydrogen levels and of temperature.

The design equations followed the concept for the fatigue design criterion according to the ASME Boiler and Pressure Vessel Code, Section III.

it is recognized that a possible limitation to the satisfactory behavior of the fuel rods in a reactor which is subjected to daily load follow is the failure of the cladding by low cycle strain fatigue. During their normal residence time in reactor, the fuel rods may be subjected to ~1000 cycles with typical changes in power level from 50% to 100% of their steady-state values.

The assessment of the fatigue life of the fuel rod cladding is subject to a considerable uncertainty due to the difficulty of evaluating the strain range which results from the cyclic interaction of the fuel pellets and cladding. This difficulty arises, for example, from such high unpredictable phenomena as pellet cracking, fragmentation, and relocation. Since early 1968, this particular phenomenon has been investigated analytically and experimentally.

Strain fatigue tests on irradiated and non-irradiated hydrided Zr-4 claddings were performed, which permitted a definition of a conservative fatigue life limit and recommendation on a methodology to treat the strain fatigue evaluation of Westinghouse reference fuel rod designs.

It is believed that the final proof of the adequacy of a given fuel rod design to meet the load follow requirements can only come from incore experiments performed on actual reactors. Experience in load follow operation dates back to early 1970 with the load follow operation of the Saxton reactor. Successful load follow operation has been performed on reactor A (>400 load follow cycles) and reactor B (>500 load follow cycles). In both cases, there was no significant coolant activity increase that could be associated with the load follow mode of operation.

4.2.3.2 Fuel Materials Considerations

Sintered, high density uranium dioxide fuel reacts only slightly with the clad at core operating temperatures and pressures. In the event of clad defects, the high resistance of uranium dioxide to attack by water protects against fuel deterioration although limited fuel erosion can occur. As has been shown by operating experience and extensive experimental work, the thermal design parameters conservatively account for changes in the thermal performance of the fuel elements due to pellet fracture which may occur during power operation. The consequences of defects in the clad are greatly reduced by the ability of uranium dioxide to retain fission products, including those which are gaseous or highly volatile. Observations from several operating Westinghouse-supplied pressurized water reactors (Reference 9) have shown that fuel pellets can densify under irradiation to a density higher than the manufactured values. Fuel densification and subsequent settling of the fuel pellets can result in local and distributed gaps in the fuel rods. Fuel densification has been minimized by improvements in the fuel manufacturing process and by specifying a nominal 95 percent initial fuel density.

The evaluation of fuel densification effects and its consideration in fuel design are described in References 17 and 23. The treatment of fuel swelling and fission gas release are described in References 17 and 23.

The effects of waterlogging on fuel behavior are discussed in Subsection 4.2.3.3.

4.2.3.3 Fuel Rod Performance

In the calculation of the steady state performance of a nuclear fuel rod, the following interacting factors must be considered:

a. Clad creep and elastic deflection

b. Pellet density changes, thermal expansion, gas release, and thermal properties as a function of temperature and fuel burnup

c. Internal pressure as a function of fission gas release, rod geometry, and temperature distribution.

These effects are evaluated using a fuel rod design model (References 17 and 23). The model modifications for time dependent fuel densification are given in References 17 and 23. With the above interacting factors considered, the model determines the fuel rod performance characteristics for a given rod geometry, power history, and axial power shape. In particular, internal gas pressure, fuel and clad temperatures, and clad deflections are calculated. The fuel rod is divided into several axial sections and radially into a number of annular zones. Fuel density changes are calculated separately for each segment. The effects are integrated to obtain the internal rod pressure.

The initial rod internal pressure is selected to delay fuel/clad mechanical interaction and to avoid the potential for flattened rod formation. It is limited, however, by the design criteria for the rod internal pressure (see Subsection 4.2.1.3).

The gap conductance between the pellet surface and the clad inner diameter is calculated as a function of the composition, temperature, and pressure of the gas mixture, and the gap size or contact pressure between clad and pellet. After computing the fuel temperature for each pellet annular zone, the fractional fission gas release is assessed using an empirical model derived from experimental data (References 17 and 23). The total amount of gas released is based on the average fractional release within each axial and radial zone and the gas generation rate which in turn is a function of burnup. Finally, the gas released is summed over all zones and the pressure is calculated.

The code shows good agreement with a variety of published and proprietary data on fission gas release, fuel temperatures and clad deflections (References 17 and 23). These data include variations in power, time, fuel density, and geometry.

a. Fuel/Cladding Mechanical Interaction

One factor in fuel element duty is potential mechanical interaction of fuel and clad. This fuel/clad interaction produces cyclic stresses and strains in the clad, and these in turn consume clad fatigue life. The reduction of fuel/clad interaction is therefore a goal of design. The technology of using prepressurized fuel rods has been developed to further this objective.

The gap between the fuel and clad is sufficient to prevent hard contact between the two. However, during power operation, a gradual compressive creep of the clad onto the fuel pellet occurs due to the external pressure exerted on the rod by the coolant. Clad compressive creep eventually results in the fuel/clad contact. Once fuel/clad contact occurs, changes in power level result in changes in clad stresses and strains. By using prepressurized fuel rods to partially offset the effect of the coolant external pressure, the rate of clad creep toward the surface of the fuel is reduced. Fuel rod prepressurization delays the time at which fuel/clad contact occurs and hence significantly reduces the extent of cyclic stresses and strains experienced by the clad both before and after fuel/clad contact. These factors result in an increase in the fatigue life margin of the clad and lead to greater clad reliability. If gaps should form in the fuel stacks, clad flattening will be prevented by the rod prepressurization so that the flattening time will be greater than the fuel life time.

A two-dimensional (r,θ) finite element model has been developed to investigate the effects of radial pellet cracks on stress concentrations in the clad. Stress concentration is defined here as the difference between the maximum clad stress in the θ direction and the mean clad stress. The first case has the fuel and clad in mechanical equilibrium, and as a result the stress in the clad is close to zero. In subsequent cases, the pellet power is increased in steps and the resultant fuel thermal expansion imposes tensile stress in the clad. In addition to uniform clad stresses, stress concentrations develop in the clad adjacent to radial cracks in the pellet. These radial cracks have a tendency to open during a power increase but the frictional forces between fuel and clad oppose the opening of these cracks and result in localized increases in clad stress. As the power is further increased, large tensile stresses exceed the ultimate tensile strength of UO2, and additional cracks develop in the fuel thus limiting the magnitude of the stress concentration in the clad.

As part of the standard fuel rod design analysis, the maximum stress concentration evaluated from finite element calculations is added to the volume averaged effective stress in the clad as determined from one-dimensional stress/strain calculations. The resultant clad stress is then compared to the temperature-dependent yield strength to assure that the stress/strain criteria are satisfied.

1. Transient Evaluation Method

Pellet thermal expansion due to power increases is considered the only mechanism by which significant stresses and strains can be imposed on the clad. Such increases are a consequence of fuel shuffling (e.g., Region 3 positioned near the center of the core for Cycle 2 operation after operating near the periphery during Cycle 1), reactor power escalation following extended reduced power operation, and full length control rod movement. In the mechanical design model, lead rod burnup values are obtained using best estimate power histories, as determined by core physics calculations. During burnup, the amount of diametral gap closure is evaluated based upon the pellet expansion cracking model, clad creep model, and fuel swelling model. At various times during the depletion, the power is increased locally on the rod to the burnup dependent attainable power density as determined by core physics calculations. The radial, tangential and axial clad stresses -resulting from the power increase are combined into a volume average effective clad stress.

The Von Mises criterion is used to determine if the clad yield-strength has been exceeded. This criterion states that an isotropic material in multi-axial stress will begin to yield plastically when the effective stress exceeds the yield strength as determined by an axial tensile test. The yield strength correlation is for irradiated cladding since fuel/clad interaction occurs at high burnup. Furthermore, the effective stress is increased by an allowance, which accounts for stress concentrations in the clad adjacent to radial cracks in the pellet, prior to the comparison with the yield stress. This allowance was evaluated using a two-dimensional (r,θ) finite element model.

Slow transient power increases can result in large clad strains without exceeding the clad yield strength because of clad creep and stress relaxation. Therefore, in addition to the yield strength criterion, a criterion on allowable clad strain is necessary. Based upon high strain rate burst and tensile test data on irradiated tubing, 1 percent strain was determined to be a conservative lower limit on irradiated clad deformation and was thus adopted as a design criterion.

A comprehensive review of the available strain fatigue models was conducted by Westinghouse as early as 1968. This included the Langer-O'Donnell model (Reference 12), the Yao-Munse model, and the Manson Halford model. Upon completion of this review and using the results of the Westinghouse experimental programs discussed below, it was concluded that the approach defined by Langer-O'Donnell would be retained and the empirical factors of their correlation modified in order to conservatively bound the results of the Westinghouse testing program.

The Langer-O'Donnell empirical correlation has the following form:

$$S_a = \frac{E}{4\sqrt{N_f}} \ln\left(\frac{100}{100 - RA}\right) + S_e$$

where:

S_a = 1/2 E $\Delta\varepsilon_t$ = pseudo-stress amplitude which causes failure in Nf cycles (lb./in.2)

$\Delta\varepsilon_t$ = total strain range (in./in.)

E = Young's Modulus (lb./in.2)

N_f = number of cycles to failure

RA = reduction in area at fracture in a uniaxial tensile test (percent)

S_e = endurance limit (lb/in^2)

Both RA and S_e are empirical constants which depend on the type of material, the temperature and irradiation. The Westinghouse testing program was subdivided into the following subprograms:

(a) A rotating bend fatigue experiment on unirradiated Zircaloy-4 specimens at room temperature and at 725°F. Both hydrided and nonhydrided Zircaloy-4 cladding were tested.

(b) A biaxial fatigue experiment in gas autoclave on unirradiated Zircaloy-4 cladding, both hydrided and nonhydrided

(c) A fatigue test program on irradiated cladding from the Carolina-Virginia Tube Reactor and Yankee Core V conducted at Battelle Memorial Institute.

The results of these test programs provided information on different cladding conditions including the effect of irradiation, of hydrogen level, and temperature.

The design equations followed the concept for the fatigue design criterion according to the ASME Code, Section III, namely:

(a) The calculated pseudo-stress amplitude (S_a) has to be multiplied by a factor of 2 in order to obtain the allowable number of cycles (Nf).

(b) The allowable number of cycles for a given S_a is 5 percent of N, maintaining a safety factor of 20 on cycles.

The lesser of the two allowable number of cycles is selected. The cumulative fatigue life fraction is then computed as:

$$\sum_{1}^{k} \frac{n_k}{N_{fk}} \leq 1$$

where:

n_k = number of diurnal cycles of mode k

N_{fk} = number of allowable cycles

It is recognized that a possible limitation to the satisfactory behavior of the fuel rods in a reactor which is subjected to daily load follow is the failure of the clad by low cycle strain fatigue. During their normal residence time in reactor, the fuel rods may be subjected to approximately 1000 cycles with typical changes in power level from 50 to 100 percent of their steady state values.

The assessment of the fatigue life of the fuel rod clad is subject to a considerable uncertainty due to the difficulty of evaluating the strain range which results from the cyclic interaction of the fuel pellets and clad. This difficulty arises, for example, from such highly unpredictable phenomena as pellet cracking, fragmentation, and relocation. Nevertheless, since early 1968, this particular phenomenon has been investigated analytically and experimentally (Reference 12). Strain fatigue tests on irradiated and nonirradiated hydrided Zircaloy-4 claddings were performed which permitted a definition of a conservative fatigue life limit and recommendation on a methodology to treat the strain fatigue evaluation of the Westinghouse reference fuel rod designs.

It is believed that the final proof of the adequacy of a given fuel rod design to meet the load follow requirements can only come from incore experiments performed on actual reactors. Experience in load follow operation dates back to early 1970 with the load follow operation of the Saxton reactor. Successful load follow operation has been performed on reactor A (approximately 400 load follow cycles) and reactor B (approximately 500 load follow cycles). In both cases, there was no significant coolant activity increase that could be associated with the load follow mode of operation.

b. Irradiation Experience

Westinghouse fuel operational experience is presented in Reference 1. Additional test assembly and test rod experience are given in Sections 8 and 23 of Reference 9.

c. Fuel and Cladding Temperature

The methods used for evaluation of fuel rod temperatures are presented in Subsection 4.4.2.11.

d. Waterlogging

Local cladding deformations typical for waterlogging bursts have never been observed in commercial Westinghouse-supplied fuel. (Waterlogging damage of a previously defected fuel rod has occasionally been postulated as a mechanism for subsequent rupture of the cladding. Such damage has been postulated as a consequence of a power increase on a rod after water has entered such a rod through a clad defect of appropriate size. Rupture is postulated upon power increase if the rod internal pressure increase is excessive due to insufficient venting of water to the reactor coolant.) Experience has shown that the small number of rods which have acquired clad defects, regardless of primary mechanism, remain intact and do not progressively distort or restrict coolant flow. In fact such small defects are normally observed, through reductions in coolant activity, to be progressively closed upon further operation due to the buildup of zirconium oxide and other substances. Secondary failures which have been observed in defective rods are attributed to hydrogen embrittlement of the cladding. Post-irradiation examinations point to the hydriding failure mechanism rather than a waterlogging mechanism; the secondary failures occur as axial cracks or blisters in the cladding and are similar regardless of the primary failure mechanism. Such cracks do not result in flow blockage, or increase the effects of any postulated transients. More information is provided in Reference 19.

e. Potentially Damaging Temperature Effects During Transients

The fuel rod experiences many operational transients (intentional maneuvers) during its residence in the core. A number of thermal effects must be considered when analyzing the fuel rod performance.

The clad can be in contact with the fuel pellet at some time in the fuel lifetime. Clad/pellet interaction occurs if the fuel pellet temperature is increased after the clad is in contact with the pellet. Clad/pellet interaction is discussed in Subsection 4.2.3.3a.

The potential effects of operation with waterlogged fuel are discussed in Subsection 4.2.3.3d, which concluded that waterlogging is not a concern during operational transients.

Clad flattening, as shown in Reference 6, has been observed in some operating Westinghouse supplied power reactors. Thermal expansion (axial) of the fuel rod stack against a flattened section of clad could cause failure of the clad. This is no longer a concern because clad flattening is precluded by design during the fuel residence in the core (see Subsection 4.2.3.1).

Potential differential thermal expansion between the fuel rods and the guide thimbles during a transient is considered in the design. Excessive bowing of the fuel rods is precluded because the grid assemblies allow axial movement of the fuel rods relative to the grids. Specifically, thermal expansion of the fuel rods is considered in the grid design so that axial loads imposed on the fuel rods during a thermal transient will not result in excessively bowed fuel rods.

f. Fuel Element Burnout and Potential Energy Release

As discussed in Subsection 4.4.2.2, the core is protected from DNB over the full range of possible operating conditions. In the extremely unlikely event that DNB should occur, the clad temperature will rise due to degradation in heat transfer caused by steam blanketing at the rod surface. During this time, some chemical reaction between the cladding and the coolant will occur. However, because of the relatively good film boiling heat transfer following DNB, and the short time of the transient, the energy release resulting from this reaction is insignificant compared to the power produced by the fuel.

g. Coolant Flow Blockage Effects on Fuel Rods

This evaluation is presented in Subsection 4.4.4.7.

4.2.3.4 Spacer Grids

The coolant flow channels are established and maintained by the structure composed of grids and guide thimbles. The lateral spacing between fuel rods is provided and controlled by the support dimples of adjacent grid cells. Contact of the fuel rods on the dimples is maintained by the clamping force of the grid springs. Lateral motion of the fuel rods is opposed by the spring force and the internal moments generated between the spring and the support dimples. Grid testing is discussed in Reference 13.

As shown in Reference 13, grid crushing tests and seismic and loss-of-coolant accident evaluations show that the grids will maintain a geometry that is capable of being cooled under the worst-case accident Condition IV event.

4.2.3.5 Fuel Assembly

a. Stresses and Deflections

The fuel assembly component stress levels are limited by the design. For example, stresses in the fuel rod due to axial thermal expansion and zirconium alloy irradiation growth are limited by the relative motion of the rod as it slips over the grid spring and dimple surfaces. Clearances between the fuel rod ends and nozzles are provided so that zircaloy irradiation growth does not result in rod end interferences. Stresses in the fuel assembly caused by tripping of the Rod Cluster Control Assembly have little influence on fatigue because of the small number of events during the life of an assembly. Assembly components and prototype fuel assemblies made from production parts have been subjected to structural tests to verify that the design bases requirements are met.

The fuel assembly design loads for shipping and handling have been established at 4g axial and 6g lateral. Accelerometers are permanently placed into the shipping cask to monitor and detect fuel assembly accelerations that would exceed the criteria. Past history and experience have indicated that loads which exceed the allowable limits rarely occur. Exceeding the limits requires reinspection of the fuel assembly for damage. Tests on various fuel assembly components such as the grid assembly, sleeves, inserts and structure joints have been performed to assure that the shipping design limits do not result in impairment of fuel assembly function. Seismic analysis of the fuel assembly is presented in Reference 13.

b. Dimensional Stability

A prototype fuel assembly has been subjected to column loads in excess of those expected in normal service and faulted conditions (see Reference 13).

No interference between control rod and thimble tubes will occur during insertion of the rods following a postulated loss-of-coolant accident transient due to fuel rod swelling, thermal expansion, or bowing. In the early phase of the transient following the coolant break, the high axial loads, which could be generated by the difference in thermal expansion between fuel clad and thimbles, are relieved by slippage of the fuel rods through the grids. The relatively low drag force restraint on the fuel rods will induce only minor thermal bowing, which is insufficient to lose the gap between the fuel rod and thimble tube.

Reference 13 shows that the fuel assemblies will maintain a geometry that is capable of being cooled during a combined seismic and double-ended loss-of-coolant accident.

4.2.3.6 Reactivity Control Assembly and Burnable Poison Rods

a. Internal Pressure and Cladding Stresses During Normal, Transient and Accident Conditions

The designs of the burnable poison and source rods provide a sufficient void volume to accommodate the internal pressure increase during operation caused by release of helium generated by neutron absorption. This is not a concern for the Ag-In-Cd control rods, because no gas is generated in or released by the absorber material. For the burnable poison rod, the use of glass in tubular form provides a central void volume along the length of the rods.

The stress analysis of the burnable poison end source rods assumes 100 percent gas release to the rod void volume in addition to the initial pressure within the rod.

During normal transient and accident conditions the void volume limits the internal pressures to values which satisfy the criteria in Subsection 4.2.1.6.

These limits are established not only to assure that peak stresses do not reach unacceptable values, but also limit the amplitude of the oscillatory stress component in consideration of the fatigue characteristics of the materials.

Rod, guide thimble, and dashpot flow analyses indicate that the flow is sufficient to prevent coolant boiling. Therefore, clad temperatures at which the clad material has adequate strength to resist coolant operating pressures and rod internal pressures are maintained.

b. Thermal Stability of the Absorber Material, Including Phase Changes and Thermal Expansion

The radial and axial temperature profiles have been determined by considering gap conductance, thermal expansion, and neutron or gamma heating of the contained material as well as gamma heating of the clad.

The maximum temperature of the absorber material was calculated to be less than 1010°F for Ag-In-Cd and occurs axially at only the highest flux region. This temperature is well below the absorber melting temperature stated in Subsection 4.2.1.6. The thermal expansion properties of the absorber material and the phase changes are discussed in Reference 2.

The maximum temperature of the borosilicate glass was calculated to be about 1300°F and takes place following the initial rise to power.

As the operating cycle proceeds, the glass temperature decreases for the following reasons: (1) reduction in power generation due to boron 10 depletion, (2) better gap conductance as the helium produced diffuses to the gap, and (3) external gap reduction due to borosilicate glass swelling.

Sufficient diametral and end clearances have been provided in the neutron absorber, burnable poison, and source rods to accommodate the relative thermal expansions between the enclosed material and the surrounding clad and end plug.

c. Irradiation Stability of the Absorber Material, Taking into Consideration Gas Release and Swelling

The irradiation stability of the absorber material is discussed in Reference 2. Irradiation produces no deleterious effects in the absorber material.

Sufficient diametral and end clearances are provided to accommodate swelling of the absorber material.

Based on experience with borosilicate glass, and on nuclear and thermal calculations, gross swelling or cracking of the glass tubing is not expected during operation. Some minor creep of the glass at the hot spot on the inner surface of the tube could occur, but would continue only until the glass came in contact with the inner liner. The wall thickness of the inner liner is sized to provide adequate support in the event of slumping, and to collapse locally before rupture of the exterior cladding if unexpected large volume changes, due to swelling or cracking, should occur. The ends of the inner liner are open to allow helium, which diffuses out of the glass, to occupy the central void.

d. Potential for Chemical Interaction, Including Possible Waterlogging Rupture

The structural materials selected have good resistance to irradiation damage and are compatible with the reactor environment.

Corrosion of the materials exposed to the coolant is quite low, and proper control of chloride and oxygen in the coolant will prevent the occurrence of stress corrosion. The potential for the interference with rod cluster control movement due to possible corrosion phenomena is very low.

Waterlogging rupture is not a failure mechanism associated with Westinghouse-designed control rods. However, a breach of the cladding for any postulated reason does not result in serious consequences. The silver-indium-cadmium absorber material is relatively inert and would still remain remote from high coolant velocity regions. Rapid loss of material resulting in significant loss of reactivity control material would not occur. Bettis test results (Reference 8) concluded that additions of indium and cadmium to silver, in the amounts to form the Westinghouse absorber material composition, result in small corrosion rates.

4.2.4 Testing and Inspection Plan

4.2.4.1 Quality Assurance Program

The quality assurance program plan of the Westinghouse Nuclear Fuel Division is discussed in Section 17.1.

The program provides for control over all activities affecting product quality, commencing with design and development and continuing through procurement, materials handling, fabrication, testing and inspection, storage, and transportation. The program also provides for the indoctrination and training of personnel and for the auditing of activities affecting product quality through a formal auditing program.

Westinghouse drawings and product, process, and material specifications identify the inspection to be performed.

4.2.4.2 Quality Control

Quality control philosophy is generally based on the following inspections being performed to a 95 percent confidence that at least 95 percent of the product meets specification, unless otherwise noted.

a. Fuel System Components and Parts

The characteristics inspected depends upon the component parts and includes dimensional, visual, check audits of test reports, material certification and nondestructive examination such as X-ray and ultrasonic.

All material used in this core is accepted and released by Quality Control.

b. Pellets

Inspection is performed for dimensional characteristics such as diameter, density, length and squareness of ends. Additional visual inspections are performed for cracks, chips and surface conditions according to approved standards.

Density is determined in terms of weight per unit length. Chemical analyses are taken on a specified sample basis throughout pellet production.

c. Rod Inspection

Fuel rod, control rod, burnable poison and source rod inspection consists of the following nondestructive examination techniques and methods, as applicable.

1. Leak Testing

Each rod is tested using a calibrated mass spectrometer with helium as the detectable gas.

2. Closure Welds

Rod closure welds are inspected by ultrasonic test or X-ray in accordance with a qualified technique and Westinghouse specifications.

3. Dimensional

All rods are dimensionally inspected prior to final release. The requirements include such items as length, camber, and visual appearance.

4. Plenum Dimensions

All fuel rods are inspected by gamma scanning or other approved methods as discussed in Subsection 4.2.4.4 to ensure proper plenum dimensions.

5. Pellet-to-Pellet Gaps

All fuel rods are inspected by gamma scanning or other approved methods as discussed in Subsection 4.2.4.4 to ensure that no significant gaps exist between pellets.

6. Enrichment Control

   All fuel rods are gamma scanned to verify enrichment control prior to acceptance for assembly loading.

7. Traceability

   Traceability of rods and associated rod components is established by Quality Control.

d. Assemblies

Each fuel, control, burnable poison and source rod assembly is inspected for compliance with drawing and/or specification requirements. Other incore control component inspection and specification requirements are given in Subsection 4.2.4.3.

e. Other Inspections

The following inspections are performed as part of the routine inspection operation:

1. Tool and gage inspection and control including standardization to primary and/or secondary working standards. Tool inspection is performed at prescribed intervals on all serialized tools. Complete records are kept of calibration and conditions of tools.

2. Audits are performed of inspection activities and records to assure that prescribed methods are followed and that records are correct and properly maintained.

3. Surveillance inspection, where appropriate, and audits of outside contractors are performed to ensure conformance with specified requirements.

f. Process Control

To prevent the possibility of mixing enrichments during fuel manufacture and assembly, strict enrichment segregation and other process controls are exercised.

The UO2 powder is kept in sealed containers or is processed in a closed system. The containers are either fully identified both by descriptive tagging and preselected color coding or, for the closed system, the material is monitored by a computer data management information system. For the sealed container system, a Westinghouse identification tag completely describing the contents is affixed to the containers before transfer to powder storage. Isotopic content is confirmed by analysis.

Powder withdrawal from storage can only be made by an authorized group, which directs the powder to the correct pellet production line. All pellet production lines are physically separated from each other and pellets of only a single nominal enrichment and density are produced in a given production line at any given time.

Finished pellets are transferred to segregated storage racks within the confines of the pelleting area. Samples from each pellet lot are tested for physical and chemical properties including isotopic content and impurity levels prior to acceptance by Quality Control. Physical barriers prevent mixing of pellets of different nominal designs and enrichment in this storage area. Unused powder and substandard pellets are returned to storage for disposition.

Pellets are loaded into fuel cladding tubes on isolated production lines. Each production line contains only rods of one fuel type at any one time.

A unique code is placed on each fuel tube for traceability purposes. The end plugs are inserted and welded to seal the tube. The fuel tube remains identifiable by this code throughout the fabrication process.

At the time of installation into an assembly, a matrix is generated to identify each rod in its position within a given assembly. After the fuel rods are installed, an inspector verifies that all fuel rods in an assembly carry the correct identification character describing the fuel enrichment and density for the core region being fabricated. The top nozzle is inscribed with a permanent identification number providing traceability of the assembly and the fuel rods contained in the assembly.

Similar traceability is provided for burnable poison, source rods and control rodlets as required.

4.2.4.3 Core Component Testing and Inspection

Tests and inspections are performed on each reactivity control component to verify the mechanical characteristics. In the case of the Rod Cluster Control Assembly, prototype testing has been conducted and both manufacturing test/inspections and functional testing at the plant site are performed.

During the component manufacturing phase, the following requirements apply to the reactivity control components to assure the proper functioning during reactor operation:

a. All materials are procured to specifications to attain the desired standard of quality.

b. A spider from each braze lot is proof tested by applying a 5000 pound load to the spider body, so that approximately 310 pounds is applied to each vane. This proof load provides a bending moment at the spider body approximately equivalent to 1.4 times the load caused by the acceleration imposed by the control rod drive mechanism.

c. All rods are checked for integrity by methods described in Subsection 4.2.4.2, item c.

d. To assure proper fitup with the fuel assembly, the rod cluster control, burnable poison and source assemblies are installed in the fuel assembly without restriction or binding in the dry condition. Also a straightness of 0.01 in./ft is required on the entire inserted length of each rod assembly.

The Rod Cluster Control Assemblies are functionally tested following core loading but prior to criticality to demonstrate reliable operation of the assemblies. The testing performed during the initial plant startup is described in Chapter 14. Following each refueling, each assembly is fully withdrawn and dropped at full flow/operating temperature conditions specified by Technical Specifications.

In order to demonstrate continuous free movement of the Rod Cluster Control Assemblies, and to ensure acceptable core power distributions during operations, partial movement checks are performed on every Rod Cluster Control Assembly as required by the Technical Specifications.

If a Rod Cluster Control Assembly cannot be moved by its mechanism, adjustments in the boron concentration ensure that adequate shutdown margin would be achieved following a trip. Thus inability to move one Rod Cluster Control Assembly can be tolerated. More than one inoperable Rod Cluster Control Assembly could be tolerated, but would impose additional demands on the plant operator. Therefore, the number of inoperable Rod Cluster Control Assemblies has been limited to one.

4.2.4.4 Tests and Inspections by Others

If any tests and inspections are to be performed on behalf of Westinghouse, Westinghouse will review and approve the quality control procedures, inspection plans, etc., to be utilized to ensure that they are equivalent to the description provided in Subsections 4.2.4.1 and 4.2.4.3 and are performed properly to meet all Westinghouse requirements.

4.2.4.5 In-Service Surveillance

Westinghouse has extensive experience with the use of 17x17 standard fuel assemblies in other operating plants. This experience is summarized in WCAP-8183, Reference 1, which is periodically updated to provide the most recent information operating plants. Additional test assembly and test rod experience is given in Sections 8 and 23 of Reference 9.

4.2.4.6 Onsite Inspection

Detailed written procedures are used by the station staff and nuclear fuel quality assurance personnel for the receipt inspection of all new fuel and associated components such as control rods and plugs. The procedures are specific and are written to take into account the manufacturer's procedures and processes. The specific procedures incorporate the following minimum requirements:

a. Survey of the new fuel shipping containers for radiation and contamination levels

b. External inspection of shipping container for visible signs of damage, including integrity of seals

c. Check of condition of new fuel shipping container accelerometers

d. Inspection of physical condition of inside of shipping containers including hardware utilized to secure the component and protective covers if used

e. Verification of serial numbers if serial numbers are required

f. Visual inspection of component for dirt, debris, water, deep scars, abrasions and other irregularities or evidence of damage

g. Survey of radiation and contamination levels of new fuel assembly.

Surveillance of fuel and reactor performance is routinely conducted. Power distribution is monitored using excore fixed and incore detectors. Coolant activity and chemistry are followed to permit early detection of any fuel clad defects.

Visual irradiated fuel inspections will be conducted as necessary during each refueling. Selected fuel assemblies may be inspected for fuel rod failure, structural integrity, crud deposition, rod bow and other irregularities. Fuel assemblies will be selected for inspection based upon performance history and recommendations made by the fuel supplier.

The fuel inspection program will be expanded to include more fuel assemblies or greater detail of examination if high coolant activity is experienced during operation, irregularities are noted in fuel performance, irregularities are noted during routine inspections, or if a new fuel design is incorporated.

4.2.5 References

1. Slagle, W. H., "Operational Experience with Westinghouse Cores," WCAP-8183, (latest revision).

2. Beaumont, M. D., and Iorii, J .A., "Properties of Fuel and Core Component Materials," WCAP-9179, Revision 1 (Proprietary), July 1978.

3. Not used

4. Hellman, J. M. (Ed.), "Fuel Densification Experimental Results and Model for Reactor Application," WCAP-8218-P-A (Proprietary) and WCAP-8219-A (Nonproprietary), March 1975.

5. Not used

6. George, R. A., Lee, Y. C. and Eng. G. H., "Revised Clad Flattening Model," WCAP-8377 (Proprietary) and WCAP-8381 (Nonproprietary), July 1974.

7. Risher, D. H., et al., "Safety Analysis for the Revised Fuel Rod Internal Pressure Design Basis," WCAP-8963 (Proprietary), November 1976 and WCAP-8964 (Nonproprietary), August 1977.

8. Cohen, J., "Development and Properties of Silver Base Alloys as Control Rod Materials for Pressurized Water Reactors," WAPD-214, December 1959.

9. Eggleston, F. T., "Safety-Related Research and Development for Westinghouse Pressurized Water Reactors, Program Summaries-Winter 1977-Summer 1978," WCAP-8768, Revision 2, October 1978.

10. Demario, E. E., "Hydraulic Flow Test of the 17x17 Fuel Assembly," WCAP-8278 (Proprietary) and WCAP-8279 (Nonproprietary), February 1974.

11. Skaritka, J., et al., "Fuel Rod Bow Evaluation," WCAP-8691, Revision l (Proprietary) and WCAP-8692, Revision 1 (Nonproprietary), July 1979.

12. O'Donnell, W. J. and Langer, B. F., "Fatigue Design Basis for Zircaloy Components," Nuclear Science and Engineering 20 l-12, 1964.

13. Gesinski, L., and Chiang, D., "Safety Analysis of the 17x17 Fuel Assembly for Combined Seismic and Loss-of-Coolant Accident," WCAP-8236 (Proprietary) and WCAP-8288 (Nonproprietary) December 1973.

14. Davidson. S. L. (Ed.), et. al., "VANTAGE-5 Fuel Assembly, Reference Core Report," WCAP-10444-P-A, Westinghouse Electric Corporation, September 1985.

15. Davidson, S. L. (Ed.), et. al., "VANTAGE-5H Fuel Assembly," WCAP-10444-P-A Addendum 2-A, Westinghouse Electric Corporation, April 1988.

16. Davidson, S. L. and Ryan, T.L., "VANTAGE+ Fuel Assembly Reference Core Report," WCAP-12610-P-A and Appendices A through D, Westinghouse Electric Corporation, April 1995.

17. Weiner, R. A., et al., "Improved Fuel Performance Models for Westinghouse Fuel Rod Design and Safety Evaluations," WCAP-10851-P-A (Proprietary) and WCAP-11873-A (Non-Proprietary), August 1988.

18. Kersting, P. J., et al., "Assessment of Clad Flattening and Densification Power Spike Factor Elimination in Westinghouse Nuclear Fuel," WCAP-13589-A, March 1995.

19. Stephan, L. A., "The Effects of Cladding Material and Heat Treatment on the Response of Water Logged UO_2 Fuel Rods to Power Bursts," IN-ITR 1970.

20. Davidson, S. L., "Westinghouse Fuel Criteria Evaluation Process," WCAP-12488-A, October 1994.

21. "Addendum 1 to WCAP-12488-A, Revision To Design Criteria," WCAP-12488-A, Addendum 1-A, Revision 1, January 2002. (Westinghouse Proprietary)

22. Letter from N. J. Liparolu (Westinghouse) to R. S. Jones (NRC), "Westinghouse Interpretation of Staff's Position on Extended Burnup (Proprietary)," NTD-NRC-94-4275, August 29, 1994.

23. Slagle, W. G., (Ed.), "Westinghouse Improved Performance Analysis and Design Model (PAD 4.0)," WCAP-15063-P-A, Rev. 1 w/ errata July 2000.

4.3 NUCLEAR DESIGN

4.3.1 Design Bases

This section describes the design bases and functional requirements used in the nuclear design of the Fuel and Reactivity Control System, and relates these design bases to the General Design Criteria (GDC) in 10 CFR 50, Appendix A. Where appropriate, supplemental criteria such as 10 CFR 50.46, Acceptance Criteria for Emergency Core Cooling Systems for Light Water Nuclear Power Reactors are addressed. Before discussing the nuclear design bases, it is appropriate to briefly review the four major categories ascribed to conditions of plant operation.

The full spectrum of plant conditions is divided into four categories, in accordance with the anticipated frequency of occurrence and risk to the public (as defined in ANSI Standard N18.2):

1. Condition I - Normal Operation
2. Condition II - Incidents of Moderate Frequency
3. Condition III - Infrequent Faults
4. Condition IV - Limiting Faults

In general, the Condition I occurrences are accommodated with margin between any plant parameter and the value of that parameter which would require either automatic or manual protective action. Condition II incidents are accommodated with, at most, a shutdown of the reactor with the plant capable of returning to operation after corrective action. Fuel damage (fuel damage as used here is defined as penetration of the fission product barrier; i.e., the fuel rod clad) is not expected during Condition I and Condition II events. It is not possible, however, to preclude a very small number of rod failures. These are within the capability of the plant cleanup system and are consistent with the plant design basis.

Condition III incidents shall not cause more than a small fraction of the fuel elements in the reactor to be damaged, although sufficient fuel element damage might occur to preclude immediate resumption of operation. The release of radioactive material due to Condition III incidents should not be sufficient to interrupt or restrict public use of these areas beyond the exclusion radius. Furthermore, a Condition III incident shall not, by itself generate a Condition IV fault or result in a consequential loss of function of the reactor coolant or reactor containment barriers.

Condition IV occurrences are faults that are not expected to occur, but are defined as limiting faults which must be designed against. Condition IV faults shall not cause a release of radioactive material that results in an undue risk to public health and safety.

The core design power distribution limits related to fuel integrity are met for Condition I occurrences through conservative design, and maintained by the action of the control system. The requirements for Condition II occurrences are met by providing an adequate protection system which monitors reactor parameters. The control and protection systems are described in Chapter 7, and the consequences of Condition II, III and IV occurrences are given in Chapter 15.

4.3.1.1 Fuel Burnup

a. Basis

The fuel rod design basis is described in Section 4.2. The nuclear design basis is to install sufficient reactivity in the fuel to attain a region average discharge burnup of between 45,000 and 50,000 MWd/Mtu. The above, along with the design basis in Subsection 4.3.1.3, satisfies GDC-10.

b. Discussion

Fuel burnup is a measure of fuel depletion, which represents the integrated energy output of the fuel (MWd/Mtu), and is a convenient means for quantifying fuel exposure criteria.

The core design lifetime or design discharge burnup is achieved by installing sufficient initial excess reactivity in each fuel region and by following a fuel replacement program (such as that described in Subsection 4.3.2) that meets all safety-related criteria in each cycle of operation.

Initial excess reactivity installed in the fuel, although not a design basis, must be sufficient to maintain core criticality at full power operating conditions throughout cycle life with equilibrium xenon, samarium, and other fission products present. The end of design cycle life is defined to occur when the chemical shim concentration is essentially zero with control rods present to the degree necessary for operational requirements (e.g., the controlling bank at the "bite" position). In terms of chemical shim boron concentration this represents approximately 10 parts per million (ppm) with no control rod insertion.

A limitation on initial installed excess reactivity is not required other than as is quantified in terms of other design bases such as core reactivity feedback and shutdown margin discussed below.

4.3.1.2 Reactivity Feedbacks (Reactivity Coefficient)

a. Basis

The fuel temperature coefficient will be negative and the moderator temperature coefficient of reactivity will be nonpositive for power operating conditions, above 20% power, thereby providing negative reactivity feedback characteristics. The design basis conservatively includes analysis for positive moderator temperature coefficients; however, actual core loading designs meet the above restrictions and thus GDC 11.

b. Discussion

When compensation for a rapid increase in reactivity is considered, there are two major effects. These are the resonance absorption effects (Doppler) associated with changing fuel temperature, and the spectrum effect resulting from changing moderator density. These basic physics characteristics are often identified by reactivity coefficients. The use of slightly enriched uranium ensures that the Doppler coefficient of reactivity is negative. This coefficient provides the most rapid reactivity compensation. The core is also designed to have an overall negative moderator temperature coefficient of reactivity so that average coolant temperature or void content provides another, slower compensatory effect. Nominal power operation is permitted only in a range of overall negative moderator temperature coefficient. The negative moderator temperature coefficient can be achieved through use of fixed burnable poison and/or control rods by limiting the reactivity held down by soluble boron.

Burnable poison content (quantity and distribution) is not stated as a design basis other than as it relates to accomplishment of a nonpositive moderator temperature coefficient at power operating conditions discussed above.

4.3.1.3 Control of Power Distribution

a. Basis

The nuclear design basis is that, with at least a 95 percent confidence level:

1. The fuel will not be operated at greater than 14.6 kW/ft* under normal operating conditions.

2. Under abnormal conditions including the maximum overpower condition, the fuel peak power will not cause melting as defined in Subsection 4.4.1.2.

3. The fuel will not operate with a power distribution that violates the Departure from Nucleate Boiling (DNB) design basis (i.e., the DNBR shall not be less than the safety analysis limit value, as discussed in Subsection 4.4.1.1) under Condition I and II events including the maximum overpower condition.

4. Fuel management will be such to produce rod powers and burnups consistent with the assumptions in the fuel rod mechanical integrity analysis of Section 4.2.

The above basis meets GDC-10.

b. Discussion

Calculation of extreme power shapes which affect fuel design limits is performed with proven methods and verified frequently with measurements from operating reactors. The conditions under which limiting power shapes are assumed to occur are chosen conservatively with regard to any permissible operating state.

---

* Due to LOCA analysis.
Average kW/ft (5.84), (assuming maximum reactor rated thermal power of ≤ 3659 MWt) x F_Q (2.50) = 14.6 kW/ft

Even though there is good agreement between peak power calculations and measurements, a nuclear uncertainly margin (see Subsection 4.3.2.2g) is applied to calculated peak local power. Such a margin is provided both for the analysis for normal operating states and for anticipated transients.

4.3.1.4 Maximum Controlled Reactivity Insertion Rate

a. Basis

The maximum reactivity insertion rate due to withdrawal of Rod Cluster Control Assemblies at power or by boron dilution is limited. During normal at power operation with normal control rod overlap, the maximum controlled reactivity rate change is limited to less than 110 pcm/sec. (1 pcm = 10^{-5} $\Delta\rho$, see footnote to Table 4.3-2.) At zero power conditions, a maximum reactivity change rate of 75 pcm/sec for accidental simultaneous withdrawal of two control banks is set so that peak heat generation rate and DNBR do not exceed the maximum allowable at overpower conditions. This satisfies GDC-25.

The maximum reactivity worth of control rods and the maximum rates of reactivity insertion employing control rods are limited to preclude rupture of the coolant pressure boundary or disruption of the core internals to a degree which would impair core cooling capacity due to a rod withdrawal or ejection accident (see Chapter 15).

Following any Condition IV event (rod ejection, steam line break, etc.), the reactor can be brought to the shutdown condition and the core will maintain acceptable heat transfer geometry. This satisfies GDC-28.

b. Discussion

Reactivity addition associated with an accidental withdrawal of a control bank (or banks) is limited by the maximum rod speed (or travel rate) and by the worth of the bank(s). The maximum control rod speed is 45 inches per minute and the maximum rate of reactivity change considering two control banks moving is less than 75 pcm/sec. During normal operation at power and with normal control rod overlap, the maximum reactivity change rate is limited to less than 110 pcm/sec.

The reactivity change rates are conservatively calculated assuming unfavorable axial power and xenon distributions. The peak xenon burnout rate is 25 pcm/min, significantly lower than the maximum reactivity addition rate of 110 pcm/sec for normal operation and 75 pcm/sec for accidental withdrawal of two banks.

4.3.1.5 Shutdown Margins

a. Basis

Minimum shutdown margin as specified in Technical Specifications and the Core Operating Limits Report is required at any power operating condition, in the hot standby shutdown condition and in the cold shutdown condition.

In all analyses involving reactor trip, the single, highest worth Rod Cluster Control Assembly is postulated to remain untripped in its full out position (stuck rod criterion). This satisfies GDC-26.

b. Discussion

Two independent reactivity control systems are provided, namely control rods and soluble boron in the coolant. The Control Rod System can compensate for the reactivity effects of the fuel and water temperature changes accompanying power level changes over the range from full-load to no-load. In addition, the Control Rod System provides the minimum shutdown margin under Condition I events and is capable of making the core subcritical rapidly enough to prevent exceeding acceptable fuel damage limits assuming that the highest worth control rod is stuck out upon trip.

The boron system can compensate for all xenon burnout reactivity changes and will maintain the reactor in the cold shutdown condition. Thus, backup and emergency shutdown provisions are provided by a mechanical and a chemical shim control system, which satisfies GDC-26.

c. Basis

When fuel assemblies are in the pressure vessel and the vessel head is not in place, k_{eff} will be maintained at or below 0.95 with control rods and soluble boron. Further, the fuel will be maintained sufficiently subcritical that removal of all Rod Cluster Control Assemblies will not result in criticality.

d. Discussion

ANSI Standard N18.2 specifies a k_{eff} not to exceed 0.95 in spent fuel storage racks and transfer equipment flooded with pure water and a k_{eff} not to exceed 0.98 in normally dry new fuel storage racks assuming optimum moderation. No criterion is given for the refueling operation; however, a 5 percent margin, which is consistent with spent fuel storage and transfer, is adequate for the controlled and continuously monitored operations involved.

The boron concentration required to meet the refueling shutdown criteria is specified in the Technical Specifications. Verification that this shutdown criteria is met, including uncertainties, is achieved using qualified nuclear design methods such as the CASMO Code (Reference 1) and SIMULATE Code (Reference 2), per the Phoenix-P/ANC Code System (Reference 11). The subcriticality of the core is continuously monitored as described in the Technical Specifications.

4.3.1.6 Stability

a. Basis

The core will be inherently stable to power oscillations at the fundamental mode. This satisfies GDC-12. Spatial power oscillations within the core with a constant core power output, should they occur, can be reliably and readily detected and suppressed.

b. Discussion

Oscillations of the total power output of the core, from whatever cause, are readily detected by the loop temperature sensors and by the nuclear instrumentation. The core is protected by these systems and a reactor trip would occur if power increased unacceptably, preserving the design margins to fuel design limits. The stability of the Turbine/Steam Generator/Core Systems and the Reactor Control System is such that total core power oscillations are not normally possible. The redundancy of the protection circuits ensures an extremely low probability of exceeding design power levels.

The core is designed so that diametral and azimuthal oscillations due to spatial xenon effects are self-damping and no operator action or control action is required to suppress them. The stability to diametral oscillations is so great that this excitation is highly improbable. Convergent azimuthal oscillations can be excited by prohibited motion of individual control rods. Such oscillations are readily observable and alarmed using the excore long ion chambers. Indications are also continuously available from incore thermocouples and loop temperature measurements. Moveable and fixed incore detectors can be activated to provide more detailed information.

In all presently proposed cores, these horizontal plane oscillations are self-damping by virtue of reactivity feedback effects designed into the core.

However, axial xenon spatial power oscillations may occur late in core life. The control banks and excore detectors are provided for control and monitoring of axial power distributions. Assurance that fuel design limits are not exceeded is provided by reactor Overpower ΔT and Overtemperature ΔT trip functions which use the measured axial power imbalance as input.

4.3.1.7 Anticipated Transients without Trip

The effects of anticipated transients with failure to trip are not considered in the design bases for transients analyzed in Chapter 15. Analysis has shown that the likelihood of such a hypothetical event is negligibly small. Furthermore, analysis of the consequences of a hypothetical failure to trip following anticipated transients has shown that no significant core damage would result, system peak pressures would be limited to acceptable values and no failure of the Reactor Coolant System would result (see Reference 3). The final NRC ATWTS Rule (Reference 4) requires that Westinghouse-designed plants install ATWTS mitigation systems to initiate a turbine trip and actuate emergency feedwater flow independent of the Reactor Protection System. The Seabrook ATWTS mitigation system is described in Subsection 7.6.12.

4.3.2 Description

4.3.2.1 Nuclear Design Description

The reactor core consists of a specified number of fuel rods which are held in bundles by spacer grids and top and bottom fittings. The fuel rods are constructed of zirconium alloy cylindrical tubes containing UO_2 fuel pellets. The bundles, known as fuel assemblies, are arranged in a pattern which approximates a right circular cylinder.

Each fuel assembly contains a 17x17 rod array composed of 264 fuel rods, 24 rod cluster control thimbles and an incore instrumentation thimble. Figure 4.2-1 shows a cross-sectional view of a 17x17 fuel assembly and the related rod cluster control locations. Further details of the fuel assembly are given in Section 4.2.

The fuel rods within a given assembly have the same uranium enrichment in both the radial and axial planes. Fresh fuel assemblies of different enrichments are used in the reload core to establish a favorable radial power distribution. Figure 4.3-1 shows a sample fuel loading pattern to be used in the reload cores. The premise for reload designs is for low radial leakage, achieved by placing low reactivity assemblies around the perimeter of the core. Fresh assemblies are then distributed within the core interior to generate a favorable radial power distribution. The enrichments for these cores vary with the expected cycle length; typical values are shown in Table 4.3-1. Axial fuel blankets composed by mid-enriched annular fuel pellets may be used to reduce axial neutron leakage and improve fuel utilization.

The reference reloading pattern is typically similar to Figure 4.3-1, with depleted fuel on the periphery and fresh fuel interspersed in the center with depleted fuel. The core will operate between eighteen and twenty-four months between refueling, accumulating between 16,000 MWd/Mtu and 24,000 MWd/Mtu per cycle. The exact reloading pattern, initial and final positions of assemblies, number of fresh assemblies and their placement are dependent on the energy requirement for the next cycle, and burnup and power histories of the previous cycles.

The core average enrichment is determined by the amount of fissile material required to provide the desired core lifetime and energy requirements, namely a region average discharge burnup of between 45,000 and 50,000 MWd/Mtu. The physics of the burnout process is such that operation of the reactor depletes the amount of fuel available due to absorption of neutrons by the U-235 atoms and their subsequent fission. The rate of U-235 depletion is directly proportional to the power level at which the reactor is operated. In addition, the fission process results in the formation of fission products, some of which readily absorb neutrons. These effects, depletion and the buildup of fission products, are partially offset by the buildup of plutonium shown in Figure 4.3-2 for the 17x17 fuel assembly, which occurs due to the nonfission absorption of neutrons in U-238. Therefore, at the beginning of any cycle a reactivity reserve equal to the depletion of the fissionable fuel and the buildup of fission product poisons over the specified cycle life must be "built" into the reactor. This excess reactivity is controlled by removable neutron absorbing material in the form of boron dissolved in the primary coolant and burnable poison rods.

The concentration of boric acid in the primary coolant is varied to provide control and to compensate for long-term reactivity requirements. The concentration of the soluble neutron absorber is varied to compensate for reactivity changes due to fuel burnup, fission product poisoning including xenon and samarium, burnable poison depletion, and the cold-to-operating moderator temperature change. Using its normal makeup path, the Chemical and Volume Control System (CVCS) is capable of inserting negative reactivity at a rate of approximately 30 pcm/min when the reactor coolant boron concentration is 1000 ppm and approximately 35 pcm/min when the reactor coolant boron concentration is 100 ppm. If the emergency boration path is used, the CVCS is capable of inserting negative reactivity at a rate of approximately 65 pcm/min when the reactor coolant concentration is 1000 ppm and approximately 75 pcm/min when the reactor coolant boron concentration is 100 ppm. The peak burnout rate for xenon is 25 pcm/min (Subsection 9.3.4 discusses the capability of the CVCS to counteract xenon decay). Rapid transient reactivity requirements and safety shutdown requirements are met with control rods.

As the boron concentration is increased, the moderator temperature coefficient becomes less negative. The use of a soluble poison alone would result in a positive moderator coefficient at beginning-of-life for the cycle. Therefore, burnable absorber fuel rods are used to reduce the soluble boron concentration sufficiently to ensure that the moderator temperature coefficient is negative for power operating conditions above 20% power*. During operation the poison content in these rods is depleted thus adding positive reactivity to offset some of the negative reactivity from fuel depletion and fission product buildup. The depletion rate of the burnable absorber fuel rods is not critical since chemical shim is always available and flexible enough to cover any possible deviations in the expected burnable absorber depletion rate. Figure 4.3-3 is a graph of a typical core depletion.

In addition to reactivity control, the burnable absorber fuel rods are strategically located to provide a favorable radial power distribution. Figure 4.3-4 shows the integral burnable absorber fuel rod distribution within a fuel assembly for the several fuel rod patterns used in a 17x17 array. A typical integral burnable absorber fuel rod loading pattern is shown in Figure 4.3-5.

Control rods are located for use in the core to provide control for rapid changes in reactivity. The reactivity worth of the control rods is dependent on the particular absorber material used, but the power distribution effects and reactivity worth depend primarily on the number and location of the inserted control rods.

---

* Note: A non-negative moderator temperature coefficient is allowed by Technical Specifications for all power levels, provided that compliance with the ATWS Rule and its basis are maintained, as described in the Bases for Technical Specification 3/4.1.1.3. The Seabrook core design philosophy meets this requirement by ensuring that a non-positive MTC exists for operating conditions above 20% power.

Table 4.3-1, Table 4.3-2 and Table 4.3-3 contain a summary of the reactor core design parameters for a typical reload fuel cycle, including reactivity coefficients, delayed neutron fraction and neutron lifetimes. Sufficient information is included to permit an independent calculation of the nuclear performance characteristics of the core.

4.3.2.2 Power Distributions

The accuracy of power distribution calculations has been confirmed through analytic benchmarks and experience of operation under conditions very similar to those expected. Details of this confirmation are given in Reference 2 and in Subsection 4.3.2.2f.

a. Definitions

Power distributions are quantified in terms of hot channel factors. These factors are a measure of the peak pellet power within the reactor core and the total energy produced in a coolant channel and are expressed in terms of quantities related to the nuclear or thermal design, namely:

1. Power density, is the thermal power produced per unit volume of the core (kW/liter).

2. Linear power density, is the thermal power produced per unit length of active fuel (kW/ft). Since fuel assembly geometry is standardized, this is the unit of power density most commonly used. For all practical purposes, it differs from kW/liter by a constant factor which includes geometry and the fraction of the total thermal power which is generated in the fuel rod.

3. Average linear power density, is the total thermal power produced in the fuel rods divided by the total active fuel length of all rods in the core.

4. Local heat flux, is the heat flux at the surface of the cladding (Btu/ft^2-hr). For nominal rod parameters, this differs from linear power density by a constant factor.

5. Rod power or rod integral power, is the length integrated linear power density in one rod (kW).

6. Average rod power, is the total thermal power produced in the fuel rods divided by the number of fuel rods (assuming all rods have equal length).

7. The hot channel factors used in the discussion of power distribution in this section are defined as follows:

   (a) F_Q, heat flux hot channel factor is defined as the maximum local heat flux on the surface of a fuel rod divided by the average fuel rod heat flux, allowing for manufacturing tolerances on fuel pellets and rods.

   (b) F^N_Q, nuclear heat flux hot channel factor, is defined as the maximum local fuel rod linear power density divided by the average fuel rod linear power density, assuming nominal fuel pellet and rod parameters.

   (c) F^E_Q, engineering heat flux hot channel factor is the allowance on heat flux required for manufacturing tolerances. The engineering factor allows for local variations in enrichment, pellet density and diameter, surface area of the fuel rod and eccentricity of the gap between pellet and clad. Combined statistically, the net effect is a factor of 1.03 to be applied to fuel rod surface heat flux.

   (d) $F_{\Delta H}{}^N$ nuclear enthalpy rise hot channel factor is defined as the ratio of the integral of linear power along the rod with the highest integrated power to the average rod power.

Manufacturing tolerances, hot channel power distribution and surrounding channel power distributions are treated in the calculation of the DNBR as described in Section 4.4.

It is convenient for the purposes of discussion to define subfactors of F_Q; however, design limits are set in terms of the total peaking factor.

F_Q = Total peaking factor or heat flux hot-channel factor

$$= \frac{\text{Maximum kW/ft}}{\text{Average kW/ft}}$$

Without densification effects,

$$F_Q = F^N_Q \times F^E_Q \times F^N_U$$

where

F^N_Q and F^E_Q are defined above.

F^N_U = uncertainty associated with the incore detector system, given in the COLR.

To include the allowances made for densification effect, which are height dependent, the following quantities are defined.

S(Z) = the allowance made for densification effects at height Z in the core. See Subsection 4.3.2.2e.

Then

F_Q = Total peaking factor

$$= \frac{\text{Maximum kW/ft}}{\text{Average kW/ft}}$$

Including densification allowance

$$F_Q = \max (S(Z) \times F^N_Q \times F^E_Q \times F^N_U$$

b. Radial Power Distributions

While radial power distributions in various axial planes of the core contribute to the axial F_Q, the core radial enthalpy rise distribution as determined by the integral of power up each channel is of greater interest. The power shape is axially integrated to yield a two dimensional representation of assembly and pin powers ($F_{\Delta H}^N$). Figure 4.3-6, Figure 4.3-7, Figure 4.3-8, Figure 4.3-9, Figure 4.3-10 and Figure 4.3-11 show typical representative operating conditions. These conditions are: (1) hot full power (HFP) near beginning-of-life (BOL) - unrodded - no xenon, (2) HFP near BOL - unrodded - equilibrium xenon, (3) HFP near BOL - bank D in - equilibrium xenon (4) HFP near middle-of-life (MOL) - unrodded - equilibrium xenon, (5) HFP near end-of-life (EOL) - unrodded - equilibrium xenon, and (6) HFP near EOL - bank D in - equilibrium xenon.

c. Assembly Power Distributions

For the purpose of illustration, assembly power distributions from the BOL and EOL conditions corresponding to Figure 4.3-7 and Figure 4.3-10, respectively, are given for the same assembly in Figure 4.3-12 and Figure 4.3-13, respectively.

d. Axial Power Distributions

The shape of the power profile in the axial, or vertical, direction is largely under the control of the operator either through the manual operation of the full length control rods or automatic motion of full length rods responding to manual operation of the CVCS. Nuclear effects which cause variations in the axial power shape include moderator density, Doppler effect on resonance absorption, spatial xenon and burnup.

Automatically controlled variations in total power output and full length rod motion are also important in determining the axial power shape at any time. Signals are available to the operator from the excore ion chambers, which are long ion chambers outside the reactor vessel running parallel to the axis of the core. Separate signals are taken from the top and bottom halves of the chambers. The difference between top and bottom signals from each of four pairs of detectors is displayed on the control panel and called the flux difference, ΔI. Calculations of core average peaking factor for many plants and measurements from operating plants under many operating situations are associated with either ΔI or axial offset in such a way that an upper bound can be placed on the peaking factor. For these correlations, axial offset is defined as:

$$\text{axial offset} = \frac{\varphi_t - \varphi_b}{\varphi_t + \varphi_b}$$

where φ_t and φ_b are the top and bottom detector readings, respectively.

Representative axial power shapes for typical BOL and EOL unrodded conditions are shown in Figure 4.3-14 and Figure 4.3-15. Comparative partially rodded axial power shapes are shown in Figure 4.3-16. These figures cover a wide range of axial offset including values not permitted at full power.

The radial power distributions shown in Figure 4.3-8 and Figure 4.3-11 involving the partial insertion of control rods represent a synthesis of power shapes from the rodded and unrodded planes. The applicability of the separability assumption upon which this procedure is based is assured through extensive three-dimensional calculations of possible rodded conditions. As an example, Figure 4.3-17 compares the axial power distribution for several assemblies at different distances from inserted control rods with the core average distribution.

The only significant difference from the average occurs in the low power peripheral assemblies, thus confirming the validity of the separability assumption.

e. Local Power Peaking

Fuel densification, which has been observed to occur under irradiation in several operating reactors, causes the fuel pellets to shrink both axially and radially. The pellet shrinkage combined with random hang-up of fuel pellets results in gaps in the fuel column when the pellets below the hung-up pellet settle in the fuel rod. The gaps vary in length and location in the fuel rod. Because of decreased neutron absorption in the vicinity of the gap, power peaking occurs in the adjacent fuel rods resulting in an increased power peaking factor. A quantitative measure of this local peaking is given by the power spike factor S(Z), where Z is the axial location in the core.

Results reported in Reference 5 show that fuel manufactured by Westinghouse will not densify to the point that significant axial gaps will occur in the fuel stack, and that no power spike penalty should be included in the safety analysis.

f. Limiting Power Distributions

According to the ANSI classification of plant conditions (see Chapter 15), Condition I occurrences are those which are expected frequently or regularly in the course of power operation, maintenance, or maneuvering of the plant. As such, Condition I occurrences are accommodated with margin between any plant parameter and the value of that parameter which would require either automatic or manual protective action. Inasmuch as Condition I occurrences occur frequently or regularly, they must be considered from the point of view of affecting the consequences of fault conditions (Conditions II, III, and IV). In this regard, analysis of each fault condition described is generally based on a conservative set of initial conditions corresponding to the most adverse set of conditions which can occur during Condition I operation.

The list of steady state and shutdown conditions, permissible deviations, and operational transients is given in Chapter 15. Implicit in the definition of normal operation is proper and timely action by the reactor operator. That is, the operator follows recommended operating procedures for maintaining appropriate power distributions and takes any necessary remedial actions when alerted to do so by the plant instrumentation. Thus, as stated above, the worst or limiting power distribution which can occur during normal operation is to be considered as the starting point for analysis of ANSI Condition II, III and IV events.

Improper procedural actions or errors by the operator are assumed in the design as occurrences of moderate frequency (ANSI Condition II). Some of the consequences which might result are listed in Chapter 15. Therefore, the limiting power shapes which result from such Condition II events are those power shapes which deviate from the normal operating condition at the recommended axial offset band; e.g., due to lack of proper action by the operator during a xenon transient following a change in power level brought about by control rod motion. Power shapes which fall in this category are used for determination of the reactor protection system setpoints so as to maintain margin to overpower or DNB limits.

The means for maintaining power distributions within the required hot channel factor limits are described in the Surveillance and Action requirements of Technical Specifications.

The calculations used to establish the limits on core power distribution are described in Reference 15. All of the nuclear effects which influence the radial and/or axial power distributions throughout core life for various modes of operation, including load follow, reduced power operation, and axial xenon transients are considered.

Power distributions are calculated for the full power condition and reduced power operation with fuel and moderator temperature feedback effects included. The steady state nuclear design calculations are done for normal flow with the same mass flow in each channel. Flow redistribution is calculated explicitly where it is important in the DNB analysis of accidents. The effect of xenon on radial power distribution is small (compare Figure 4.3-6 and Figure 4.3-7) but is included as part of the normal design process.

The core average axial profile can experience significant changes which can occur rapidly as a result of rod motion and load changes and more slowly due to xenon distribution. For the study of points of closest approach to axial power distribution limits, several thousand cases are examined. Since the properties of the nuclear design dictate what axial shapes can occur, boundaries on the limits of interest can be set in terms of the parameters which are readily observed on the plant. Specifically, the nuclear design parameters which are significant to the axial power distribution analysis are:

1. Core power level

2. Core height

3. Coolant temperature and flow

4. Coolant temperature program as a function of reactor power

5. Fuel cycle lifetimes

6. Rod bank worths

7. Rod bank overlaps

Normal operation of the plant assumes compliance with the following conditions:

1. Control rods in a single bank move together with no individual rod insertion differing by more than 12 steps (indicated) from the bank demand position;

2. Control banks are sequenced with overlapping banks;

3. The control bank insertion limits are not violated; and

4. Axial power distribution procedures, which are given in terms of flux difference control and control bank position, are observed.

The axial power distribution procedures referred to above are part of the required operating procedures which are followed in normal operation. Briefly, they require control of the axial offset (flux difference divided by fractional power) at all power levels within a permissible operating band.

Calculations are performed for normal operation of the reactor, including axial xenon transients. Beginning, middle and end-of-cycle conditions are included in the calculations. These cases represent many possible reactor states in the life of one fuel cycle, and they have been chosen as sufficiently definitive of the cycle. It is not possible to single out any transient or steady-state condition which defines the most limiting case. The process of generating a myriad of power distributions is essential to the philosophy that leads to the required level of confidence for the level of protection provided by the core thermal limit protection function setpoints and core power distribution limits.

The calculated power distributions are the result of power level and control rod configurations run with reconstructed axial xenon distributions. The specific xenon distributions are preconditioned by the presence of control rods and then allowed to redistribute for several hours. A detailed discussion of the method used to generate allowable xenon conditions may be found in Reference 15.

The envelope drawn over the calculated max (F_Q x Power) points in Figure 4.3-21 represents an upper bound envelope on local power density versus elevation in the core. The calculated values have been increased by the nuclear uncertainty factor F^N_U for conservatism and a factor of 1.03 for the engineering factor F^E_Q. It should be emphasized that this envelope is a conservative representation of the bounding values of local power density. Expected values are considerably smaller.

Allowing for fuel densification effects, the average linear power at a maximum analyzed power level of 3659 MWt is 5.84 kW/ft. From Figure 4.3-21, the conservative upper bound value of normalized local power density, including uncertainly allowances, is 2.50 corresponding to a peak linear power of 14.6 kW/ft at full power.

The confirmation of protection system setpoints with respect to power distributions is described in Reference 15. In evaluating the required setpoints the core is assumed to be operating within the four constraints described above.

The required Overpower ΔT and Overtemperature ΔT reactor trip setpoints as a function of power and flux difference are cycle dependent. Setpoints for a typical reload core are shown in Figure 4.3-22 and Figure 4.3-23. The peak power density which can occur in the core assuming reactor trip at the Overpower ΔT reactor trip setpoint is less than that required for center-line melt including uncertainties. Similarly, assuming the reactor is tripped at the Overtemperature ΔT setpoint, the minimum DNBR during events for which the Overtemperature ΔT provides protection will be greater than the safety analysis limit value.

It should be noted that a reactor overpower accident is not assumed to occur coincident with an independent operator error. Additional detailed discussion of these analyses is presented in Reference 15.

F_Q can be increased with decreasing power as shown in the Technical Specifications. Increasing $F_{\Delta H}$ with decreasing power is also permitted. The allowance for increased $F_{\Delta H}$ permitted is cycle-dependent and shown in the Core Operating Limits Report. The allowed increase for a typical reload core is shown in Figure 4.3-26.

Typical radial factors and radial power distributions are shown in Figure 4.3-6, Figure 4.3-7, Figure 4.3-8, Figure 4.3-9, Figure 4.3-10 and Figure 4.3-11. The worst values generally occur when the rods are assumed to be at their insertion limits.

When a situation is possible in normal operation which could result in local power densities in excess of those assumed as the precondition for a subsequent hypothetical accident, but which would not itself cause fuel failure, administrative controls and alarms are provided for returning the core to a safe condition. These alarms are described in detail in Chapters 7 and 16.

g. Experimental Verification of Power Distribution Analysis

This subject is discussed in depth in Reference 2. A summary of this report is given below. It should be noted that power distribution-related measurements are incorporated into the evaluation of calculated power distribution information using the FINC code described in Reference 8. The measured versus calculational comparison is normally performed periodically throughout the cycle lifetime of the reactor as required by Technical Specifications.

In a measurement of the heat flux hot channel factor, F_Q, with the incore detector system described in Subsections 7.7.1 and 4.4.6, the following uncertainties have to be considered:

1. Reproducibility of the measured signal

2. Errors in the physics analytical methods employed in inferring the power distribution.

3. Errors in the calculated relationship between detector flux and peak rod power some distance from the measurement thimble.

4. Errors in constructing an axial power profile from five fixed points.

The appropriate allowance for category 1 above has been quantified by repetitive measurements made with the Incore Detector System. This system stores data every minute, thus the reproducibility of the detector's signal can be determined by monitoring the signals over time with the core in steady state. Local power distribution predictions are verified in critical experiments on arrays of rods with simulated guide thimbles, control rods, burnable poisons, etc. These critical experiments provide quantification of errors of types 2 and 3 above. Errors in category 3 above are quantified to the extent possible, by using the comparisons of data measured and predicted over 22 full core measurements. Axial power construction was verified by direct measurements of the incore axial neutron flux profile to the predictions of the analytical prediction of that profile. As well as comparisons of axial offset determined from both the fixed incore detector system and other means.

Reference 8 describes the foundations and results of the uncertainty analysis, along with comparisons to data collected with the movable detector system. The report concludes that the uncertainty associated with F_Q (heat flux) is 5.21 percent at the 95 percent confidence level with only 5 percent of the measurements greater than the inferred value. This is the equivalent of a 1.645σ limit on a normal distribution and is the uncertainty to be associated with a full core flux map with fixed detectors reduced with a reasonable set of input data incorporating the influence of burnup on the radial power distribution.

In comparing measured power distributions (or detector currents) against the calculations for the same situation, it is not possible to subtract out the detector reproducibility. Thus a comparison between measured and predicted power distributions has to include some measurement error. Such a comparison is given in Figure 4.3-24 for one of the maps used in Reference 8. The report results confirm the adequacy of the 5.21 percent uncertainty allowance on the calculated F_Q.

A similar analysis for the uncertainty in $F^N_{\Delta H}$ (rod integral power) measurements results in an allowance of 4.12 percent at the equivalent of a 1.645σ confidence level. For historical reasons, an 8 percent uncertainty factor is allowed in the nuclear design calculational basis; that is, the predicted rod integrals at full power must not exceed the design $F^N_{\Delta H}$ less 8 percent.

The accumulated data on power distributions in actual operation is basically of three types:

1. Much of the data is obtained in steady state operation at constant power in the normal operating configuration;

2. Data with unusual values of axial offset are obtained as part of the excore detector calibration exercise which is performed quarterly;

3. Special tests have been performed in load-follow and other transient xenon conditions which have yielded useful information on power distributions.

These data are presented in detail in Reference 2.

h. Testing

A very extensive series of physics tests is performed on the first cores. These tests and the criteria for satisfactory results are described in detail in Chapter 14. Since not all limiting situations can be created at BOL, the main purpose of the tests is to provide a check on the calculational methods used in the predictions for the conditions of the tests. Tests performed at the beginning of each reload cycle are limited to verification of steady state power distributions, on the assumption that the reload fuel is supplied by the first core designer.

i. Monitoring Instrumentation

The adequacy of instrument numbers, spatial deployment, required correlations between readings and peaking factors, calibration and errors are described in Reference 8. The relevant conclusions are summarized here in Subsections 4.3.2.2g and 4.4.6.1.

Provided the limitations given in Subsection 4.3.2.2f on rod insertion and flux difference are observed, the Excore Detector System provides adequate online monitoring of power distributions. Further details of specific limits on the observed rod positions and power distributions are given in the Technical Specifications together with a discussion of their bases.

Limits for alarms, reactor trip, etc., are given in the Technical Specifications. Descriptions of the systems provided are given in Section 7.7.

4.3.2.3 Reactivity Coefficients

The kinetic characteristics of the reactor core determine the response of the core to changing plant conditions or to operator adjustments made during normal operation, as well as the core response during abnormal or accidental transients. These kinetic characteristics are quantified in reactivity coefficients. The reactivity coefficients reflect the changes in the neutron multiplication due to varying plant conditions such as power, moderator or fuel temperatures, or less significantly due to a change in pressure or void conditions. Since reactivity coefficients change during the life of the core, ranges of coefficients are employed in transient analysis to determine the response of the plant throughout life. The results of such simulations and the reactivity coefficients used are presented in Chapter 15. The reactivity coefficients are calculated on a corewise basis by advanced nodal analysis methods. The effects of radial and axial power distribution on core average reactivity coefficients is implicit in those calculations and is not significant under normal operating conditions. For example, a skewed xenon distribution which results in changing axial offset by 5 percent changes the moderator and Doppler temperature coefficients by less than 0.01 pcm/°F and 0.03 pcm/°F, respectively. An artificially skewed xenon distribution which results in changing the radial $F^{N}_{\Delta H}$ by 3 percent changes the moderator and Doppler temperature coefficients by less than 0.03 pcm/°F and 0.001 pcm/°F, respectively. The spatial effects are accentuated in some transient conditions; for example, in postulated rupture of a main steam line and rupture of rod cluster control assembly mechanism housing described in Subsections 15.1.5 and 15.4.8, and are included in these analyses.

The analytical methods and calculational models used in calculating the reactivity coefficients are given in Subsection 4.3.3. These models have been confirmed through extensive testing of more than thirty cores similar to the plant described herein; results of these tests are discussed in Subsection 4.3.3.

Quantitative information for calculated reactivity coefficients, including fuel-Doppler coefficient, moderator coefficients (density, temperature, pressure, void) and power coefficient is given in the following sections.

a. Fuel Temperature (Doppler) Coefficient

The fuel temperature (Doppler) coefficient is defined as the change in reactivity per degree change in effective fuel temperature and is primarily a measure of the Doppler broadening of U-238 and Pu-240 resonance absorption peaks. Doppler broadening of other isotopes such as U-236, Np-237 etc., are also considered but their contributions to the Doppler effect is small. An increase in fuel temperature increases the effective resonance absorption cross sections of the fuel and produces a corresponding reduction in reactivity.

The fuel temperature coefficient is calculated by performing calculations using the SIMULATE-3 code (Reference 2) or the ANC code (Reference 12). Moderator temperature reactivity changes are removed as the power level is varied. Spatial variation of fuel temperature is taken into account by calculating the effective fuel temperature as a function of power density as discussed in Subsection 4.3.3.1.

The Doppler temperature coefficient is shown in Figure 4.3-27 as a function of the effective fuel temperature (at BOL and EOL conditions). The effective fuel temperature is lower than the volume averaged fuel temperature since the neutron flux distribution is nonuniform through the pellet and gives preferential weight to the surface temperature. The Doppler-only contribution to the power coefficient, defined later, is shown in Figure 4.3-28 as a function of relative core power. The integral of the differential curve on Figure 4.3-28 is the Doppler contribution to the power defect and is shown in Figure 4.3-29 as a function of relative power. The Doppler coefficient becomes more negative as a function of life as the Pu-240 content increases, thus increasing the Pu-240 resonance absorption, but overall becomes less negative since the fuel temperature changes with burnup as described in Subsection 4.3.3.1. The upper and lower limits of Doppler coefficient used in accident analyses are given in Chapter 15.

b. Moderator Coefficients

The moderator coefficient is a measure of the change in reactivity due to a change in specific coolant parameters such as density, temperature, pressure or void. The coefficients so obtained are moderator density, temperature, pressure and void coefficients.

1. Moderator Density and Temperature Coefficients

The moderator temperature (density) coefficient is defined as the change in reactivity per unit change in the moderator temperature. Generally, the effect of the changes in moderator density as well as the temperature are considered together. A decrease means less moderation which results in a negative moderation coefficient. An increase in coolant temperature, keeping the density constant, leads to a hardened neutron spectrum and results in an increase in resonance absorption in U-238, Pu-240 and other isotopes. The hardened spectrum also causes a decrease in the fission to capture ratio in U-235 and Pu-239. Both of these effects make the moderator coefficient more negative. Since water density changes more rapidly with temperature as temperature increases, the moderator temperature coefficient becomes more negative with increasing temperature.

The soluble boron used in the reactor as a means of reactivity control also has an effect on moderator temperature coefficient since the soluble boron poison density as well as the water density is decreased when the coolant temperature rises. A decrease in the soluble poison concentration introduces a positive component in the moderator temperature coefficient.

Thus, if the concentration of soluble poison is large enough, the net value of the coefficient may be positive. With the burnable poison rods present, however, the initial hot boron concentration is sufficiently low that the moderator temperature coefficient is negative at power operating conditions above 20% power*. The effect of control rods is to make the moderator coefficient more negative by reducing the required soluble boron concentration and by increasing the "leakage" of the core.

With burnup, the moderator temperature coefficient becomes more negative primarily as a result of boric acid dilution but also to an extent from the effects of the buildup of plutonium and fission products.

---

* Note: A non-negative moderator temperature coefficient is allowed by Technical Specifications for all power levels, provided that compliance with the ATWS Rule and its basis are maintained, as described in the Bases for Technical Specification 3/4.1.1.3. The Seabrook core design philosophy meets this requirement by ensuring that a non-positive MTC exists for operating conditions above 20% power.

The moderator coefficient is calculated for the various plant conditions discussed above by performing two-group nodal calculations, varying the moderator temperature (and density) by about ±5°F about each of the mean temperatures. The moderator coefficient is shown as a function of core temperature and boron concentration for the unrodded and rodded core in Figure 4.3-30, Figure 4.3-31 and Figure 4.3-32. The temperature range covered is from cold (68°F) to about 600°F. The contribution due to Doppler coefficient (because of change in moderator temperature) has been subtracted from these results. Figure 4.3-33 shows the hot, full power moderator temperature coefficient plotted as a function of cycle lifetime for the just critical boron concentration condition based on the design boron letdown condition.

The moderator coefficients presented here are calculated on a corewide basis, since they are used to describe the core behavior in normal and accident situations when the moderator temperature changes can be considered to affect the entire core.

2. Moderator Pressure Coefficient

The moderator pressure coefficient relates the change in moderator density, resulting from a reactor coolant pressure change, to the corresponding effect on neutron production. This coefficient is of much less significance in comparison with the moderator temperature coefficient. A change of 50 psi in pressure has approximately the same effect on reactivity as a half degree change in moderator temperature. This coefficient can be determined from the moderator temperature coefficient by relating change in pressure to the corresponding change in density.

3. Moderator Void Coefficient

The moderator void coefficient relates the change in neutron multiplication to the presence of voids in the moderator. In a PWR, this coefficient is not very significant because of the low void content in the coolant. The core void content is less than one-half of one percent and is due to local or statistical boiling. The void coefficient can be determined from the moderator temperature coefficient by relating change in void to corresponding change in density.

c. Power Coefficient

The combined effect of moderator and fuel temperature change as the core power level changes is called the total power coefficient and is expressed in terms of reactivity change per percent power change. The power coefficient at BOL and EOL conditions is given in Figure 4.3-34.

It becomes more negative with burnup reflecting the combined effect of moderator and fuel temperature coefficients with burnup. The power defect (integral reactivity effect) at BOL and EOL is given in Figure 4.3-35.

d. Comparison of Calculated and Experimental Reactivity Coefficients

Subsection 4.3.3 describes the comparison of calculated and experimental reactivity coefficients in detail. Based on the data presented there, the accuracy of the current analytical model is:

1. ±0.2 percent $\Delta\rho$ for Doppler defect

2. ±2 pcm/°F for the moderator coefficient

Experimental evaluation of the calculated coefficients will be completed during the physics tests described in Chapter 14.

e. Reactivity Coefficients Used in Transient Analysis

Table 4.3-2 gives the limiting values as well as the best estimate values for the reactivity coefficients. The limiting values are used as design limits in the transient analysis. The exact values of the coefficient used in the analysis depend on whether the transient of interest is examined at the BOL or EOL, whether the most negative or the most positive (least negative) coefficients are appropriate, and whether spatial nonuniformity must be considered in the analysis. Conservative values of coefficients, considering various aspects of analysis are used in the transient analysis. This is completely described in Chapter 15.

The reactivity coefficients shown in Figure 4.3-27, Figure 4.3-28, Figure 4.3-29, Figure 4.3-30, Figure 4.3-31, Figure 4.3-32, Figure 4.3-33, Figure 4.3-34 and Figure 4.3-35 are best estimate values calculated for this cycle and apply to the core described in Table 4.3-1. The limiting values shown in Table 4.3-2 are chosen to encompass the best estimate reactivity coefficients, including the uncertainties given in Subsection 4.3.3.3 over appropriate operating conditions calculated for this cycle and the expected values for the subsequent cycles. The most positive as well as the most negative values are selected to form the design basis range used in the transient analysis. A direct comparison of the best estimate and design limit values shown in Table 4.3-2 can be misleading since in many instances, the most conservative combination of reactivity coefficients is used in the transient analysis even though the extreme coefficients assumed may not simultaneously occur at the condition of lifetime, power level, temperature and boron concentration assumed in the analysis. The need for re-evaluation of any accident in a subsequent cycle is contingent upon whether or not the coefficients for that cycle fall within the identified range used in the analysis presented in Chapter 15 with due allowance for the calculational uncertainties given in Subsection 4.3.3.3. Control rod requirements are given in Table 4.3-3 for the core described and for a hypothetical equilibrium cycle since these are markedly different. These latter numbers are provided for information only and their validity in a particular cycle would be an unexpected coincidence.

4.3.2.4 Control Requirements

To ensure the shutdown margin stated in the Technical Specifications and the Core Operating Limits Report under conditions where a cooldown to ambient temperature is required, concentrated soluble boron is added to the coolant. Boron concentrations for several core conditions are listed in Table 4.3-2. For all core conditions including refueling, the boron concentration is well below the solubility limit. The Rod Cluster Control Assemblies are employed to bring the reactor to the hot shutdown condition. The minimum required shutdown margin is given in the Technical Specifications.

The ability to accomplish the shutdown for hot conditions is demonstrated in Table 4.3-3 by comparing the difference between the Rod Cluster Control Assembly reactivity available with an allowance for the worst stuck rod with that required for control and protection purposes. The shutdown margin includes an allowance of 10 percent for analytic uncertainties (see Subsection 4.3.2.4i). The largest reactivity control requirement appears at the EOL when the moderator temperature coefficient reaches its peak negative value as reflected in the larger power defect.

The control rods are required to provide sufficient reactivity to account for the power defect from full power to zero power and to provide the required shutdown margin. The reactivity addition resulting from power reduction consists of contributions from Doppler, variable average moderator temperature, flux redistribution, and reduction in void content as discussed below.

a. Doppler

The Doppler effect arises from the broadening of U-238 and Pu-240 resonance peaks with an increase in effective pellet temperature. This effect is most noticeable over the range of zero power to full power due to the large pellet temperature increase with power generation.

b. Variable Average Moderator Temperature

When the core is shutdown to the hot, zero power condition, the average moderator temperature changes from the equilibrium full load value determined by the steam generator and turbine characteristics (steam pressure, heat transfer, tube fouling, etc.) to the equilibrium no load value, which is based on the steam generator shell side design pressure. The design change in temperature is conservatively increased by 6°F to account for the control dead band and measurement errors.

c. Redistribution

During full power operation, the coolant density decreases with core height, and this, together with partial insertion of control rods, results in less fuel depletion near the top of the core. Under steady state conditions, the relative power distribution will be slightly asymmetric towards the bottom of the core. On the other hand, at Hot Zero Power conditions, the coolant density is uniform up the core, and there is no flattening due to the Doppler. The result will be a flux distribution which at zero power can be skewed toward the top of the core. The reactivity insertion due to the skewed distribution is calculated with an allowance for effects of xenon distribution.

d. Void Content

A small void content in the core is due to nucleate boiling at full power. The void collapse coincident with power reduction makes a small reactivity contribution.

e. Rod Insertion Allowance

At full power, the control bank is operated within a prescribed band of travel to compensate for small periodic changes in boron concentration, changes in temperature and very small changes in the xenon concentration not compensated for by a change in boron concentration. When the control bank reaches either limit of this band, a change in boron concentration is required to compensate for additional reactivity changes. Since the insertion limit is set by a rod travel limit, a conservatively high calculation of the inserted worth exceeds the normally inserted reactivity.

f. Burnup

Excess reactivity of 10 percent $\Delta\rho$ (hot) is installed at the beginning of each cycle to provide sufficient reactivity to compensate for fuel depletion and fission products throughout the cycle. This reactivity is controlled by the addition of soluble boron to the coolant and by burnable poison. The soluble boron concentration for several core configurations, the unit boron worth, and burnable poison worth are given in Table 4.3-1 and Table 4.3-2. Since the excess reactivity for burnup is controlled by soluble boron and/or burnable poison, it is not included in control rod requirements.

g. Xenon and Samarium Poisoning

Changes in xenon and samarium concentrations in the core occur at a sufficiently slow rate, even following rapid power level changes, that the resulting reactivity change is controlled by changing the soluble boron concentration.

h. pH Effects

Changes in reactivity due to a change in coolant pH, if any, are sufficiently small in magnitude and occur slowly enough to be controlled by the boron system. Further details are available in Reference 9.

i. Experimental Confirmation

Following a normal shutdown, the total core reactivity change during cooldown with a stuck rod has been measured on a 121 assembly, 10-foot high core and 121 assembly, 12-foot high core. In each case, the core was allowed to cool down until it reaches criticality simulating the steamline break accident. For the 10-foot core, the total reactivity change associated with the cooldown is over-predicted by about 0.3 percent $\Delta\rho$ with respect to the measured result. This represents an error of about 5 percent in the total reactivity change and is about half the uncertainty allowance for this quantity. For the 12-foot core, the difference between the measured and predicted reactivity change was an even smaller 0.2 percent $\Delta\rho$. These measurements and others demonstrate the ability of the methods described in Subsection 4.3.3.

j. Control

Core reactivity is controlled by means of a chemical poison dissolved in the coolant, Rod Cluster Control Assemblies, and burnable absorber fuel rods as described below.

k. Chemical Poison

Boron in solution as boric acid is used to control relatively slow reactivity changes associated with:

1. The moderator temperature defect in going from cold shutdown at ambient temperature to the hot operating temperature at zero power,

2. The transient xenon and samarium poisoning, such as that following power changes or changes in rod cluster control position,

3. The excess reactivity required to compensate for the effects of fissile inventory depletion and buildup of long-life fission products,

4. The burnable absorber fuel rod depletion.

The boron concentration for various core conditions is presented in Table 4.3-2.

l. Rod Cluster Control Assemblies

Full length Rod Cluster Control Assemblies exclusively are employed in this reactor.

The number of respective full length assemblies is shown in Table 4.3-1. The full length Rod Cluster Control Assemblies are used for shutdown and control purposes to offset fast reactivity changes associated with:

1. The required shutdown margin in the Hot Zero Power, stuck rod condition,

2. The reactivity compensation as a result of an increase in power above Hot Zero Power (power defect including Doppler, and moderator reactivity changes),

3. Unprogrammed fluctuations in boron concentration, coolant temperature or xenon concentration (with rods not exceeding the allowable rod insertion limits),

4. Reactivity ramp rates resulting from load changes.

The allowed full length control bank insertion is limited at full power to maintain shutdown capability. As the power level is reduced, control rod reactivity requirements are also reduced and more rod insertion is allowed. The control bank position is monitored and the operator is notified by an alarm if the limit is approached. The determination of the insertion limit uses conservative xenon distributions and axial power shapes. In addition, the rod cluster control assembly withdrawal pattern determined from these analyses is used in determining power distribution factors and in determining the maximum worth of an inserted rod cluster control assembly ejection accident. For further discussion, refer to the Technical Specifications on rod insertion limits.

Power distribution, rod ejection and rod misalignment analyses are based on the arrangement of the shutdown and control groups of the Rod Cluster Control Assemblies shown in Figure 4.3-36. All shutdown Rod Cluster Control Assemblies are withdrawn before withdrawal of the control banks is initiated. In going from zero to 100 percent power, control banks A, B, C and D are withdrawn sequentially. The limits of rod positions and further discussion on the basis for rod insertion limits are provided in the Technical Specifications and the Core Operating Limits Report.

m. Reactor Coolant Temperature

Reactor coolant (or moderator) temperature control has added flexibility in reactivity control of the Westinghouse PWR. This feature takes advantage of the negative moderator temperature coefficient inherent in a PWR to:

1. Maximize return to power capabilities

2. Provide ±5 percent power load regulation capabilities without requiring control rod compensation

3. Extend the time in cycle life to which daily load follow operation can be accomplished.

Reactor coolant temperature control supplements the dilution capability of the plant by lowering the reactor coolant temperature to supply positive reactivity through the negative moderator coefficient of the reactor. After the transient is over, the system automatically recovers the reactor coolant temperature to the programmed value.

Moderator temperature control of reactivity, like soluble boron control, has the advantage of not significantly affecting the core power distribution. However, unlike boron control, temperature control can be rapid enough to achieve reactor power change rates of 5 percent/minute.

n. Integral Fuel Burnable Absorber Rods

Integral Fuel Burnable Absorber (IFBA) rods provide partial control of the excess reactivity available during the beginning of the fuel cycle. In doing so, these rods prevent the moderator temperature coefficient from being positive at normal operating conditions above 20% power. They perform this function by reducing the requirement of soluble poison in the moderator at the beginning of the fuel cycle as described previously. For purposes of illustration, a typical IFBA rod pattern in the core together with the number of rods per assembly are shown in Figure 4.3-5, while the arrangements within an assembly are displayed in Figure 4.3-4. The reactivity worth of these rods is shown in Table 4.3-1. The boron in the rods is depleted with burnup but at a sufficiently slow rate so that the resulting critical concentration of soluble boron is such that the moderator temperature coefficient remains negative at all times for power operating conditions above 20% power[*].

o. Peak Xenon Startup

Compensation for the peak xenon buildup is accomplished using the Boron Control System. Startup from the peak xenon condition is accomplished with a combination of rod motion and boron dilution. The boron dilution may be made at any time, including during the shutdown period, provided the shutdown margin is maintained.

p. Load Follow Control and Xenon Control

During load follow maneuvers, power changes are accomplished using control rod motion and dilution or boration by the boron system as required. Control rod motion is limited by the control rod insertion limits on full length rods as provided in the Technical Specifications and discussed in Subsections 4.3.2.4l and 4.3.2.4m. The power distribution is maintained within acceptable limits through the location of the full length rod bank. Reactivity changes due to the changing xenon concentration can be controlled by rod motion and/or changes in the soluble boron concentration. Late in cycle life, extended load follow capability is obtained by augmented the limited boron dilution capability at low soluble boron concentration by temporary moderator temperature reductions.

---

[*] Note: A non-negative moderator temperature coefficient is allowed by Technical Specifications for all power levels, provided that compliance with the ATWS Rule and its basis are maintained, as described in the Bases for Technical Specification 3/4.1.1.3. The Seabrook core design philosophy meets this requirement by ensuring that a non-positive MTC exists for operating conditions above 20% power.

Rapid power increases (5 percent/min) from part power load follow operation are accomplished with a combination of rod motion, moderator temperature reduction, and boron dilution. Compensation for the rapid power increase is accomplished initially by a combination of rod withdrawal and moderator temperature reduction. As the slower boron dilution takes affect after the initial rapid power increase, the moderator temperature returns to the programmed value.

q. Burnup

Control of the excess reactivity for burnup is accomplished using soluble boron and/or burnable poison. The boron concentration must be limited during operating conditions to ensure the moderator temperature coefficient is negative. Sufficient burnable poison is installed at the beginning of a cycle to give the desired cycle lifetime without exceeding the boron concentration limit. The practical minimum boron concentration is 10 ppm.

4.3.2.5 Control Rod Patterns and Reactivity Worth

The full length Rod Cluster Control Assemblies are designated by function as the control groups and the shutdown groups. The terms "group" and "bank" are used synonymously throughout this report to describe a particular grouping of control assemblies. The rod cluster assembly pattern is displayed in Figure 4.3-36, which is not expected to change during the life of the plant. The control banks are labeled A, B, C, and D and the shutdown banks are labeled SA, SB, etc., as applicable. Each bank, although operated and controlled as a unit, is comprised of two subgroups. The axial position of full length Rod Cluster Control Assemblies may be controlled manually or automatically. The Rod Cluster Control Assemblies are all dropped into the core following actuation of reactor trip signals.

Two criteria have been employed for selection of the control groups. First, the total reactivity worth must be adequate to meet the requirements specified in Table 4.3-3. Second, in view of the fact that these rods may be partially inserted at power operation, the total power peaking factor should be low enough to ensure that the power capability requirements are met. Analyses indicate that the first requirement can be met either by a single group or by two or more banks whose total worth equals at least the required amount. The axial power shape would be more peaked following movement of a single group of rods worth three to four percent $\Delta\rho$; therefore, four banks (described as A, B, C, and D in Figure 4.3-36) each worth approximately one percent $\Delta\rho$ have been selected.

The position of control banks for criticality under any reactor condition is determined by the concentration of boron in the coolant. On an approach to criticality, boron is adjusted to ensure that criticality will be achieved with control rods above the insertion limit set by shutdown and other considerations (see the Technical Specifications and the Core Operating Limits Report).

Ejected rod worths are given in Subsection 15.4.8 for several different conditions.

Allowable deviations due to misaligned control rods are noted in the Technical Specifications.

A representative calculation for two banks of control rods withdrawn simultaneously (rod withdrawal accident) is given in Figure 4.3-37.

Calculation of control rod reactivity worth versus time following reactor trip involves both control rod velocity and differential reactivity worth. The rod position versus time of travel after rod release, assumed is given in Figure 4.3-38. For nuclear design purposes, the reactivity worth versus rod position is calculated by a series of steady state calculations at various control rod positions assuming all rods out of the core as the initial position in order to minimize the initial reactivity insertion rate. Also to be conservative, the rod of highest worth is assumed stuck out of the core and the flux distribution (and thus reactivity importance) is assumed to be skewed to the bottom of the core. The result of these calculations is shown in Figure 4.3-39.

The shutdown groups provide additional negative reactivity to assure an adequate shutdown margin. Shutdown margin is defined as the amount by which the core would be subcritical at hot shutdown if all Rod Cluster Control Assemblies are tripped, but assuming that the highest worth assembly remains fully withdrawn and no changes in xenon or boron take place. The loss of control rod worth due to the material irradiation is negligible since only bank D and bank C may be in the core under normal operating conditions (near full power).

The values given in Table 4.3-3 show that the available reactivity in withdrawn rod cluster control assemblies provides the design bases minimum shutdown margin allowing for the highest worth cluster to be at its fully withdrawn position. An allowance for the uncertainty in the calculated worth of N-1 rods is made before determination of the shutdown margin.

4.3.2.6 Criticality of the Reactor During Refueling and Criticality of Fuel Assemblies

Criticality of fuel assemblies outside the reactor is precluded by adequate design of fuel transfer, shipping and storage facilities and by administrative control procedures. The two principal methods of preventing criticality are limiting the fuel assembly array size and limiting assembly and/or inserting neutron poisons between assemblies.

The design basis for preventing criticality outside the reactor is that, considering possible variation, there is a 95 percent probability at a 95 percent confidence level that the effective multiplication factor, K_{eff}, of the fuel assembly array will be less than 0.95. In areas like the new fuel vault where sources of moderation such as those that could arise during fire fighting operations are included, the maximum design basis K_{eff} is 0.98 under conditions of low density, "optimum moderation." For further description of the criticality safety limits in the new fuel vault and spent fuel pool, see Subsections 9.1.1.3 and 9.1.2.3, respectively.

4.3.2.7 Stability

a. Introduction

The stability of the PWR cores against xenon-induced spatial oscillations and the control of such transients are discussed extensively in References 10, 13, and 14. A summary of these reports is given in the following discussion and the design bases are given in Subsection 4.3.1.6.

In a large reactor core, xenon-induced oscillations can take place with no corresponding change in the total power of the core. The oscillation may be caused by a power shift in the core which occurs rapidly by comparison with the xenon-iodine time constants. Such a power shift occurs in the axial direction when a plant load change is made by control rod motion and results in a change in the moderator density and fuel temperature distributions. Such a power shift could occur in the diametral plane of the core as a result of abnormal control action.

Due to the negative power coefficient of reactivity, PWR cores are inherently stable to oscillations in total power. Protection against total power instabilities is provided by the Control and Protection System as described in Section 7.7. Hence, the discussion on the core stability will be limited here to xenon-induced spatial oscillations.

b. Stability Index

Power distributions, either in the axial direction or in the X-Y plane, can undergo oscillations due to perturbations introduced in the equilibrium distributions without changing the total core power. The overtones in the current PWRs, and the stability of the core against xenon-induced oscillations can be determined in terms of the eigenvalues of the first flux overtones. Writing, either in the axial direction or in the X-Y plane, the eigenvalue of the first harmonic as:

$$\xi = b + ic, \tag{4.3-1}$$

then b is defined as the stability index and $T = 2\pi/c$ as the oscillation period of the first harmonic. The time-dependence of the first harmonic in the power distribution can now be represented as:

$$\delta\varphi(t) = A\, e^{\xi t} = ae^{bt} \cos ct, \tag{4.3-2}$$

where A and a are constants. The stability index can also be obtained approximately by:

$$b = \frac{1}{T} \ln \frac{A_{n+1}}{A_n} \tag{4.3-3}$$

where A_n, A_{n+1} are the successive peak amplitudes of the oscillation and T is the time period between the successive peaks.

c. Prediction of the Core Stability

The stability of the core described herein (i.e., with 17x17 fuel assemblies) against xenon-induced spatial oscillations is expected to be equal to or better than that of earlier designs. The prediction is based on a comparison of the parameters which are significant in determining the stability of the core against the xenon-induced oscillations, namely: (1) the overall core size is unchanged and spatial power distributions will be similar, (2) the moderator temperature coefficient is expected to be similar to or slightly more negative, and (3) the Doppler coefficient of reactivity is expected to be equal to or slightly more negative at full power.

Analysis of both the axial and X-Y xenon transient tests, discussed in Subsection 4.3.2.7e, shows that the calculational model is adequate for the prediction of core stability.

d. Stability Measurements

1. Axial Measurements

Two axial xenon transient tests conducted in a PWR with a core height of 12 feet and 121 fuel assemblies are reported in Reference 14, and will be briefly discussed here. The tests were performed at approximately 50 percent and 100 percent of cycle life.

Both transients lasted about 40 hours with the regulating control bank ranging in insertion from 214 steps to 179 steps withdrawn. These maneuvers produced measured axial offsets that ranged from 3.5% to -11.6%. Figure 4.3-40 shows the axial offset as a function of time through these measurements.

The total core power was maintained constant during these spatial xenon tests, and the stability index and the oscillation period were obtained from a least-square fit of the axial offset data in the form of Equation (4.3-2). The axial offset of power is the quantity that properly represents the axial stability in the sense that it essentially eliminates any contribution from even order harmonics including the fundamental mode. The conclusions of the tests are:

(a) The core was stable against induced axial xenon transients both at the core average burnups of 1550 MWd/Mtu and 7700 MWd/Mtu. The measured stability indices are -0.041 hr^{-1} for the first test (Curve 1 of Figure 4.3-40) and -0.014 hr^{-1} for the second test (Curve 2 of Figure 4.3-40). The corresponding oscillation periods are 32.4 hrs and 27.2 hrs, respectively.

(b) The reactor core becomes less stable as fuel burnup progresses and the axial stability index was essentially zero at 12,000 MWd/Mtu.

Additional tests conducted on a PWR 12 foot core with 193 assemblies indicate that full length control rods can be used to dampen axial xenon oscillations effectively.

2. Measurements in the X-Y Plane

Two X-Y xenon oscillation tests were performed at a PWR plant with a core height of 12 feet and 157 fuel assemblies. The first test was conducted at a core average burnup of 1540 MWd/Mtu and the second at a core average burnup of 12,900 MWd/Mtu. Both of the X-Y xenon tests show that the core was stable in the X-Y plane at both burnups. The second test shows that the core became more stable as the fuel burnup increased and all Westinghouse PWRs with 121 and 157 assemblies are expected to be stable throughout their burnup cycles.

In each of the two X-Y tests, a perturbation was introduced to the equilibrium power distribution through an impulse motion of one rod cluster control unit located along the diagonal axis. Following the perturbation, the uncontrolled oscillation was monitored using the moveable detector and thermocouple system and the excore power range detectors. The quadrant tilt difference (QTD) is the quantity that properly represents the diametral oscillation in the X-Y plane of the reactor core in that the differences of the quadrant average powers over two symmetrically opposite quadrants essentially eliminate the contributions to the oscillation from the azimuthal mode. The QTD data were fitted in the form of Equation (4.3-2) through a least-square method. A stability index of -0.076 hr^{-1} with a period of 29.6 hours was obtained from the thermocouple data shown in Figure 4.3-41.

It was observed in the second X-Y xenon test that the PWR core with 157 fuel assemblies had become more stable due to an increased fuel depletion and the stability index was not determined.

e. Comparison of Calculations with Measurements

Analysis of the axial xenon transients above was performed by Westinghouse using its neutronics methods. The results of the stability calculation for the axial tests are compared with the experimental data in Table 4.3-4. The calculations show conservative results for both of the axial tests with a margin of approximately -0.01 hr^{-1} in the stability index.

An analytical simulation of the first X-Y xenon oscillation test shows a calculated stability index of -0.081 hr^{-1}, in good agreement with the measured value of -0.076 hr^{-1}. As indicated earlier, the second X-Y xenon test showed that the core had become more stable compared to the first test and no evaluation of the stability index was attempted. This increase in the core stability in the X-Y plane due to increased fuel burnup is due mainly to the increased magnitude of the negative moderator temperature coefficient.

f. Stability Control and Protection

The Excore Detector System is utilized to provide indications of xenon-induced spatial oscillations. The readings from the multi-section excore detectors are available to the operator and also form part of the protection system.

1. Axial Power Distribution

For maintenance of proper axial power distributions, the operator is instructed to maintain axial power distribution within axial flux difference operating limit band specified in the Core Operating Limits Report, based on the excore detector readings. Should the axial flux difference move outside this band, power level will be reduced by the operators per Technical Specification requirements. If the operators do not reduce power, the protection limit will be reached and the reactor will be tripped.

Twelve foot PWR cores become less stable to axial xenon oscillations as fuel burnup progresses. However, free xenon oscillations are not allowed to occur except for special tests. The full-length control rod banks are sufficient to dampen and control any axial xenon oscillations present. Should the axial flux difference move outside the specified operating limit band due to a axial xenon oscillation, or any other reason, the core power level will be reduced by the operators per Technical Specification requirements, or the protection limit on axial flux difference will be reached and the reactor will be tripped.

2. Radial Power Distribution

The core described herein is calculated to be stable against X-Y xenon induced oscillations at all times in life.

The X-Y stability of large PWRs has been further verified as part of the startup physics test program for cores with 193 fuel assemblies. The measured X-Y stability of the cores with 157 and 193 assemblies was in good agreement with the calculated stability as discussed in Subsections 4.3.2.7d and 4.3.2.7e. In the unlikely event that X-Y oscillations occur, backup actions are possible and would be implemented if necessary, to increase the natural stability of the core as discussed in the Technical Specifications. This is based on the fact that several actions could be taken to make the moderator temperature coefficient more negative, which will increase the stability of the core in the X-Y plane.

Provisions for protection against nonsymmetric perturbations in the X-Y power distribution that could result from equipment malfunctions are made in the protection system design. This includes control rod drop, rod misalignment and asymmetric loss of coolant flow.

4.3.2.8 Vessel Irradiation

A brief review of the methods and analyses used in the determination of neutron and gamma ray flux attenuation between the core and the pressure vessel is given below. A more complete discussion on the pressure vessel irradiation and surveillance program is given in Section 5.3.

The materials that serve to attenuate neutrons originating in the core and gamma rays from both the core and structural components consist of the core baffle, core barrel, neutron pads and associated water annuli, all of which are within the region between the core and the pressure vessel.

In general, few group neutron diffusion theory codes are used to determine fission power density distributions within the active core, and the accuracy of these analyses is verified by incore measurements on operating reactors. Region and rodwise power sharing information from the core calculations is then used as source information in two-dimensional S_n transport calculations which compute the flux distributions throughout the reactor.

The neutron flux distribution and spectrum in the various structural components varies significantly from the core to the pressure vessel. Representative values of the neutron flux distribution and spectrum are presented in Table 4.3-5. The values listed are based on time averaged equilibrium cycle reactor core parameters and power distributions; and, thus, are suitable for long-term nvt projections and for correlation with radiation damage estimates.

As discussed in Section 5.3, the irradiation surveillance program utilizes actual test samples to verify the accuracy of the calculated fluxes at the vessel.

4.3.3 Analytical Methods

Calculations required in nuclear design consist of three distinct types, which are performed in sequence:

1. Determination of effective fuel temperatures
2. Generation of macroscopic few-group parameters
3. Space-dependent, few-group diffusion calculations.

These calculations are carried out by computer codes which can be executed individually; however, most of the codes required have been linked to form an automated design sequence which minimizes design time, avoids errors in transcription of data, and standardizes the design methods.

4.3.3.1 Fuel Temperature (Doppler) Calculations

Temperatures vary radially within the fuel rod, depending on the heat generation rate in the pellet, the conductivity of the materials in the pellet, gap, and clad, and the temperature of the coolant.

The fuel temperatures for use in nuclear design Doppler calculations are obtained from the fuel rod design model described in Subsection 4.2.1.3 which considers the effect of radial variation of pellet conductivity, expansion-coefficient and heat generation rate, elastic deflection of the clad, and a gap conductance which depends on the initial fill gap, the hot open gap dimension, fuel swelling, fission gas release, and plastic clad deformation. Further gap closure occurs with burnup and accounts for the decrease in Doppler defect with burnup.

4.3.3.2 Macroscopic Group Constants

Macroscopic few-group constants and analogous microscopic cross sections (needed for feedback and microscopic depletion calculations) are generated for fuel cells by a recent version of the CASMO or PHOENIX-P (References 1 and 11) code, which provide burnup dependent cross sections. Fast and thermal cross section library tapes contain microscopic cross sections taken from the ENDF/B-VI library, with a few exceptions where other data provided good agreement with critical experiments, isotopic measurements, and plant critical boron values. The effect on the unit fuel cell of nonlattice components in the fuel assembly is obtained by supplying an appropriate volume fraction of these materials in an extra region which is homogenized with the unit cell in the fast and thermal flux calculations. In the thermal calculation, the fuel rod, clad, and moderator are homogenized by energy-dependent disadvantage factors derived from an analytical fit to integral transport theory results.

Group constants for control rods, IFBA rods, guide thimbles, instrument thimbles and interassembly gaps are generated in a manner analogous to the fuel cell calculation. Baffle and reflector group constants are taken from two dimensional PHOENIX-P models of the core and baffle/reflector interface.

Nodal group constants are obtained by a flux-volume homogenization of the fuel cells, burnable poison cells, guide thimbles, instrumentation thimbles, interassembly gaps, and control rod cells from one mesh internal per cell X-Y unit fuel assembly diffusion calculations.

Validation of the cross section method is based on analysis of isotopic data, plant critical boron (C_B) values at HZP, BOL and at HFP as a function of burnup as shown in Reference 11. Control rod worth measurements are also shown in Reference 11.

Confirmatory critical experiments on burnable poisons are described in Reference 1.

4.3.3.3 Spatial Three Dimensional Calculations

Spatial three dimensional calculations consist primarily of two-group advanced nodal calculations using a version of ANC (Reference 12) or SIMULATE (Reference 2). Full three dimensional calculations are performed using four radial nodes per assembly and at least twenty four axial nodes. Pin power reconstruction is performed within the code to determine discrete pin powers and detailed detector reaction rates. The code also contains means to follow the core spectral history to compensate for depletion of nodes not at the general conditions used in generating the cross sections.

Validation of ANC and SIMULATE calculations is associated with the validation of the group constants themselves, as discussed in Subsection 4.3.3.2. Validation of the Doppler calculations is associated with the fuel temperature validation discussed in Subsection 4.3.3.1. Validation of the moderator coefficient calculations is obtained by comparison with plant measurements at Hot Zero Power conditions.

Validation of the spatial codes for calculating power distributions involves the use of incore and excore detectors and is discussed in Subsection 4.3.2.2g.

4.3.4 References

1. A.S. DiGiovine, K.B. Spinney, D.G. Napolitano, J. Pappas, "CASMO-3G Validation", YAEC-1363, April, 1988.

2. A.S. DiGiovine, J.P. Gorski, M.A. Tremblay, "SIMULATE-3 Validation and Verification", YAEC-1659, September, 1998.

3. "Westinghouse Anticipated Transients Without Reactor Trip Analysis", WCAP-8330, August 1974.

4. ATWS Final Rule - Code of Federal Regulations 10 CFR 50.62 and Supplementary Information Package, "Reduction of Risk from Anticipated Transient without Scram (ATWS) Events for Light Water-Cooled Nuclear Power Plants."

5. Oelrich, R. L. and Kersting, P. J., "Assessment of Clad Flattening and Densification Power Spike Factor Elimination in Westinghouse Nuclear Fuel," WCAP-13589-A, March 1995.

6. Meyer, R.O., "The Analysis of Fuel Densification," Division of Systems Safety, USNRC, NUREG-0085, July 1976.

7. Guimond, P. J., et al., "Core Thermal Limit Protection Function Setpoint Methodology for Seabrook Station", YAEC-1854-P-A, October 1992.

8. J.P. Gorski, "Seabrook Station Unit 1 Fixed Incore Detector System Analysis", YAEC-1855-P-A, October 1992.

9. Cermek, J. O., et al., "Pressurized Water Reactor pH - Reactivity Effect Final Report," WCAP-3696-8 (EURAEC-2074), October 1968.

10. Moore, J. S., Power Distribution Control of Westinghouse Pressurized Water Reactors," WCAP-7811, December 1971.

11. Nguyen, T. Q., et. al. "Qualification of the PHOENIX-P/ANC Nuclear Design System for Pressurized Water Reactor Cores", WCAP-11596-P-A, June 1998 (Westinghouse Proprietary)

12. Liu, Y. S, Meliksetion, A, Rathkopt, J. A., Little D. C., Nakano, F., Poploski, M. J., "ANC-A Westinghouse Advanced Nodal Computer Code", WCAP-10965-P-A, September, 1986 (Westinghouse Proprietary)

13. Skogen, F. B. and McFarlane, A. F., "Xenon-Induced Spatial Instabilities in Three-Dimensions," WCAP-3680-22 (EURAEC-2116), September 1969.

14. Lee, J. C., et al., "Axial Xenon Transient Tests at the Rochester Gas and Electric Reactor," WCAP-7964, June 1971.

15. Miller, R. W., et al., "Relaxation of Constant Axial Offset Control, F_Q Surveillance Technical Specification," WCAP-10216-P-A, Revision 1A, February 1994.

4.4 THERMAL AND HYDRAULIC DESIGN

4.4.1 Design Bases

The overall objective of the thermal and hydraulic design of the reactor core is to provide adequate heat transfer which is compatible with the heat generation distribution in the core such that heat removal by the Reactor Coolant System or the Emergency Core Cooling System (when applicable) assures that the following performances and safety criteria requirements are met:

a. Fuel damage (defined as penetration of the fission product barrier, i.e., the fuel rod clad) is not expected during normal operation and operational transients (Condition I) or any transient conditions arising from faults of moderate frequency (Condition II). It is not possible, however, to preclude a very small number of rod failures. These will be within the capability of the plant cleanup system, and are consistent with the plant design bases.

b. The reactor can be brought to a safe state following a Condition III event with only a small fraction of fuel rods damaged (see above definition) although sufficient fuel damage might occur to preclude resumption of operation without considerable outage time.

c. The reactor can be brought to a safe state and the core can be kept subcritical with acceptable heat transfer geometry following transients arising from Condition IV events.

In order to satisfy the above criteria, the following design bases have been established for the thermal and hydraulic design of the reactor core.

4.4.1.1 Departure From Nucleate Boiling Design Basis

a. Basis

There will be at least 95 percent probability that departure from nucleate boiling (DNB) will not occur on the limiting fuel rods during normal operation and operational transients and any transient conditions arising from faults of moderate frequency (Conditions I and II events), at 95 percent confidence level.

The design limit DNBR value for RFA is 1.22 for typical cells and 1.22 for thimble cells. For use in the DNB safety analyses, the limit DNBR is conservatively increased to provide DNB margin to offset the effect of rod bow, RCS flow anomaly and any other DNB penalties that may occur, and to provide flexibility in design and operation of the plant. For RFA fuel, Safety Analysis Limit DNBR value of 1.47 for both typical and thimble cells is employed in the analysis.

b. Discussion

By preventing DNB, adequate heat transfer is assured between the fuel clad and the reactor coolant, thereby preventing clad damage as a result of inadequate cooling. Maximum fuel rod surface temperature is not a design basis, as it will be within a few degrees of coolant temperature during operation in the nucleate boiling region.

Limits provided by the nuclear control and protection systems are such that this design basis will be met for transients associated with Condition II events including overpower transients. There is an additional large DNBR margin at rated power operation and during normal operating transients.

The thermal-hydraulic analysis of the RFA (w/IFMs) fuel used in Seabrook Station incorporates the use of the VIPRE-01 computer code and the Revised Thermal Design Procedure (RTDP). The WRB-2M DNB correlation is used for the RFA. The W-3 correlations are still used when conditions are outside the range of theWRB-2 or WRB-2M correlation and applicability of the RTDP.

The WRB-2M DNB correlation is based on rod bundle data and takes advantage of the DNB benefit of reduced grid spacings associated with IFMs. The approval of the NRC that a 95/95 limit DNBR of 1.14 is appropriate for RFA and has been documented.

The W-3 correlation with a 95/95 limit DNBR of 1.30 is used below the fuel assembly first mixing vane grid. The W-3 correlation with a 95/95 limit DNBR of 1.45 is used in the pressure range of 500 to 1000 psia.

With RTDP methodology, variations in plant operating parameters, nuclear and thermal parameters, fuel fabrication parameters, and DNB correlation predictions are considered statistically to obtain the overall DNBR uncertainty factor which is used to define the design limit DNBR that satisfies the DNB design criterion. The criterion is that the probability that DNB will not occur on the most limiting fuel rod is at least 95 percent (at 95 percent confidence level) for any Condition I or II event. Conservative uncertainty values are used to calculate the design limit DNBR. Since the uncertainties are all included in the uncertainty factor, the accident analysis is done with input parameters at their nominal or best-estimate values. RTDP analyses use the minimum measured flow (MMF), equal to thermal design flow (TDF) plus a flow uncertainty. Analyses by standard methods continue to use TDF.

The Standard Thermal Design Procedure (STDP) is used for those analyses where RTDP is not applicable. In the STDP method, the parameters used in analysis are treated in a conservative way from a DNBR standpoint. The parameter uncertainties are applied directly to the plant safety analyses input values to give the lowest minimum DNBR. The DNBR limit for STDP is the appropriate DNB correlation limit increased by sufficient margin to offset the applicable DNBR penalties.

4.4.1.2 Fuel Temperature Design Basis

a. Basis

During modes of operation associated with Condition I and Condition II events, there is at least a 95 percent probability that the peak kW/ft fuel rods will not exceed the $U0_2$ melting temperature at the 95 percent confidence level. The melting temperature of $U0_2$ is taken as 5080°F (Reference 1), unirradiated, decreasing 58°F per 10,000 MWd/Mtu exposure.

Design evaluations for Condition I and II events have shown that fuel melting will not occur for achievable local burnups to 75,000 MWd/Mtu, Reference 5. The NRC approved design evaluations up to 60,000 MWd/Mtu in Reference 5 and up to 62,000 MWd/Mtu in Reference 6.

b. Discussion

By precluding $U0_2$ melting, the fuel geometry is preserved and possible adverse effects of molten $U0_2$ on the cladding are eliminated. Cycle-specific values for the peak linear heat generation rate precluding centerline melt are determined as a function of fuel rod average exposure. The determination of these values includes allowance of sufficient margin to accommodate the uncertainties in the thermal evaluations described in Subsection 4.4.2.9a. To preclude fuel centerline melting, these values are observed as an overpower limit for Condition I and II events, and employed as a basis for overpower protection system setpoints.

Fuel rod thermal evaluations are performed at various burnups to assure that this design basis as well as the fuel integrity design bases given in Section 4.2 is met.

4.4.1.3 Core Flow Design Basis

a. Basis

A minimum of 91.7 percent of the thermal flow rate will pass through the fuel rod region of the core and be effective for fuel rod cooling. Coolant flow through the thimble tubes, as well as the leakage from flow paths outside the core including the core barrel-baffle region, are not considered effective for heat removal.

b. Discussion

As noted in section 4.4.1.1, in core cooling evaluations the flow rate entering the reactor vessel is assumed to be the minimum measured flow rate (MMF), when the WRB-2M correlation and RTDP are applicable, and the thermal design flow rate (TDF) otherwise. A maximum of 6.8 percent of the MMF value is allotted as bypass flow. Similarly, a maximum of 8.3 percent of the TDF value is allotted as bypass flow. These values include rod cluster control guide thimble cooling flow for the case of all thimble plug assemblies removed, head cooling flow, baffle leakage, leakage to the vessel outlet nozzle, and the effect of IFM grids.

4.4.1.4 Hydrodynamic Stability Design Basis

Modes of operation associated with Conditions I and II events shall not lead to hydrodynamic instability.

4.4.1.5 Other Considerations

The above design bases, together with the fuel clad and fuel assembly design bases given in Subsection 4.2.1, are sufficiently comprehensive so additional limits are not required.

Fuel rod diametral gap characteristics, moderator-coolant flow velocity and distribution, and moderator void are not inherently limiting. Each of these parameters is incorporated into the thermal and hydraulic models used to ensure the above-mentioned design criteria are met. For instance, the fuel rod diametral gap characteristics change with time (see Subsection 4.2.3.3) and the fuel rod integrity is evaluated on that basis. The effect of the moderator flow velocity and distribution (see Subsection 4.4.2.2) and moderator void distribution (see Subsection 4.4.2.4) are included in the core thermal (VIPRE-01) evaluation and thus affect the design bases.

Meeting the fuel clad integrity criteria covers possible effects of clad temperature limitations. As noted in Subsection 4.2.3.3, the fuel rod conditions change with time. A single clad temperature limit for Condition I or Condition II events is not appropriate since, of necessity, it would be overly conservative. A clad temperature limit is applied to the loss-of-coolant accident (Subsection 15.6.5), control rod ejection accident, and locked rotor accident.

4.4.2 Description

4.4.2.1 Summary Comparison

Values of pertinent parameters, along with critical heat flux ratios, fuel temperatures and linear heat generation rates, are presented in Table 4.4-1 for both the Seabrook Station cycle 10 and the uprate cycles for all coolant loops in service. The thermal and hydraulic analyses cover both an uprate to 3659 MWt and any intermediate uprates between 3411 and 3659 MWt. It is also noted, that in this power capability evaluation there has not been any change in the design criteria. The reactor is still designed to meet the DNB design criterion of Section 4.4.1.1, as well as no fuel centerline melting during normal operation, operational transients and faults of moderate frequency.

All DNB analyses were performed such that the DNBR margins are available for offsetting rod bow penalties, RCS flow anomaly and any other DNB penalties that may occur and for flexibility in design.

Fuel densification has been considered in the DNB and fuel temperature evaluations.

4.4.2.2 Critical Heat Flux Ratio or Departure from Nucleate Boiling Ratio and Mixing Technology

The minimum DNBRs for the rated power, design overpower and anticipated transient conditions are given in Table 4.4-1. The minimum DNBR in the limiting flow channel is usually downstream of the peak heat flux location (hot spot) due to the increased downstream enthalpy rise.

DNBRs are calculated by using the correlation and definitions described in the following Subsections 4.4.2.2a and 4.4.2.2b. The VIPRE-01 computer code (discussed in Subsection 4.4.4.5a) is used to determine the flow distribution in the core and the local conditions in the hot channel for use in the DNB correlation. The use of hot channel factors is discussed in Subsection 4.4.4.3a (nuclear hot channel factors) and in Subsection 4.4.2.2d (hot channel factors).

a. Departure from Nucleate Boiling Technology

The WRB-2M DNB correlation is used to evaluate critical heat flux in the fuel assemblies. The W-3 or the WRB-2 correlation is used where the WRB-2M correlation is not applicable. These correlations are tested against DNB test data in order to establish correlation limits which satisfy the DNB design basis stated in Section 4.4.1.1.

b. Definition of Departure from Nucleate Boiling Ratio (DNBR)

The DNB heat flux ratio (DNBR) as applied to this design when all flow cell walls are heated, is:

$$DNBR = \frac{q''_{DNB,N}}{q''_{loc}} \qquad (4.4\text{-}1)$$

where:

$$q''_{DNB,N} = \frac{q''_{DNB,EU}}{F} \qquad (4.4\text{-}2)$$

$q''_{DNB,EU}$ is the uniform DNB heat flux as predicted by the WRB-2M (Reference 9), WRB-2 (References 79 and 80) or W-3 (Reference 8) DNB correlation.

F is the flux shape factor to account for nonuniform axial heat flux distributions (Reference 8) with the "C" term modified as in Reference 3.

q''_{loc} is the actual local heat flux.

A multiplier of 0.88 is applied for all DNB analyses using the W-3 correlation.

The DNBR when a cold wall is present is the same as equation 4.4-1 above when the WRB-2M correlation is applied. When the W-3 correlation is applied, the DNBR is:

$$DNBR = \frac{q''_{DNB,\,N,\,CW}}{q''_{loc}} \tag{4.4-4}$$

where:

$$CWF = 1.0 - Ru\left[13.76 - 1.37e^{1.78x} - 4.732\left\{\frac{G}{10^6}\right\}^{-0.0535} - 0.0619\left\{\frac{P}{1000}\right\}^{0.14} - 8.50Dh^{0.107}\right] \tag{4.4-6}$$

and Ru = 1 - De/Dh.

Values of minimum DNBR provided in Table 4.4-1 and Table 4.4-2 are the limiting values obtained by applying the above two definitions of DNBR to the appropriate cell (typical cell with all walls heated, or a thimble cold wall cell with a partial heated wall condition).

c. Mixing Technology

1. Flow Mixing

The subchannel mixing model incorporated in the VIPRE-01 Code and used in reactor design is based on experimental data (Reference 17). The mixing vanes incorporated in the spacer grid design induce additional flow mixing between the various flow channels in a fuel assembly as well as between adjacent assemblies. This mixing reduces the enthalpy rise in the hot channel resulting from local power peaking or unfavorable mechanical tolerances.

2. Thermal Diffusion

The rate of heat exchange by mixing between flow channels is proportional to the difference in the local mean fluid enthalpy of the respective channels of the local fluid density and flow velocity. The proportionality is expressed by the dimensionless thermal diffusion coefficient (TDC) which is defined as:

$$TDC = \frac{w'}{\rho V a} \qquad (4.4\text{-}7)$$

where:

w' = flow exchange rate per unit length, (lb_m/ft-sec)

ρ = fluid density, lb_m/ft^3

V = fluid velocity, ft/sec

a = lateral flow area between channels per unit length, ft^2/ft

The application of the TDC in the VIPRE-01 analysis for determining the overall mixing effect or heat exchange rate is presented in Reference 81.

As a part of an ongoing research and development program, Westinghouse has sponsored and directed mixing tests at Columbia University (Reference 12). These series of tests, using the "R" mixing vane grid design on 13, 26 and 32 inch grid spacing, were conducted in pressurized water loops at Reynolds numbers similar to that of PWR core under the following single and two phase (subcooled boiling) flow conditions:

Pressure	1500 to 2400 psia
Inlet temperature	332 to 642°F
Mass velocity	1.0 to 3.5×10^6 $lb_m/hr\text{-}ft^2$
Reynolds number	1.34 to 7.45×10^5
Bulk outlet quality	-52.1 to 13.5%

TDC is determined by comparing code predictions with the measured subchannel exit temperatures. Data for 26 inch axial grid spacing are presented in Figure 4.4-1 where the thermal diffusion coefficient is plotted versus the Reynolds number. TDC is found to be independent of Reynolds number, mass velocity, pressure and quality over the ranges tested. The two-phase data (local, subcooled boiling) fell within the scatter of the single-phase data. The effect of two-phase flow on the value of TDC has been demonstrated by Cadek (Reference 12), Rowe and Angle (References 13 and 14), and Gonzalez-Santalo and Griffith (Reference 15). In the subcooled boiling region, the values of TDC were indistinguishable from the single-phase values. In the quality region, Rowe and Angle show that in the case with rod spacing similar to that in PWR reactor core geometry, the value of TDC increased with quality to a point and then decreased, but never below the single-phase value. Gonzalez-Santalo and Griffith showed that the mixing coefficient increased as the void fraction increased.

The data from these tests on the "R" grid showed that a design TDC value of 0.038 (for 26 inch grid spacing) can be used in determining the effect of coolant mixing.

A mixing test program similar to the one described above was conducted at Columbia University for the 17x17 geometry and mixing vane grids on 26 inch spacing (Reference 16). The mean value of TDC obtained from these tests was 0.059, and all data was well above the current design value of 0.038.

Since the actual reactor grid spacing is approximately 20 inches, additional margin is available for this design, as the value of TDC increases as grid spacing decreases (Reference 12).

The inclusion of three intermediate flow mixer grids in the upper span of the RFA (w IFMs) results in a grid spacing of approximately 10 inches. Per Reference 80, a TDC value of 0.038 was chosen as a conservatively low value for use in RFA (w IFMs) to determine the effect of constant mixing in the core thermal performance analysis.

3. Inlet Flow Maldistribution

A conservatively low total core inlet flow is used in VIPRE-01 subchannel analysis. The applicable core inlet flow is reduced by a cycle-specific factor accounting for the effect of inlet flow maldistribution on core thermal performance. Determination of the flow reduction factor is discussed in Subsection 4.4.4.2b.

4. Flow Redistribution

Redistribution of flow in the hot channel resulting from the high flow resistance in the channel due to local or bulk boiling and the effect of the nonuniform power distribution is inherently considered in the VIPRE-01 analysis for every operating condition which is evaluated.

d. Hot Channel Factors

The total hot channel factors for heat flux and enthalpy rise are defined as the maximum-to-core average ratios of these quantities. The heat flux hot channel factor considers the local maximum linear heat generation rate at a point (the hot spot), and the enthalpy rise hot channel factor involves the maximum integrated value along a channel (the hot channel).

Each of the total hot channel factors considers a nuclear hot channel factor (see Subsection 4.4.4.3) describing the neutron power distribution and an engineering hot channel factor which allows for fabrication tolerances.

1. Heat Flux Engineering Hot Channel Factor, F_Q^E

   The heat flux engineering hot channel factor is used to evaluate the maximum heat flux. This subfactor has a value of 1.03 and is determined by statistically combining the tolerances for the fuel pellet diameter, density, enrichment, and burnable absorber. Measured manufacturing data on Westinghouse 17x17 fuel were used to verify that this value was not exceeded for 95 percent of the limiting fuel rods at a 95 percent confidence level. Thus, it is expected that a statistical sampling of the fuel assemblies of this plant will yield a value no larger than 1.03. As shown in Reference 30, no DNB penalty needs to be taken for the relatively low intensity heat flux spikes caused by variations in the above parameter as well as fuel pellet eccentricity and fuel rod diameter variations.

2. Enthalpy Rise Engineering Hot Channel Factor, $F_{\Delta H}^E$

   The effect of fabrication tolerances on the hot channel enthalpy rise is also considered in the core thermal subchannel analysis. The development of the WRB-2M DNBR design limit used with the RTDP included consideration of the fabrication tolerances for density, enrichment, and burnable absorber.

   Values employed in the analysis related to the above fabrication variations are based on applicable limiting tolerances, such that design values are met for 95 percent of the limiting channels at a 95 percent confidence level. Measured manufacturing data on Westinghouse 17x17 fuel show the tolerances used are conservative. In addition, each fuel assembly is checked to assure the channel spacing design criteria are met.

   When the W-3 or WRB-2 correlations are employed the effect of fabrication variations is applied in the VIPRE-01 analysis as a direct multiplier on the hot channel enthalpy rise.

e. Effects of Rod Bow on DNBR

The phenomenon of fuel rod bowing, as described in Reference 83, must be accounted for in the DNBR safety analysis of Condition I and Condition II events for each plant application. Applicable generic credits for margin resulting from retained conservatism in the evaluation of DNBR are used to offset the effect of rod bow.

For the safety analysis of Seabrook Unit I, sufficient DNBR margin was maintained to accommodate full and low flow rod bow DNBR penalties identified in Reference 4. The referenced penalties are applicable to the analyses using the WRB-2M and the WRB-2 DNB correlations.

The maximum rod bow penalty (1.3 percent DNBR) accounted for in the design safety analysis is based on an assembly average burnup of 24,000 MWd/Mtu. At burnups greater than 24,000 MWd/Mtu, credit is taken for the effect of F_H burndown, due to the decrease in fissionable isotopes and the buildup of fission product inventory, and no additional rod bow penalty is required (Reference 85).

In the upper spans of the RFA (w IFMs) fuel assembly, additional restraint is provided with the intermediate flow mixer grids such that the grid-to-grid spacing in those spans with IFM grids is approximately 10 inches compared to approximately 20 inches in the other spans. Using the NRC approved scaling factor results in predicted channel closure in the limiting 10-inch spans of less than 50-percent closure. Therefore, no rod bow DNBR penalty is required in the 10-inch spans in RFA (w IFMs) safety analyses.

4.4.2.3 Linear Heat Generation Rate

The core average and maximum LHGRs are given in Table 4.4-1. The method of determining the maximum LHGR is given in Subsection 4.3.2.2.

4.4.2.4 Void Fraction Distribution

The calculated core average and the hot subchannel maximum and average void fractions are presented in Table 4.4-2 for operation at full power with the original design hot channel factors. The void models used in the VIPRE-01 computer code are described in Subsection 4.4.2.7c. Typical normalized core flow and enthalpy rise distributions are shown in Figure 4.4-2, Figure 4.4-3 and Figure 4.4-4 for the Cycle 1 core design. The distributions are also typical of those which would be found in later operating cycles.

4.4.2.5 Core Coolant Flow Distribution

Assembly average coolant mass velocity and enthalpy at various radial and axial core locations are given below. Typical coolant enthalpy rise and flow distributions are shown for the 4 foot elevation (1/3 of core height) in Figure 4.4-2, and 8 foot elevation (2/3 of core height) in Figure 4.4-3 and at the core exit in Figure 4.4-4. These distributions are for the full power conditions as given in Table 4.4-1 and for the radial power density distribution shown in Figure 4.3-7, which correspond to the Cycle 1 core design. The values are also typical for later operating cycles. The analysis for this case utilized a uniform core inlet enthalpy and inlet flow distribution. No orificing is employed in the reactor design.

4.4.2.6 Core Pressure Drops and Hydraulic Loads

a. Core Pressure Drops

The analytical model and experimental data used to calculate the pressure drops shown in Table 4.4-1 are described in Subsection 4.4.2.7. The core pressure drop includes the fuel assembly, lower core plate, and upper core plate pressure drops. The full power operation pressure drop values shown in Table 4.4-1 are the unrecoverable pressure drops across the vessel, including the inlet and outlet nozzles, and across the core. These pressure drops are based on a best estimate flow of 402,000 gpm, 3659 MWt and core inlet temperature of 556.8°F.

Uncertainties associated with the core pressure drop values are discussed in Subsection 4.4.2.9b.

b. Hydraulic Loads

The fuel assembly hold down springs, Figure 4.2-2, are designed to keep the fuel assemblies in contact with the lower core plate under all Condition I and II events, with the exception of the turbine overspeed transient associated with a loss of external load. The hold down springs are designed to tolerate the possibility of an over deflection associated with fuel assembly liftoff for this case, and provide contact between the fuel assembly and the lower core plate following this transient. More adverse flow conditions occur during a loss-of-coolant accident. These conditions are presented in Subsection 15.6.5.

Hydraulic loads at normal operating conditions are calculated considering the best estimate flow and accounting for the best estimate core bypass flow based on manufacturing tolerances. Core hydraulic loads at cold plant startup conditions are based on the cold best estimate flow, but are adjusted to account for the coolant density difference. Conservative core hydraulic loads for a pump overspeed transient, which could possibly create flow rates 18 percent greater than the best estimate flow, are evaluated to be approximately twice the fuel assembly weight. Applicable uncertainties are applied to these results.

4.4.2.7 Correlation and Physical Data

a. Surface Heat Transfer Coefficients

Forced convection heat transfer coefficients are obtained from the familiar Dittus-Boelter correlation (Reference 20), with the properties evaluated at bulk fluid conditions:

$$\frac{hDe}{K} = 0.023\left(\frac{D_e G}{\mu}\right)^{0.8}\left(\frac{C_p \mu}{K}\right)^{0.4} \qquad (4.4\text{-}8)$$

where:

h = heat transfer coefficient, (Btu/hr-ft^2°F)

D_e = equivalent diameter, (ft)

K = thermal conductivity, (Btu/hr-ft-°F)

G = mass velocity, (lb_m/hr-ft^2)

μ = dynamic viscosity, (lb_m/ft-hr)

C_P = heat capacity, (Btu/lb_m -°F)

This correlation has been shown to be conservative (Reference 21) for rod bundle geometries with pitch-to-diameter ratios in the range used by PWRs.

The onset of nucleate boiling occurs when the clad wall temperature reaches the amount of superheat predicted by Thom's correlation, Reference 22. After this occurrence the outer clad wall temperature is determined by:

$$\Delta T_{sat} = (0.072 \exp(-P/1260))\,(q'')^{0.5} \qquad (4.4\text{-}9)$$

where:

ΔT_{sat} = wall superheat, $T_w - T_{sat}$, (°F)

q" = wall heat flux, (Btu/hr-ft^2)

P = pressure, (psia)

T_w = outer clad wall temperature, (°F)

T_{sat} = saturation temperature of coolant at P, (°F)

b. Total Core and Vessel Pressure Drop

Unrecoverable pressure losses occur as a result of viscous drag (friction) and/or geometry changes (form) in the fluid flow path. The flow field is assumed to be incompressible, turbulent, single- phase water. These assumptions apply to the core and vessel pressure drop calculations for the purpose of establishing the primary loop flow rate. Two-phase considerations are neglected in the vessel pressure drop evaluation because the core average void is negligible (see Table 4.4-2). Two-phase flow considerations in the core thermal subchannel analyses are considered and the models are discussed in Subsection 4.4.4.2c. Core and vessel pressure losses are calculated by equations of the form:

$$P_L = \left(K + \frac{F L}{D_e} \right) \frac{\rho V^2}{2 g_c (144)} \qquad (4.4\text{-}10)$$

Where:

P_L = unrecoverable pressure drop, (lb_f/in^2)

ρ = fluid density, (lb_m/ft^3)

L = length, (ft)

D_e = equivalent diameter, (ft)

V = fluid velocity, (ft/sec)

g_c = $32.174 \frac{lb_m - ft}{lb_f - sec^2}$

K = form loss coefficient, dimensionless

F = friction loss coefficient, dimensionless

Fluid density is assumed to be constant at the appropriate value for each component in the core and vessel. Because of the complex core and vessel flow geometry, precise analytical values for the form and friction loss coefficients are not available. Therefore, experimental values for these coefficients are obtained from geometrically similar models.

Values are quoted in Table 4.4-1 for unrecoverable pressure loss across the reactor vessel, including the inlet and outlet nozzles and across the core. The results of full-scale tests of core components and fuel assemblies were utilized in developing the core pressure loss characteristic. The pressure drop for the vessel was obtained by combining the core loss with correlation of 1/7th scale model hydraulic test data on a number of vessels (References 23 and 24) and form loss relationships (Reference 25). Moody curves (Reference 26) were used to obtain the single-phase friction factors.

c. Void Fraction Correlation

Empirical correlations are used in VIPRE to model the void fraction in two-phase flow. The subcooled void correlation used to model the non-equilibrium transition from single phase to nucleate boiling is given in Reference 81. The bulk (saturated) void model relates flow quality with void fraction which can account for phase slip.

4.4.2.8 Thermal Effects of Operational Transients

DNB core safety limits are generated as a function of coolant temperature, pressure, core power and axial power imbalance. Steady state operation within these safety limits insures that the minimum DNBR is not less than the safety analysis limit. Figure 15.0-1 shows the safety analysis limit lines and the resulting Overtemperature ΔT trip lines (which become part of the Technical Specifications or Core Operating Limits Report), plotted as ΔT, versus T_{avg} for various pressures. This system provides adequate protection against anticipated operational transients that are slow with respect to fluid transport delays in the primary system. In addition, for fast transients, e.g., uncontrolled rod bank withdrawal at power incident (Subsection 15.4.2), specific protection functions are provided as described in Section 7.2 and the use of these protection functions is described in Chapter 15.

4.4.2.9 Uncertainties in Estimates

a. Uncertainties in Fuel and Clad Temperatures

As discussed in paragraph 4.4.2.11, the fuel temperature is a function of crud, oxide, clad, pellet-clad gap, and pellet conductances. Uncertainties in the fuel temperature calculation are essentially of two types: fabrication uncertainties, such as variations in the pellet and clad dimensions and the pellet density; and model uncertainties, such as variations in the pellet conductivity and the gap conductance. These uncertainties have been quantified by comparison of the thermal model to the inpile thermocouple measurements, (References 40 - 46) by out-of-pile measurements of the fuel and clad properties, (References 47 - 58) and by measurements of the fuel and clad dimensions during fabrication. The resulting uncertainties are then used in all evaluations involving the fuel temperature. The effect of densification on fuel temperature uncertainties is also included in the calculation of the total uncertainty.

In addition to the temperature uncertainty described above, the measurement uncertainty in determining the local power and the effect of density and enrichment variations on the local power are considered in establishing the heat flux hot channel factor. These uncertainties are described in paragraph 4.3.2.2.1. Reactor trip setpoints, as specified in the Technical Specifications, include allowance for instrument and measurement uncertainties such as calorimetric error, instrument drift and channel reproducibility, temperature measurement uncertainties, noise, and heat capacity variations.

Uncertainty in determining the cladding temperature results from uncertainties in the crud and oxide thicknesses. Because of the excellent heat transfer between the surface of the rod and the coolant, the film temperature drop does not appreciably contribute to the uncertainty.

b. Uncertainties in Pressure Drops

Core and vessel pressure drops based on a measured flow, as described in Section 5.1, are quoted in Table 4.4-1. The uncertainties quoted are based on the uncertainties in both the test results and the analytical extension of these values to the reactor application.

A major use of the core and vessel pressure drops was to determine the primary system coolant flow rates as discussed in Section 5.1. As discussed in Subsection 4.4.5.1, tests on the primary system prior to initial criticality were made to verify

that conservative primary system coolant flow has been used in the mechanical design and safety analyses of the plant.

c. Uncertainties Due to Inlet Flow Maldistribution

The effects of uncertainties in the inlet flow maldistribution criteria used in the core thermal analyses are discussed in Subsection 4.4.4.2b.

d. Uncertainty in DNB Correlation

The uncertainty in the DNB correlation (Subsection 4.4.2.2) can be written as a statement on the probability of not being in DNB based on the statistics of the DNB data. This is discussed in Subsection 4.4.2.2b.

e. Uncertainties in DNBR Calculations

The uncertainties in the DNBRs calculated by VIPRE-01 analysis (see Subsection 4.4.4.5a) with the RTDP are accounted for as discussed in Section 4.4.1.1. For those transients that do not use RTDP, the uncertainties are applied directly to the VIPRE-01 input parameters. The results of a sensitivity study (Reference 18) show that the minimum DNBR in the hot channel is relatively insensitive to variations in the core-wide-radial power distribution (for the same value of F_H).

The ability of the VIPRE-01 computer code to accurately predict flow and enthalpy distributions in rod bundles is discussed in Subsection 4.4.4.5a and in Reference 81.

f. Uncertainties in Flow Rates

The uncertainties associated with loop flow rates are discussed in Section 5.1. For core thermal performance evaluations, a minimum loop flow is used which is less than the best estimate loop flow. In addition, up to 8.3 percent of the thermal design flow is assumed to be ineffective for core heat removal capability because it bypasses the core through the various available vessel flow paths described in Subsection 4.4.4.2a.

g. Uncertainties in Hydraulic Loads

As discussed in Subsection 4.4.2.6b, applicable uncertainties are applied to the hydraulic loads on the fuel assembly that are calculated using best estimate flows.

h. Uncertainty in Mixing Coefficient

The value of the mixing coefficient, TDC, used in VIPRE-01 analyses for this application is 0.038. The mean value of TDC obtained in the "R" grid mixing tests described in Subsection 4.4.2.2a was 0.042 (for 26 inch grid spacing). The value 0.038 is one standard deviation below the mean value; approximately 90 percent of the data give values of TDC greater than 0.038 (Reference 12).

The results of the mixing tests done on 17x17 geometry, as discussed in Subsection 4.4.2.2c, had a mean value of TDC of 0.059 and standard deviation of $\sigma = 0.007$. Hence the current design value of TDC is almost 3 standard deviations below the mean for 26 inch grid spacing.

4.4.2.10 Flux Tilt-Considerations

Significant quadrant power tilts are not anticipated during normal operation since this phenomenon is caused by some asymmetric perturbation. A dropped or misaligned Rod Cluster Control Assembly could cause changes in hot channel factors. However, these events are analyzed separately in Chapter 15.

Other possible causes for quadrant power tilts include X-Y xenon transients, inlet temperature mismatches, enrichment variations within tolerances and so forth.

In addition to unanticipated quadrant power tilts as described above, other readily explainable asymmetries may be observed during calibration of the excore detector quadrant power tilt alarm. During operation, incore maps are taken at least once per month and, periodically, additional maps are obtained for calibration purposes. Each of these maps is reviewed for deviations from the expected power distributions. Asymmetry in the core, from quadrant to quadrant, is frequently a consequence of the design when assembly and/or component shuffling and rotation requirements do not allow exact symmetry preservation. In each case, the acceptability of an observed asymmetry, planned or otherwise, depends solely on meeting the required accident analyses assumptions.

In practice, once acceptability has been established by review of the incore maps, the quadrant power tilt alarms and related instrumentation are adjusted to indicate zero Quadrant Power Tilt Ratio as the final step in the calibration process. This action ensures that the instrumentation is correctly calibrated to alarm in the event an unexplained or unanticipated change occurs in the quadrant to quadrant relationships between calibration intervals. Proper functioning of the quadrant power tilt alarm is significant because no allowances, beyond accounting for the maximum tilt allowed by Technical Specifications, are made in the design for increased hot channel factors due to unexpected developing flux tilts, since all likely causes are prevented by

design or procedures, or are specifically analyzed. Finally, in the event that unexplained flux tilts do occur, the Technical Specifications (Subsection 3/4.2.4) provide appropriate corrective actions to ensure continued safe operation of the reactor.

4.4.2.11 Fuel and Cladding Temperatures

Consistent with the thermal-hydraulic design bases described in Subsection 4.4.1, the following discussion pertains mainly to fuel pellet temperature evaluation. A discussion of fuel clad integrity is presented in Subsection 4.2.3.1.

The thermal-hydraulic design assures that the maximum fuel temperature is below the melting point of $U0_2$ (melting point of 5080°F (Reference 1) unirradiated and decreasing by 58°F per 10,000 MWd/Mtu). To preclude center melting, and as a basis for overpower protection system setpoints, cycle-specific values for the peak linear heat generation rate precluding centerline melt are determined as a function of fuel rod average exposure. These are observed as an overpower limit for Condition I and II events. They provide sufficient margin for uncertainties in the thermal evaluations described in Subsection 4.4.2.9a. The temperature distribution within the fuel pellet is predominantly a function of the local power density and the $U0_2$ thermal conductivity. However, the computation of radial fuel temperature distributions combines crud, oxide, clad gap and pellet conductances. The factors which influence these conductances, such as gap size (or contact pressure), internal gas pressure, gas composition, pellet density, and radial power distribution within the pellet, etc., have been combined into a Westinghouse semi-empirical thermal model (see Subsection 4.2.3.3) with the model modifications for time dependent fuel densification given in Reference 2. This thermal model enables the determination of these factors and their net effects on temperature profiles. The temperature predictions have been compared to inpile fuel temperature measurements (References 40-46 and 59) and melt radius data (References 60 and 61).

As described in Reference 2, fuel rod thermal evaluations (fuel centerline, average and surface temperatures) are determined throughout the fuel rod life-time with consideration of time dependent densification. To determine the maximum fuel temperatures, various burnup rods, including the highest burnup rod, are analyzed over the rod linear power range of interest.

The principal factors which are employed in the determination of the fuel temperature are discussed below.

a. $U0_2$ Thermal Conductivity

The thermal conductivity of uranium dioxide was evaluated from data reported from a number of measurements.

At the higher temperatures, thermal conductivity is best obtained by utilizing the integral conductivity to melt which can be determined with more certainty. From an examination of the data, it has been concluded that the best estimate for the value of 2800°C Kdt is 93 watts/cm.

The design curve is in excellent agreement with the recommendation of the IAEA panel (Reference 36).

b. Radial Power Distribution in $U0_2$ Fuel Rods

An accurate description of the radial power distribution as a function of burnup is needed for determining the power level for incipient fuel melting and other important performance parameters such as pellet thermal expansion, fuel swelling and fission gas release rates.

Radial power distribution in UO_2 fuel rods is determined with the neutron transport code LASER. The LASER code has been validated by comparing the code predictions on radial burnup and isotopic distributions with measured radial microdrill data (References 62 and 63). A "radial power depression factor," f, is determined using radial power distributions predicted by LASER. The factor, f, enters into the determination of the pellet centerline temperature, T_C, relative to the pellet surface temperature, T_S, through the expression:

$$\int_{T_s}^{T_c} K(T)\, dT = \frac{q'' f}{4\pi}$$

where:

K(T) = the thermal conductivity for $U0_2$ with a uniform density distribution

q' = the linear power generation rate.

c. Gap Conductance

The temperature drop across the pellet-clad gap is a function of the gap size and the thermal conductivity of the gas in the gap. The gap conductance model is selected such that when combined with the UO_2 thermal conductivity model, the calculated fuel centerline temperatures reflect the inpile temperature measurements. A more detailed discussion of the gap conductance model is presented in Reference 64.

d. Surface Heat Transfer Coefficients

The fuel rod surface heat transfer coefficients during subcooled forced convection and nucleate boiling are presented in Subsection 4.4.2.7a.

e. Fuel Clad Temperatures

The outer surface of the fuel rod at the hot spot operates at a temperature of approximately 660°F for steady operation at rated power throughout core life due to the onset of nucleate boiling. Initially (beginning-of-life), this temperature is that of the clad metal outer surface.

During operation over the life of the core, the buildup of oxides and crud on the fuel rod surface causes the clad surface temperature to increase. Allowance is made in the fuel center melt evaluation for this temperature rise. Since the thermal-hydraulic design basis limits DNB, adequate heat transfer is provided between the fuel clad and the reactor coolant so that the core thermal output is not limited by considerations of clad temperature.

f. Treatment of Peaking Factors

The total heat flux hot channel factor, F_Q, is defined by the ratio of the maximum to core average heat flux. As presented in Table 4.3-2 and discussed in Subsection 4.3.2.2f, the design value of F_Q for normal operation is 2.50. This results in a peak linear power of 14.6 kW/ft at full power conditions.

The centerline temperature must be below the $U0_2$ melt temperature over the lifetime of the rod, including allowances for uncertainties. The fuel temperature design basis is discussed in Subsection 4.4.1.2. The centerline temperature resulting from overpower transients/operator errors is below that required to produce melting.

4.4.3 Description of the Thermal and Hydraulic Design of the Reactor Coolant System

4.4.3.1 Plant Configuration Data

Plant configuration data for the thermal hydraulic and fluid systems external to the core are provided in the appropriate Chapters 5, 6, and 9. Implementation of the Emergency Core Cooling System (ECCS) is discussed in Chapter 15. Some specific areas of interest are the following:

a. Total coolant flow rates for the Reactor Coolant System (RCS) and each loop are provided in Table 5.1-1. Flow rates employed in the evaluation of the core are presented in Section 4.4.

b. Total RCS volume including pressurizer and surge line, RCS liquid volume including pressurizer water at steady state power conditions are given in Table 5.1-1.

c. The flow path length through each volume may be calculated from physical data provided in the above referenced tables.

d. The height of fluid in each component of the RCS may be determined from the physical data presented in Section 5.4. The components of the RCS are water filled during power operation with the pressurizer being approximately 60 percent water filled.

e. Components of the ECCS are to be located so as to meet the criteria for net positive suction head described in Section 6.3.

f. Line lengths and sizes for the Safety Injection System are determined so as to guarantee a total system resistance which will provide, as a minimum, the fluid delivery rates assumed in the safety analyses described in Chapter 15.

g. The parameters for components of the RCS are presented in Section 5.4, component and subsystem design.

h. The steady state pressure drops and temperature distributions through the RCS are presented in Table 5.1-1.

4.4.3.2 Operating Restrictions on Pumps

The minimum net positive action head (NPSH) and minimum seal injection flow rate must be established before operating the reactor coolant pumps. With the minimum 6 gpm labyrinth seal injection flow rate established, the operator will have to verify that the system pressure satisfies NPSH requirements.

4.4.3.3 Power-Flow Operating Map (BWR)

Not applicable to pressurized water reactors.

4.4.3.4 Temperature-Power Operating Map

The relationship between Reactor Coolant System temperature and power is shown in Figure 4.4-6.

The effects of reduced core flow due to inoperative pumps is discussed in Subsections 5.4.1, 15.3.1, and 15.3.2. Natural circulation capability of the system is demonstrated in Subsection 15.2.6.

4.4.3.5 Load Following Characteristics

The Reactor Coolant System is designed on the basis of steady state operation at full power heat load. The reactor coolant pumps utilize constant speed drives. The reactor coolant pump assembly is described in Section 5.4. Reactor power is controlled to maintain average coolant temperature at a value which is a linear function of load, as described in Section 7.7.

4.4.3.6 Thermal and Hydraulic Characteristics Summary Table

The thermal and hydraulic characteristics are given in Table 4.4-1 and Table 4.4-2.

4.4.4 Evaluation

4.4.4.1 Critical Heat Flux

The critical heat flux correlation utilized in the core thermal analysis is explained in detail in Subsection 4.4.2.

4.4.4.2 Core Hydraulics

a. Flow Paths Considered in Core Pressure Drop and Thermal Design

The following flow paths for core bypass flow are considered:

1. Flow through the spray nozzles into the upper head for head cooling purposes.

2. Flow entering into the RCC guide thimbles to cool the control rods.

3. Leakage flow from the vessel inlet nozzle directly to the vessel outlet nozzle through the gap between the vessel and the barrel.

4. Flow introduced between the baffle and the barrel for the purpose of cooling these components and which is not considered available for core cooling.

5. Flow in the gaps between the fuel assemblies on the core periphery and the adjacent baffle wall.

The above contributions are evaluated to confirm that the design value of the core bypass flow is met. The design value of core bypass flow for Seabrook Station is equal to 8.3 percent of the total vessel flow when all thimble plugs are deleted.

Of the total allowance, 4.0 percent is associated with the core, item 2 above, and the remainder is associated with the internals (items 1, 3, 4 and 5 above). Calculations have been performed using drawing tolerances on a worst case basis and accounting for uncertainties in pressure losses. Based on these calculations, the core bypass flow for the plant is < 8.3 percent when all thimble plugs are deleted.

b. Inlet Flow Distributions

Data have been considered from several 1/7th scale hydraulic reactor model tests (References 23, 24, and 37) and from sensitivity studies, Reference 18, in arriving at the core inlet flow maldistribution criteria to be used in the VIPRE-01 analyses (see Subsection 4.4.4.5a).

The effect of the total flow rate on the inlet velocity distribution was studied in the experiments of Reference 23. As was expected, on the basis of the theoretical analysis, no significant variation could be found in inlet velocity distribution with reduced flow rate.

c. Empirical Friction Factor Correlations

Two empirical friction factor correlations are used in the VIPRE-01 computer code (described in Subsection 4.4.4.5a).

The friction factor in the axial direction, parallel to the fuel rod axis, is evaluated using the correlations described in Reference 81).

The flow in the lateral directions, normal to the fuel rod axis, views the reactor core as a large tube bank. Thus, the lateral friction factor proposed by Idel'chik (Reference 25) is applicable. This correlation is of the form:

$$F_L = A\ Re_L^{-0.2} \qquad (4.4\text{-}12)$$

where:

A is a function of the rod pitch and diameter as given in Reference 25.

Re_L is the lateral Reynolds number based on the rod diameter.

4.4.4.3 Influence of Power Distribution

The core power distribution, which is largely established at beginning-of-life by fuel enrichment, loading pattern, and core power level is also a function of variables such as control rod worth and position, and fuel depletion throughout lifetime. Radial power distributions in various planes of the core are often illustrated for general interest; however, the core radial enthalpy rise distribution as determined by the integral of power up each channel is of greater importance for DNB analyses. These radial power distributions, characterized by F_H (defined in paragraph 4.3.2.2.1), as well as axial heat flux profiles are discussed in the following two paragraphs.

4.4.4.3.1 Nuclear Enthalpy Rise Hot Channel Factor, FH

Given the local power density q' (kW/ft) at a point x, y, z in a core with N fuel rods and height H,

$$F_{\Delta H}^{N} = \frac{\text{Hot rod power}}{\text{average rod power}} = \frac{MAX \int_0^H q'(x_0, y_0, z_0)dz}{\frac{1}{N}\sum_{\substack{all \\ rods}} \int_0^H q'(x, y, z)dz}$$

The way in which F_H is used in the DNB calculation is important. The location of minimum DNBR depends on the axial profile, and the value of DNBR depends on the enthalpy rise to that point. Basically, the maximum value of the rod integral is used to identify the most likely rod for minimum DNBR. An axial power profile is obtained which, when normalized to the design value of F_H, recreates the axial heat flux along the limiting rod. The surrounding rods are assumed to have the same axial profile with rod average powers which are typical distributions found in hot assemblies. In this manner, worst-case axial profiles can be combined with worst-case radial distributions for reference DNB calculations.

It should be noted again that F_H is an integral and is used as such in DNB calculations. Local heat fluxes are obtained by using hot channel and adjacent channel explicit power shapes which take into account variations in horizontal power shapes throughout the core.

For operation at a fraction of full power, the design F_H used is given by:

$$F^N_{\Delta H} = F^{RTD}_{\Delta H} [1 + PF_{\Delta H}(1 - P)]$$

$F^{RTP}_{\Delta H}$ is the limit at rated thermal power (RTP) specified in the core Operating Limits Report (COLR).

$PF_{\Delta H}$ is the power factor multiplier for F_H specified in the COLR.

P is the fraction of rated thermal power.

The permitted relaxation of F_H is included in the DNB protection setpoints and allows radial power shape changes with rod insertion to the insertion limits, (Reference 84) thus allowing greater flexibility in the nuclear design.

4.4.4.3.2 Axial Heat Flux Distributions

As discussed in paragraph 4.3.2.2, the axial heat flux distribution can vary as a result of rod motion or power change or as a result of a spatial xenon transient which may occur in the axial direction. Consequently, it is necessary to measure the axial power imbalance by means of the excore nuclear detectors (as discussed in paragraph 4.3.2.2.7) and to protect the core form excessive axial power imbalance. The reference axial shape used in establishing core DNB limits (that is, overtemperature $\triangle T$ protection system setpoints) is a chopped cosine with a peak-to-average value of 1.55. The reactor trip system provides automatic reduction of the trip setpoints on excessive axial power imbalance. To determine the magnitude of the setpoint reduction, the reference shape is supplemented by other axial shapes skewed to the bottom and top of the core.

The course of those accidents in which DNB is a concern is analyzed in chapter 15 assuming that the protection setpoints have been set on the basis of these shapes. In many cases, the axial power distribution in the hot channel changes throughout the course of the accident due to rod motion, coolant temperature, and power level changes.

The initial conditions for the accidents for which DNB protection is required are assumed to be those permissible within the specified axial offset control limits described in paragraph 4.3.2.2. In the case of the loss-of-flow accident, the hot channel heat flux profile is very similar to the power density profile in normal operation preceding the accident.

4.4.4.4 Core Thermal Response

A general summary of the steady state thermal-hydraulic design parameters including thermal output, flow rates, etc., is provided in Table 4.4-1 for all loops in operation.

As stated in Subsection 4.4.1, the design bases of the application are to prevent DNB and to prevent fuel melting for Condition I and II events. The protective systems described in Chapter 7 are designed to meet these bases. The response of the core to Condition II transients is given in Chapter 15.

4.4.4.5 Analytical Techniques

a. Core Analysis

The objective of reactor core thermal design is to determine the maximum heat-removal capability in all flow subchannels and to show that the core safety limits are not exceeded using the most conservative power distribution. The thermal design takes into account local variations in dimensions, power generation, flow redistribution, and mixing. VIPRE-01 is a realistic three-dimensional matrix model which has been developed to account for hydraulic and nuclear effects on the enthalpy rise in the core. (Reference 81). The behavior of the hot assembly is determined by superimposing the power distribution among the assemblies upon the inlet flow distribution while allowing for flow mixing and flow distribution between assemblies. The local variations in power, fuel rod and pellet fabrication, and mixing within the hottest assembly are superimposed on the average conditions of the hottest assembly in order to determine the conditions in the hot channel.

b. Steady State Analysis

The VIPRE-01 computer program and subchannel analysis methodology, as approved by the NRC (Reference 81) is used to determine coolant density, mass velocity, enthalpy, vapor void, static pressure, and DNBR distributions within the reactor core hot subchannel under all expected operating conditions. The VIPRE-01 code is described in detail in Reference 81, including models and correlations used.

c. Experimental Verification

Experimental verification of VIPRE-01 is presented in References 11 and 81.

The VIPRE-01 analysis methodology is based on a knowledge and understanding of the heat transfer and hydrodynamic behavior of the coolant flow and the mechanical characteristics of the fuel elements. VIPRE-01 analysis provides a realistic evaluation of the core performance and is used in the thermal analyses as described above.

d. Transient Analysis

The approved VIPRE-01 methodology (Reference 81) was shown to be conservative for transient thermal-hydraulic analysis.

4.4.4.6 Hydrodynamic and Flow Power Coupled Instability

Boiling flows may be susceptible to thermohydrodynamic instabilities, (Reference 69). These instabilities are undesirable in reactors since they may cause a change in thermohydraulic conditions that may lead to a reduction in the DNB heat flux relative to that observed during a steady flow condition or to undesired forced vibrations of core components. Therefore, a thermohydraulic design criterion was developed which states that modes of operation under Conditions I and II events shall not lead to thermohydrodynamic instabilities.

Two specific types of flow instabilities are considered for Westinghouse PWR operation. These are the Ledinegg or flow excursion type of static instability and the density wave type of dynamic instability.

A Ledinegg instability involves a sudden change in flow rate from one steady state to another. This instability occurs (Reference 69) when the slope of the reactor coolant system pressure drop-flow rate curve ($\delta\Delta P/\delta G$ internal) becomes algebraically smaller than the loop supply (pump head) pressure drop-flow rate curve ($\delta\Delta P/\delta G$ external). The criterion for stability is thus ($\delta\Delta P/\delta G$ internal > $\delta\Delta P/\delta G$ external). The Westinghouse pump head curve has a negative slope ($\delta\Delta P/\delta G$external < 0) whereas the reactor coolant system pressure drop-flow rate curve has a positive slope ($\delta\Delta P/\delta G$ internal > O) over the Condition I and Condition II operational ranges. Thus, the Ledinegg instability will not occur.

The mechanism of density wave oscillations in a heated channel has been described by Lahey and Moody (Reference 70). Briefly, an inlet flow fluctuation produces an enthalpy perturbation. This perturbs the length and the pressure drop of the single phase region and causes quality or void perturbations in the two phase regions which travel up the channel with the flow. The quality and length perturbations in the two-phase region create two-phase pressure drop perturbations. However, since the total pressure drop across the core is maintained by the characteristics of the fluid system external to the core, then the two-phase pressure drop perturbation feeds back to the single phase region. These resulting perturbations can be either attenuated or self-sustained.

A simple method has been developed by Ishii (Reference 71) for parallel closed channel systems to evaluate whether a given condition is stable with respect to the density wave type of dynamic instability. This method has been used to assess the stability of typical Westinghouse reactor designs (References 72, 73, 74), under Conditions I and II operation. The results indicate that a large margin to density wave instability exists, e.g., increases on the order of 150 to 200 percent of rated reactor power would be required for the predicted inception of this type of instability.

The application of the method of Ishii, Reference 71, to Westinghouse reactor designs is conservative due to the parallel open channel feature of Westinghouse PWR cores. For such cores, there is little resistance to lateral flow leaving the flow channels of high power density. There is also energy transfer from channels of high power density to lower power density channels. This coupling with cooler channels has led to the opinion that an open channel configuration is more stable than the above closed channel analysis under the same boundary conditions. Flow stability tests (Reference 75) have been conducted where the closed channel systems were shown to be less stable than when the same channels were cross connected at several locations. The cross connections were such that the resistance to channel-to-channel cross flow and enthalpy perturbations would be greater than that which would exist in a PWR core which has a relatively low resistance to cross flow.

Flow instabilities which have been observed have occurred almost exclusively in closed channel systems operating at low pressures relative to the Westinghouse PWR operating pressures. Kao, Morgan and Parker (Reference 76) analyze parallel closed channel stability experiments simulating a reactor core flow. These experiments were conducted at pressures up to 2200 psia. The results showed that for flow and power levels typical of power reactor conditions, no flow oscillations could be induced above 1200 psia.

Additional evidence that flow instabilities do not adversely affect thermal margin is provided by the data from the rod bundle DNB tests. Many Westinghouse rod bundles have been tested over wide ranges of operating conditions with no evidence of premature DNB or of inconsistent data which might be indicative of flow instabilities in the rod bundle.

In summary, it is concluded that thermohydrodynamic instabilities will not occur under Condition I and II modes of operation for Westinghouse PWR reactor designs. A large power margin, greater than doubling rated power, exists to predicted inception of such instabilities. Analysis has been performed which shows that minor plant to plant differences in Westinghouse reactor design such as fuel assembly arrays, core power to flow ratios, fuel assembly length, etc., will not result in gross deterioration of the above power margins.

4.4.4.7 Fuel Rod Behavior Effects from Coolant Flow Blockage

Coolant flow blockages can occur within the coolant channels of a fuel assembly or external to the reactor core. The effects of fuel assembly blockage within the assembly on fuel rod behavior is more pronounced than external blockages of the same magnitude. In both cases, the flow blockages cause local reductions in coolant flow. The amount of local flow reduction, where it occurs in the reactor, and how far along the flow stream the reduction persists are considerations which will influence the fuel rod behavior. The effects of coolant flow blockages in terms of maintaining rated core performance are determined both by analytical and experimental methods. The experimental data are usually used to augment analytical tools such as computer programs. Inspection of the DNB correlation (Subsection 4.4.2.2 and Reference 8) shows that the predicted DNBR is dependent upon the local values of quality and mass velocity.

Thermal-hydraulic codes are capable of predicting the effects of local flow blockages on DNBR within the fuel assembly on a subchannel basis, regardless of where the flow blockage occurs. In Reference 19, it is shown that for a fuel assembly similar to the Westinghouse design, the flow distribution within the fuel assembly when the inlet nozzle is completely blocked can be accurately predicted. Full recovery of the flow was found to occur about 30 inches downstream of the blockage. With the reference reactor operating at the nominal full power conditions specified in Table 4.4-1, the effects of an increase in enthalpy and decrease in mass velocity in the lower portion of the fuel assembly would not result in the reactor reaching a minimum DNBR below the safety analysis limit.

From a review of the open literature it is concluded that flow blockage in "open lattice cores" similar to the Westinghouse cores cause flow perturbations which are local to the blockage. For instance, A. Ohtsubol, et al. (Reference 77), show that the mean bundle velocity is approached asymptotically about 4 inches downstream from a flow blockage in a single flow cell. Similar results were also found for 2 and 3 cells completely blocked. P. Basmer, et al. (Reference 78) tested an open lattice fuel assembly in which 41 percent of the subchannels were completely blocked in the center of the test bundle between spacer grids. Their results show the stagnant zone behind the flow blockage essentially disappears after 1.65 L/De or about 5 inches for their test bundle. They also found that leakage flow through the blockage tended to shorten the stagnant zone or, in essence the complete recovery length. Thus, local flow blockages within a fuel assembly have little effect on subchannel enthalpy rise. The reduction in local mass velocity

is the main parameter which affects the DNBR. Westinghouse analysis results presented in the original Seabrook FSAR demonstrated that if the plant was operating at full power and nominal steady state conditions as specified in Table 4.4-1, a substantial reduction in local mass velocity would be required to reduce the DNBR close to the DNBR Safety Analysis Limits. The above mass velocity effect on the DNB correlation was based on the assumption of fully developed flow along the full channel length. In reality, a local flow blockage is expected to promote turbulence and thus would likely not effect DNBR at all.

Coolant flow blockages induce local crossflows as well as promote turbulence. Fuel rod behavior is changed under the influence of a sufficiently high crossflow component. Fuel rod vibration could occur, caused by this crossflow component, through vortex shedding or turbulent mechanisms. If the crossflow velocity exceeds the limit established for fluid elastic stability, large amplitude whirling results. The limits for a controlled vibration mechanism are established from studies of vortex shedding and turbulent pressure fluctuations. The crossflow velocity required to exceed fluid elastic stability limits is dependent on the axial location of the blockage and the characterization of the crossflow (jet flow or not). These limits are greater than those for vibratory fuel rod wear. Crossflow velocity above the established limits can lead to mechanical wear of the fuel rods at the grid support locations. Fuel rod wear due to flow induced vibration is considered in the fuel rod fretting evaluation (Section 4.2).

4.4.5 Testing and Verification

4.4.5.1 Tests Prior to Initial Criticality

A reactor coolant flow test was performed following fuel loading but prior to initial criticality. Elbow tap pressure drop data obtained in this test allowed determination of the coolant flow rates at reactor operating conditions. This test verified that conservative coolant flow rates have been used in the core thermal and hydraulic analysis.

4.4.5.2 Initial Power and Plant Operation

Core power distribution measurements are made at several core power levels (see Chapter 14). These tests are used to insure that conservative peaking factors are used in the core thermal and hydraulic analysis.

4.4.5.3 Component and Fuel Inspections

Inspections performed on the manufactured fuel are delineated in Subsection 4.2.4. Fabrication measurements critical to thermal and hydraulic analysis are obtained to verify that the engineering hot channel factors in the design analyses (Subsection 4.4.2.2d) are met.

4.4.6 Instrumentation Requirements

4.4.6.1 Incore Instrumentation

Instrumentation is located in the core so that radial, axial, and azimuthal core characteristics may be obtained for all core quadrants.

The incore instrumentation thimbles enter the core from the bottom and are positioned in the full length instrumentation guide tubes that are located in the center of the fuel assemblies. Figure 4.4-7 shows the location of the 58 instrumented assemblies in the core. Each thimble consists of the calibration tube for the moveable incore detectors, five fixed platinum detectors at various core heights, and a core-exit thermocouple at the tip of the thimble. The platinum detectors measure the gamma and neutron flux and are processed to determine the local power distribution. Each thermocouple measures the temperature of the fluid in the guide tube that is heated by conduction from the bulk core fluid and by gamma heating of the components in the guide tube.

The core-exit thermocouples provide a backup to the flux monitoring instrumentation for monitoring power distribution. The routine, systematic collection of thermocouple readings by the main plant computer system provides a data base. From this data base, abnormally high or abnormally low readings, quadrant temperature tilts, or systematic departures from a prior reference map can be deduced.

The Incore Detector System would be used for more detailed mapping if the thermocouple system were to indicate an abnormality. These two complementary systems are more useful when taken together than either system alone would be. The Incore Instrumentation System is described in more detail in Subsection 7.7.1.9.

The incore instrumentation is provided to obtain data from which fission power density distribution in the core, coolant enthalpy distribution in the core, and fuel burnup distribution may be determined.

4.4.6.2 Overtemperature and Overpower ΔT Instrumentation

The Overtemperature ΔT trip protects the core against low DNBR. The Overpower ΔT trip protects against excessive power (fuel rod rating protection).

As discussed in Subsection 7.2.1.1b, factors included in establishing the Overtemperature ΔT and Overpower ΔT trip setpoints include the reactor coolant temperature in each loop and the axial distribution of core power through the use of the two section excore neutron detectors.

4.4.6.3 Instrumentation to Limit Maximum Power Output

The output of the three ranges (source, intermediate, and power) of detectors, with the electronics of the nuclear instruments, is used to limit the maximum power output of the reactor within their respective ranges.

There are six radial locations containing a total of eight neutron flux detectors installed around the reactor in the primary shield, two proportional counters for the source range installed on opposite "flat" portions of the core containing the primary startup sources at an elevation approximately one quarter of the core height. Two compensated ionization chambers for the intermediate range, located in the same instrument wells and detector assemblies as the source range detectors, are positioned at an elevation corresponding to one half of the core height; four dual section uncompensated ionization chamber assemblies for the power range installed vertically at the four corners of the core and located equidistant from the reactor vessel at all points and, to minimize neutron flux pattern distortions, within one foot of the reactor vessel. Each power range detector provides two signals corresponding to the neutron flux in the upper and in the lower sections of a core quadrant. The three ranges of detectors are used as inputs to monitor neutron flux from a completely shutdown condition to 120 percent of full power with the capability of recording overpower excursions up to 200 percent of full power.

The output of the power range channels is used for:

a. The rod speed control function

b. To alert the operator to an excessive power unbalance between the quadrants

c. To protect the core against rod ejection accidents

d. To protect the core against adverse power distributions resulting from dropped rods.

Details of the neutron detectors and nuclear instrumentation design and the control and trip logic are given in Chapter 7. The limits on neutron flux operation and trip setpoints are given in the Technical Specifications and Core Operating Limits Report.

4.4.6.4 Loose Parts Monitoring System (LPMS)

The LPMS is a system provided for the detection of loose metallic parts in the primary system during preoperational testing, startup and power operation modes. The LPMS, together with the associated programmatic and reporting procedures, comprise the Loose Part Detection Program described in Regulatory Guide 1.133, Rev. 1.

A detailed comparison of the LPMS with each of the specific positions of Section C of Regulatory Guide 1.133 is presented below with exceptions and clarifications.

Reg. Guide Position	Discussion
C.1.a C.1.b	A total of sixteen loose part sensors are provided to detect loose part impacts with a kinetic energy of 0.5 ft-lb. of parts weighing between .25 lb. and 30 lbs. in the vicinity of six natural collection regions in the nuclear steam supply system. a) Two sensors on the exterior of the reactor vessel in the vicinity of the lower plenum and two sensors on the reactor vessel head lifting lugs. b) Three sensors on the exterior of each steam generator in the vicinity of the reactor coolant inlet plenum. Two sensors are normally active and one is normally passive. The normally passive sensor may be switched into the system to replace a normally active sensor or to aid in the localization of a loose part in a steam generator.
C.1.c	Two or more independently monitored sensors are provided at each natural collection region. Each of these channels is physically separated from each other at the sensors up to and including the charge converters. From there, sensor signals are routed by individual shielded cables through seismically qualified conduit and tray associated with safety-related Train A up to penetration EDE-MM-126. Outside containment, all signal cabling is routed in seismically qualified tray associated with safety-related Train A up to the control room electronics.
C.1.d C.4.e	The Automatic Data Acquisition System of the LPMS will be actuated (all active channels simultaneously) by the system electronics when the measured magnitude of the acoustic signal from any one channel exceeds the predetermined alert level for that channel. An audible alarm will alert control room personnel of any excursion above the predetermined alert level. To ensure that the data provided at the output of the system electronics is recorded to allow accurate offline analysis, the recorder is wide-band with respect to the bandwidth of the filtered data. The analog recorder

Reg. Guide Position	Discussion
	provided will use the direct (as opposed to FM) recording mode. Two selectable tape speeds are provided, allowing selection of recording bandwidth. The Automatic Data Acquisition System has a manual override.
C.1.e C.2 C.3	The alert logic of the LPMS has the following features and capabilities
C.4.b	a) Minimization of false alarms due to flow or other disturbances not indicative of metallic loose part impacts. b) Maintenance of sensitivity to metallic loose part impacts under conditions of varying background noise. c) The signal filtering process attenuates the signals due to operational disturbances outside the filter system's bandwidth. d) The alert logic is capable of functioning satisfactorily in varying background noise levels. e) To differentiate between valid impacts and plant noise associated with one-time transient events (as opposed to steady state noise), the alert module common to each group of six electronic channels of the LPMS incorporates a variable timer circuit. The alert module will not perform its functions (alarm actuation and automatic recorder actuation) unless a predetermined number of impacts (excursions above the alert level) occur within a predetermined time period. This time circuit may be disabled, by use of a selector switch, so that any single excursion above the alert level will cause the alarm module to perform its functions. f) To vary the alert level from one sensor to the other to compensate for various background noises at each sensor location. The alert level for each channel is a function of the steady state background noises measured by that channel, according to the relation:

Reg. Guide Position

Discussion

$$AL = (1 + K) BN$$

Where AL is the alert level, BN is the background noise level, and K is the fraction of the background noise level by which an impact must exceed the background in order to be detected. The K value was individually determined for each channel following initial system calibration. The K value for each channel was initially determined within two constraints:

a) The value (1 + K) BN shall be greater than the largest signal presented to the impact detection module when noise of magnitude BN is applied to the input terminals of the system electronics, as determined by factory acceptance testing of the LPMS and in situ monitoring of the signals presented to each impact detector.

b) The value (1 + K) BN (for the largest expected BN level) shall be less than the magnitude of the signal associated with the specified detectable loose part impact, as determined during initial LPMS calibration.

c) The minimum value of K consistent with the above criterion (a) was chosen and the satisfaction of criterion (b) was then verified. Satisfaction of these criteria will be periodically verified during operation in accordance with Regulatory Position 3.e of Regulatory Guide 1.133.

The alert level for power operation was submitted to the commission (in the startup report) following completion of the startup test program. If the alert level is exceeded, diagnostic steps will be taken within 72 hours to determine if a loose part is present. The safety significance of any identified loose part will be determined.
During initial startup, power operation and refueling, channel checks, monitoring audio channels, channel functional tests, background noise measurements, and channel calibrations will be performed as prescribed in the regulatory guide. A channel calibration includes the adjustments recommended by the vendor and an assessment of the overall channel

Reg. Guide Position	Discussion
	response by observing the response to a known mechanical input or by comparing the background noise spectra to baseline background noise spectra. Calibration equipment and procedures are available for review at Seabrook Station.
C.1.f	The LPMS has the capability for periodic on-line channel checks and channel functional tests in addition to on-line and off-line channel calibration.
C.1.g C.4.k	The LPMS is designed to operate under normal environmental conditions The LPMS (excluding the recording equipment) has been seismically qualified to IEEE 344-75 to be functional up to and including the Operating Basis Earthquake (OBE). The LPMS sensor, charge converter, and system cabinet are seismically supported.
C.1.h	The LPMS will be included in the Seabrook surveillance and maintenance program. Maintenance and surveillance actions will be performed in accordance with approved procedures. The documented maintenance history will be maintained and evaluated over the life of the plant. Components will be of a quality that is consistent with minimal maintenance requirements and low failure rates. In lieu of the recommendations to replace components prior to end of service life, LPMS components will be maintained on a run to failure basis. This maintenance philosophy is considered to be acceptable since the system performs no active safety functions and a minimum of two diverse sensors will be provided for each collection region. A single random failure of one sensor in a collection region will not preclude monitoring of the region. The Seabrook maintenance and corrective action programs will trend LPMS equipment degradation and increases in failure rates will initiate augmented system maintenance.
C.1.i	Recognition of a faulty channel is easily identified by a blinking LED condition. All Control Room electronics are rack-mounted, designed for the ease of replacement or repair in the event of a malfunctioning channel.

Reg. Guide Position	Discussion
C.4.a	The loose parts monitoring sensors are piezoelectric accelerometers designed for use in high temperature and high radiation environments. Two accelerometers are mounted on the reactor vessel head. These accelerometers are mounted into two of the vessel head lifting lugs. Two accelerometers are threaded into clamps on the bottom-mounted instrumentation tubes. These locations allow monitoring of the reactor vessel upper and lower plenums and facilitated the mounting of the sensors. There are three accelerometers on each steam generator, two which are normally active and the third normally passive. The two normally active sensors are located in a vertical line approximately 16 inches above and below the centerline of the tube sheet, oriented 20° on the hot leg side of the tube lane centerline. The normally passive accelerometer is located on the tube sheet centerline 90° from the other sensors but still on the hot leg side of the tube lane centerline. These accelerometers are mounted on the side of the steam generator. All steam generator sensors are capable of monitoring the steam generator reactor coolant inlet plenum. They are dispersed to assist in localization of a loose part.
C.4.c	Anticipated major sources of external and internal noises are pump starts, reactor trip, and control rod stepping.
C.4.d	By meeting the criteria as defined in position C.3, the acquisition of quality data is ensured.
C.4.f C.5	Operability and surveillance requirements for the LPMS are included in Technical Requirements Manual.
C.4.g	Seabrook procedures provide a diagnostic program using information from other plant systems and operating history to confirm the presence of a loose part.
C.4.h	The procedures for performing channel check, channel functional test, and background noise measurements are available at Seabrook Station.
C.4.i	Radiation protection procedures have been developed to provide guidance and direction to station personnel for minimizing radiation

Reg. Guide Position	Discussion
	exposure during maintenance, calibration, and diagnostic work activities. The overall radiation protection program is described in the Updated FSAR Chapter 12.
C.4.j	Seabrook's non-licensed training program provides pertinent training for plant personnel involved with system operation, and maintenance. Loose part diagnosis is performed by an organization qualified to interpret loose part data.
C.6	If the presence of a loose part is confirmed and is evaluated to have safety significance, it will be reported to the NRC in accordance with 10 CFR 50.72.

4.4.6.5 Instrumentation for Detection of Inadequate Core Cooling

The Inadequate Core Cooling Monitoring System installed at Seabrook Station includes the following:

- Core Exit Thermocouple Monitoring
- Core Subcooling Margin Monitor
- Reactor Vessel Level Monitoring

The inadequate core cooling monitor provides improved information presentation and display to the plant operators on the status of core heat removal capability. The system monitors core exit thermocouples and wide-range reactor pressure and calculates core subcooling margin utilizing redundant channels of instrumentation and control room displays.

The monitoring system displays several levels of information including: (a) bulk average core exit thermocouple trending (b) a spatial map exhibiting the thermocouple temperature at its respective location in the core (c) a core map showing minimum, average, and maximum quadrant temperatures (d) subcooling margin (e) a detailed data list exhibiting thermocouple location, tag designation, temperature; and (f) hot channel core exit temperature. The Reactor Vessel Level Instrumentation System (RVLIS) consists of two redundant independent trains that monitor the reactor vessel water levels. Each train provides two vessel level indications: full range and dynamic head. The full range RVLIS reading provides an indication of reactor vessel water level from the bottom of the vessel to the top of the vessel during natural circulation

conditions. The dynamic head reading provides an indication of reactor core, internals, and outlet nozzle pressure drop for any combination of operating reactor coolant pumps. Comparison of the measured pressure drop with the normal, single phase pressure drop provides an approximate indication of the relative void content of the circulating fluid.

4.4.6.6 Instrumentation for Mid-loop Operation

Generic Letter 88-17, "Loss of Decay Heat Removal," recommended that licensees implement certain actions prior to operation in a reduced Reactor Coolant System (RCS) inventory condition with irradiated fuel in the core. The concern stated in the Generic Letter is the potential consequences involved in preventing and recovering from loss of shutdown cooling while operating in a reduced inventory condition. The NRC recommended expeditious action and programmed enhancements to maintain sufficient equipment in an operable or available status so as to mitigate a loss of shutdown cooling or RCS inventory should they occur. Reduced inventory is defined by the NRC to be an RCS level lower than three feet below the reactor vessel flange.

In response to the NRC recommendations, the design includes (1) reliable indications of parameters that describe the state of the RCS and the performance of systems normally used to cool the RCS for both normal and accident conditions, (2) procedures to cover reduced inventory operation and (3) provisions for alternate sources of inventory for addition if necessary. The following is a brief description of the plant equipment, instrumentation and procedures that are used to comply with the recommendations of Generic Letter 88-17:

Reactor Coolant System Level Monitoring: At least two diverse RCS level indications are operational during reduced inventory conditions with irradiated fuel in the core. Continuous level indications are monitored in the Control Room and audible alarms sound on inadvertent transition in RCS level from the existing operating condition. The RCS level instrumentation consists of an RCS sight glass, wide range level indication provided by differential pressure measurement and three diverse narrow range level indicators provided by ultrasonic measurements (2) and differential pressure measurement (1). With exception of the sight glass, the RCS level instrumentation provides diverse indication, trend and low-level alarm capability in the control room via the Main Plant Computer System (MPCS) during all phases of operation under reduced inventory.

Reactor Coolant System Temperature Monitoring: When the reactor vessel head is located on the reactor vessel, two independent core exit temperature measurements are demonstrated to be operable prior to draining the RCS down to reduced inventory. The core exit temperature measurements are provided using the core exit thermocouple portion of the redundant Class 1E safety-related Inadequate Core Cooling Monitor.

Thermocouple readings are displayed on the Main Control Board and input into the MPCS. Mid-loop high temperature alarms are provided by the MPCS based on selection of the maximum reliable thermocouple temperature.

Residual Heat Removal System Performance: Continuous monitoring and trend capability of Residual Heat Removal System performance is provided in the Control Room by the MPCS. The RHR system parameters that are monitored include RHR loop flow, RHR heat exchanger inlet and outlet temperatures, RHR pump suction pressures and RHR pump motor current indications.

Administrative Controls: Controls are in place to implement specific actions to be taken when draining the RCS with irradiated fuel in the core. Required actions are based on the Westinghouse Owners Group reduced inventory project guidance and plant specific analyses. Plant procedures include the necessary information to determine equipment and/or operational requirements and limitations, including:

1. Prior to entry into a reduced inventory condition, controls are established to provide reasonable assurance that containment closure can be achieved before core is uncovered as a result of loss of decay heat removal. With the exception of penetrations that are in use or undergoing maintenance which are administratively controlled, at least one boundary of each containment penetration is maintained intact during reduced inventory operation. In the event of a loss of decay heat removal, administratively controlled penetrations are closed.

2. Prior to entering a reduced inventory condition, communication is established between the control room and a local nuclear systems operator in containment.

3. When operating at reduced inventory with steam generator nozzle dams in place, one centrifugal charging pump and one safety injection pump are available with a specified flow path to the reactor core. A gravity flow path from the Reactor Water Storage Tank (RWST) to the RCS is also made available as a secondary source. An adequate vent is provided to preclude RCS pressurization that could prevent gravity feed from the RWST and/or damage to the steam generator nozzle dams. Administrative controls assure availability of the redundant centrifugal charging and safety injection pumps upon unavailability of the operable pump.

4. When operating at reduced inventory with nozzle dams removed and the RCS vent closed for evacuation and fill, one centrifugal charging pump and one safety injection pump are available with specified flow paths to the reactor core. A gravity feed flow path from the RWST is also available for inventory addition as a secondary source. Administrative controls assure availability of the redundant

centrifugal charging and safety injection pumps upon unavailability of the operable pump.

4.4.7 References

1. Christensen, J. A., Allio, R. J. and Biancheria, A., "Melting Point of Irradiated $U0_2$," WCAP-6065, February 1965.

2. Hellman, J. M. (Ed.), "Fuel Densification Experimental Results and Model for Reactor Application," WCAP-8218-P-A (Proprietary), March 1975 and WCAP-8219-A, March 1975.

3. Tong, L. S., "Boiling Crisis and Critical Heat Flux," AEC Critical Review Series, TID-25887, 1972.

4. "Evaluation of Westinghouse Request for Generic Approval", ENCLOSURE to letter from Carl Berlinger (NRC) to E. P. Rahe, Jr., (Westinghouse), "Request for Reduction in Fuel Assembly Burnup Limit for Calculation of Maximum Rod Bow Penalty", dated June 18, 1986.

5. Davidson, S. L. (Ed.), "VANTAGE + Fuel Assembly Reference Core Report," WCAP-12610-P-A, April 1995.

6. Davidson, S. L. (Ed.), "Westinghouse Fuel Criteria Evaluation Report," WCAP-12488-A, October 1994.

7. Not used

8. Tong, L. S., "Prediction of Departure from Nucleate Boiling for an Axially Non-Uniform Heat Flux Distribution," J. Nucl. Energy, 21, 241-248 (1967).

9. Smith, L. D., et al, "Modified WRB-2 Correlation, WRB-2M, for predicting Critical Heat Flux in 17x17 Rod Bundles with Modified LPD Mixing Vane Grids," WCAP-15025-P-A, April 1999.

10. Not used

11. NP-2511-CCM Volumes 1-5, "VIPRE-01: A Thermal-Hydraulic Code for Reactor Cores", Electric Power Research Institute.

12. Cadek, F. F., Motley, F. E. and Dominicis, D. P., "Effect of Axial Spacing on Interchannel Thermal Mixing with the R Mixing Vane Grid," WCAP-7941-P-A (Proprietary), January 1975 and WCAP-7959-A, January 1975.

13. Rowe, D. S., Angle, C. W., "Crossflow Mixing Between Parallel Flow Channels During Boiling, Part II Measurements of Flow and Enthalpy in Two Parallel Channels," BNWL-371, part 2, December 1967.

14. Rowe, D. S., Angle, C. W., "Crossflow Mixing Between Parallel Flow Channels During Boiling, Part III Effect of Spacers on Mixing Between Two Channels," BNWL-371, part 3, January 1969.

15. Gonzalez-Santalo, J. M. and Griffith, P., "Two-Phase Flow Mixing in Rod Bundle Subchannels," ASME Paper 72-WA/NE-19.

16. Motley, F. E., Wenzel A. H., Cadek, F. F., "The Effect of 17x17 Fuel Assembly Geometry on Interchannel Thermal Mixing," WCAP-8298-P-A (Proprietary), January 1975 and WCAP-8299-A, January 1975.

17. Cadek, F. F., "Interchannel Thermal Mixing Vane Grids," WCAP-7667-P-A (Proprietary), January 1975 and WCAP-7755-A, January 1975.

18. Hochreiter, L. F., "Application of the THINC-IV Program to PWR Design," WCAP-8054 (Proprietary), October 1973, and WCAP-8195, October 1973.

19. Hochreiter, L. E., Chelemer, H. and Chu, P. T., "THINC-IV An Improved Program for Thermal-Hydraulic Analysis of Rod Bundle Cores," WCAP-7956, June 1973.

20. Dittus, F. W., and Boelter, L. M. K., "Heat Transfer in Automobile Radiators of the Tubular Type," Calif. Univ. Publication In Eng., 2, No. 13, 443461 (1930).

21. Weisman, J., "Heat Transfer to Water Flowing Parallel to Tube Bundles," Nucl. Sci. Eng., 6, 78-79 (1959).

22. Thom, J. R. S., Walker, W. M., Fallon, T. A. and Reising, G. F. S., "Boiling in Sub-Cooled Water During Flow up Heated Tubes or Annuli," Prc. Instn. Mech. Engrs., 180, Pt. C, 226-46 (1955-66).

23. Hetsroni, G., "Hydraulic Tests of the San Onofre Reactor Model," WCAP-3269-8, June 1964.

24. Hetsroni, G., "Studies of the Connecticut-Yankee Hydraulic Model," NYO-3250-2, June 1965.

25. Idel'chik, I. E., "Handbook of Hydraulic Resistance," AEC-TR-6630, 1960.

26. Moody, L. F., "Friction Factors for Pipe Flow," Transaction of the American Society of Mechanical Engineers, 66, 671-684 (1944).

27. Not used.

28. Not used.

29. Not used.

30. Hill, K. W., Motley, F. E., Catek, F. F., "Effect of Local Heat Flux Spikes on DNB in Non-Uniform Heated Rod Bundles," WCAP-8174, August 1973.

31. Not used

32. Not used

33. Not used

34. Not used

35. Not used

36. International Atomic Energy Agency, "Thermal Conductivity of Uranium Dioxide," Report of the Panel held in Vienna, April 1965, IAEA Technical Reports Series, No. 59, Vienna, The Agency, 1966.

37. Carter, F. D., "Inlet Orificing of Open PWR Cores," WCAP-9004, January 1969 (Proprietary) and WCAP-7836, January 1972 (Nonproprietary).

38. Not used

39. Not used

40. Kjaerheim, G., and Rolstad, E., "In-Pile Determination of $U0_2$ Thermal Conductivity, Density Effects, and Gap conductance," HPR-80, December 1967.

41 Kjaerheim, G., In-Pile Measurements of Center Fuel Temperatures and Thermal Conductivity Determination of Oxide Fuels, Paper IFA-175 Presented at the European Atomic Energy Society Symposium on Performance Experience of Water-Cooled Power Reactor Fuel, Stockholm, Sweden, October 1969.

42. Cohen, I., Lustman, B., and Eichenberg, D., "Measurement of the Thermal Conductivity of Metal-Clad Uranium Oxide Rods During Irradiation," WAPD-228, 1960.

43. Clough, D. J., and Sayers, J. B., "The Measurement of the Thermal Conductivity of $U0_2$ under Irradiation in the Temperature Range 150 to 1600C," AERE-R-4690, UKAEA Research Group, Harwell, December 1964.

44. Stora, J. P., et al., "Thermal Conductivity of Sintered Uranium Oxide under In-Pile Conditions," EURAEC-1095, 1964.

45. Devold, I., "A Study of the Temperature Distribution in $U0_2$ Reactor Fuel Elements," AE-318, Aktiebolaget Atomenergi, Stockholm, Sweden, 1968.

46. Balfour, M. G., Christensen, J. A., and Ferrari, H. M., "In-Pile Measurement of $U0_2$ Thermal Conductivity," WCAP-2923, 1966.

47. Howard, V. C., and Gulvin, T. G., "Thermal Conductivity Determinations on Uranium Dioxide by a Radial Flow Method," UKAEA IG-Report 51, November 1960.

48. Lucks, C. F., and Deem, H. W., "Thermal Conductivity and Electrical Conductivity of $U0_2$," in Progress Reports Relating to Civilian Applications, BMI-1448 (Revised) for June 1960, BNI-1489 (Revised) for December 1960, and BMI-1518 (Revised) for May 1961.

49. Daniel, J. L., Matolich, J., Jr., and Deem, H. W., "Thermal Conductivity of $U0_2$" HW-69945, September 1962.

50. Feith, A. D., "Thermal Conductivity of $U0_2$ by a Radial Heat Flow Method," TID-21668, 1962.

51. Vogt, J., Grandell, L., and Runfors, U., "Determination of the Thermal Conductivity of Unirradiated Uranium Dioxide," AB Atomenergi Report RMB-527, 1964, Quoted by IAEA Technical Report Series No. 59, "Thermal Conductivity of Uranium Dioxide."

52. Nishijima, T., Kawada, T., and Ishihata, A., "Thermal Conductivity of Sintered $U0_2$ and $A1_2/0_3$ at High Temperatures," Journal of the American Ceramic Society 48, pp 31-34, 1965.

53. Ainscough, J. B., and Wheeler, M. J., "Thermal Diffusivity and Thermal Conductivity of Sintered Uranium Dioxide, "Proceedings of the Seventh Conference of Thermal Conductivity, National Institute of Standards and Technology, Washington, p 467, 1968.

54. Godfrey, T. G., et al., "Thermal Conductivity of Uranium Dioxide and Armco Iron by an Improved Radial Heat Flow Technique," ORNL-3556, June 1964.

55. Stora, J. P., et al., "Thermal Conductivity of Sintered Uranium Oxide Under In-Pile Conditions," EURAEC-1095, August 1964.

56. Bush, A. J., "Apparatus for Measuring Thermal Conductivity to 2500C," Report 64-1P6-401-43 (Proprietary), Westinghouse Research Laboratories, February 1965.

57. Asamoto, R. R., Anselin, F. L., and Conti, A. E., "The Effect of Density on the Thermal Conductivity of Uranium Dioxide," GEAP-5493, April 1968.

58. Kruger, O. L., Heat Transfer Properties of Uranium and Plutonium Dioxide, Paper 11-N-68F, Presented at the Fall Meeting of Nuclear Division of American Ceramic Society, Pittsburgh, September 1968.

59. Leech, W. J., et al., "Revised PAD Code Thermal Safety Model, WCAP-8720, Addendum 2, October 1982.

60. Duncan, R. N., "Rabbit Capsule Irradiation of $U)_2$," CVTR Project, CVNA-142, June 1962.

61. Nelson, R. C., et al., "Fission Gas Release from $U0_2$ Fuel Rods with Gross Central Melting," GEAP-4572, July 1964.

62. Poncelet, C. G., "Burnup Physics of Heterogeneous Reactor Lattices," WCAP-6069, June 1965.

63. Nodvick, R. J., "Saxton Core II Fuel Performance Evaluation," WCAP-3385-56, Part II, "Evaluation of Mass Spectrometric and Radiochemical Analyses or Irradiated Saxton Plutonium Fuel," July 1970.

64. Weiner, R. A., et al., "Improved Fuel Performance Models for Westinghouse Fuel Rod Design-and Safety Evaluation," WCAP-10851-P-A, August 1988.

References 65 through 68 are not used.

69. J. A. Boure, A. E. Bergles, and L. S. Tong, "Review of Two-Phase Flow Instability," Nucl. Engr. Design 25 (1973) p. 165-192.

70. R. T. Lahey and F. J. Moody, "The Thermal Hydraulics of a Boiling Water Reactor," American Nuclear Society, 1977.

71. P. Saha, M. Ishii, and N. Zuber, "An Experimental Investigation of the Thermally Induced Flow Oscillations in Two-Phase Systems," J. of Heat Transfer, Nov. 1976, pp. 616-662.

72. Virgil C. Summer FSAR, Docket #50-395.

73. Byron/Braidwood FSAR, Docket #50-456.

74. South Texas FSAR, Docket #50-498.

75. S. Kakac, T. N. Veziroglu, K. Akyuzlu, 0. Berkol, "Sustained and Transient Boiling Flow Instabilities in a Cross-Connected Four- Parallel-Channel Upflow System," Proc. of 5th International Heat Transfer Conference, Tokyo, Sept. 3-7, 1974.

76. H. S. Kao, C. D. Morgan, and W. B. Parker, "Prediction of Flow Oscillation in Reactor Core Channel," Trans. ANS, Vol. 16, 1973, pp. 212-213.

77. Ohtsubo A., and Uruwashi, S., "Stagnant Fluid due to Local Flow Blockage," J. Nucl. Sci. Technol., 9, No. 7, 433-434, (1972).

78. Basmer, P., Kirsh, D. and Schultheiss, G. F., "Investigation of the Flow Pattern in the Recirculation Zone Downstream of Local Coolant Blockages in Pin Bundles," Atomwirtschaft, 17, No. 8, 416-417, (1972). (In German).

79. Letter from H. A. Sepp (Westinghouse) to T. E. Collins (NRC), "Notification of FCEP Application for WRB-1 and WRB-2 Applicability to the 17x17 Modified LPD Grid Design for Robust Fuel Assembly Application," NSD-NRC-98-5618, March 25, 1998.

80. Davidson, S. L. (Editor), "Reference Core Report - VANTAGE 5 Fuel Assembly," WCAP-10444-P-A, September 1985, "VANTAGE 5H Fuel Assembly," WCAP-10444-P-A, Addendum 2-A, April 1988.

81. WCAP-14565, "VIPRE-01 Modeling and Qualification for Pressurized Water Reactor Non-LOCA Thermal-Hydraulic Safety Analysis," Y X Sung, et al., April 1997.

82. Not used

83. Skaritka, J., ed, "Fuel Rod Bow Evaluation," WCAP-8691, Revision 1, July 1979.

84. McFarlane, A. F., "Power Peaking Factors," WCAP-7912-P-A (Proprietary) and WCAP-7912-A (Nonproprietary), January 1975.

85. Letter From C. Berlinger (NRC) to E. P. Rahe Jr. (W), Subject: "Request for Reduction in Fuel Assembly Burnup Limit for Calculation of Maximum Rod Bow Penalty," June 18, 1986.

86. Not used

87. Not used

88. Not used

89. Not used

90. Not used

91. Not used

92. Generic Letter 88-17, "Loss of Decay Heat Removal," dated October 17, 1988.

93. NAESCO letter NYN-93154 from T. C. Feigenbaum (NAESCO) to USNRC, "Revised Commitment Related to Generic Letter 88-17," November 5, 1993.

94. PSNH letter NYN-89001 from G. S. Thomas (PSNH) to USNRC, "Response to Generic Letter 88-17," January 3, 1989.

95. PSNH letter NYN-89012 from G. S. Thomas (PSNH) to USNRC, "Response to Generic Letter 88-17," February 3, 1989.

4.5 REACTOR MATERIALS

4.5.1 Control Rod Drive System Structural Materials

4.5.1.1 Materials Specifications

All parts of the Control Rod Drive System exposed to the reactor coolant are made of metals which resist the corrosive action of the water. Three types of metals are used exclusively: stainless steels, nickel-chromium-iron and cobalt-based alloys. In the case of stainless steels, only austenitic and martensitic stainless steels are used. The martensitic stainless steels are not used in the heat-treated conditions which cause susceptibility to stress corrosion cracking or accelerated corrosion in the Westinghouse pressurized water reactor water chemistry. Materials with yield strength greater than 90,000 psi are 410 stainless steel, Haynes 25 and Inconel X-750; their usage and properties are presented in the following subsections.

a. Pressure Vessel

All pressure-containing parts of the CRDM comply with Section III of the ASME Boiler and Pressure Vessel Code, and are fabricated from austenitic (Type 304) stainless steel.

b. Coil Stack Assembly

The coil housings require a magnetic material. Both low carbon cast steel and ductile iron have been successfully tested for this application, with ductile iron eventually specified for the control rod drive mechanism (CRDM). The finished housings are zinc plated or flame sprayed to provide corrosion resistance.

Coils are wound on bobbins of molded Dow Corning 302 material, with double glass insulated copper wire. Coils are then vacuum impregnated with silicon varnish. A wrapping of mica sheet is secured to the coil outside diameter. The result is a well-insulated coil capable of sustained operation at 200°C.

c. Latch Assembly

Magnetic pole pieces are fabricated from Type 410 stainless steel. All nonmagnetic parts, except pins and springs, are fabricated from Type 304 stainless steel. Haynes 25 is used to fabricate link pins. Springs are made from nickel-chromium-iron alloy (Inconel X-750). Latch arm tips are clad with Stellite-6 to provide improved wearability. Hard chrome plate and Stellite-6 are used selectively for bearing and wear surfaces.

d. Drive Rod Assembly

The major portion of the drive rod assembly is a Type 410 stainless steel. The coupling is machined from Type 403 stainless steel. Other parts are Type 304 stainless steel with the exception of the springs which are nickel-chromium-iron alloy and the locking button which is Haynes 25.

4.5.1.2 Fabrication and Processing of Austenitic Stainless Steel Components

The discussions provided in Subsection 5.2.3 concerning the processes, inspections and tests on austenitic stainless steel components to assure freedom from increased susceptibility to intergranular corrosion caused by sensitization, and the discussions provided in Subsection 5.2.3 on the control of welding of austenitic stainless steels, especially control of delta ferrite, are applicable to the austenitic stainless steel pressure housing components of the CRDM.

4.5.1.3 Contamination Protection and Cleaning of Austenitic Stainless Steel

The CRDMs are cleaned prior to delivery in accordance with the guidance of ANSI 45.2.1. Process specifications in packaging and shipment are discussed in Subsection 5.2.3. Westinghouse personnel do conduct surveillance to ensure that manufacturers and installers adhere to appropriate requirements, as discussed in Subsection 5.2.3.

4.5.2 Reactor Internals Materials

4.5.2.1 Materials Specifications

The structural material for the reactor internals is Type 304 stainless steel. Parts not fabricated from Type 304 stainless steel include bolts and dowel pins which are fabricated from Type 316 stainless steel and radial support key bolts which are fabricated of Inconel X-750. There are no other materials used in the reactor internals or core support structures which are not otherwise included in the ASME Code, Section III, Appendix I.

4.5.2.2 Controls on Welding

The discussions provided in Subsection 5.2.3 are applicable to the welding of reactor internals and core support components.

4.5.2.3 Nondestructive Examination of Wrought Seamless Tubular Products and Fittings

The nondestructive examination of wrought seamless tubular products and fittings is in accordance with Section III of the ASME Code.

4.5.2.4 Fabrication and Processing of Austenitic Stainless Steel Components

The discussions provided in Subsection 5.2.3 and Section 1.8 verify conformance of reactor internals and core support structures with Regulatory Guide 1.31. The discussion provided in Section 1.8 verifies conformance of reactor internals with Regulatory Guide 1.34.

The discussion provided in Section 1.8 verifies conformance of reactor internals and core support structures with Regulatory Guide 1.71.

4.5.2.5 Contamination Protection and Cleaning of Austenitic Stainless Steel

The discussions provided in Subsection 5.2.3 and Section 1.8 are applicable to the reactor internals and core support structures, and verify conformance with ANSI 45 specifications and Regulatory Guide 1.37.

4.6 FUNCTIONAL DESIGN OF REACTIVITY CONTROL SYSTEMS

4.6.1 Information for Control Rod Drive System (CRDS)

The CRDS controls the power to the rod drive mechanism for rod movement in response to signals received from the Reactor Control System or from signals generated by reactor operator action.

The control rod drive mechanism is described in Subsection 3.9(N).4.1. The instrumentation and controls for the Reactor Trip System are described in Section 7.2 and the Reactor Control System is described in Section 7.7.

4.6.2 Evaluation of the CRDS

The analysis used to evaluate the CRDS is that known as a failure mode and effects analysis. Failure modes of several systems of the CRDS are identified, failure mechanisms attributable to identified failure modes are postulated, the methods used for failure detection are determined, and the effects of a failure on the CRDS operation are analyzed. This analysis is presented in tabular form in Reference 1. This study, and the analyses presented in Chapter 15, demonstrate that the CRDS performs its intended safety function by putting the reactor in a subcritical condition when a safety system setting is approached, with any assumed credible failures of a single active component.

Despite the extremely low probability of a common mode failure impairing the ability of the Reactor Trip System to perform its safety function, analyses have been performed in accordance with the requirements of WASH-1270. These analyses, documented in References 2 and 3, have demonstrated that acceptable safety criteria would not be exceeded even if the CRDS were rendered incapable of functioning during a reactor transient for which their function would normally be expected.

4.6.3 Testing and Verification of the CRDS

The tests performed on the CRDS are: (1) prototype tests of components of the CRDS prior assembly, (2) prototype tests of the CRDS in a simulated reactor environment, (3) tests of components following manufacturing, (4) onsite preoperational and initial startup tests and (5) periodic in-service tests. The test methods and acceptance criteria are discussed in Sections 4.2, 14.2, Subsection 3.9(N).4, and Technical Specification 3/4.1.3.

4.6.4 Information for Combined Performance of Reactivity Systems

As is indicated in Chapter 15, the only postulated events which assume credit for reactivity control systems, other than a reactor trip, to render the plant subcritical are the steam line break, feedwater line break, and loss-of-coolant accident. The Reactivity Control Systems for which credit is taken in these accidents are the Reactor Trip System and the Safety Injection System (SIS). Additional information on the CRDS is presented in Subsection 3.9(N).4 and on the SIS in Section 6.3. No credit is taken for the boration capabilities of the Chemical and Volume Control System (CVCS) as a system in the analysis of transients presented in Chapter 15. Information on the capabilities of the CVCS is provided in Subsection 9.3.4. The adverse boron dilution possibilities due to the operation of the CVCS are investigated in Subsection 15.4.6. Prior proper operation of the CVCS has been presumed as an initial condition to evaluate transients, and appropriate Technical Specifications have been prepared to ensure the correct operation or remedial action.

4.6.5 Evaluation of Combined Performance

The evaluation of the steam line break, feedwater line break, and the loss-of-coolant accident, which presume the combined actuation of the Reactor Trip System to the CRDS and the SIS, are presented in Subsections 15.1.5, 15.2.8 and 15.6.5. Reactor trip signals and safety injection signals for these events are generated from functionally diverse sensors and actuate diverse means of reactivity control, i.e., control rod insertion and injection of soluble poison.

Nondiverse but redundant types of equipment are utilized only in the processing of the incoming sensor signals into appropriate logic which initiates the protective action. This equipment is described in detail in Sections 7.2 and 7.3. In particular, note that protection from equipment failures is provided by redundant equipment and periodic testing. Effects of failures of this equipment have been extensively investigated as reported in Reference 4. This failure mode and effects analysis verifies that any single failure will not have a deleterious effect on the Engineered Safety Features Actuation System. Adequacy of the Emergency Core Cooling System and SIS performance under faulted conditions is verified in Section 6.3.

4.6.6 References

1. Shopsky, W. E., "Failure Mode and Effects Analysis (FMEA) of the Solid State Full Length Rod Control System," WCAP-8976, September 1977.

2. "Westinghouse Anticipated Transients Without Trip Analysis," WCAP-8330, August 1974.

3. Gangloff, W. C. and Loftus, W. D., "An Evaluation of Solid State Logic Reactor Protection in Anticipated Transients," WCAP-7706-L (Proprietary) and WCAP-7706 (Nonproprietary), July 1971.

4. Eggleston, F. T., Rawlins, D. H. and Petrow, J. R., "Failure Mode and Effects Analysis (FMEA) of the Engineering Safeguard Features Actuation System," WCAP-8584 (Proprietary) and WCAP-8760 (Nonproprietary), April 1976.

Table 4.1-1 REACTOR DESIGN COMPARISON TABLE INITIAL CORE

Thermal and Hydraulic Design Parameters	Seabrook Unit 1	W. B. McGuire Units 1 & 2
Reactor core heat output (MWt)	3411	3411
Reactor core heat output (10^6 Btu/hr)	11,641	11,641
Heat generated in fuel (%)	97.4	97.4
System pressure, nominal (psia)	2250	2250
System pressure, minimum steady state (psia)	2200	2220
Coolant Flow		
Total thermal flow rate (10^6 lbm/hr)	142.1	140.3
Effective flow rate for heat transfer 10^6 lbm/hr)	133.9	134.0
(Effective flow area for heat transfer ft^2)	51.1	51.1
Average velocity along fuel rods (ft/sec)	16.7	16.7
Average mass velocity (10^6 lbm/hr-ft^2)	2.62	2.62
Coolant Temperature		
Nominal inlet (°F)	558.8	558.1
Average rise in vessel (°F)	59.4	60.2
Average rise in core (°F)	62.6	62.7
Average in core (°F)	591.8	589.4
Average in vessel (°F)	588.5	588.2
Heat Transfer		
Active heat transfer surface area (ft^2)	59,700	59,700
Average heat flux, (Btu/hr-ft^2)	189,800	189,800
Maximum heat flux for normal operation, (Btu/hr-ft^2)	474,400[a]	440,300[a]
Average linear power (kW/ft)	5.44	5.44
Peak linear power for normal operation (kW/ft)	13.6[a]	12.6[a]
Heat flux hot channel factor, F_Q	2.50[b]	2.32[b]
Peak fuel central temperature at peak linear power for prevention of centerline melt (°F)	4700	4700

Thermal and Hydraulic Design Parameters	Seabrook Unit 1	W. B. McGuire Units 1 & 2
Core Mechanical Design Parameters		
Design	RCC canless, 17x17	RCC canless, 17x17
Number of fuel assemblies	193	193
$U0_2$ rods per assembly	264	264
Rod pitch (in.)	0.496	0.496
Overall dimensions (in.)	8.426x8.426	8.426x8.426
Fuel weight, as $U0_2$ (lb.)	222,739	222,739
Clad weight (lb.)	45,234	45,234
Number of grids per assembly	8 - Type R	8 - Type R
Loading technique	3 region nonuniform	3 region nonuniform
Fuel Rods		
Number	50,952	50,952
Outside diameter (in.)	0.374	0.374
Diametral gap (in.)	0.0065	0.0065
Clad thickness (in.)	0.0225	0.0225
Clad material	Zirconium Alloy	Zircaloy-4
Fuel Pellets		
Material	$U0_2$ sintered	$U0_2$ sintered
Density (% of Theoretical)	95	95
Diameter (in.)	0.3225	0.3225
Length (in.)	0.387	0.530
Rod Cluster Control Assemblies		
Neutron absorber		
Full length	Ag-In-Cd	Ag-In-Cd

Thermal and Hydraulic Design Parameters	Seabrook Unit 1	W. B. McGuire Units 1 & 2
Part length	---	Ag-In-Cd
Cladding Material	Austenitic SS	Type 304 SS-cold worked
Clad thickness		
Ag-In-Cd (in.)	0.0185	---
Number of clusters, full length/part length	57/0	53/8
Number of absorber rods per cluster	24	24
Core Structure		
Core barrel, I.D./O.D. (in.)	148.0/152.5	148.0/152.5
Thermal shield	Neutron pad design	Neutron pad design
Structure Characteristics		
Core diameter, equivalent (in.)	132.7	132.7
Core height, active fuel (in.)	144.0	144.0
Reflector Thickness and Composition		
Top, water plus steel (in.)	~10	~10
Bottom, water plus steel (in.)	~10	~10
Side, water plus steel (in.)	~15	~15
H_20/U molecular ratio lattice (cold)	2.41	2.41

---

a. This limit is associated with the maximum value of F_Q for normal operation.

b. This is the maximum value of F_Q for normal operation.

TABLE 4.1-2 ANALYTICAL TECHNIQUES IN CORE DESIGN

Analysis	Technique	Computer Code	Section Reference
Mechanical design core internals loads, deflections, and stress analysis	Static and dynamic modeling	Blowdown code, FORCE, finite element, structural analysis code, and others	3.7(N) 3.9(N) 3.9(N)
Fuel rod design			
Fuel performance characteristics (temperature, internal pressure, clad stress, etc.)	Semi-empirical thermal model of fuel rod with consideration of fuel changes, heat transfer, fission gas release, etc.	Westinghouse fuel rod design model	4.2 4.3 4.4
Nuclear design			
1. Cross sections	40 Group 2D neutron transport theory	CASMO-3 Phoenix – P	4.3
2. 3D power distributions, boron concentrations, reactivity coefficients, kinetic parameters, control rod worths, reactor and fuel assembly criticality	3D 2 Group advanced	SIMULATE-3 ANC	4.3
3. Steam line break, rod ejection doppler flattening factor	3D 2 Group advanced	ANC	15.0
Thermal-hydraulic design			
1. Steady state	Subchannel analysis of local fluid conditions in rod bundles, including inertial and crossflow resistance terms	VIPRE-01	4.4
2. Transient departure from nucleate boiling	Subchannel analysis of local fluid conditions in rod bundles during transient	VIPRE-01	4.4

TABLE 4.1-3 DESIGN LOADING CONDITIONS FOR REACTOR CORE COMPONENTS

1. Fuel assembly weight
2. Fuel assembly spring forces
3. Internals weight
4. Control rod trip (equivalent static load)
5. Differential pressure
6. Spring preloads
7. Coolant flow forces (static)
8. Temperature gradients
9. Differences in thermal expansion
   a. Due to temperature differences
   b. Due to expansion of different materials
10. Interference between components
11. Vibration (mechanically or hydraulically induced)
12. One or more loops out of service
13. All operational transients listed in Table 3.9(N)-1
14. Pump overspeed
15. Seismic loads (Operating Basis Earthquake and Safe Shutdown Earthquake)
16. Blowdown forces (due to cold and hot leg reactor coolant pipe breaks)

TABLE 4.3-1 REACTOR CORE DESCRIPTION (Typical Low Leakage Cycle Design)

Active Core	
Equivalent diameter (in.)	132.7
Active fuel height, first core (in.)	144.0
Height-to-diameter ratio	1.08
Total cross section area (ft^2)	96.06
H_20/U molecular ratio, lattice (Cold)	2.41
Reflector Thickness and Composition	
Top, water plus steel (in.)	~10
Bottom, water plus steel (in.)	~10
Side, water plus steel (in.)	~15
Fuel Assemblies	
Number	193
Rod array	17x17
Rods per assembly	264
Rod pitch (in.)	0.496
Overall transverse dimensions (in.)	8.426x8.426
Fuel weight (as UO_2) (lb.)	~220,000
Zirlo/Zircaloy weight (lb.)	46,920 – 53,300
Number of grids per assembly	8 – Structural 3 – IFM 1 – P-Grid
Composition of grids	Inconel or Zirconium Alloy
Weight of grids, effective in core (lb.)	2324 – 3150
Number of guide thimbles per assembly	24
Composition of guide thimbles	Zirconium Alloy
Diameter of guide thimbles, upper part (in.)	
(17x17 RFA)	0.442 I.D. x 0.482 O.D.
Diameter of guide thimbles, lower part (in.)	
(17x17 RFA)	0.397 I.D. x 0.439 O.D.
Diameter of instrument guide thimbles (in.)	
(17x17 RFA)	0.442 I.D. x 0.482 O.D.

Fuel Rods	
Number	50,952
Outside diameter (in.)	0.374
Diameter gap (in.)	0.0065
Clad thickness (in.)	0.0225
Clad material	Zirconium Alloy
Fuel Pellets	
Material	UO_2 Sintered
Density (percent of theoretical)	95
Fresh Fuel enrichments w/o	
Typical Low Enrichment in Split	3.6-4.4
Typical High Enrichment in Split	4.0-4.8
Diameter (in.)	0.3225
Length (in.)	0.387
Mass of UO_2 per foot of fuel rod (lb./ft)	~0.36
Rod Cluster Control Assemblies	
Neutron absorber	Ag-In-Cd
Composition	80%-15%-5%
Diameter (in.)	0.341 Ag-In-Cd
Density (lb./in.^{3})	0.367 Ag-In-Cd
Cladding material	Type 304, Cold Worked Stainless Steel
Clad thickness (in.)	0.0185
Number of clusters - full length	57
Number of absorber rods per cluster	24
Integral Fuel Burnable Absorbers (IFBA)	
Number	6,000 – 12,000 (typical)
Material	Zr_2B
Coating Thickness (in.)	0.0002 – 0.0004
Boron loading (mg/in)	1.57 - 3.14
Initial reactivity worth (%$\Delta\rho$)	Dependent on Number in Assembly
Excessive Reactivity	
Maximum fuel assembly k_∞ (cold clean, unborated water)	1.430
Maximum core reactivity (cold, zero power, beginning of cycle)	1.210

TABLE 4.3-2 NUCLEAR DESIGN PARAMETERS (Typical Low Leakage Cycle Design)

Core Average Linear Power, kW/ft, including densification effects	5.84	
Total Heat Flux Hot Channel Factor, F_Q	2.50	
Nuclear Enthalpy Rise Hot Channel Factor, $F_{\Delta H}$	1.65	
Reactivity Coefficients[+]	Design Limits	Best Estimate
Doppler-only Power, Upper Curve Coefficients, pcm/% power[++], H2P to HFP	-19.4 to -12.6	-16 to -9
(See Figure 15.1-3, Sh. 1), Lower Curve	-9.55 to -6.05	-13 to -8.5
Doppler Temperature Coefficient pcm/°F[++]	-3.2 to –0.9	-2.1 to –1.3
Moderator Temperature Coefficient, pcm/°F[++]	+5. to –55	+2. to –43.
Boron Coefficient, pcm/ppm[++]	-16 to –5	-14.5 to –6.5
Rodded Moderator Density, pcm/gm/cc[++]	$\leq 0.54 \times 10^5$	$\leq 0.41 \times 10^5$
Delayed Neutron Fraction and Lifetime		
β_{eff} BOL, (EOL)	0.0075, (0.0044)	0.0065, (0.0048)
Control Rods		
Rod Requirements	See Table 4.3-3	
Maximum Bank Worth, pcm	< 2000	<1300
Maximum Ejected Rod Worth	See Chapter 15	

Radial Factor Peak Pin FΔh (BOL to EOL)		
Unrodded		1.44 to 1.40
D bank		1.44 to 1.40
D + C		1.55 to 1.44
Boron Concentrations		
Zero Power, k_{eff} = 0.978, Cold Rod Cluster Control Assemblies Out		2110
Zero Power, k_{eff} = 0.987, Hot Rod Cluster Control Assemblies Out		2133
Refueling Boron Concentration (Lower Limit)		2100 (or $K_{eff} \leq 0.95$)
Zero Power, $k_{eff} \leq 0.95$, Cold Rod Cluster Control Assemblies In		1809
Zero Power, k_{eff} = 1.00, Hot Rod Cluster Control Assemblies Out		1936
Full Power, No Xenon, k_{eff} = 1.0, Hot Rod Cluster Control Assemblies Out		1736
Full Power, Equilibrium Xenon, k_{eff} = 1.0, Hot Rod Cluster Control Assemblies Out		1338
Reduction with Fuel Burnup Cycle ppm/GWd/Mtu++++		See Figure 4.3-3

\+ Uncertainties are given in Subsection 4.3.3.3

++ Note: 1 pcm = (percent mille) 10^{-5} Δρ where Δρ is calculated from two statepoint values of k_{eff} by $1n(K_2/K_1)$.

++++ Gigawatt Day (GWd) = 1000 Megawatt Day (1000 MWd).

Table 4.3-3 REACTIVITY REQUIREMENTS FOR ROD CLUSTER CONTROL ASSEMBLIES

Reactivity Effects, Percent	Beginning-of-Life (First Cycle)	End-of-Life (First Cycle)	End-of-Life (Typical Low Leakage Cycle)
1. Control requirements			
Fuel temperature, Doppler (%Δρ)	1.36	1.12	1.53
Moderator temperature** (%Δρ)	0.15	1.22	1.20
Redistribution (%Δρ)	0.50	0.85	***
Rod insertion allowance (%Δρ)	0.50	0.50	0.45
2. Total control (%Δρ)	2.51	3.69	3.18
3. Estimated Rod Cluster Control Assembly worth (57 rods, Ag-In-Cd)			
a. All full length assemblies inserted (%Δρ)	8.73	8.83	7.42

** Includes void effects

*** Redistribution included in Doppler portion

Reactivity Effects, Percent	Beginning-of-Life (First Cycle)	End-of-Life (First Cycle)	End-of-Life (Typical Low Leakage Cycle)
b. All but one (highest worth) assemblies inserted (%Δρ)	7.69	7.76	6.58
4. Estimated Rod Cluster Control Assembly credit with 10 percent adjustment to accommodate uncertainties, 3b - 10 percent (%Δρ)	6.92	6.98	5.93
5. Shutdown margin available, 4-2 (%Δρ)	4.41	3.29	2.75****

**** The design basis minimum shutdown is 1.3%.

TABLE 4.3-4 **AXIAL STABILITY INDEX PRESSURIZED WATER REACTOR CORE WITH A 12 FOOT HEIGHT**

Burnup (MWd/Mtu)	F_Z	C_B (ppm)	Stability Index (hr^{-1}) Exp	Calc
1550	1.34	1065	-0.041	-0.032
7700	1.27	700	-0.014	-0.006
		Difference:	+0.027	+0.026

TABLE 4.3-5 TYPICAL NEUTRON FLUX LEVEL (N/CM2-SEC) AT FULL POWER

	E>1.0MeV	**0.111MeV<E <1.0MeV**	**0.3eV≤E <0.111MeV**	**E<0.3EV**
Core Center	$9.79x10^{13}$	$9.82x10^{13}$	$1.91x10^{14}$	$1.98x10^{13}$
Core Outer Radius At Mid-Height	$2.47x10^{13}$	$2.61x10^{13}$	$5.29x10^{13}$	$5.19x10^{13}$
Core Top, on Axis	$5.20x10^{13}$	$5.35x10^{13}$	$1.10x10^{14}$	$1.30x10^{13}$
Pressure Vessel Inner Diameter Azimuthal Peak, Core Mid-Height	$1.93x10^{10}$	$2.05x10^{10}$	$3.55x10^{10}$	$1.67x10^{10}$

TABLE 4.3-6

(DELETED)

TABLE 4.3-7

(DELETED)

TABLE 4.3-8

(DELETED)

TABLE 4.3-9

(DELETED)

TABLE 4.3-10

(DELETED)

TABLE 4.4-1 THERMAL AND HYDRAULIC COMPARISON TABLE

Design Parameters	Seabrook Cycle 10 Design	Seabrook Uprate
Reactor core heat output (MWt)	3411	3659 (analyzed)
Reactor core heat output (10^6 Btu/hr)	11,641	12,485
Heat generated in fuel (%)	97.4	97.4
System pressure, nominal (psia)	2250	2250
System pressure, minimum steady state (psia)	2200	2200
DNB Correlation	WRB-2[1]	WRB-2M[8]
Correlation Limit Value	1.17[1]	1.14[8]
Design Limit Value		
Typical flow channel	1.26	1.22
Thimble (cold wall) flow channel	1.24	1.22
Safety Analysis Limit Value		
Typical flow channel	1.91	1.47
Thimble (cold wall) flow channel	1.91	1.47
Minimum DNBR at nominal conditions		
Typical flow channel	3.02[2]	2.73[10]
Thimble (cold wall) flow channel	2.88[2]	2.67[10]
Coolant Flow		
Total thermal flow rate (10^6 lb_m /hr)	145.7[3]	142.75[9]
Effective flow rate for heat transfer (10^6 lb_m /hr)	138.7[3]	133.0[9]
Effective flow area for heat transfer (ft^2)	51.3	51.1[9]
Average velocity along fuel rods (ft/sec)	17.1[3]	15.6[9]
Average mass velocity (10^6 lb_m/hr-ft^2)	2.71[3]	2.46[9]
Coolant Temperature		
Nominal inlet (°F)	559.5[3]	557.5[4]
Average rise in vessel (°F)	58.0[3]	63.2[4]
Average rise in core (°F)	60.6[3]	67.2[4]
Average in core (°F)	591.4[3]	593.1[4]
Average in vessel (°F)	588.5	589.1

Design Parameters	Seabrook Cycle 10 Design	Seabrook Uprate
Heat Transfer		
Active heat transfer, surface area (ft^2)	59,700	59,700
Average heat flux (Btu/hr-ft^2)	189,800	203,500
Maximum heat flux for normal operation (Btu/hr-ft^2)	474,500[5]	508,800[5]
Average linear power (Kw/ft)	5.445	5.84[5]
Peak linear power for normal operation (Kw/ft)	13.6[5]	14.6[5]
Pressure Drop		
Across core (psi)	28.5±2.85[7]	28.6
Across vessel, including nozzle (psi)	48.7±7.3[7]	48.7

1 For conditions outside the range of applicability of WRB-2, the W-3 correlation is used with a correlation limit of 1.45 in the pressure range of 500 to 1000 psia and 1.30 for pressures above 1000 psia.

2 This value is associated with the current design power distribution at 100 % rated power: a 1.60/1.04 = 1.54 FΔH value for V5H and RFA (w/IFMs) chopped cosine axial power shape. Values for the most adverse power distribution within the Axial Flux Difference LCO band are cycle dependent and may be slightly lower.

3 At minimum measured flow conditions.

4 At thermal design flow conditions

5 This limit is associated with the current design value of $F_Q = 2.50$.

6 Based on the original best estimate reactor flow rate as discussed in Section 5.1, and with thimble plug assemblies inserted.

7 For RFA (w/IFMs) based on a measured flow of 404,000 GPM Thimble Plugs Inserted.

8 For conditions outside the range of applicability of WRB-2M, the WRB-2 or W-3 correlation is used. The W-3 correlation limits are 1.45 in the pressure range of 500 to 1000 psia and 1.30 for pressures above 1000 psia.

9 Based on minimum measured flow = 383,000 gpm, best estimate bypass flow = 6.8%, 2250 psia, vessel average temperature = 589.1°F.

10 This value associated with $F_{\Delta H} = 1.587 = 1.67/1.04$, 100% power and 1.55 cosine axial shape.

TABLE 4.4-2 VOID FRACTIONS AT NOMINAL REACTOR CONDITIONS

	Average (%)	Maximum (%)
Core	0.0	-
Hot Subchannel	0.3	7.0

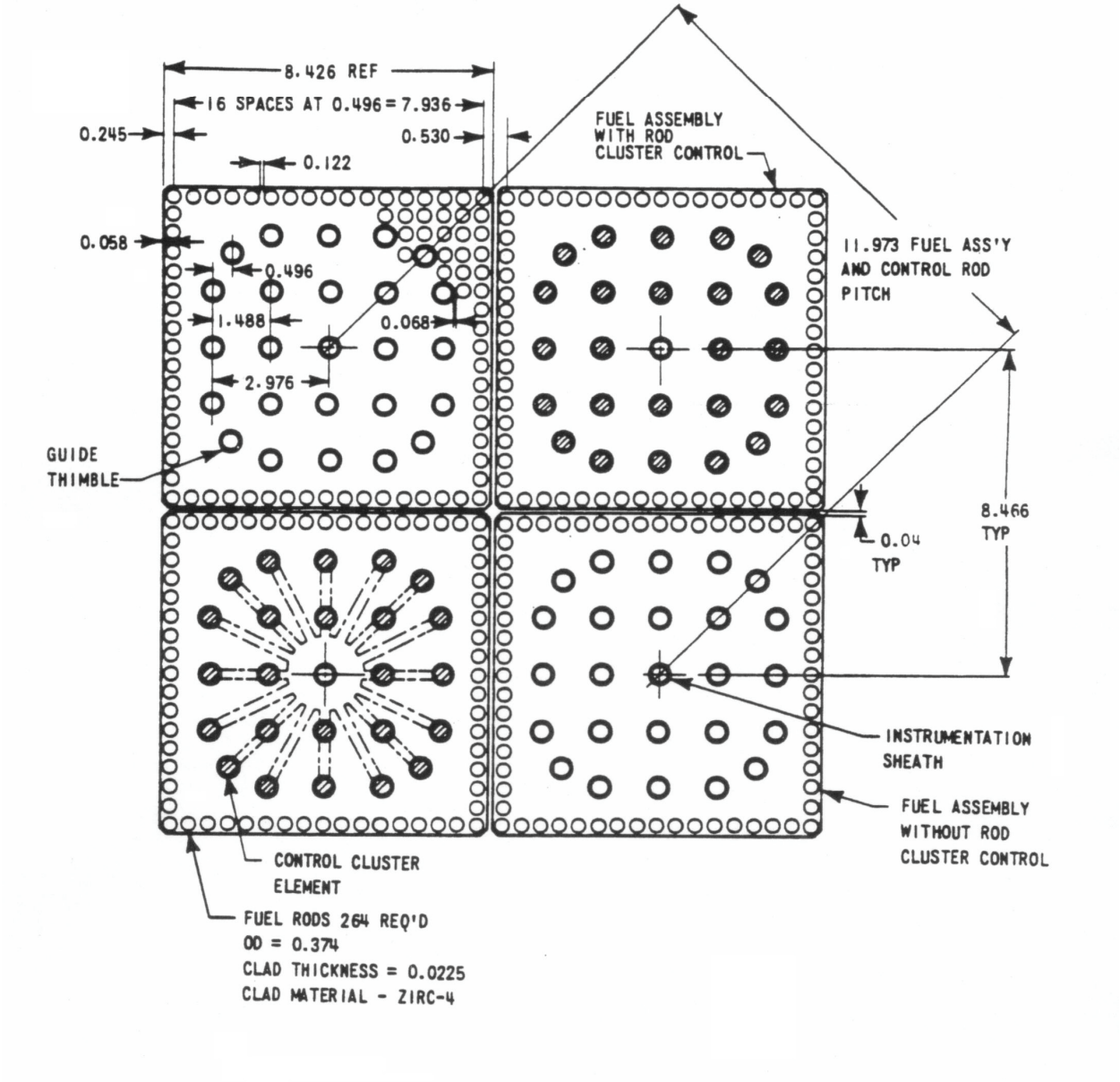

SEABROOK STATION UPDATED FINAL SAFETY ANALYSIS REPORT	Fuel Assembly Cross Section - 17x17	
		Figure 4.2-1

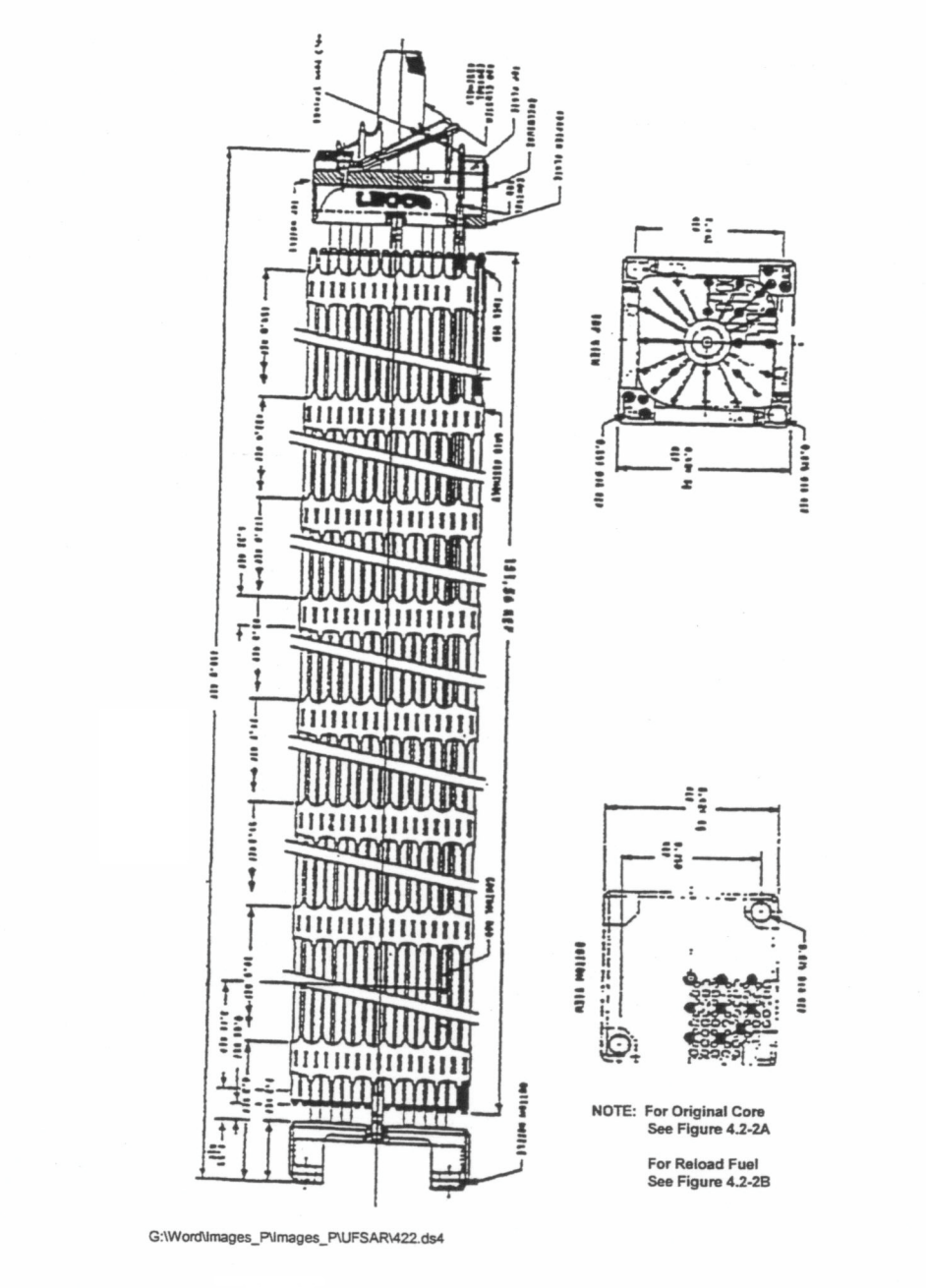

SEABROOK STATION UPDATED FINAL SAFETY ANALYSIS REPORT	Fuel Assembly Outline – 17X17	
		Figure 4.2-2

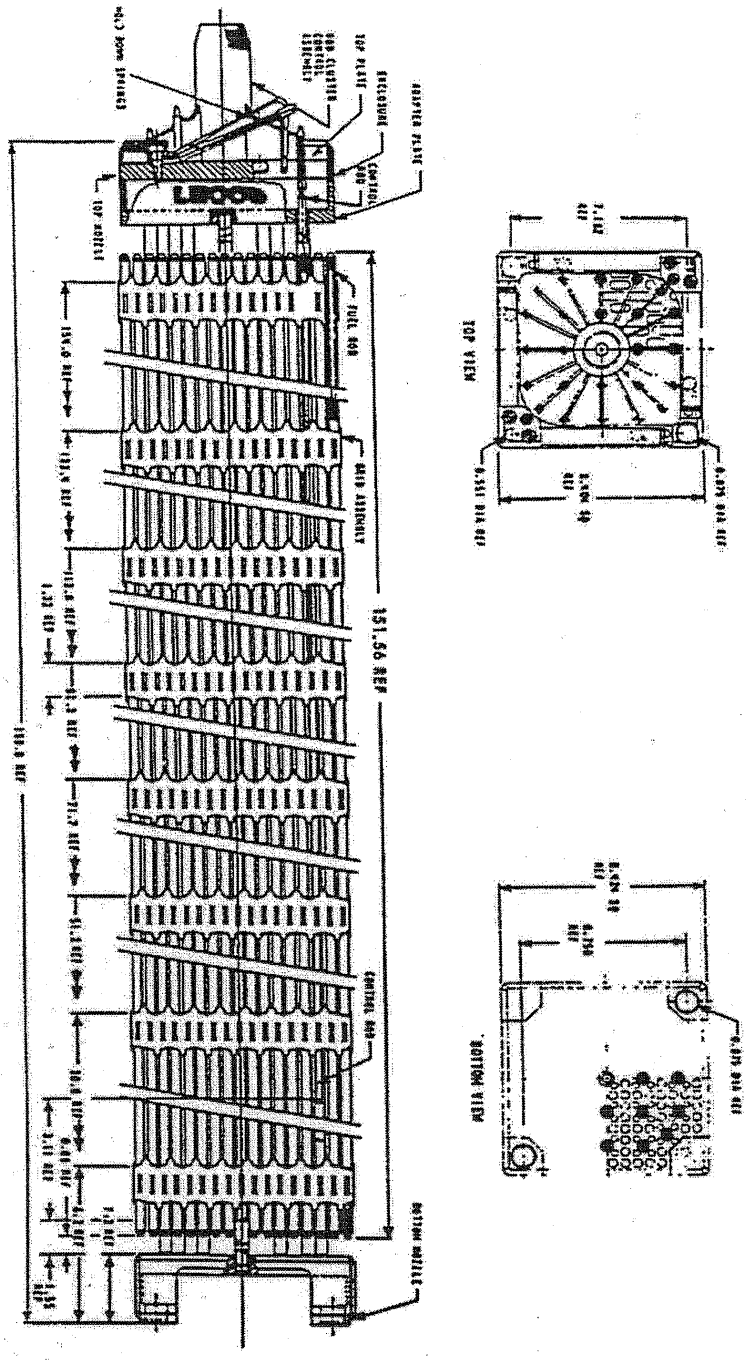

SEABROOK STATION UPDATED FINAL SAFETY ANALYSIS REPORT	Fuel Assembly Outline - 17x17 Original Core	
		Figure 4.2-2A

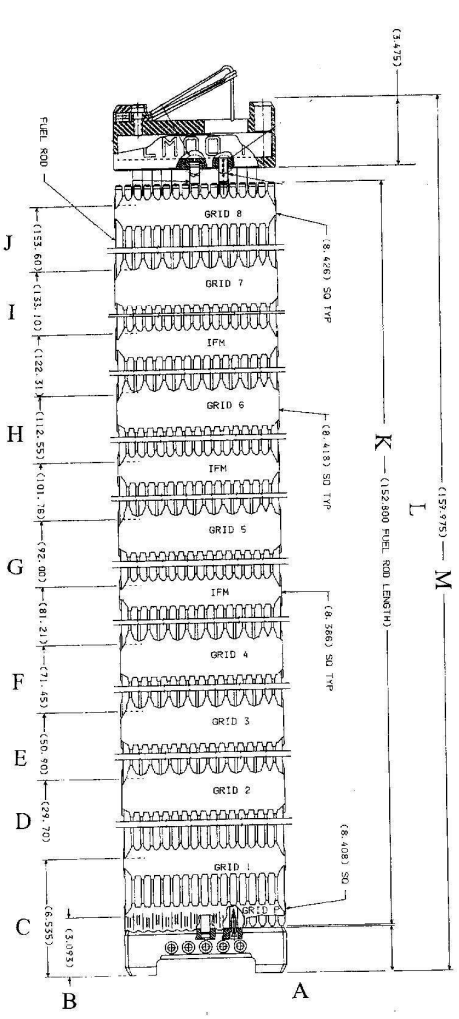

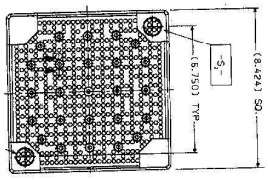

Dim.	17 X 17 STD	V5H* w/P-grid	RFA
A	2.383	2.383	2.383
B	N/A	3.093	3.093
C	5.84	6.535	6.535
D	30.26	29.70	29.70
E	50.81	50.90	50.90
F	71.36	71.45	71.45
G	91.91	92.00	92.00
H	112.46	112.55	112.55
I	133.01	133.10	133.10
J	153.60	153.40	153.60
K	152.20	152.60	152.61
L	156.50	156.30	156.50
M	159.98	159.775	159.98

*Dimensions also apply to V5H with IFMs

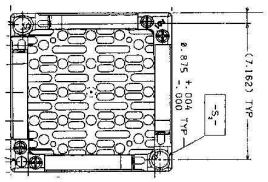

G:\Word\Images_P\UFSAR\422b.ds4

SEABROOK STATION UPDATED FINAL SAFETY ANALYSIS REPORT	Fuel Assembly Outline - 17X17 Reload Fuel	
		Figure 4.2-2B

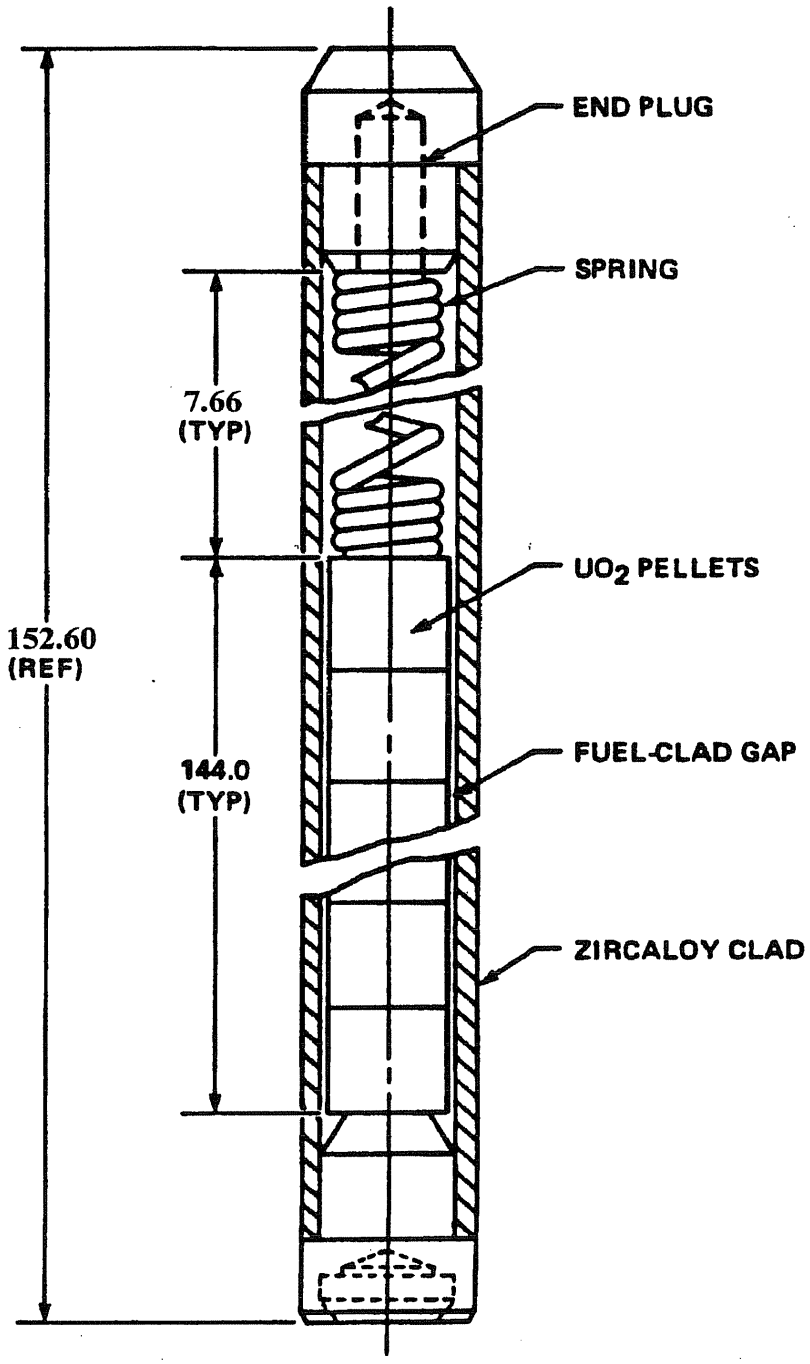

SPECIFIC DIMENSIONS DEPEND ON DESIGN VARIABLES SUCH AS PRE-PRESSURIZATION, POWER HISTORY, AND DISCHARGE BURNUP

SEABROOK STATION UPDATED FINAL SAFETY ANALYSIS REPORT	Fuel Rod Schematic	
		Figure 4.2-3

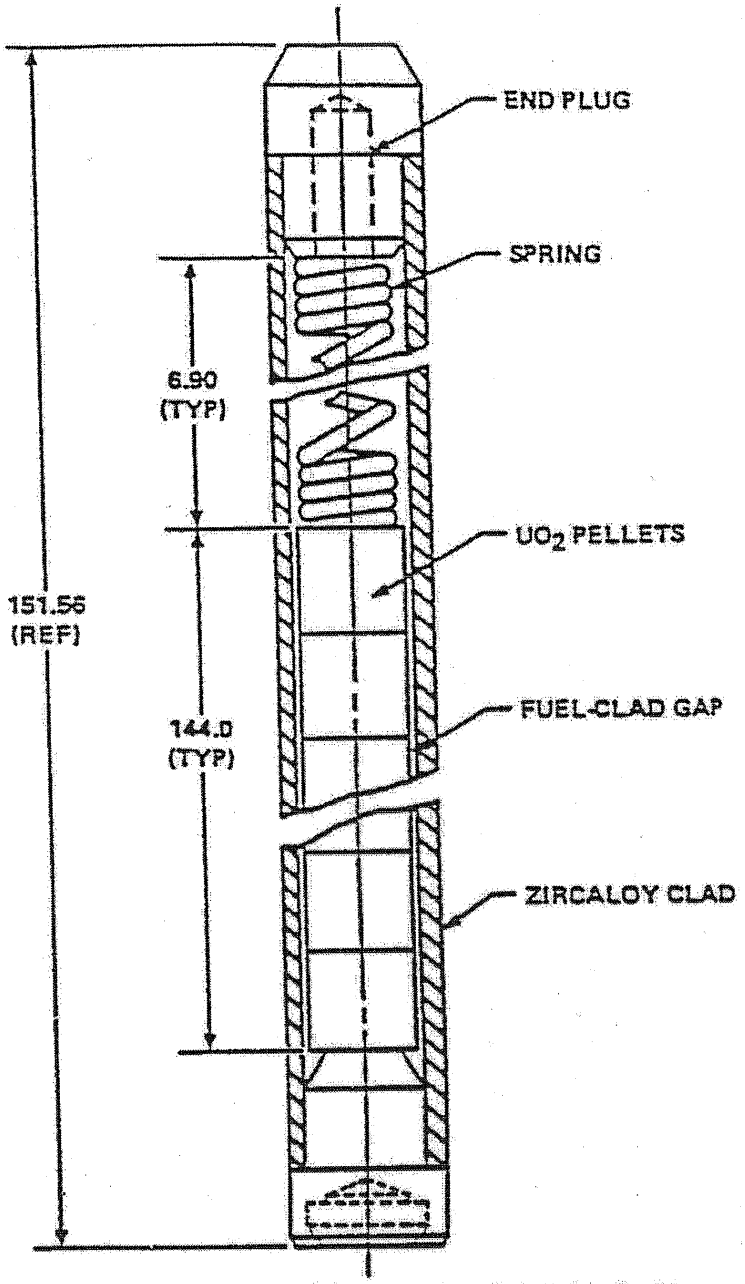

SPECIFIC DIMENSIONS DEPEND ON DESIGN VARIABLES SUCH AS PRE-PRESSURIZATION, POWER HISTORY, AND DISCHARGE BURNUP

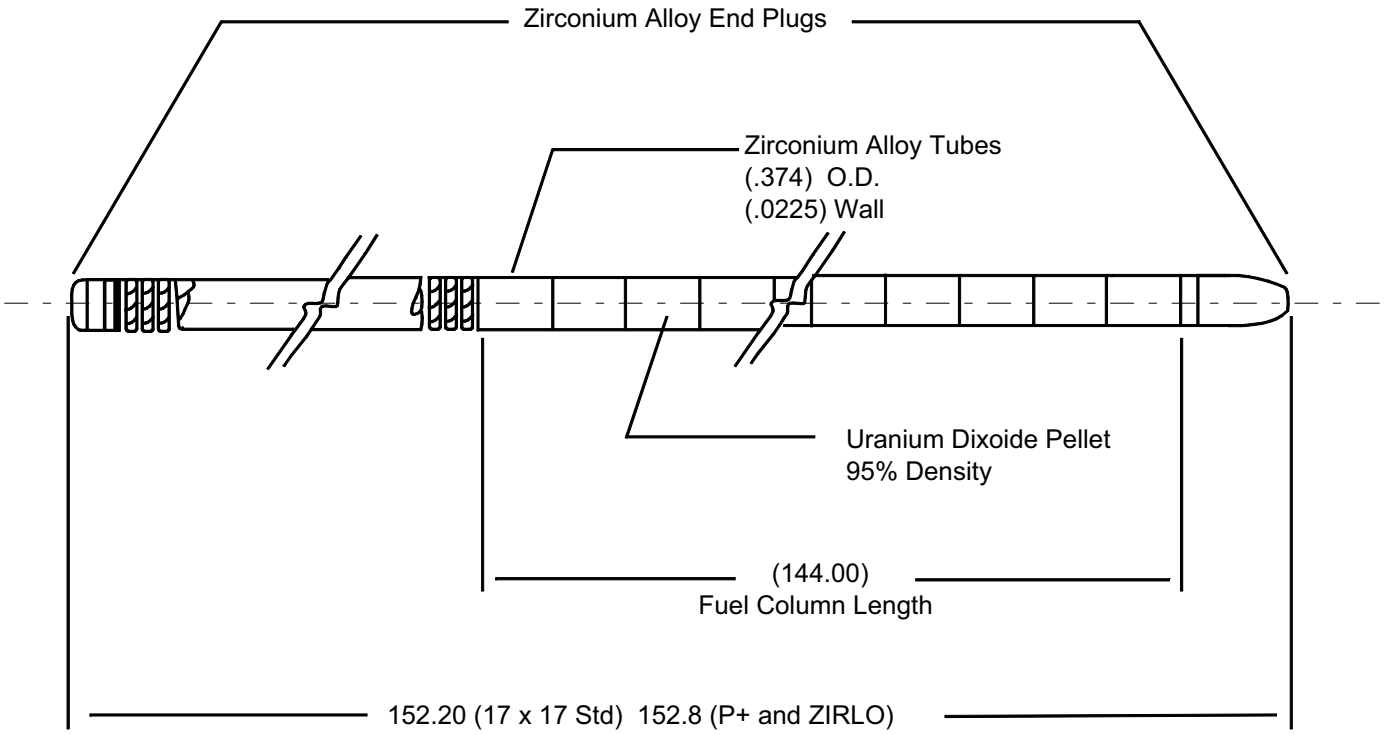

G:\Word\Images_P/UFSAR\423b.dsf

SEABROOK STATION UPDATED FINAL SAFETY ANALYSIS REPORT	Fuel Rod Schematic - Reload Fuel	
		Figure 4.2-3B

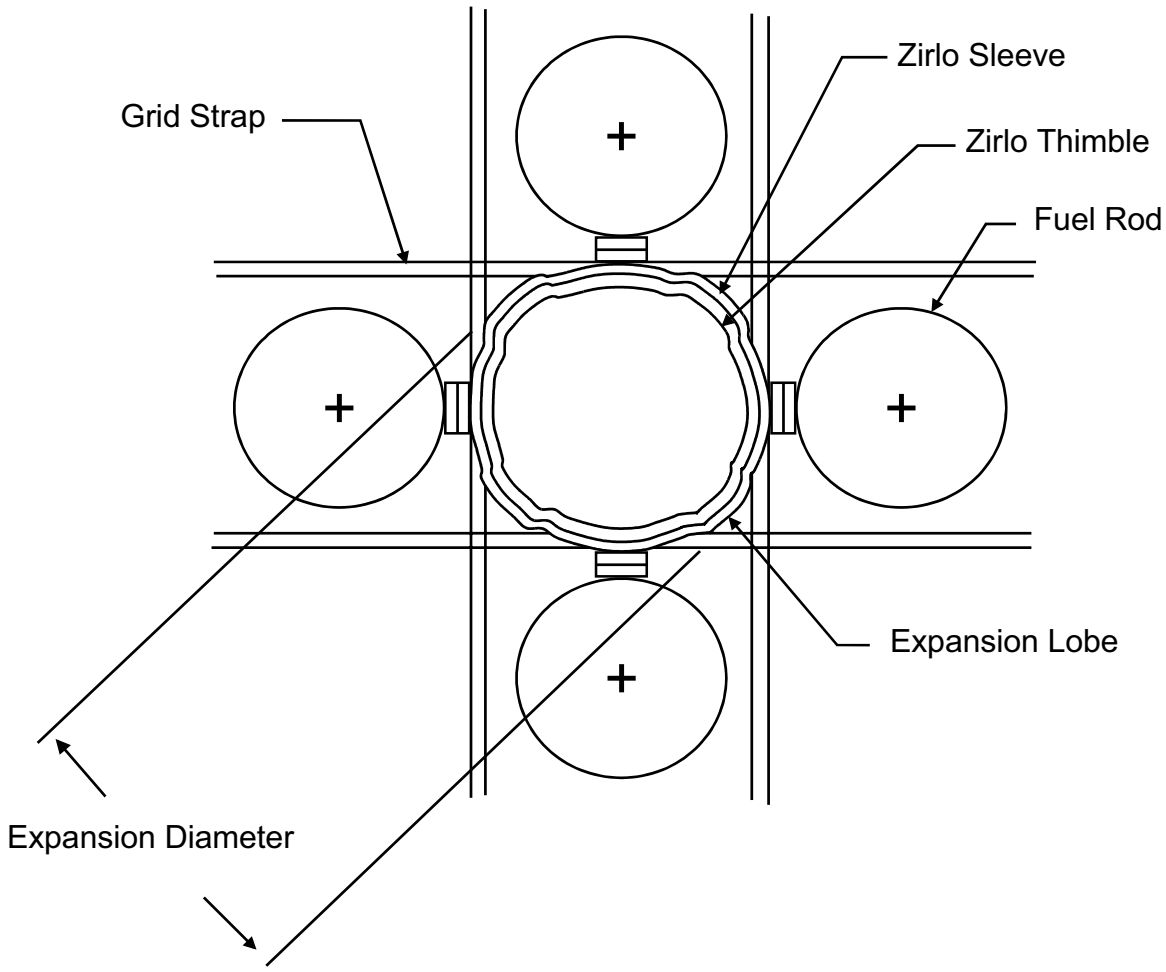

SEABROOK STATION UPDATED FINAL SAFETY ANALYSIS REPORT	Plan View	
		Figure 4.2-4

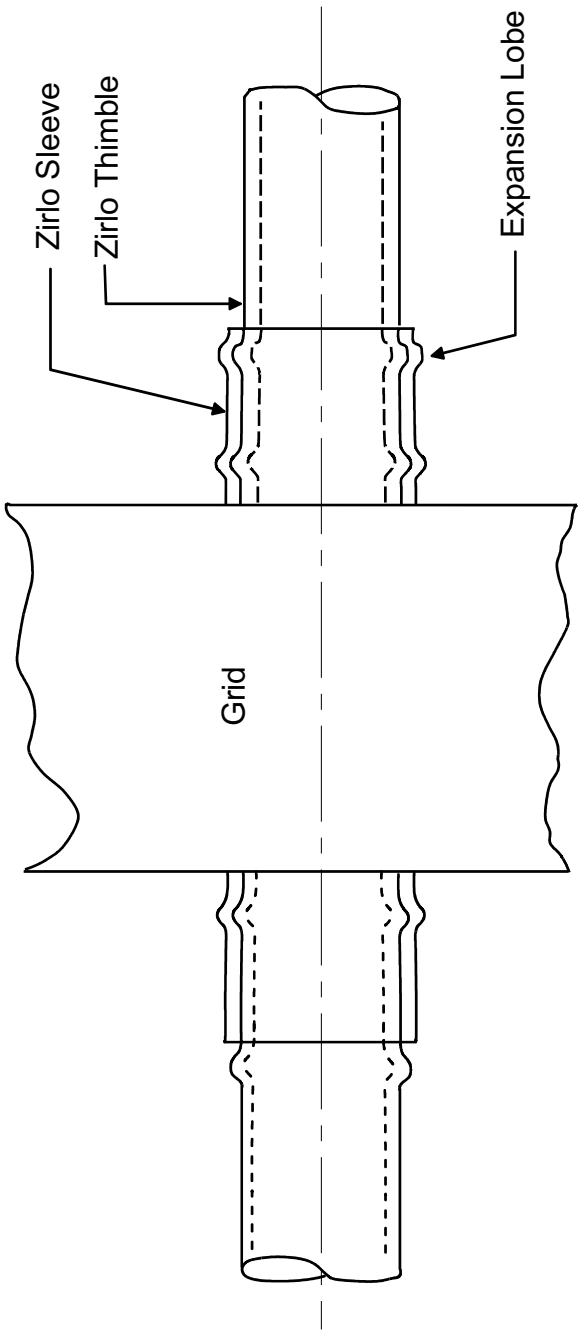

G:\Word\Images_P\UFSAR\425.ds4

SEABROOK STATION UPDATED FINAL SAFETY ANALYSIS REPORT	Elevation View	
		Figure 4.2-5

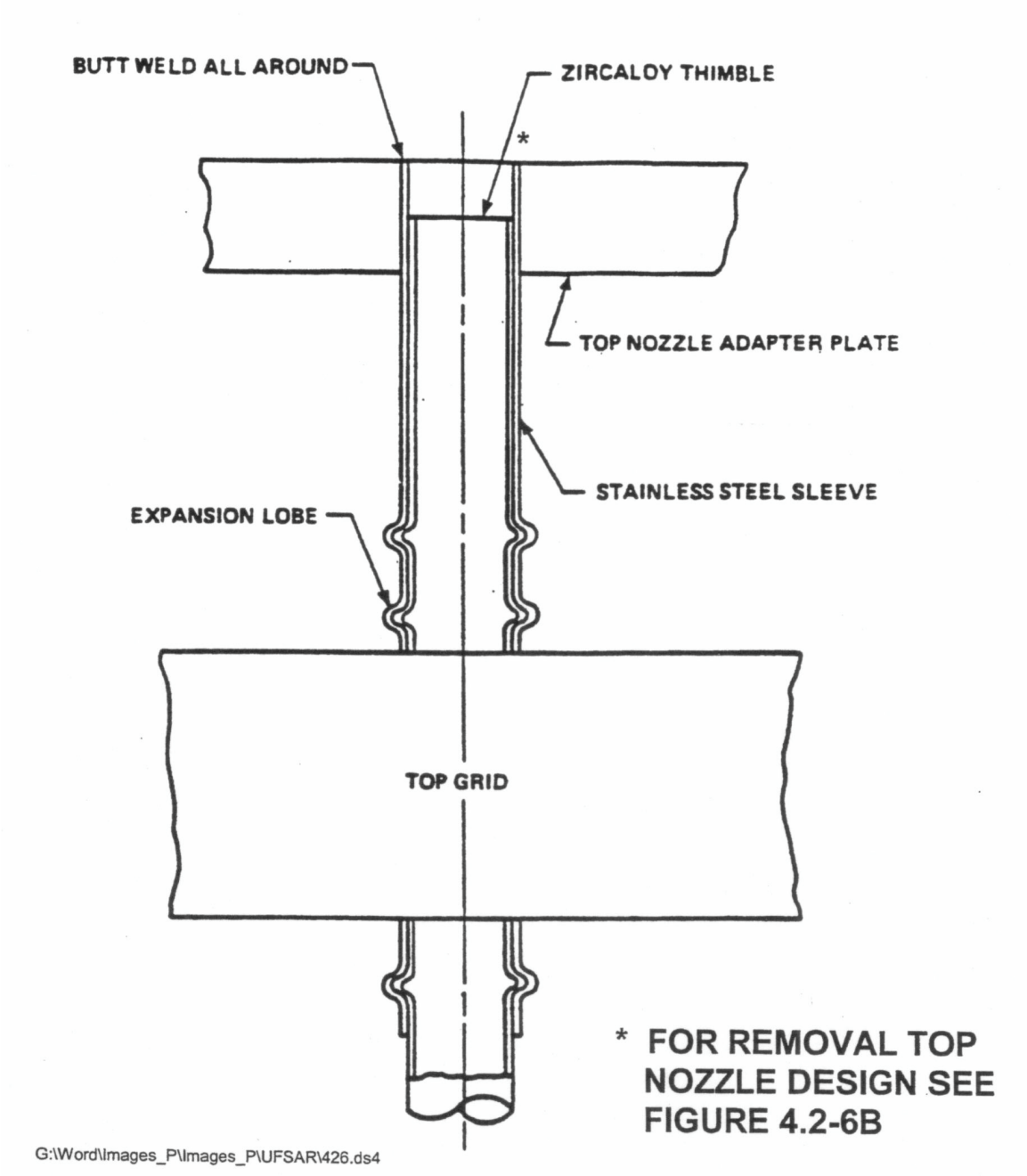

SEABROOK STATION UPDATED FINAL SAFETY ANALYSIS REPORT	Top Grid to Nozzle Attachment	
		Figure 4.2-6

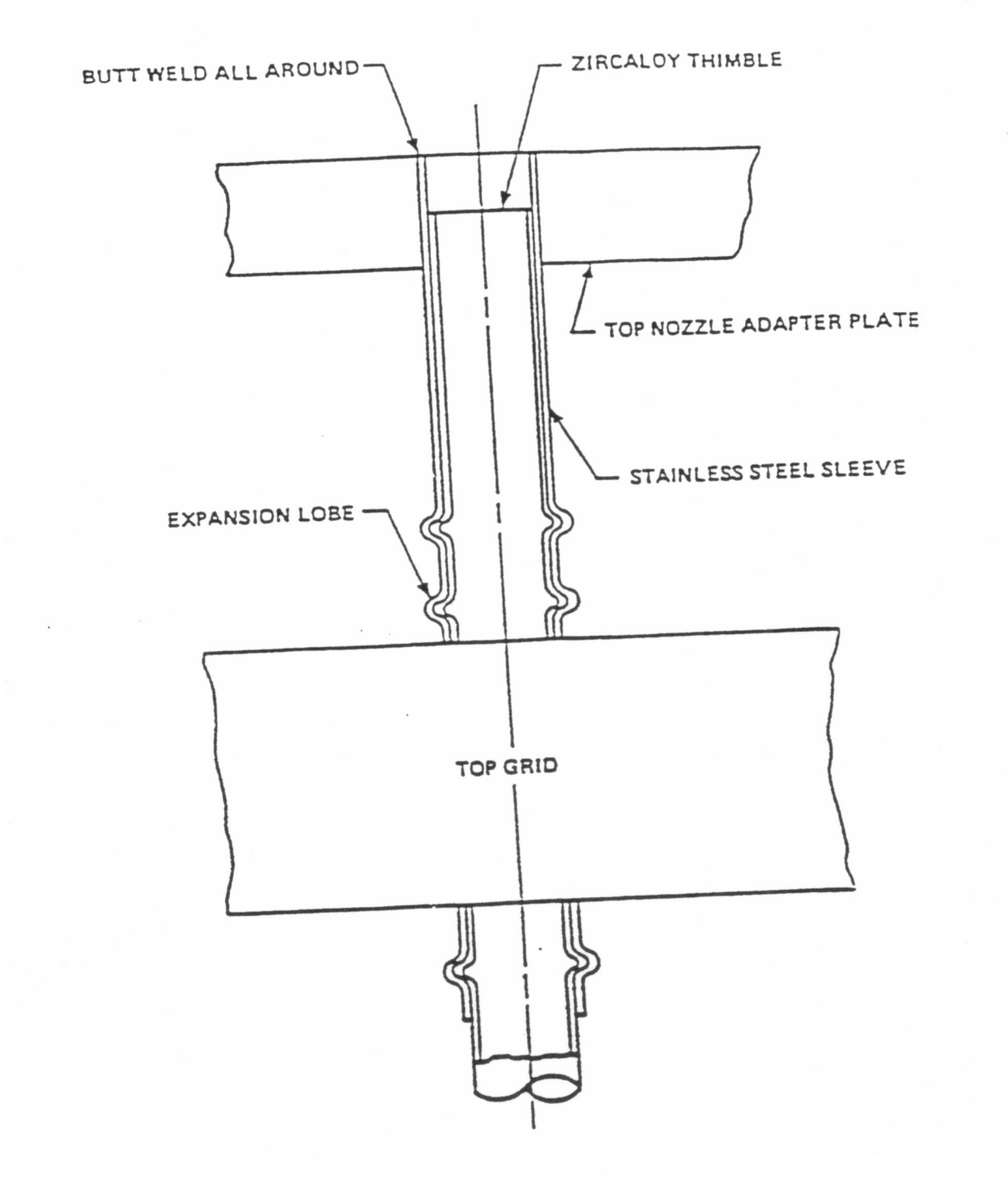

SEABROOK STATION UPDATED FINAL SAFETY ANALYSIS REPORT	Top Grid to Nozzle Attachment - Original Core	
		Figure 4.2-6A

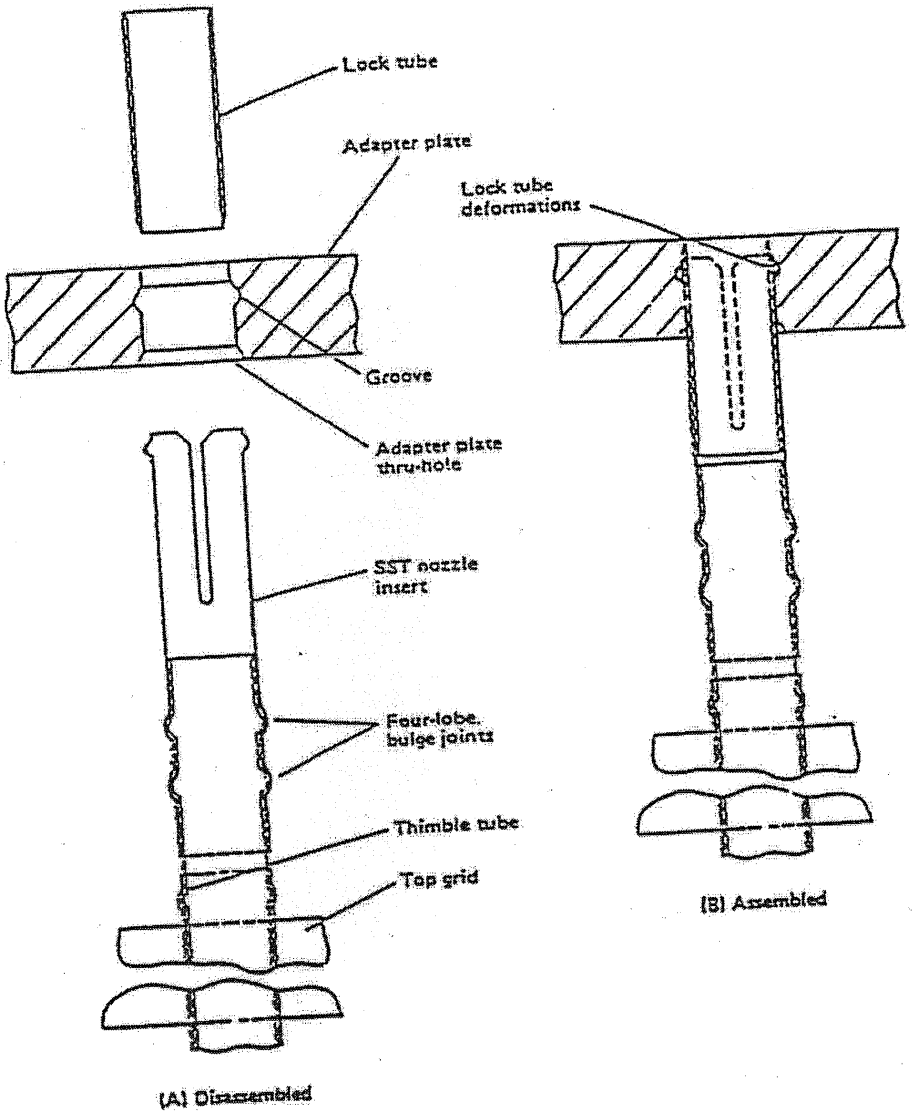

SEABROOK STATION UPDATED FINAL SAFETY ANALYSIS REPORT	Removable Top Nozzle (RTN) Top Grid to Nozzle Attachment - Reload Fuel	
		Figure 4.2-6B

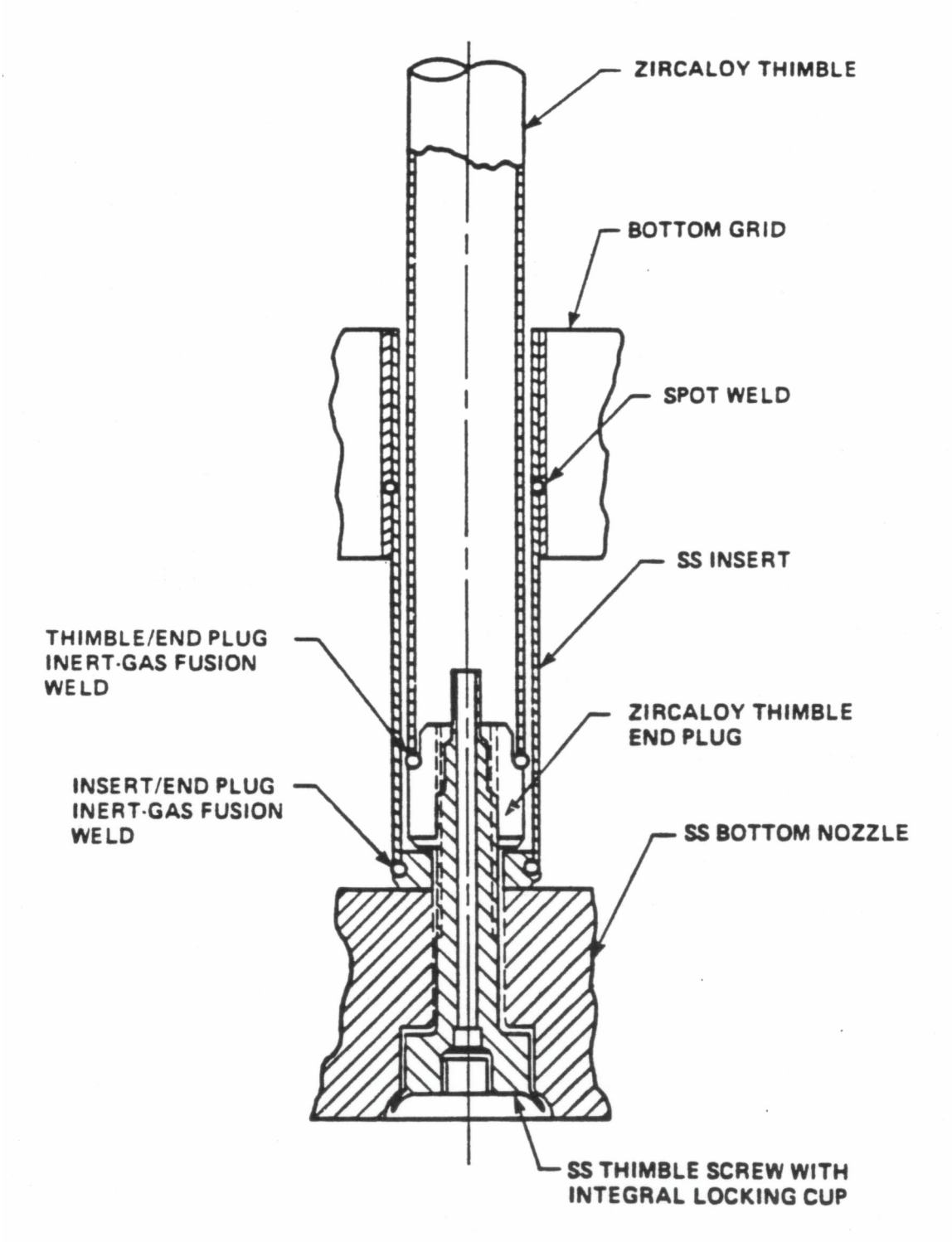

SEABROOK STATION UPDATED FINAL SAFETY ANALYSIS REPORT	Guide Thimble to Bottom Nozzle Joint	
		Figure 4.2-7

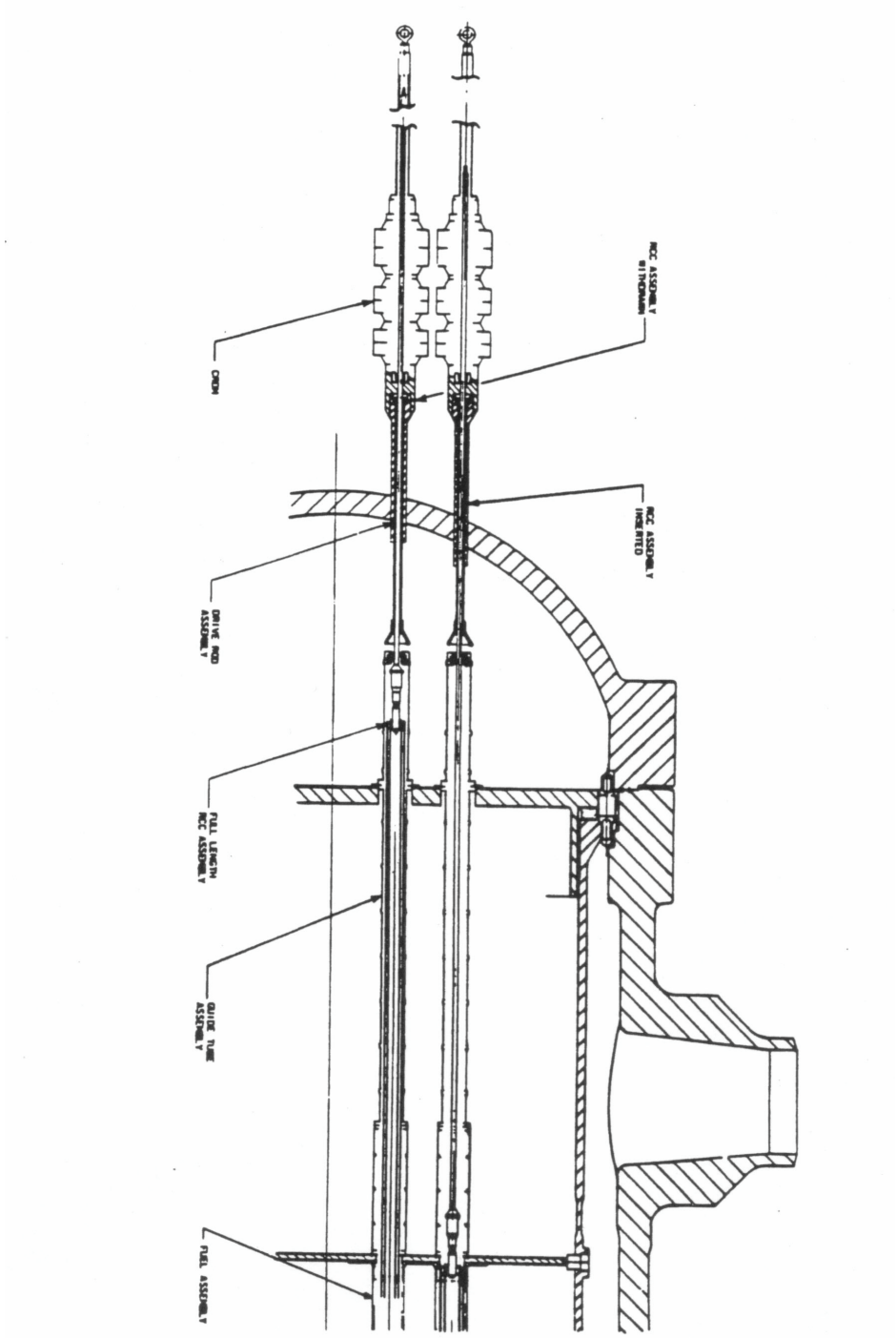

SEABROOK STATION UPDATED FINAL SAFETY ANALYSIS REPORT	Rod Cluster Control and Drive Rod Assembly with Interfacing Components	
		Figure 4.2-8

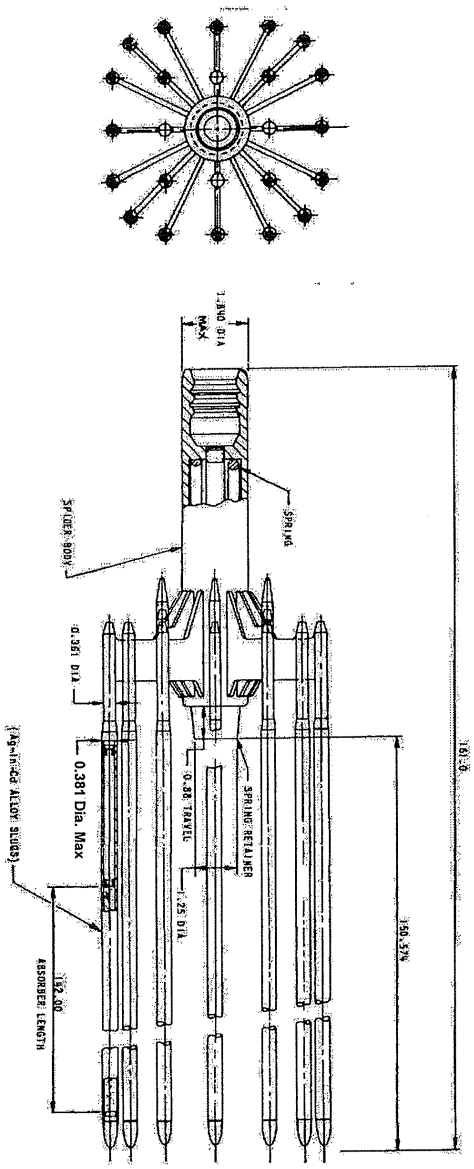

G:\Word\Images_P\UFSAR\429.ds4

SEABROOK STATION UPDATED FINAL SAFETY ANALYSIS REPORT	Rod Cluster Control Assembly Outline	
		Figure 4.2-9

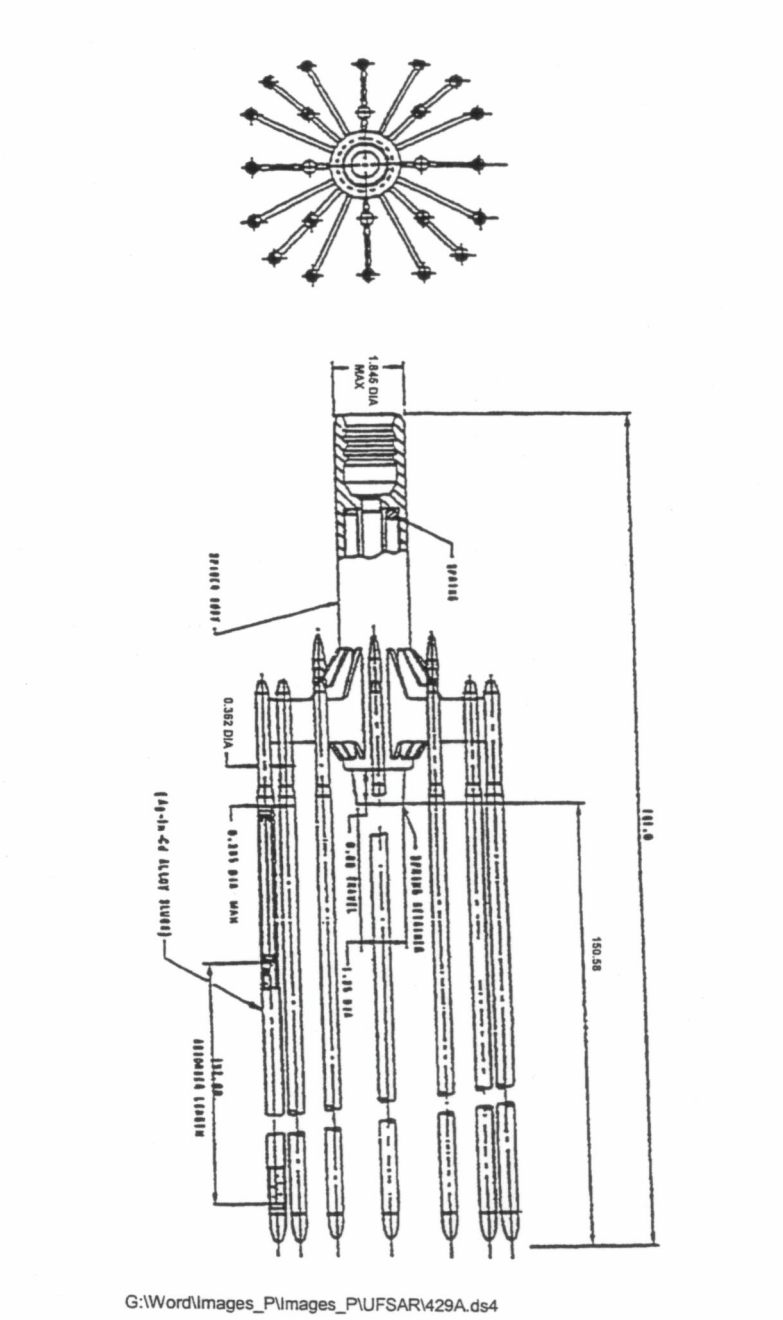

SEABROOK STATION UPDATED FINAL SAFETY ANALYSIS REPORT	Rod Cluster Control Assembly Outline - Original RCCAs	
		Figure 4.2-9A

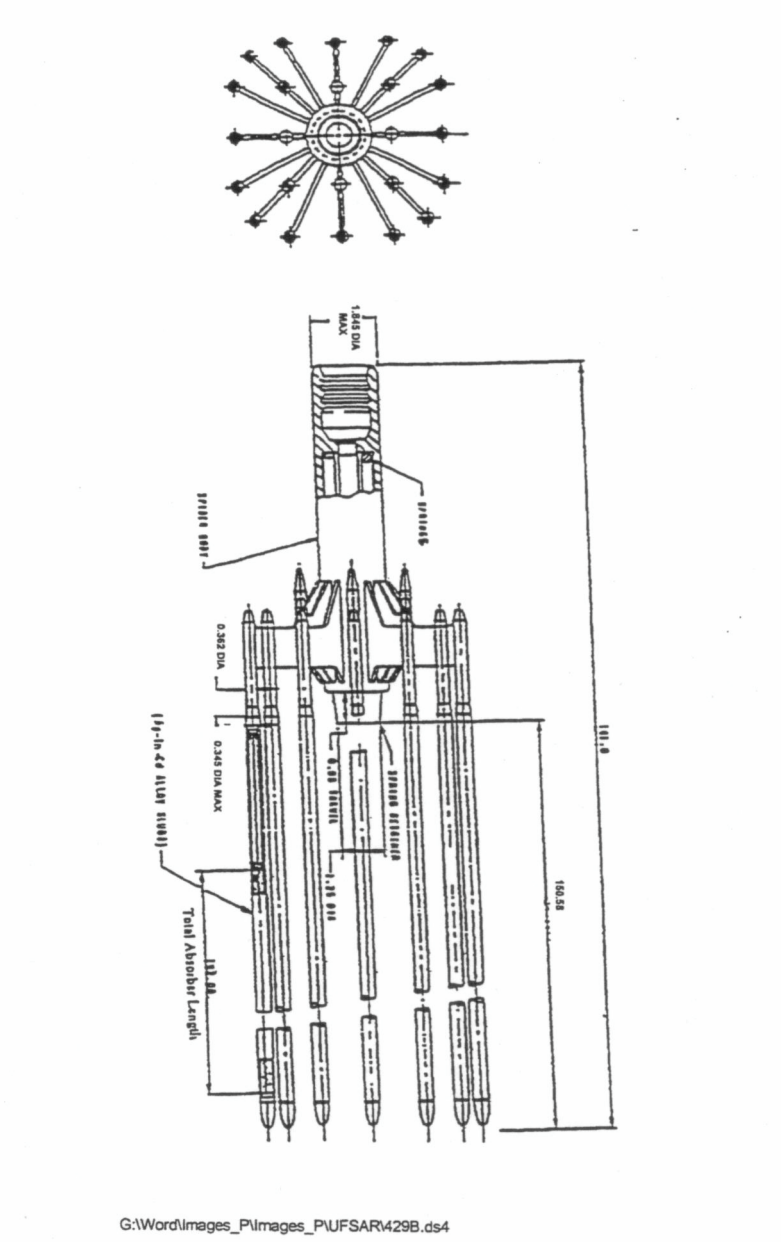

SEABROOK STATION UPDATED FINAL SAFETY ANALYSIS REPORT	Rod Cluster Control Assembly Outline - Replacement RCCAs	
		Figure 4.2-9B

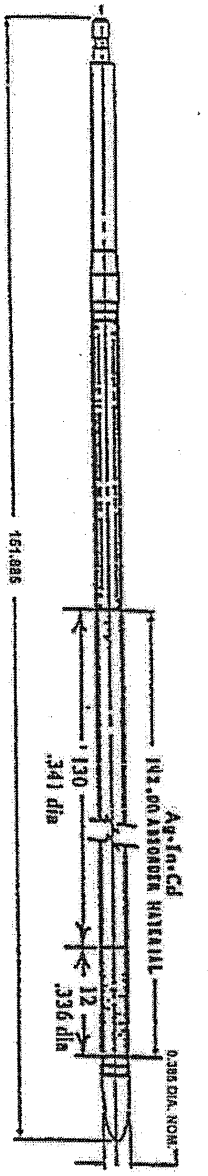

G:\Word\Images_P\Images_P\UFSAR\4210B.ds4

SEABROOK STATION UPDATED FINAL SAFETY ANALYSIS REPORT	Ag-In-Cd Absorber Rod	
		Figure 4.2-10

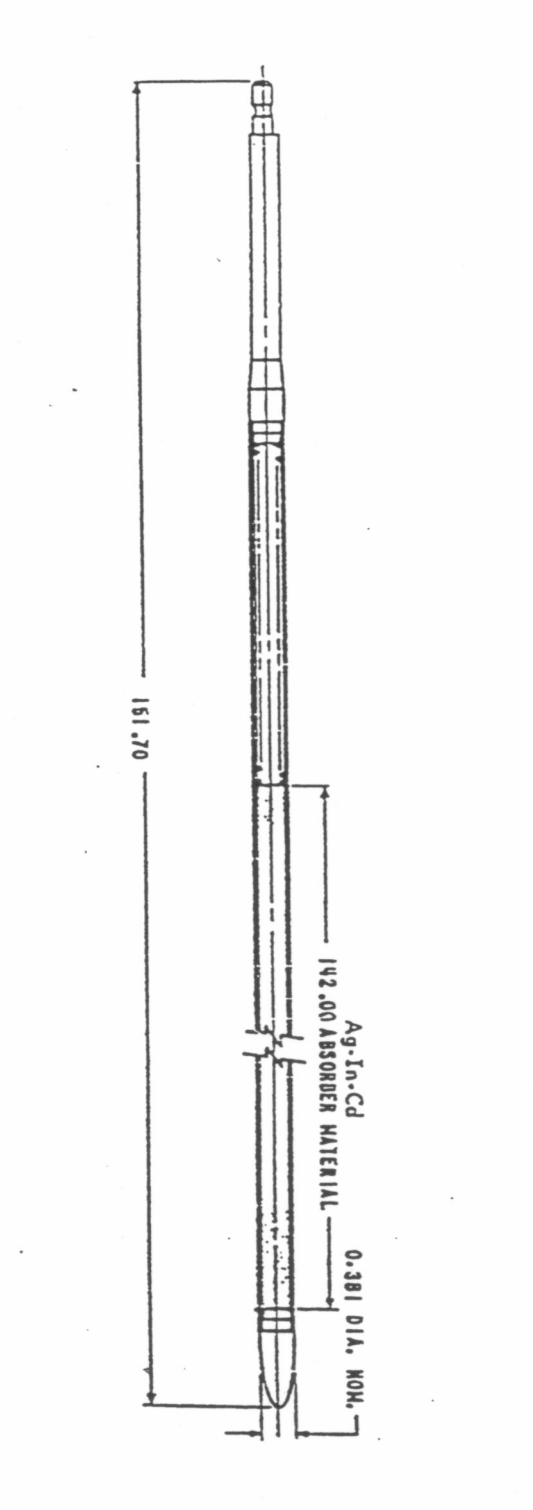

SEABROOK STATION UPDATED FINAL SAFETY ANALYSIS REPORT	Ag-In-Cd Absorber Rod - Original RCCAs	
		Figure 4.2-10A

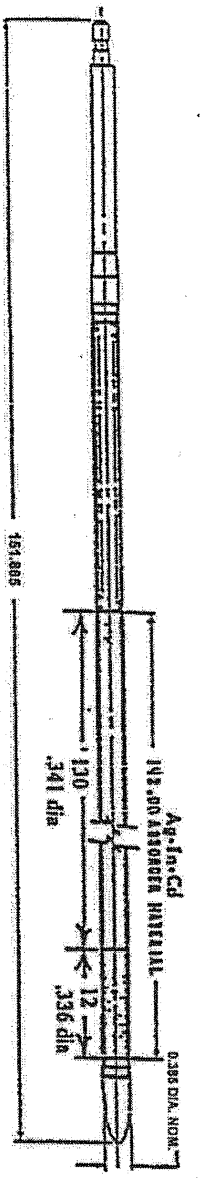

G:\Word\Images_P\Images_P\UFSAR\4210B.ds4

SEABROOK STATION UPDATED FINAL SAFETY ANALYSIS REPORT	Ag-In-Cd Absorber Rod - Replacement RCCAs	
		Figure 4.2-10B

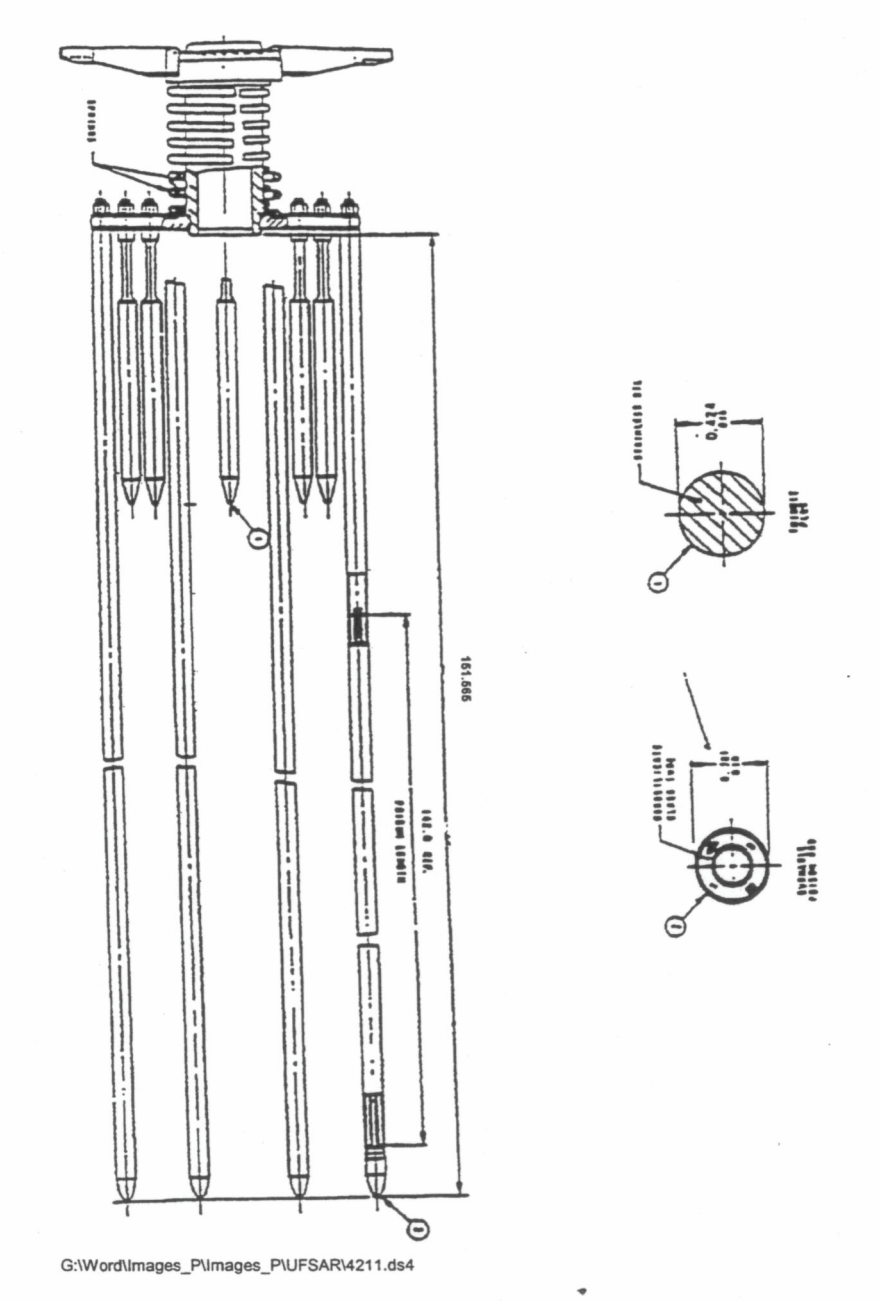

SEABROOK STATION UPDATED FINAL SAFETY ANALYSIS REPORT	Burnable Poison Assembly	
		Figure 4.2-11

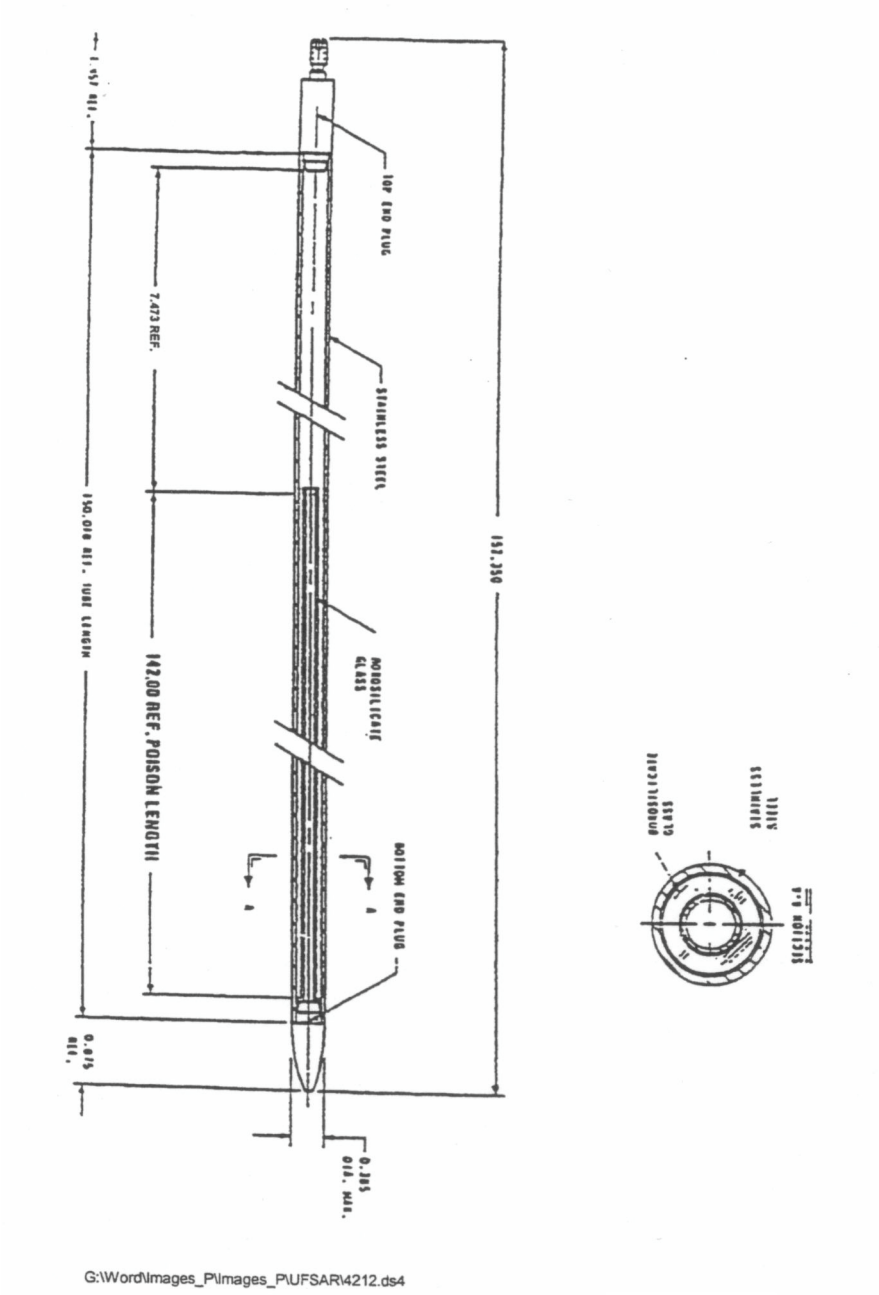

SEABROOK STATION UPDATED FINAL SAFETY ANALYSIS REPORT	Burnable Poison Rod Cross Section	
		Figure 4.2-12

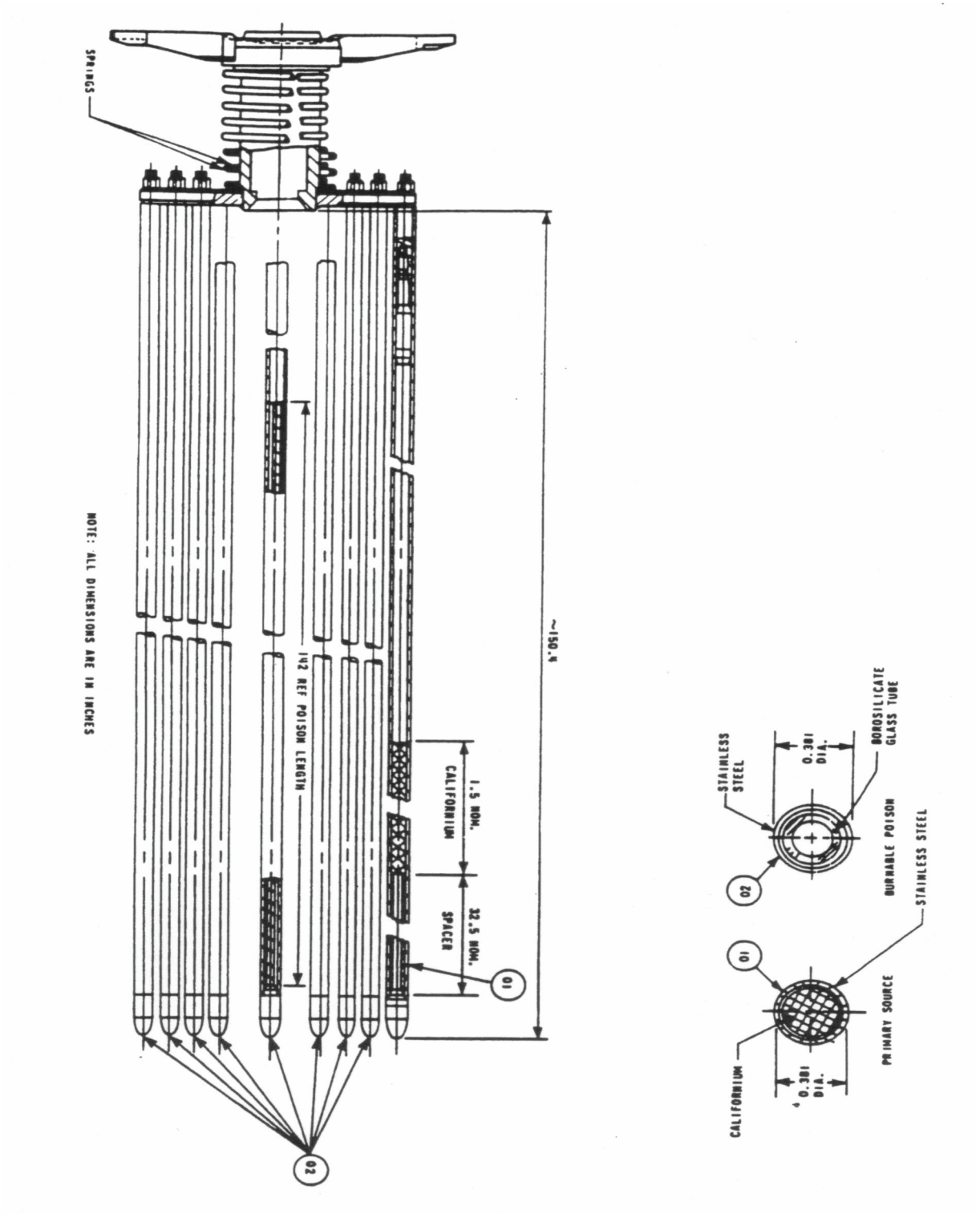

SEABROOK STATION UPDATED FINAL SAFETY ANALYSIS REPORT	Primary Source Assembly	
		Figure 4.2-13

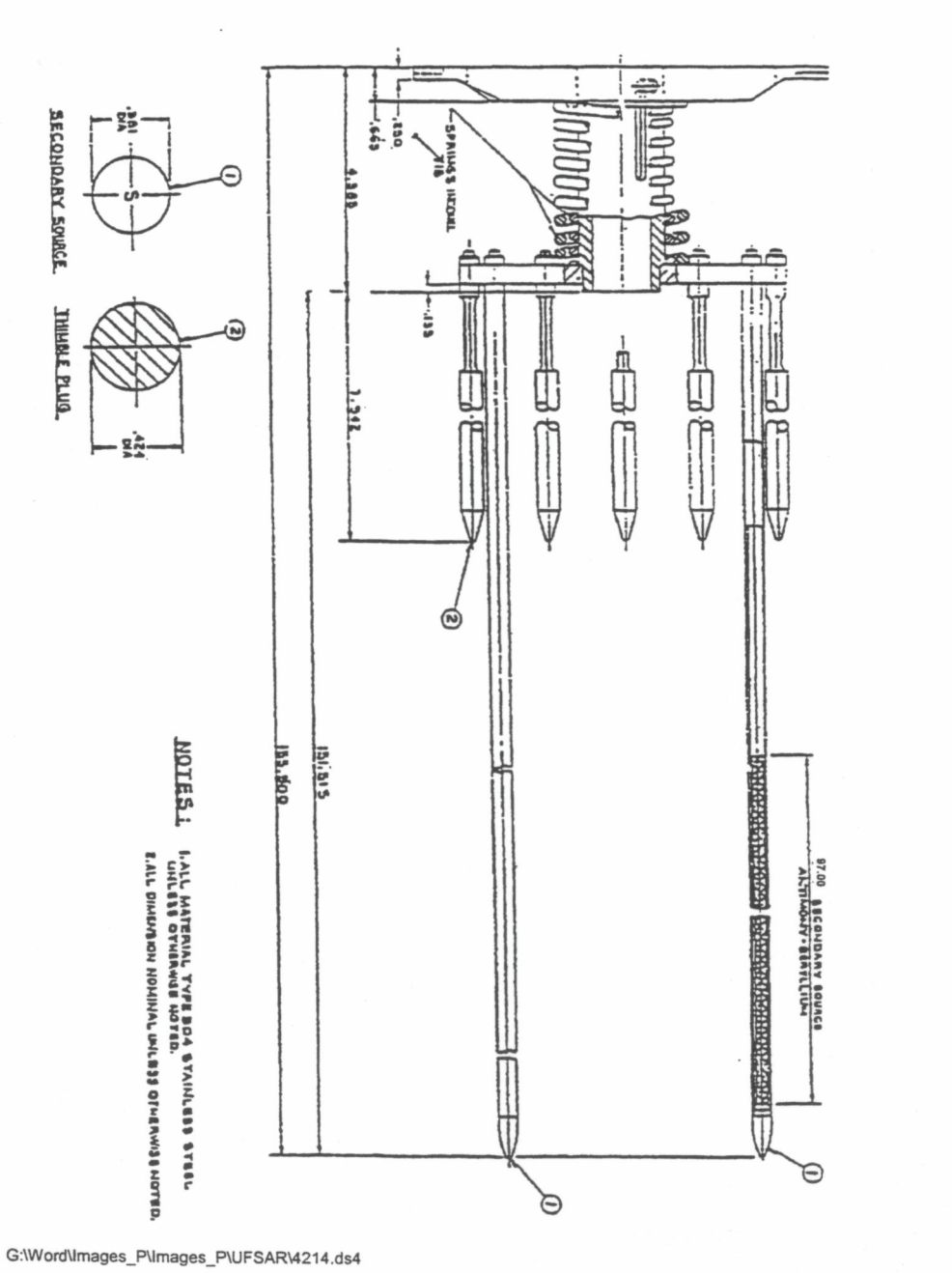

G:\Word\Images_P\Images_P\UFSAR\4214.ds4

SEABROOK STATION UPDATED FINAL SAFETY ANALYSIS REPORT	Secondary Source Assembly	
		Figure 4.2-14

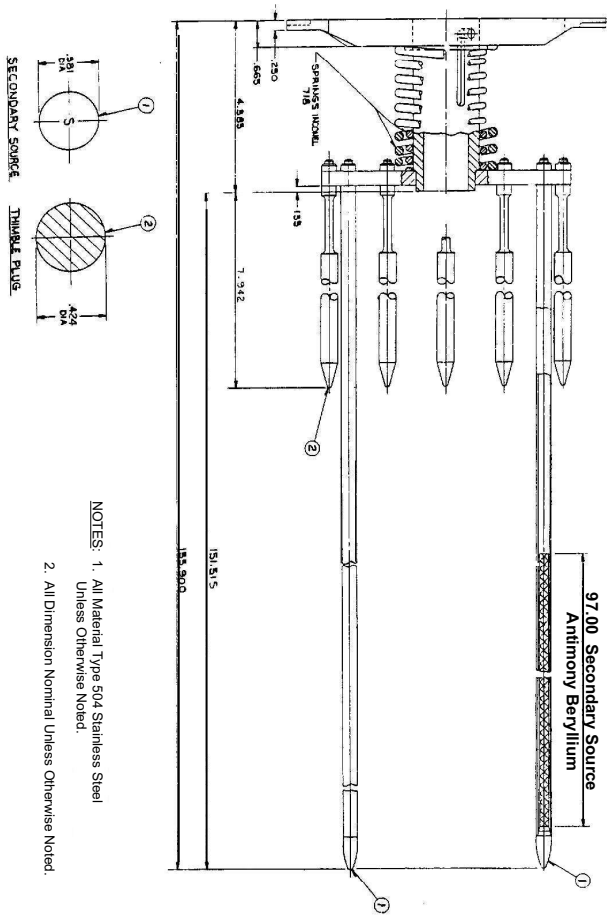

G:\Word\Images_P\UFSAR\4214a.ds4

SEABROOK STATION UPDATED FINAL SAFETY ANALYSIS REPORT	Secondary Source Assembly - Original Core	
		Figure 4.2-14A

Deleted

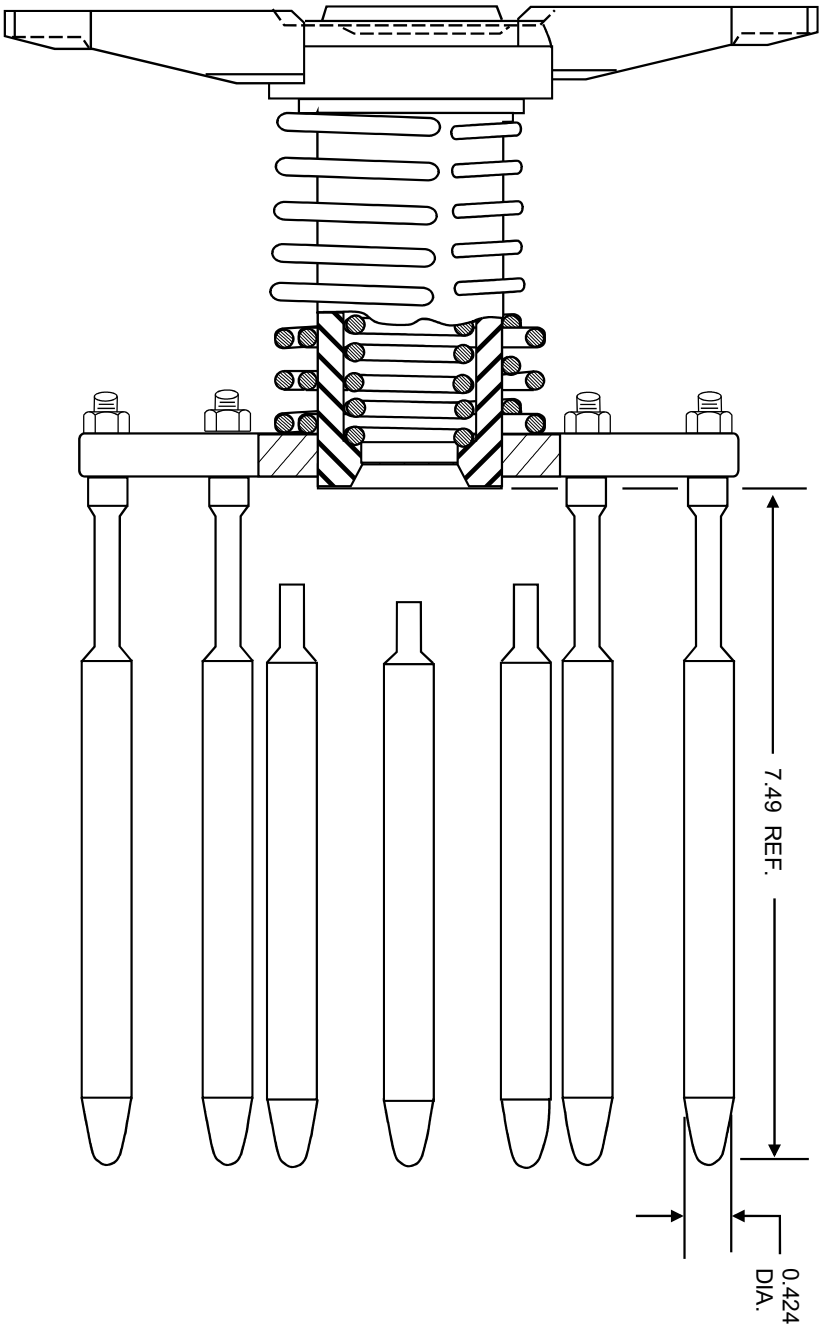

G:\Word\Images_P\UFSAR\4215.ds4

SEABROOK STATION UPDATED FINAL SAFETY ANALYSIS REPORT	Thimble Plug Assembly	
		Figure 4.2-15

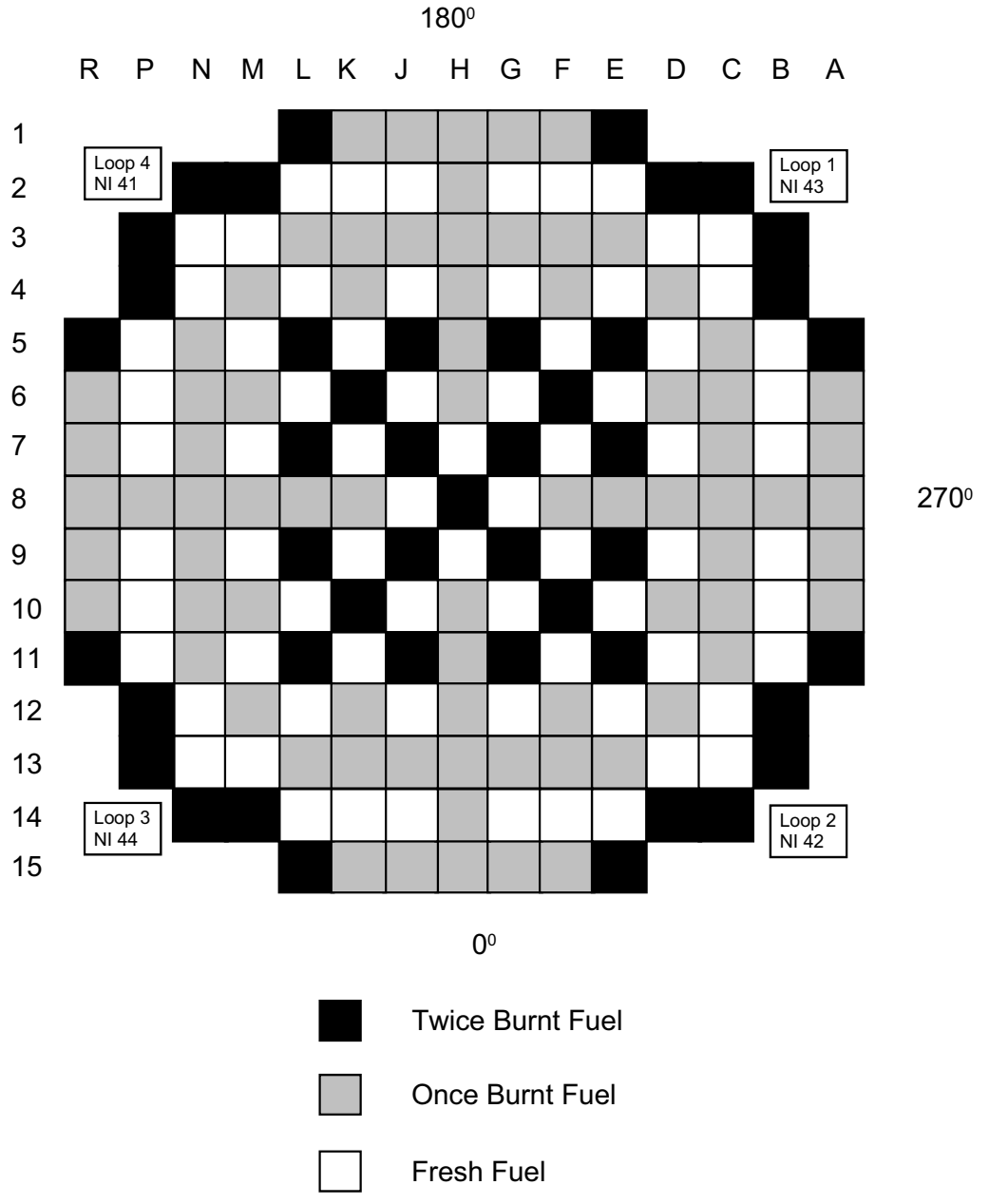

SEABROOK STATION UPDATED FINAL SAFETY ANALYSIS REPORT	Typical Low Leakage Fuel Loading Arrangement	
		Figure 4.3-1

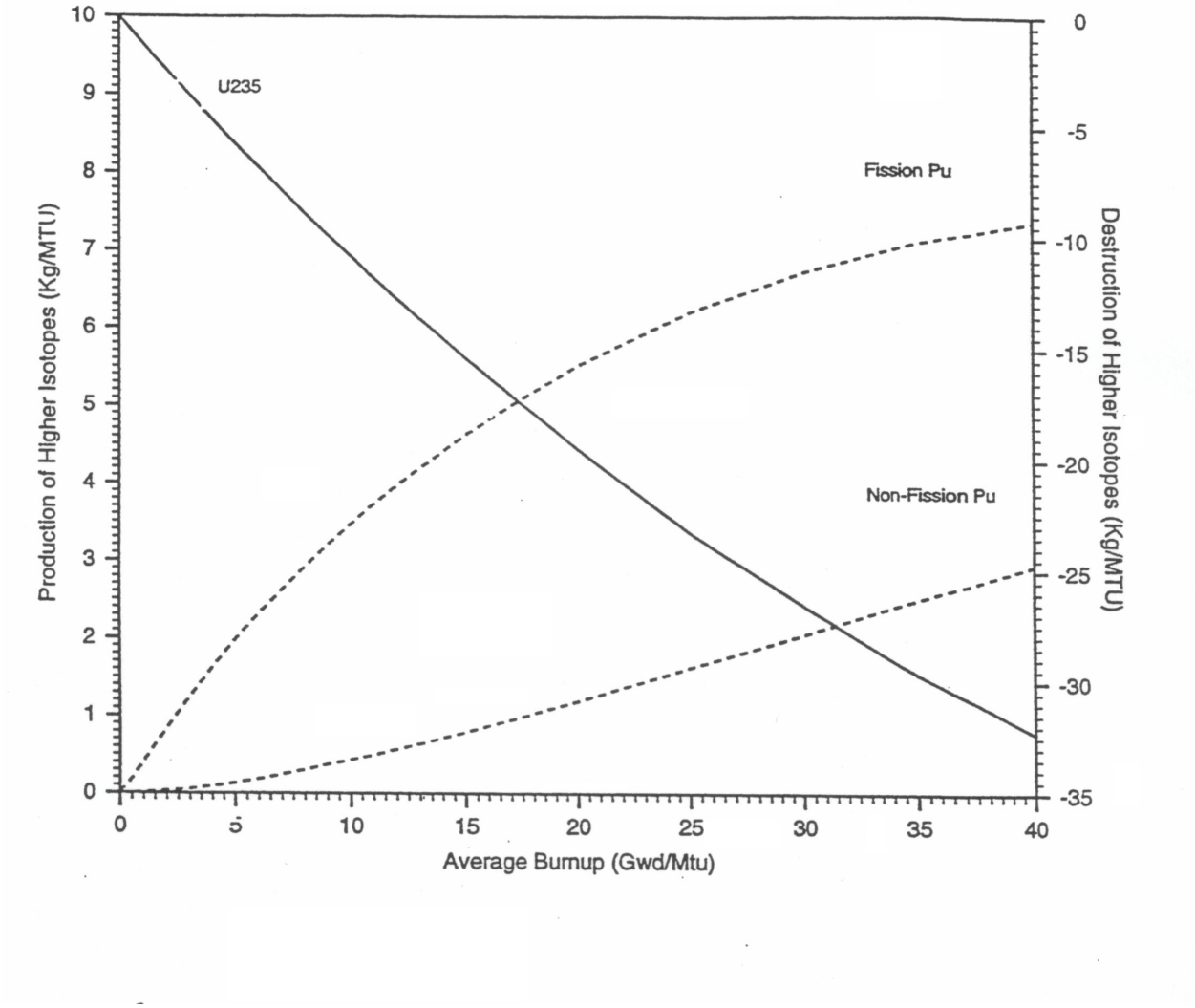

SEABROOK STATION UPDATED FINAL SAFETY ANALYSIS REPORT	Production and Destruction of Higher Isotopes for Typical Low Leakage Cycle Design Fuel	
		Figure 4.3-2

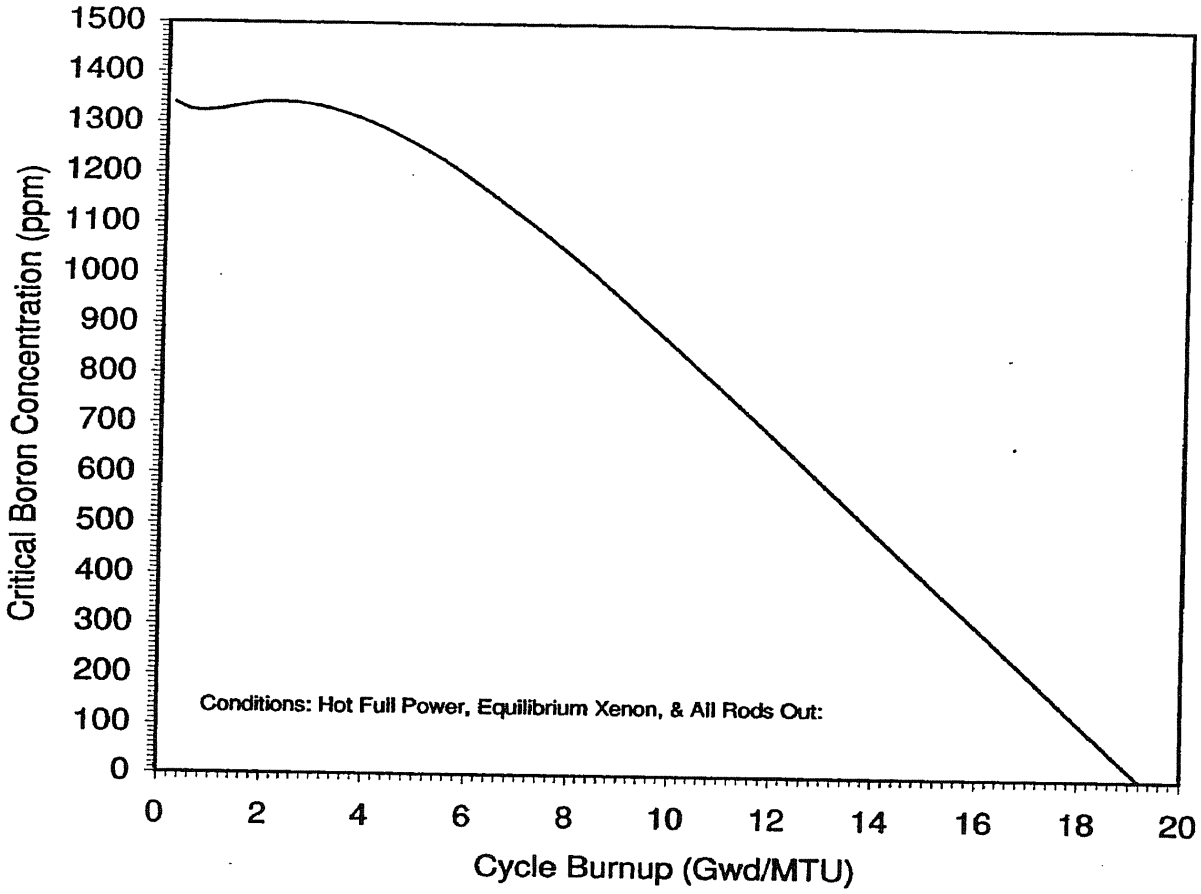

SEABROOK STATION UPDATED FINAL SAFETY ANALYSIS REPORT	Boron Concentration vs. Cycle Burnup for Typical Low Leakage Cycle Design	
		Figure 4.3-3

Standard Assembly Pin Layout

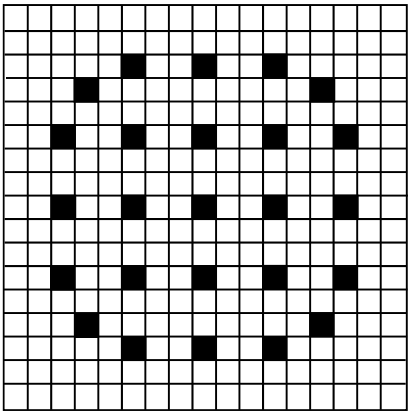

64 IFBA Pin Assembly Layout

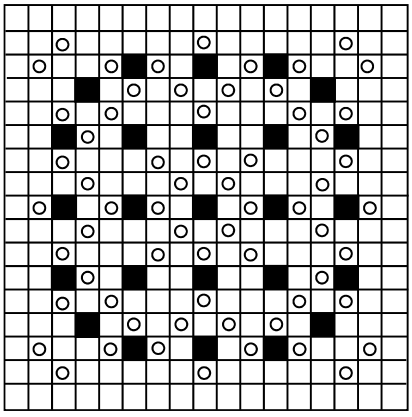

80 IFBA Pin Assembly Layout

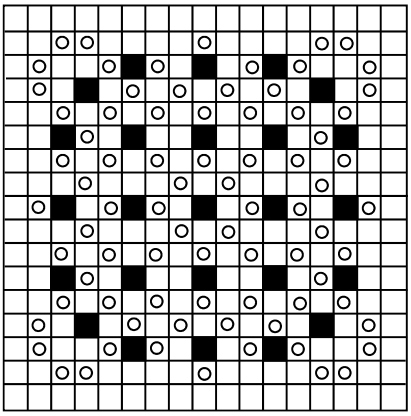

104 IFBA Pin Assembly Layout

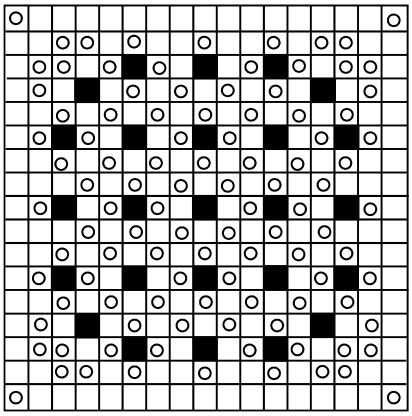

128 IFBA Pin Assembly Layout

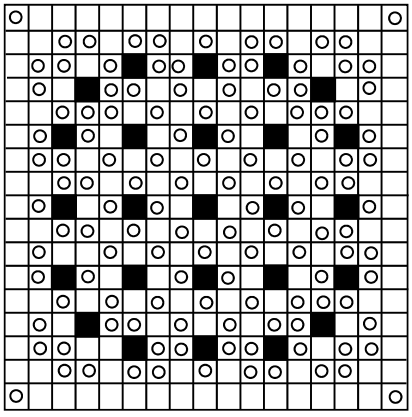

156 IFBA Pin Assembly Layout

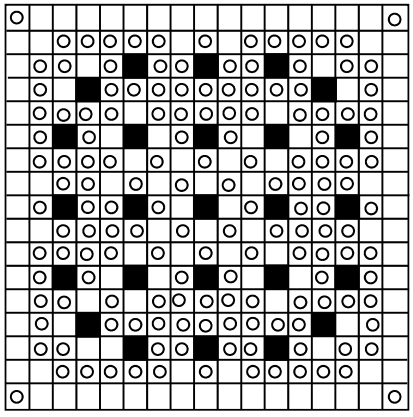

O= IFBA Rod

G:\Word\Images_P\UFSAR\434.ds4

SEABROOK STATION UPDATED FINAL SAFETY ANALYSIS REPORT	Integral Fuel Burnable Absorber Arrangement within an Assembly	
		Figure 4.3-4

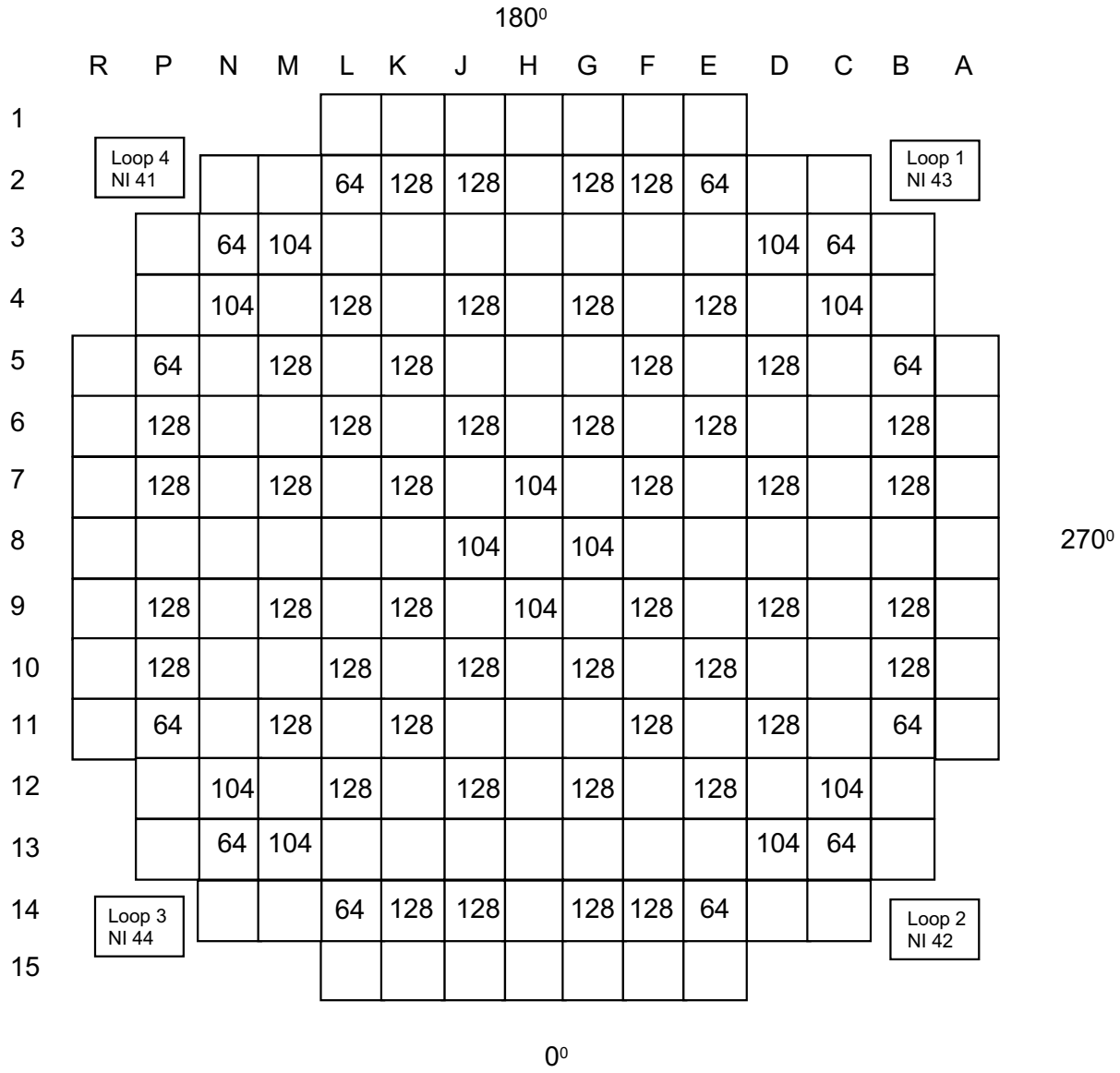

G:\Word\Images_P\UFSAR\435.ds4

SEABROOK STATION UPDATED FINAL SAFETY ANALYSIS REPORT	Typical IFBA Placement in Low Leakage Fuel Loading Arrangement	
		Figure 4.3-5

	H	G	F	E	D	C	B	A
8	0.714	1.007	1.040	1.019	1.149	1.310	1.184	0.631
9	1.007	0.861	1.012	0.929	1.217	1.246	1.226	0.634
10	1.040	1.017	0.892	1.110	1.190	1.346	1.226	0.616
11	1.019	0.930	1.112	1.019	1.280	1.345	1.108	0.304
12	1.149	1.219	1.194	1.284	1.236	1.250	0.550	
13	1.310	1.252	1.352	1.349	1.250	0.942	0.273	
14	1.184	1.238	1.233	1.112	0.549	0.265		
15	0.631	0.640	0.621	0.306				

Value Represents Assembly Relative Power

G:\Word\Images_P\UFSAR\436.ds4

SEABROOK STATION UPDATED FINAL SAFETY ANALYSIS REPORT	Typical BOL Power Density Distribution Low Leakage Fuel Loading Arrangement - Conditions: BOL, ARO, HZP, Eq Xenon
	Figure 4.3-6

	H	G	F	E	D	C	B	A
8	0.858	1.162	1.160	1.100	1.165	1.255	1.123	0.629
9	1.162	1.001	1.136	1.007	1.228	1.199	1.164	0.631
10	1.160	1.141	0.992	1.171	1.182	1.268	1.156	0.615
11	1.100	1.008	1.172	1.051	1.248	1.256	1.046	0.314
12	1.165	1.230	1.185	1.250	1.181	1.177	0.551	
13	1.255	1.203	1.272	1.258	1.177	0.909	0.286	
14	1.123	1.173	1.160	1.048	0.550	0.277		
15	0.629	0.636	0.618	0.315				

Value Represents Assembly Relative Power

G:\Word\Images_P\UFSAR\437.ds4

SEABROOK STATION UPDATED FINAL SAFETY ANALYSIS REPORT	Typical BOL Power Density Distribution Low Leakage Fuel Loading Arrangement - Conditions: BOL, ARO, HFP, Eq Xenon	
		Figure 4.3-7

	H	G	F	E	D	C	B	A
8	0.812	1.280	1.176	1.066	1.085	1.128	1.049	0.625
9	1.280	1.052	1.304	1.021	1.282	1.106	1.221	0.644
10	1.176	1.308	1.062	1.316	1.129	1.163	1.221	0.636
11	1.066	1.022	1.316	1.051	1.273	1.134	1.037	0.329
12	1.085	1.282	1.130	1.274	0.979	1.143	0.540	
13	1.128	1.107	1.164	1.134	1.142	0.900	0.293	
14	1.049	1.227	1.223	1.037	0.539	0.285		
15	0.625	0.648	0.637	0.329				

Value Represents Assembly Relative Power

G:\Word\Images_P\UFSAR\438.ds4

SEABROOK STATION UPDATED FINAL SAFETY ANALYSIS REPORT	Typical BOL Power Density Distribution Low Leakage Fuel Loading Arrangement - Conditions: BOL, Group 35% Inserted, HFP, Eq Xenon
	Figure 4.3-8

	H	G	F	E	D	C	B	A
8	0.921	1.298	1.161	1.041	1.055	1.095	1.017	0.603
9	1.298	1.052	1.283	1.000	1.252	1.078	1.187	0.625
10	1.161	1.287	1.045	1.301	1.123	1.153	1.200	0.621
11	1.041	1.000	1.302	1.065	1.318	1.161	1.039	0.326
12	1.055	1.253	1.125	1.320	1.140	1.210	0.556	
13	1.095	1.080	1.155	1.161	1.209	0.951	0.307	
14	1.017	1.193	1.203	1.040	0.555	0.298		
15	0.603	0.628	0.623	0.326				

Value Represents Assembly Relative Power

G:\Word\Images_P\UFSAR\439.ds4

SEABROOK STATION UPDATED FINAL SAFETY ANALYSIS REPORT	Typical MOL power Density Distribution Low Leakage Fuel Loading Arrangement - Conditions: MOL, ARO, HFP, Eq Xenon
	Figure 4.3-9

	H	G	F	E	D	C	B	A
8	0.908	1.235	1.108	1.019	1.034	1.083	1.043	0.682
9	1.235	1.019	1.234	0.984	1.216	1.063	1.214	0.701
10	1.108	1.236	1.018	1.248	1.080	1.123	1.219	0.696
11	1.019	0.984	1.248	1.030	1.256	1.129	1.075	0.389
12	1.034	1.215	1.080	1.257	1.100	1.208	0.620	
13	1.083	1.063	1.123	1.129	1.207	1.006	0.371	
14	1.043	1.217	1.220	1.074	0.619	0.361		
15	0.682	0.703	0.697	0.389				

Value Represents Assembly Relative Power

G:\Word\Images_P\UFSAR\4310.ds4

SEABROOK STATION UPDATED FINAL SAFETY ANALYSIS REPORT	Typical EOL Power Density Distribution Low Leakage Fuel Loading Arrangement - Conditions: EOL, ARO, HFP, Eq Xenon
	Figure 4.3-10

	H	G	F	E	D	C	B	A
8	0.787	1.210	1.122	1.046	1.065	1.119	1.080	0.709
9	1.210	1.016	1.253	1.006	1.246	1.092	1.251	0.726
10	1.122	1.255	1.035	1.261	1.085	1.133	1.241	0.715
11	1.046	1.006	1.261	1.014	1.207	1.100	1.073	0.395
12	1.065	1.246	1.085	1.208	0.930	1.136	0.603	
13	1.119	1.092	1.133	1.100	1.135	0.951	0.356	
14	1.080	1.254	1.242	1.073	0.602	0.346		
15	0.709	0.728	0.716	0.395				

Value Represents Assembly Relative Power

G:\Word\Images_P\UFSAR\4311.ds4

SEABROOK STATION UPDATED FINAL SAFETY ANALYSIS REPORT	Typical EOL Power Density Distribution Low Leakage Fuel Loading Arrangement - Conditions: EOL, Group D 35% Inserted, HFP, Eq Xenon	
		Figure 4.3-11

1.054	1.112	1.124	1.140	1.163	1.177	1.191	1.201	1.200	1.207	1.206	1.200	1.194	1.177	1.166	1.157	1.094
1.101	1.095	1.052	1.080	1.161	1.157	1.194	1.209	1.181	1.217	1.211	1.182	1.195	1.119	1.096	1.143	1.143
1.100	1.041	1.070	1.185	1.166		1.174	1.240		1.248	1.192		1.204	1.232	1.119	1.091	1.146
1.106	1.058	1.174		1.234	1.176	1.189	1.153	1.235	1.162	1.209	1.206	1.276		1.232	1.114	1.157
1.119	1.129	1.145	1.223	1.159	1.231	1.147	1.193	1.177	1.203	1.168	1.264	1.201	1.297	1.205	1.192	1.176
1.124	1.116		1.156	1.221		1.229	1.176		1.187	1.252		1.267	1.212		1.182	1.185
1.131	1.144	1.135	1.161	1.130	1.220	1.144	1.190	1.174	1.201	1.165	1.255	1.174	1.217	1.200	1.214	1.195
1.134	1.152	1.192	1.118	1.167	1.160	1.182	1.147	1.230	1.158	1.205	1.194	1.213	1.173	1.261	1.224	1.199
1.130	1.121		1.192	1.144		1.159	1.223		1.233	1.181		1.190	1.251		1.190	1.195
1.134	1.152	1.191	1.117	1.166	1.158	1.181	1.146	1.228	1.156	1.203	1.192	1.211	1.171	1.259	1.222	1.198
1.130	1.143	1.134	1.159	1.128	1.218	1.141	1.187	1.170	1.197	1.161	1.251	1.170	1.213	1.196	1.210	1.191
1.122	1.114		1.154	1.217		1.224	1.171		1.180	1.244		1.260	1.205		1.176	1.179
1.117	1.126	1.141	1.210	1.154	1.224	1.141	1.185	1.168	1.194	1.158	1.253	1.191	1.268	1.196	1.184	1.168
1.104	1.055	1.170		1.227	1.168	1.180	1.143	1.224	1.150	1.196	1.193	1.262		1.219	1.103	1.147
1.098	1.037	1.065	1.179	1.158		1.162	1.226		1.233	1.176		1.187	1.215	1.104	1.077	1.133
1.098	1.091	1.046	1.072	1.152	1.145	1.180	1.193	1.164	1.198	1.191	1.162	1.174	1.099	1.077	1.125	1.126
1.052	1.108	1.116	1.131	1.151	1.162	1.175	1.182	1.179	1.185	1.182	1.174	1.168	1.152	1.141	1.135	1.075

G:\Word\Images_P\UFSAR\4312.ds4

SEABROOK STATION UPDATED FINAL SAFETY ANALYSIS REPORT	Typical Assembly Power Density Distribution Low Leakage Fuel Loading Arrangement - Conditions: BOL, ARO, HFP, Eq Xenon	
		Figure 4.3-12

1.171	1.173	1.180	1.190	1.201	1.210	1.213	1.215	1.220	1.219	1.219	1.220	1.215	1.208	1.201	1.197	1.192
1.170	1.164	1.167	1.183	1.218	1.234	1.228	1.231	1.240	1.234	1.234	1.244	1.233	1.202	1.189	1.187	1.188
1.171	1.162	1.191	1.240	1.256		1.253	1.264		1.266	1.259		1.272	1.260	1.215	1.186	1.190
1.176	1.173	1.234		1.280	1.266	1.255	1.247	1.273	1.249	1.261	1.277	1.296		1.260	1.199	1.196
1.181	1.202	1.245	1.274	1.259	1.280	1.251	1.262	1.271	1.265	1.257	1.291	1.276	1.297	1.272	1.230	1.204
1.186	1.213		1.255	1.274		1.283	1.276		1.278	1.289		1.292	1.279		1.243	1.211
1.185	1.203	1.233	1.241	1.242	1.279	1.255	1.268	1.275	1.270	1.262	1.291	1.260	1.265	1.263	1.234	1.211
1.185	1.204	1.241	1.230	1.251	1.269	1.265	1.259	1.285	1.262	1.272	1.281	1.270	1.255	1.272	1.236	1.212
1.187	1.211		1.255	1.259		1.272	1.284		1.286	1.278		1.276	1.279		1.243	1.213
1.184	1.203	1.241	1.229	1.250	1.268	1.264	1.258	1.284	1.260	1.270	1.279	1.268	1.252	1.270	1.234	1.210
1.184	1.202	1.232	1.239	1.241	1.277	1.253	1.266	1.273	1.268	1.259	1.288	1.258	1.262	1.260	1.232	1.208
1.185	1.212		1.254	1.273		1.280	1.273		1.274	1.285		1.288	1.275		1.239	1.207
1.180	1.200	1.243	1.272	1.256	1.276	1.247	1.258	1.266	1.260	1.252	1.286	1.271	1.292	1.267	1.225	1.199
1.175	1.171	1.232		1.276	1.262	1.250	1.241	1.267	1.242	1.254	1.270	1.289		1.253	1.193	1.190
1.170	1.160	1.189	1.237	1.252		1.248	1.257		1.259	1.251		1.263	1.252	1.207	1.178	1.183
1.169	1.163	1.165	1.180	1.214	1.229	1.222	1.224	1.232	1.225	1.225	1.235	1.223	1.193	1.180	1.178	1.180
1.171	1.173	1.178	1.187	1.197	1.204	1.206	1.208	1.212	1.211	1.211	1.211	1.206	1.199	1.193	1.188	1.184

G:\Word\Images_P\UFSAR\4313.ds4

SEABROOK STATION UPDATED FINAL SAFETY ANALYSIS REPORT	Typical Assembly Power Density Distribution Low Leakage Fuel Loading Arrangement - Conditions: EOL, ARO, HFP, Eq Xenon	
		Figure 4.3-13

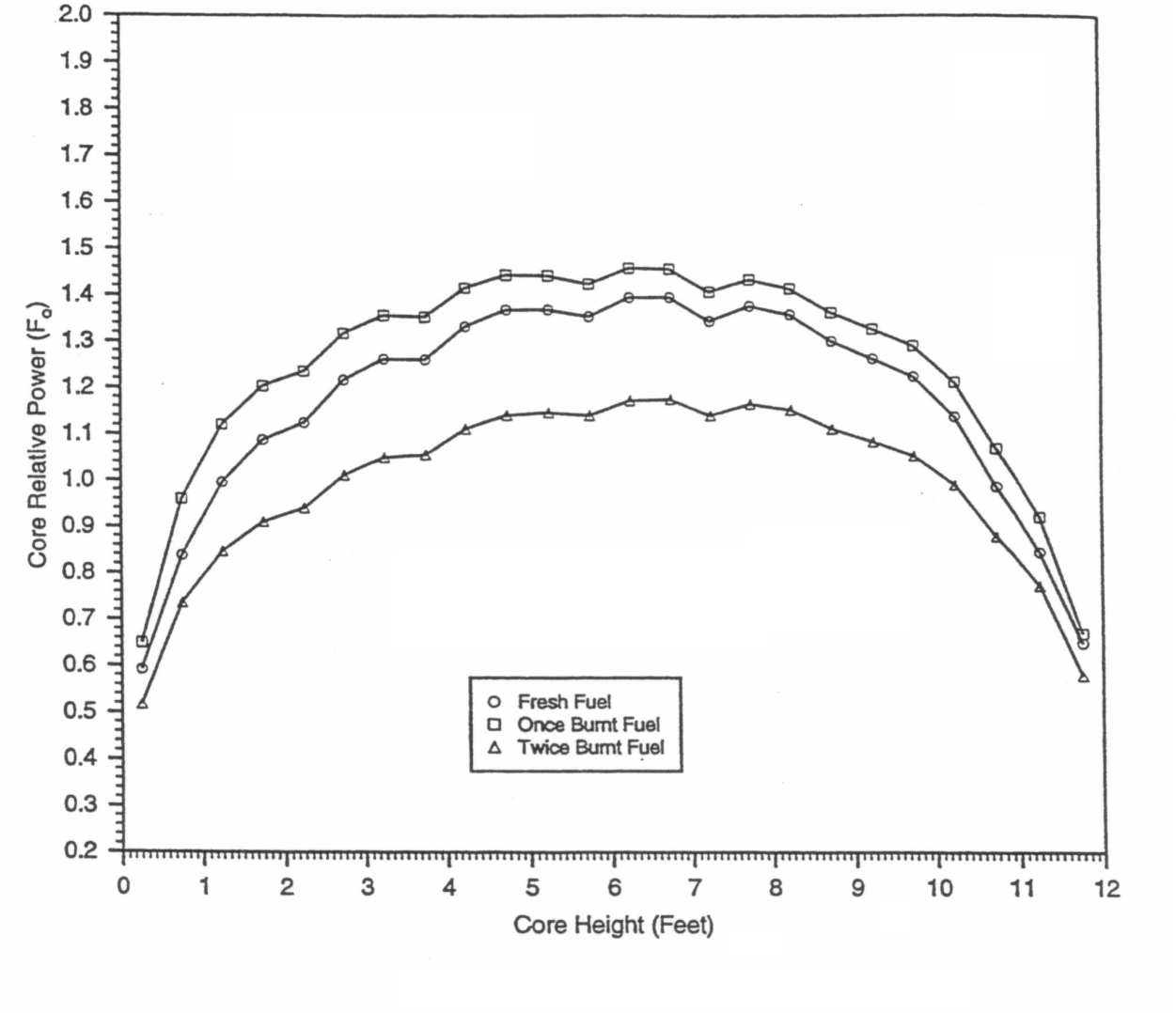

SEABROOK STATION UPDATED FINAL SAFETY ANALYSIS REPORT	Typical Axial Power Shapes at BOL During Normal Operation for Typical Low Leakage Cycle Design	
		Figure 4.3-14

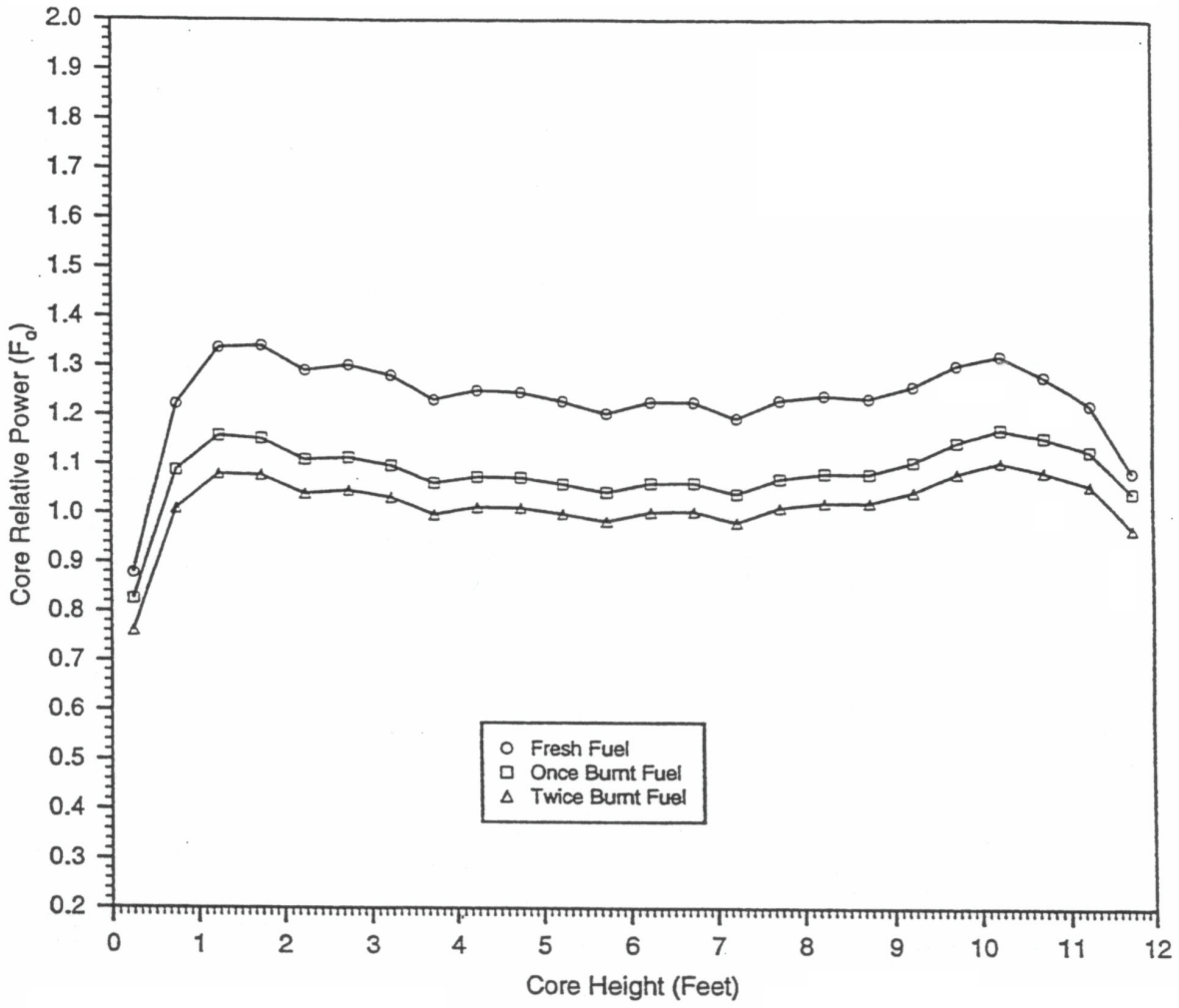

SEABROOK STATION UPDATED FINAL SAFETY ANALYSIS REPORT	Typical Axial Power Shapes at EOL During Normal Operation for Typical Low Leakage Cycle Design	
		Figure 4.3-15

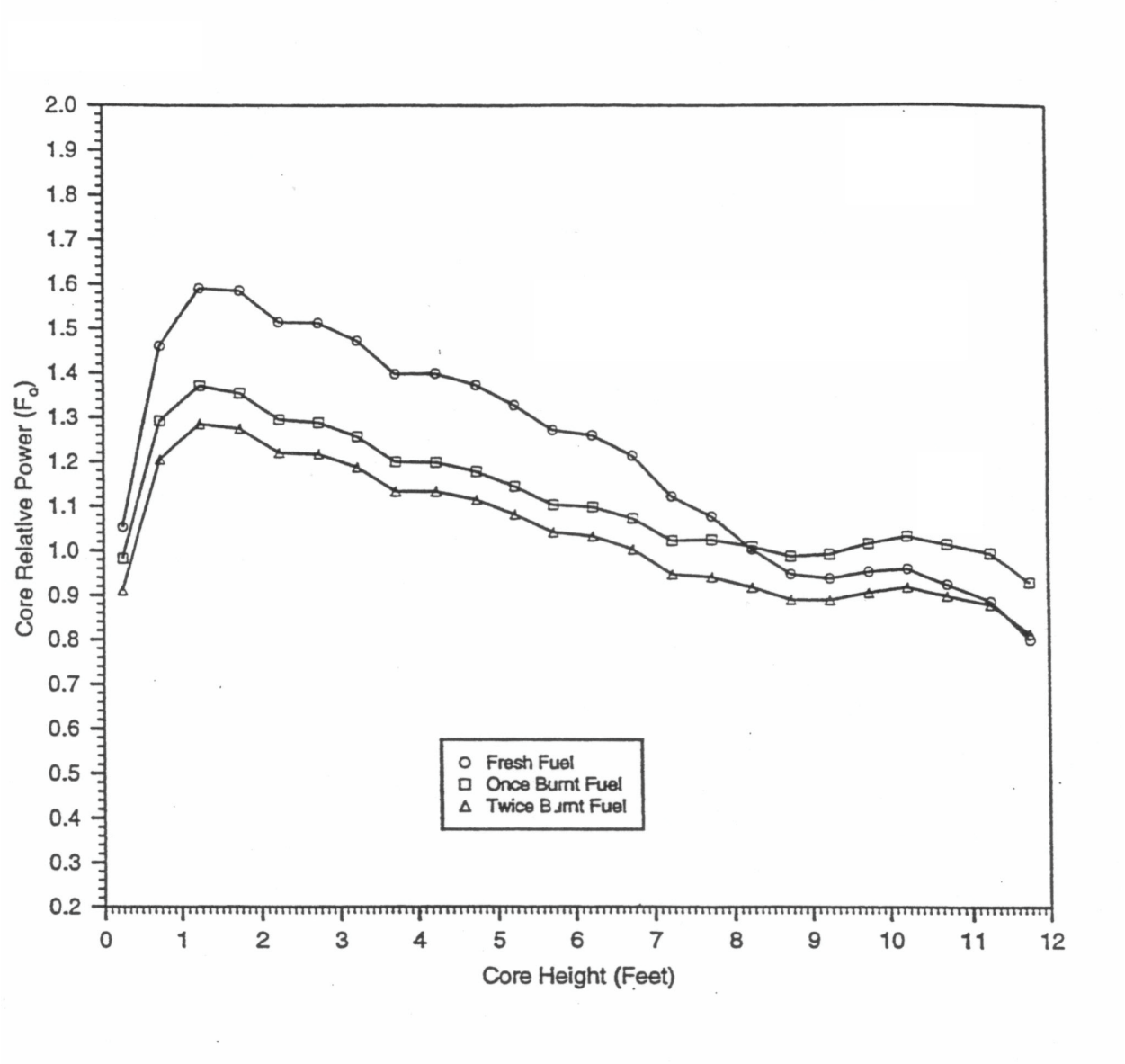

SEABROOK STATION UPDATED FINAL SAFETY ANALYSIS REPORT	Typical Axial Power Shapes During Rodded Operation for Typical Low Leakage Cycle Design	
		Figure 4.3-16

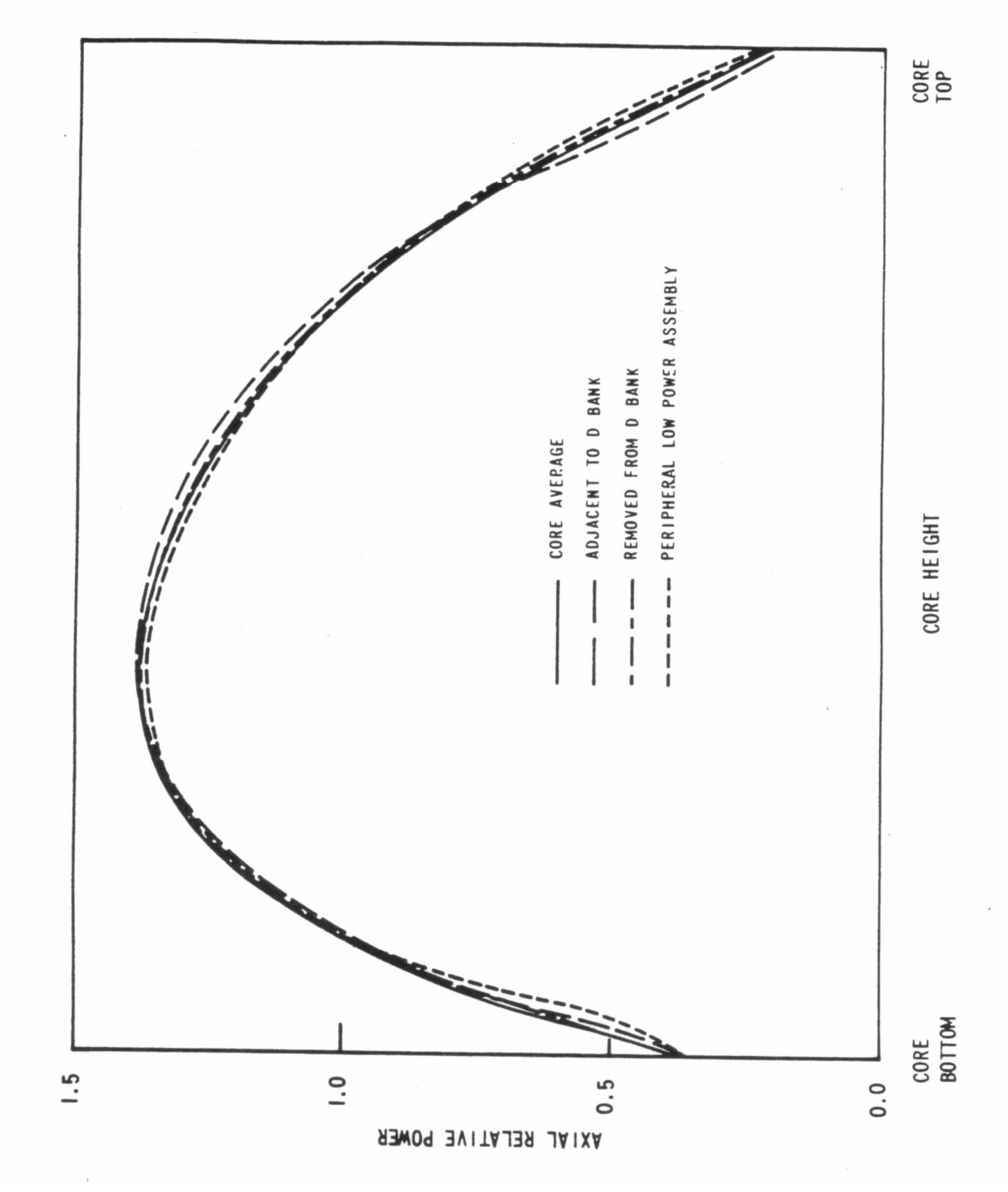

SEABROOK STATION UPDATED FINAL SAFETY ANALYSIS REPORT	Comparison of Assembly Axial Power Distribution with Core Average Axial Distribution - D Bank Slightly Inserted	
		Figure 4.3-17

DELETED

DELETED

DELETED

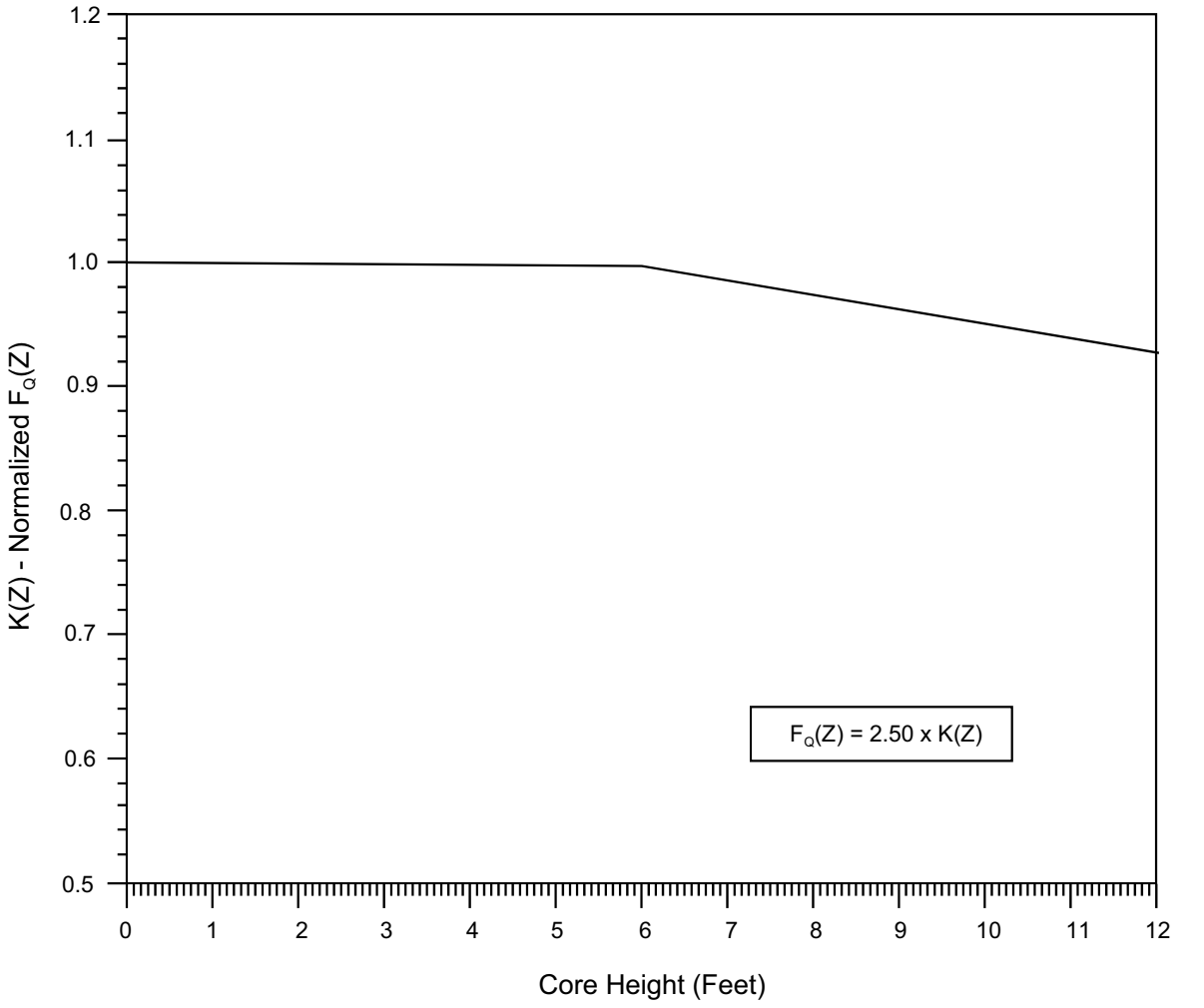

SEABROOK STATION UPDATED FINAL SAFETY ANALYSIS REPORT	Normalized Maximum F_Q versus Axial Height during Normal Operation for Typical Low Leakage Cycle Design	
		Figure 4.3-21

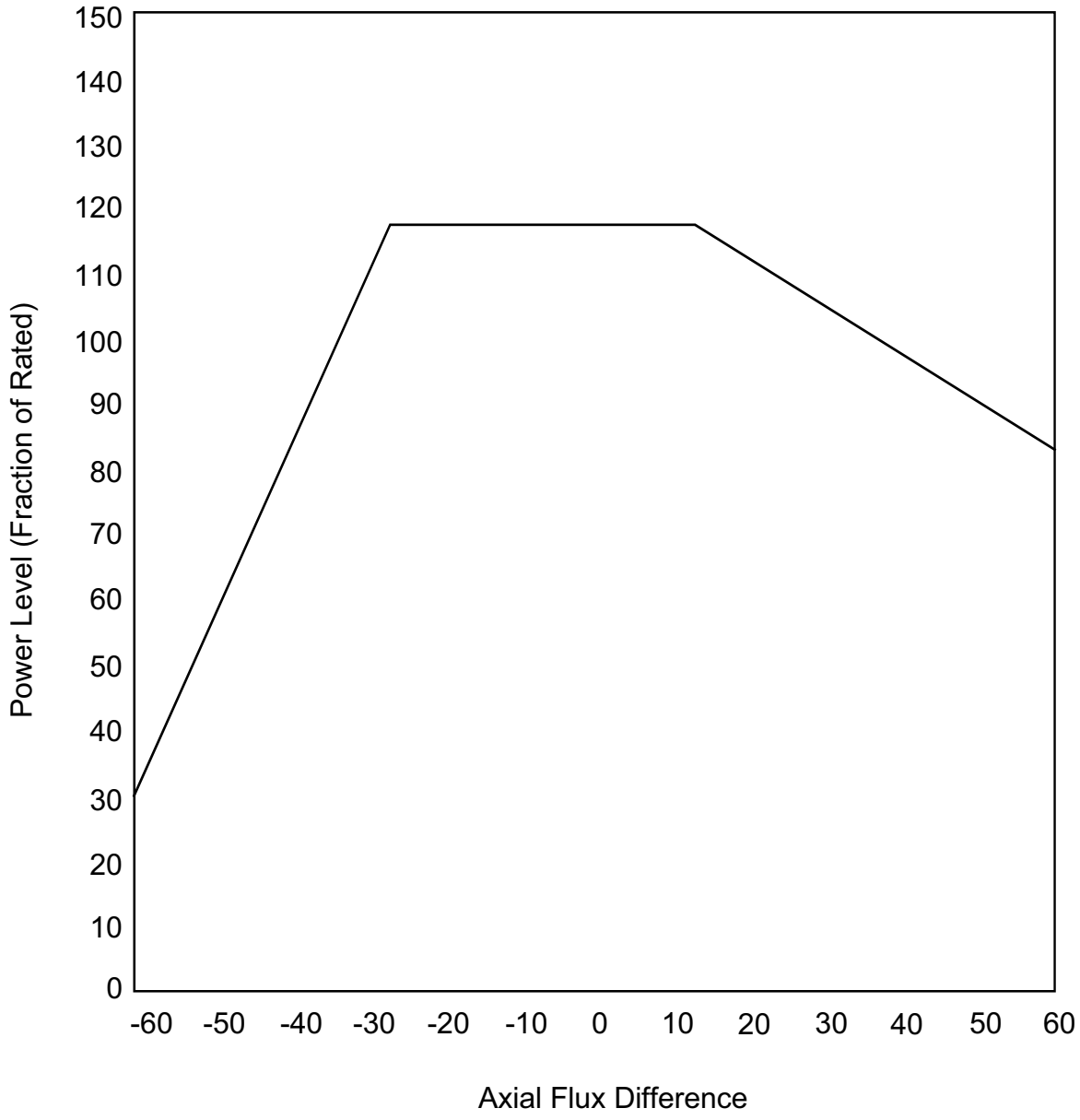

G:\Word\Images_P\UFSAR\4322.ds4

SEABROOK STATION UPDATED FINAL SAFETY ANALYSIS REPORT	Illustration of Required Overpower ΔT Setpoint for a Typical Reload core Versus Axial Flux Difference	
		Figure 4.3-22

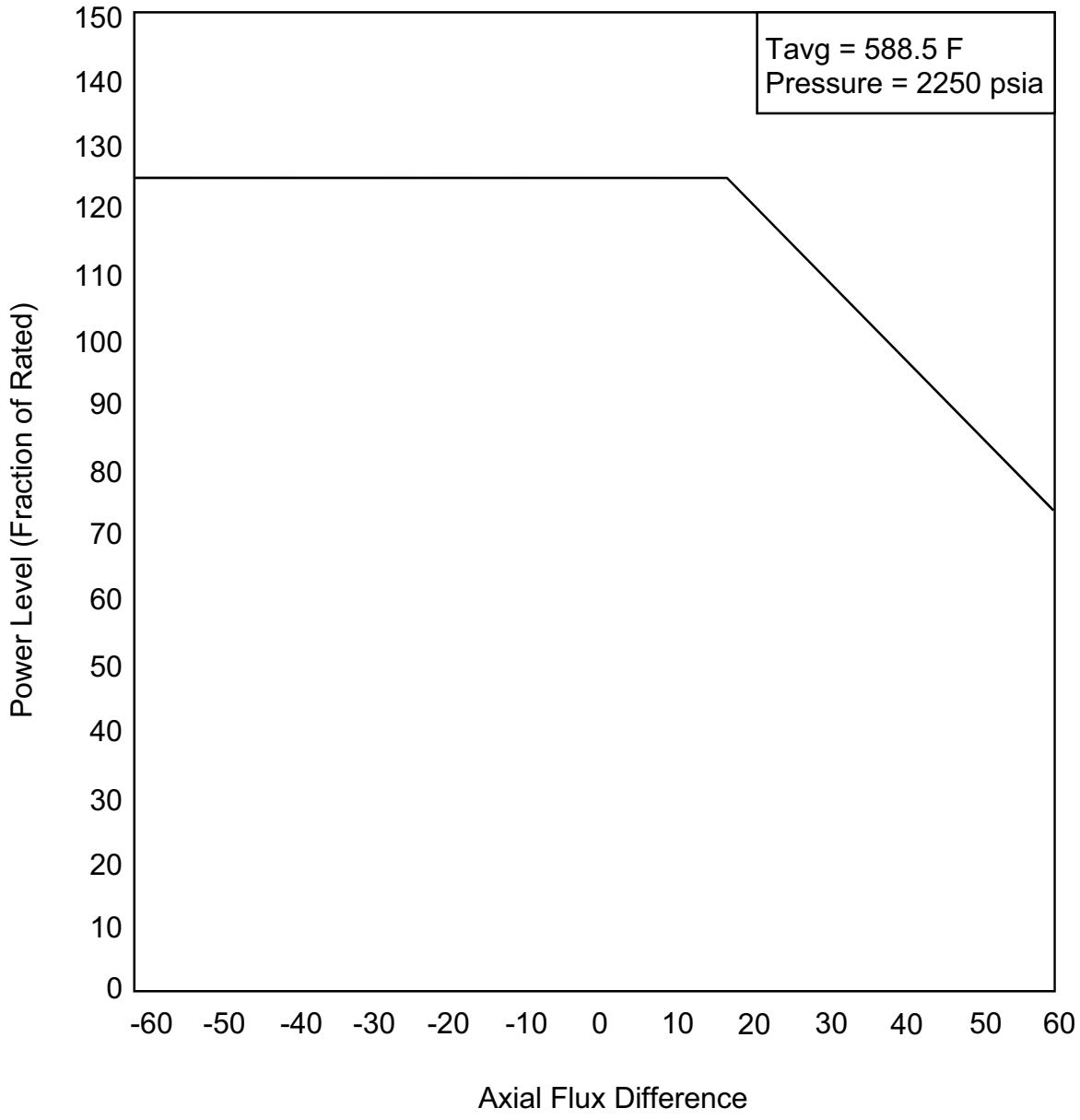

G:\Word\Images_P\UFSAR\4323.ds4

SEABROOK STATION UPDATED FINAL SAFETY ANALYSIS REPORT	Illustration of Required Overtemperature ΔT Setpoint at Nominal conditions for a Typical Reload Core versus Axial Flux Difference	
		Figure 4.3-23

180⁰

	R	P	N	M	L	K	J	H	G	F	E	D	C	B	A
1					0.313 0.311 0.687	0.615 0.609 0.924	0.631 0.624 1.157	0.620 0.612 1.384	0.614 0.619 -0.829	0.587 0.606 -3.247	0.300 0.310 -3.278				
2	Loop 4 NI 41		0.277 0.277 0.022	0.544 0.544 0.050	1.047 1.039 0.777	1.176 1.165 0.939	1.187 1.171 1.348	1.103 1.085 1.575	1.164 1.162 0.176	1.143 1.161 -1.511	1.010 1.037 -2.649	0.518 0.544 -5.012	0.273 0.285 -4.316	Loop 1 NI 43	
3		0.286 0.285 0.298	0.914 0.911 0.335	1.187 1.186 0.130	1.245 1.236 0.781	1.252 1.242 0.772	1.178 1.169 0.787	1.218 1.208 0.825	1.173 1.165 0.625	1.241 1.239 0.137	1.205 1.234 -2.353	1.129 1.186 -4.987	0.874 0.911 -4.262	0.267 0.277 -3.605	
4		0.547 0.544 0.462	1.191 1.186 0.449	1.192 1.178 1.114	1.312 1.283 2.165	1.203 1.177 2.162	1.247 1.244 0.244	1.143 1.138 0.494	1.248 1.242 0.456	1.171 1.174 -0.293	1.252 1.281 -2.319	1.154 1.178 -2.100	1.158 1.186 -2.368	0.536 0.544 -1.357	
5	0.313 0.310 0.755	1.049 1.037 1.189	1.250 1.234 1.347	1.304 1.281 1.786	1.081 1.063 1.658	1.236 1.216 1.590	1.017 1.009 0.789	1.096 1.087 0.832	1.016 1.008 0.849	1.209 1.215 -0.525	1.039 1.063 -2.275	1.275 1.283 -0.616	1.219 1.236 -1.396	1.021 1.039 -1.693	0.298 0.311 -4.538
6	0.611 0.606 0.762	1.183 1.161 1.921	1.249 1.239 0.790	1.187 1.174 1.041	1.220 1.215 0.429	1.026 1.011 1.480	1.207 1.187 1.657	1.191 1.170 1.767	1.188 1.182 0.541	0.999 1.011 -1.192	1.189 1.216 -2.329	1.172 1.177 -0.443	1.228 1.242 -1.134	1.150 1.165 -1.377	0.583 0.609 -4.501
7	0.620 0.619 0.220	1.175 1.162 1.059	1.172 1.165 0.586	1.251 1.242 0.694	1.010 1.008 0.213	1.190 1.182 0.671	1.030 1.022 0.848	1.221 1.211 0.872	1.032 1.022 1.031	1.190 1.187 0.188	1.014 1.009 0.549	1.248 1.244 0.300	1.161 1.169 -0.667	1.157 1.171 -1.198	0.610 0.624 -2.286
8	0.603 0.612 -1.493	1.077 1.085 -0.822	1.193 1.208 -1.266	1.139 1.138 0.138	1.087 1.087 0.031	1.176 1.170 0.503	1.209 1.211 -0.175	0.886 0.880 0.697	1.225 1.211 1.166	1.184 1.170 1.169	1.096 1.087 0.829	1.144 1.138 0.556	1.211 1.208 0.188	1.088 1.085 0.229	0.615 0.612 0.578
9	0.614 0.624 -1.634	1.159 1.171 -0.995	1.157 1.169 -1.093	1.250 1.244 0.452	1.012 1.009 0.313	1.182 1.187 -0.446	1.009 1.022 -1.224	1.212 1.211 0.112	1.050 1.022 2.718	1.209 1.182 2.233	1.022 1.008 1.393	1.250 1.242 0.618	1.169 1.165 0.272	1.166 1.162 0.356	0.623 0.619 0.653
10	0.613 0.609 0.681	1.171 1.165 0.448	1.207 1.242 -2.961	1.179 1.177 0.134	1.217 1.216 0.068	1.009 1.011 -0.225	1.181 1.182 0.095	1.179 1.170 0.804	1.208 1.187 1.692	1.022 1.011 1.128	1.220 1.215 0.383	1.179 1.174 0.392	1.243 1.239 0.291	1.176 1.161 1.291	0.614 0.606 1.263
11	0.324 0.311 3.861	1.080 1.039 3.859	1.243 1.236 0.551	1.286 1.283 0.230	1.070 1.063 0.713	1.219 1.215 0.363	1.013 1.008 0.568	1.080 1.087 -0.671	1.001 1.009 -0.782	1.200 1.216 -1.336	1.071 1.063 0.754	1.292 1.281 0.851	1.251 1.234 1.428	1.049 1.037 1.227	0.314 3.310 1.184
12		0.544 0.544 0.070	1.140 1.186 -3.952	1.176 1.178 -0.201	1.302 1.281 1.652	1.194 1.174 1.655	1.259 1.242 1.360	1.137 1.138 -0.017	1.241 1.244 -0.201	1.161 1.177 -1.391	1.298 1.283 1.134	1.194 1.178 1.289	1.210 1.186 2.022	0.552 0.544 1.323	
13		0.275 0.277 -0.477	0.906 0.911 -0.553	1.190 1.186 0.339	1.256 1.234 1.782	1.236 1.239 -0.245	1.159 1.165 -0.519	1.189 1.208 -1.639	1.154 1.169 -1.286	1.209 1.242 -2.777	1.231 1.236 -0.387	1.196 1.186 0.915	0.921 0.911 1.096	0.289 0.285 1.411	
14	Loop 3 NI 44		0.285 0.285 -0.102	0.546 0.544 0.237	1.044 1.037 0.722	1.147 1.161 -1.166	1.137 1.162 -2.181	1.064 1.085 -1.974	1.154 1.171 -1.448	1.130 1.165 -3.113	1.019 1.039 -1.926	0.539 0.544 -0.790	0.277 0.277 0.273	Loop 2 NI 42	
15					0.309 0.310 -0.404	0.591 0.606 -2.520	0.596 0.619 -3.815	0.590 0.612 -3.698	0.606 0.624 -2.924	0.591 0.609 -3.150	0.305 0.311 -1.990	Measured Power Predicted Power % Difference			

270⁰

0⁰

-1.0500 Axial Offset
1.6025 Maximum F_{XY}
1.4239 Maximum F_a
1.8524 Maximum F_Q
-5.0124 Maximum F_a Assembly Difference

G:\Word\Images_P\UFSAR\4324.ds4

SEABROOK STATION UPDATED FINAL SAFETY ANALYSIS REPORT	Example of a Typical Comparison between Calculated and Measured Relative Fuel Assembly Power Distribution - Conditions: BOL, HFP, ARO
	Figure 4.3-24

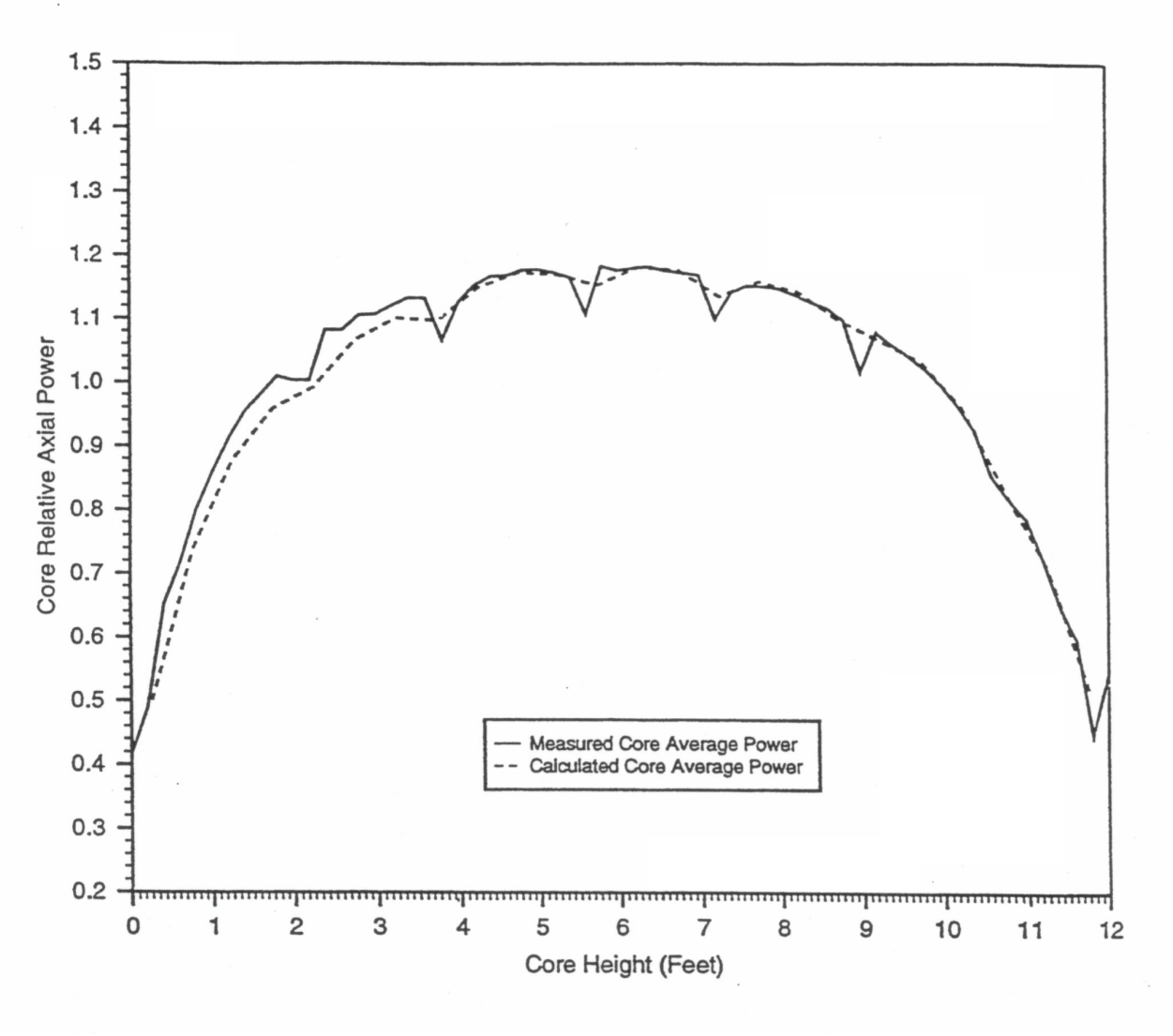

SEABROOK STATION UPDATED FINAL SAFETY ANALYSIS REPORT	Example of a Typical Comparison between Calculated and Measured Core Average Axial Power - Conditions; BOL, HFP, ARO	
		Figure 4.3-25

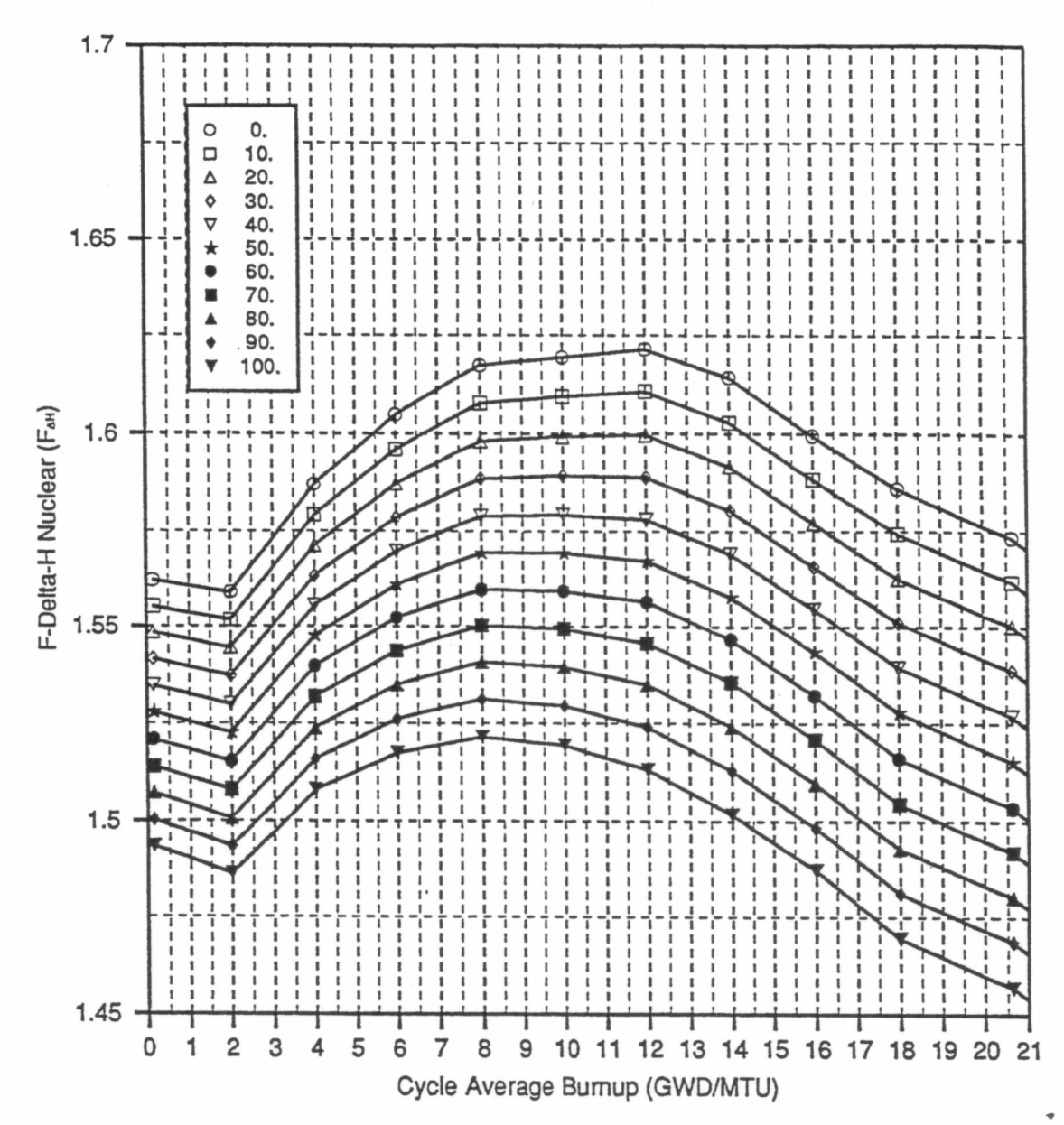

SEABROOK STATION UPDATED FINAL SAFETY ANALYSIS REPORT	All-Rods-Out Nuclear Enthalpy Rise Hot Channel Factor versus Power Level	
		Figure 4.3-26

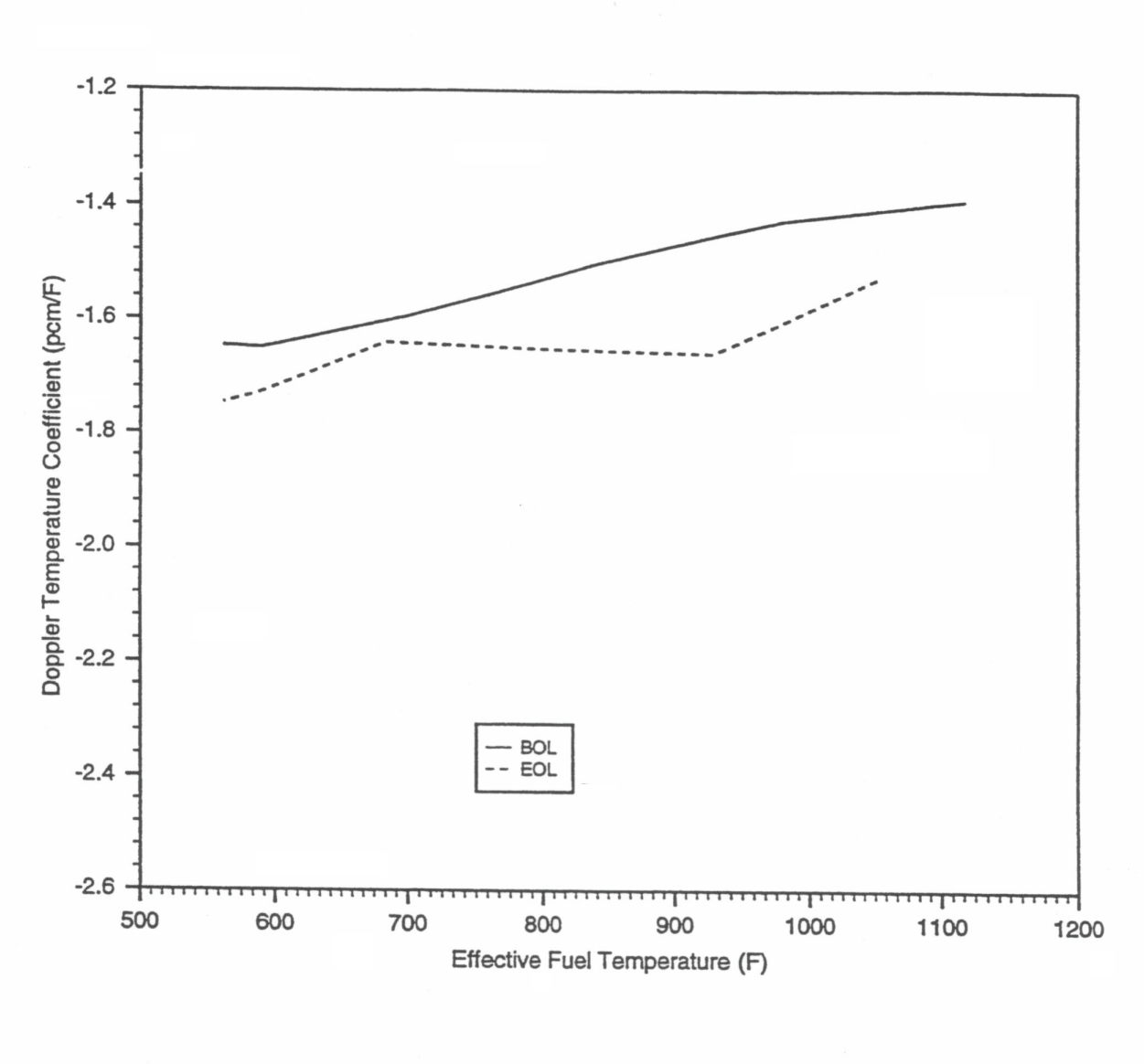

SEABROOK STATION UPDATED FINAL SAFETY ANALYSIS REPORT	Typical Low Leakage Core Design Doppler Temperature Coefficient at BOL and EOL	
		Figure 4.3-27

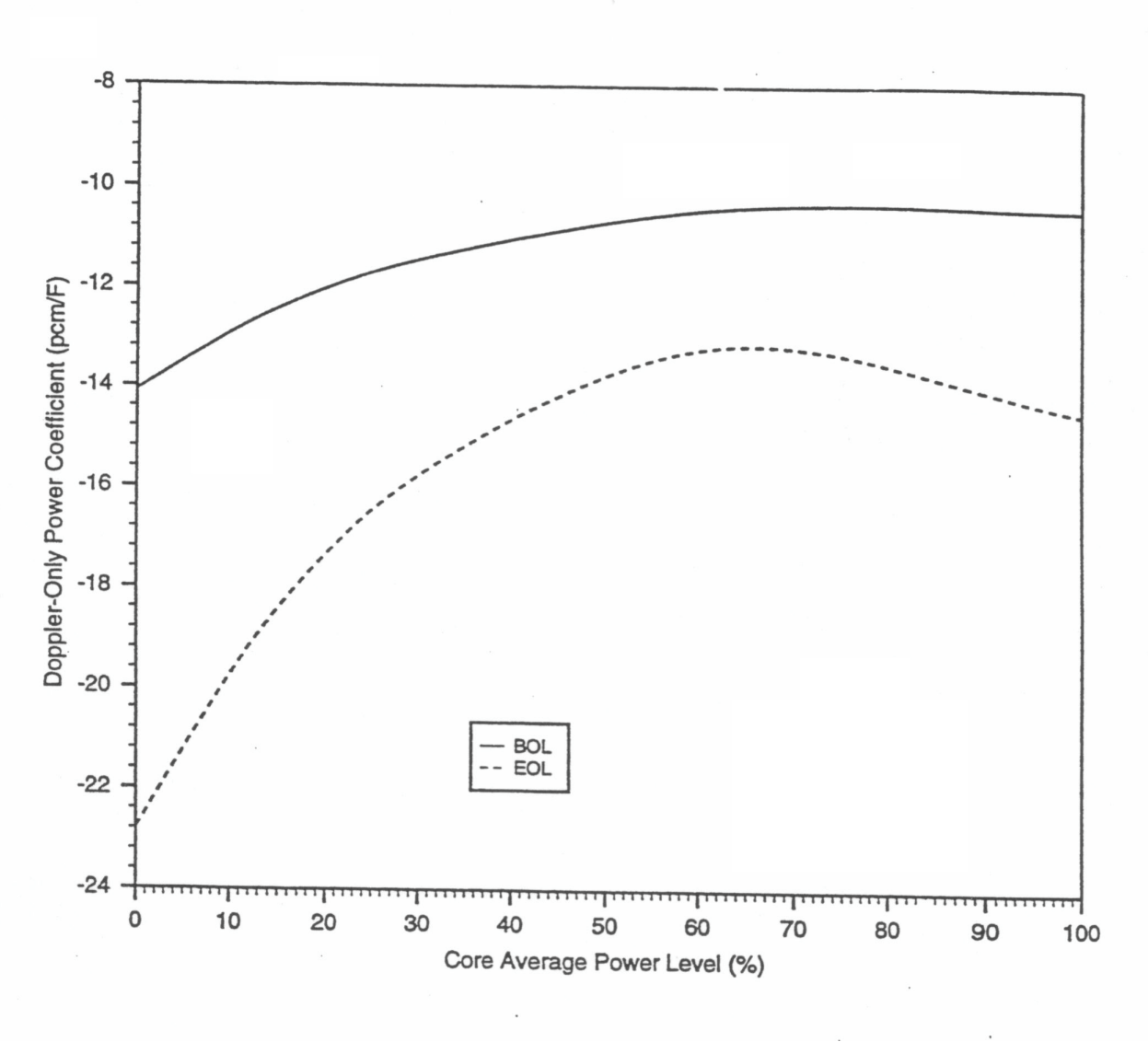

SEABROOK STATION UPDATED FINAL SAFETY ANALYSIS REPORT	Typical Low Leakage Core Design Doppler-Only Power Coefficient - BOL, & EOL	
		Figure 4.3-28

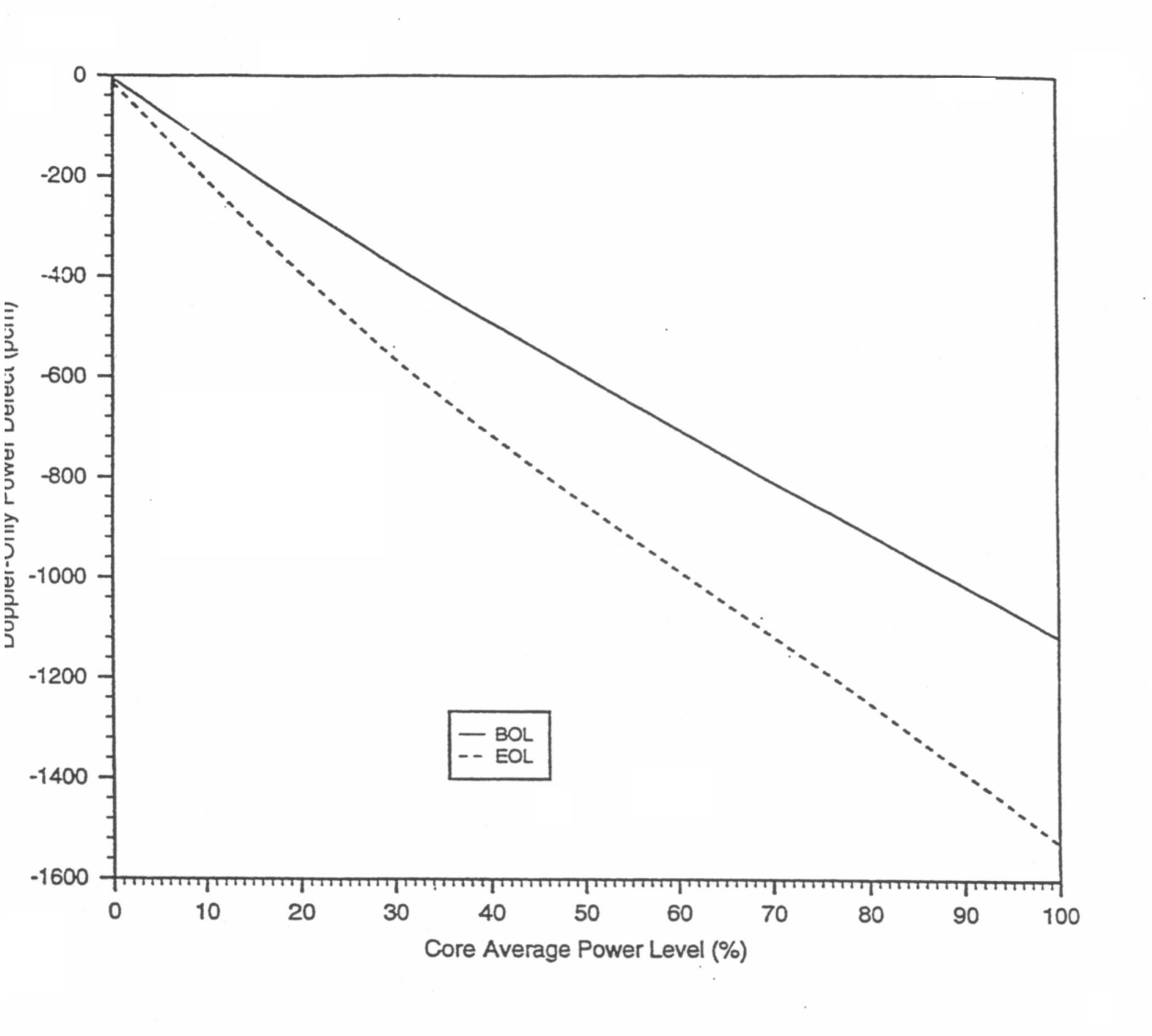

SEABROOK STATION UPDATED FINAL SAFETY ANALYSIS REPORT	Typical Low Leakage Core Design Doppler-Only Power Defect - BOL, & EOL	
		Figure 4.3-29

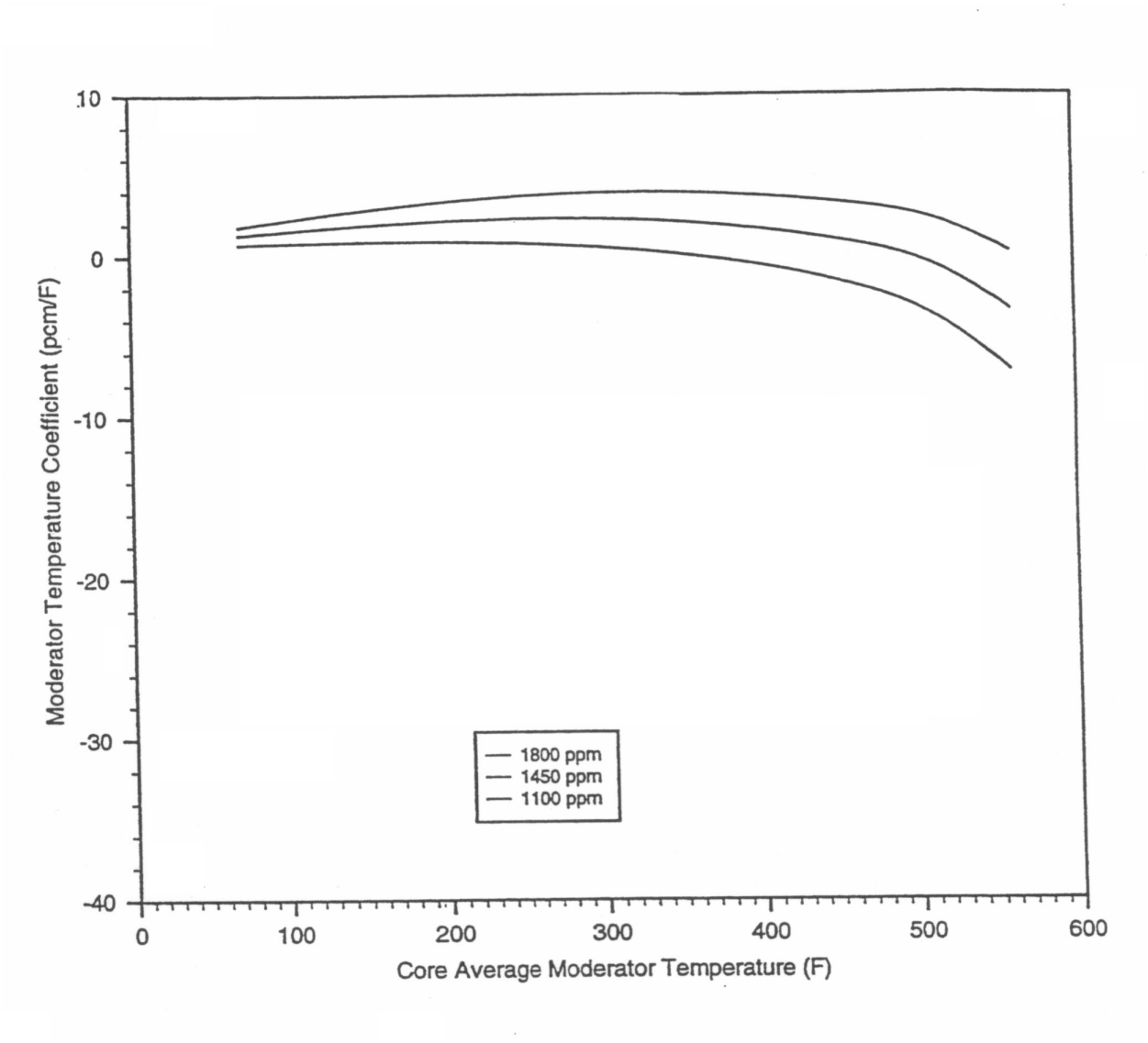

SEABROOK STATION UPDATED FINAL SAFETY ANALYSIS REPORT	Typical Low Leakage Core Design Moderator Temperature Coefficient at BOL, ARO	
		Figure 4.3-30

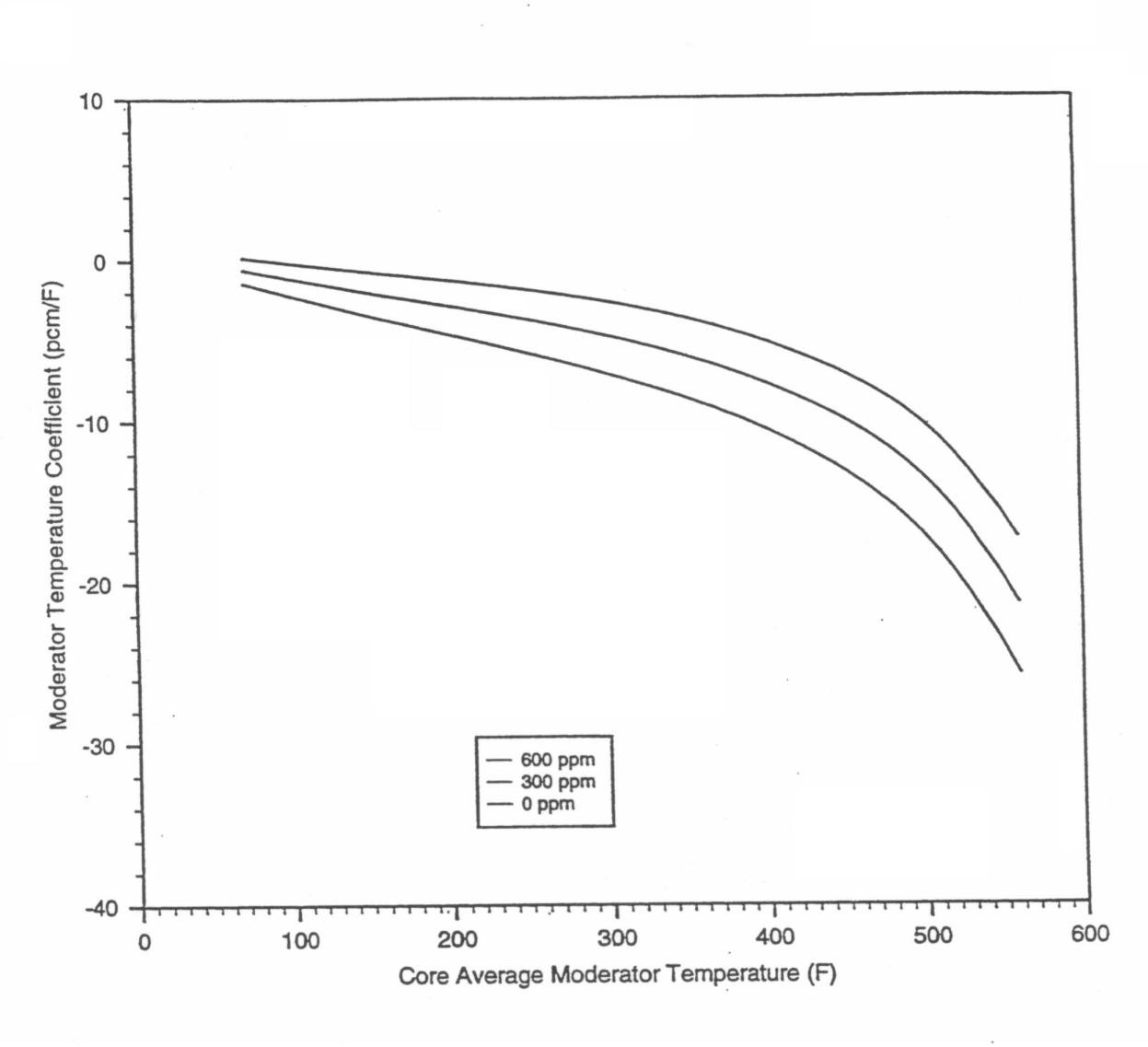

SEABROOK STATION UPDATED FINAL SAFETY ANALYSIS REPORT	Typical Low Leakage Core Design Moderator Temperature Coefficient at EOL, ARO	
		Figure 4.3-31

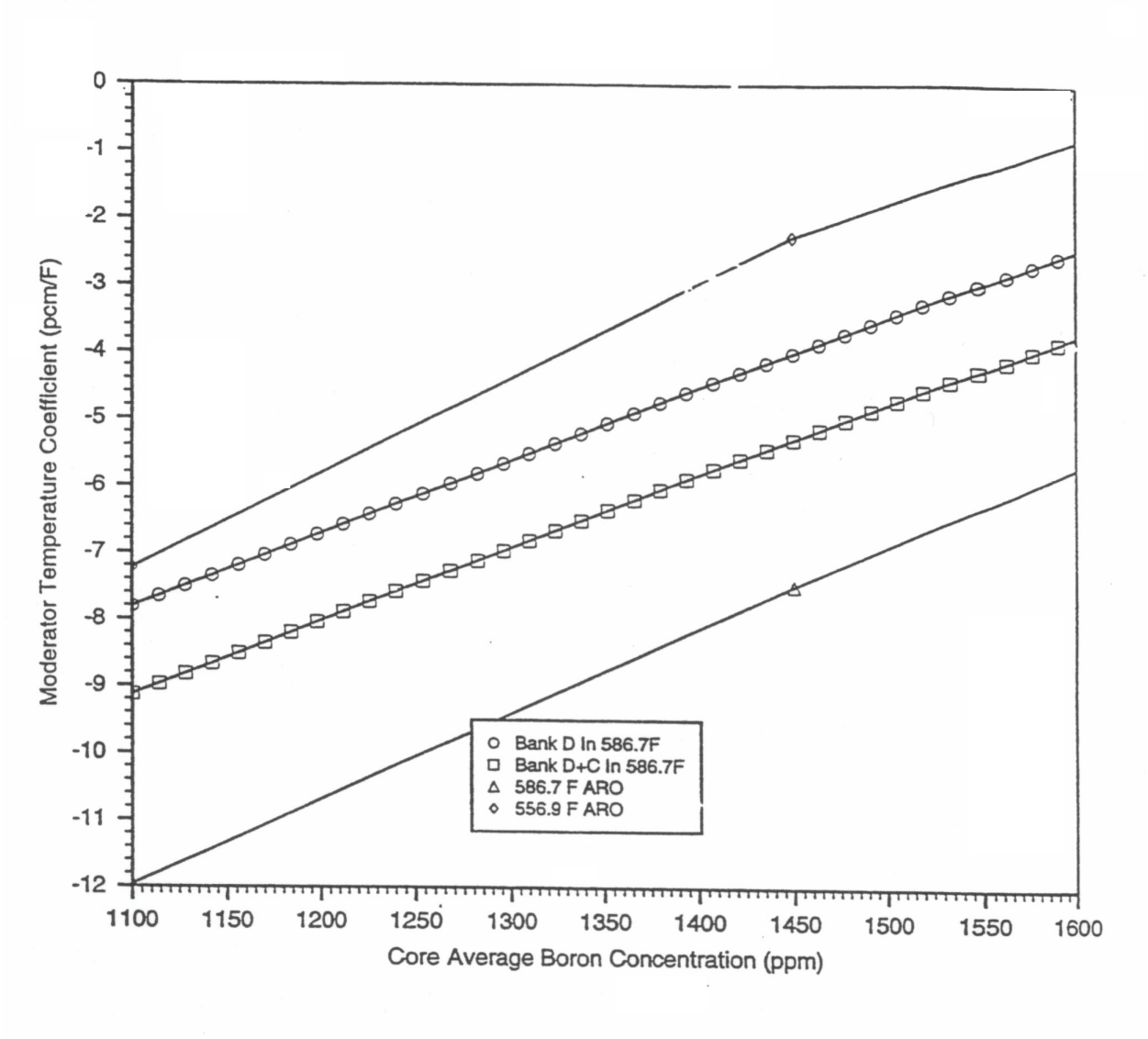

SEABROOK STATION UPDATED FINAL SAFETY ANALYSIS REPORT	Typical Low Leakage Core Design Moderator Temperature Coefficient at BOL versus Boron Concentration	
		Figure 4.3-32

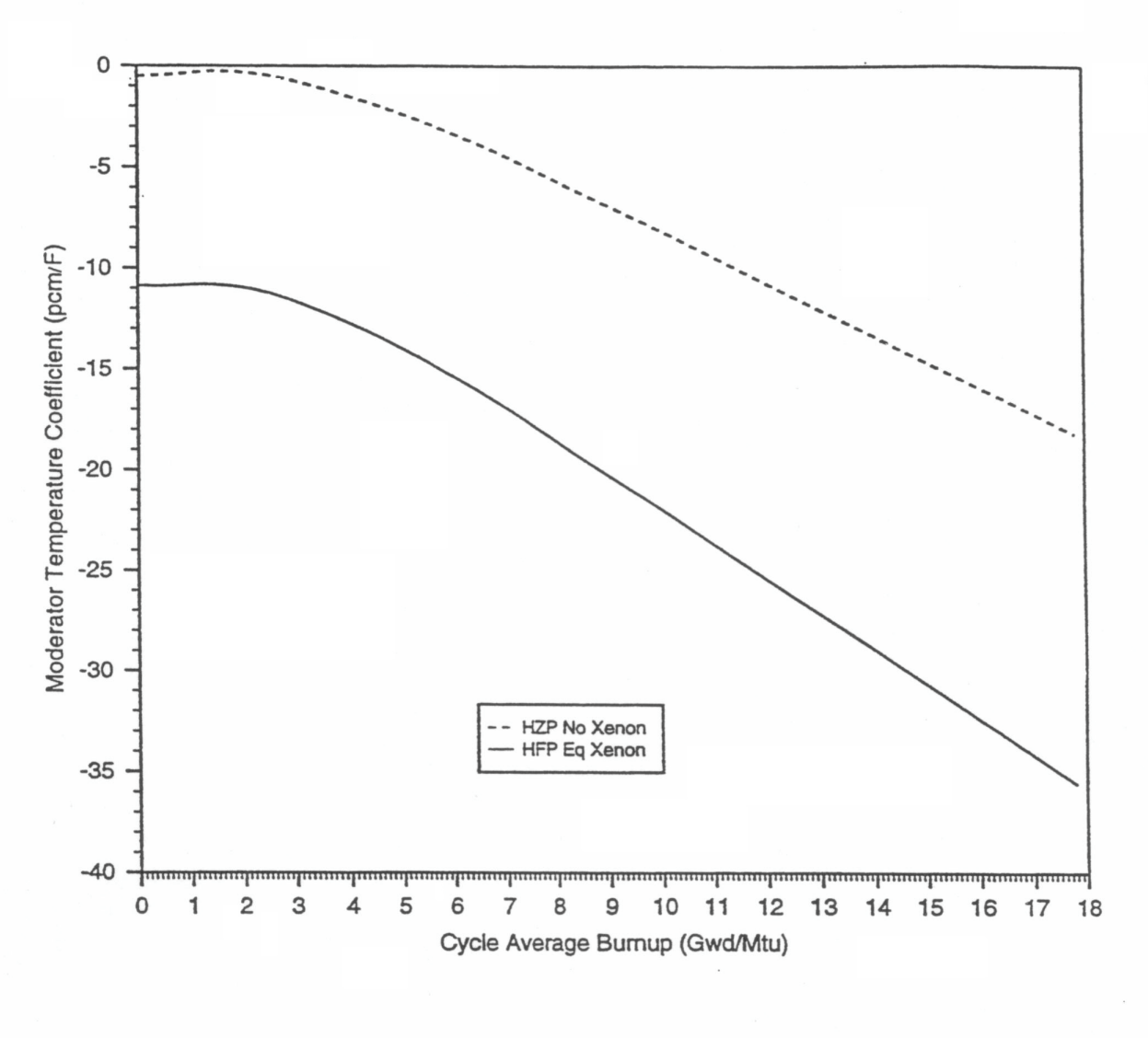

SEABROOK STATION UPDATED FINAL SAFETY ANALYSIS REPORT	Typical Low Leakage Core Design Moderator Temperature Coefficient versus cycle Burnup	
		Figure 4.3-33

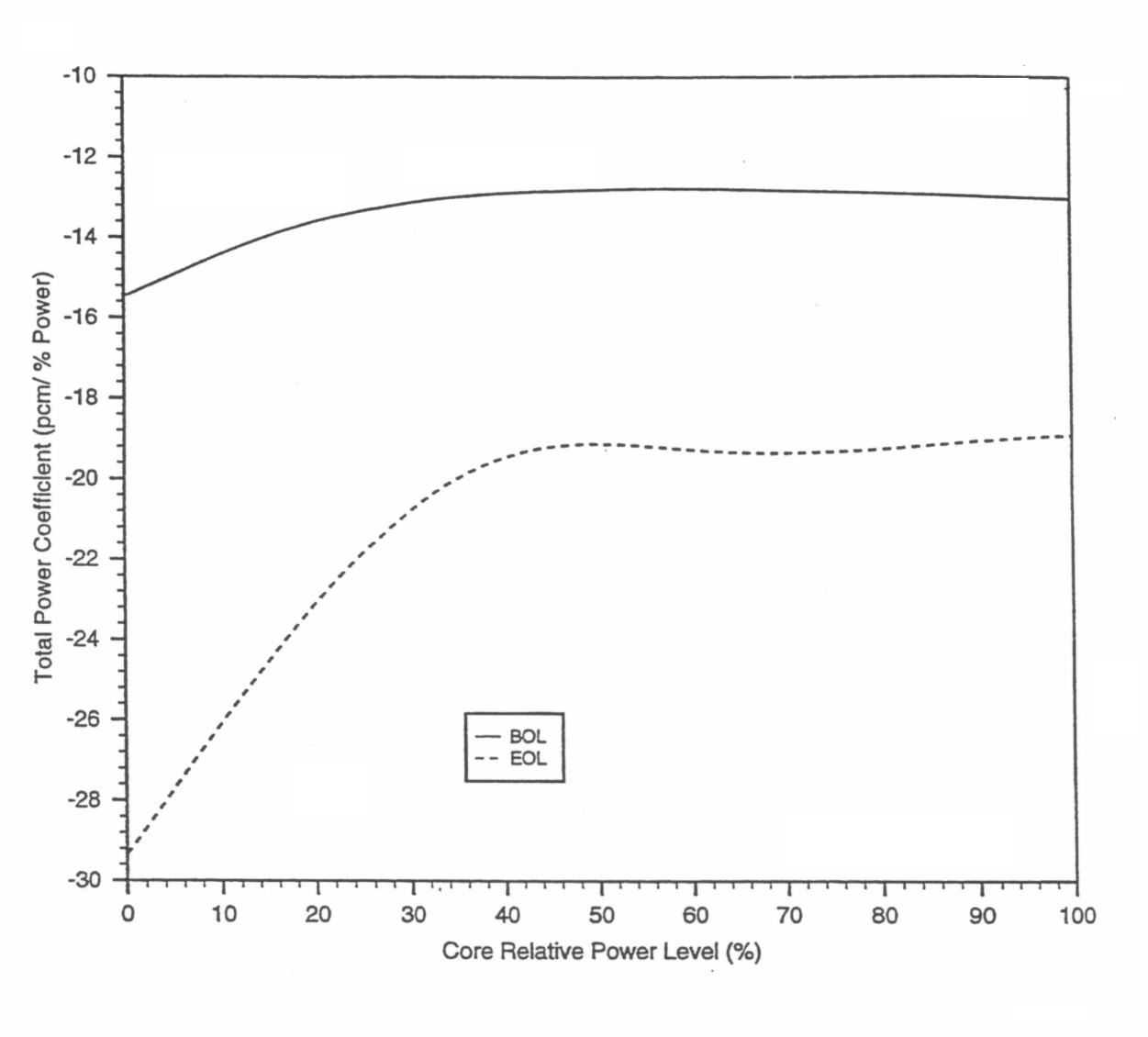

SEABROOK STATION UPDATED FINAL SAFETY ANALYSIS REPORT	Typical Low Leakage Core Design Total Power Coefficient at BOL & EOL	
		Figure 4.3-34

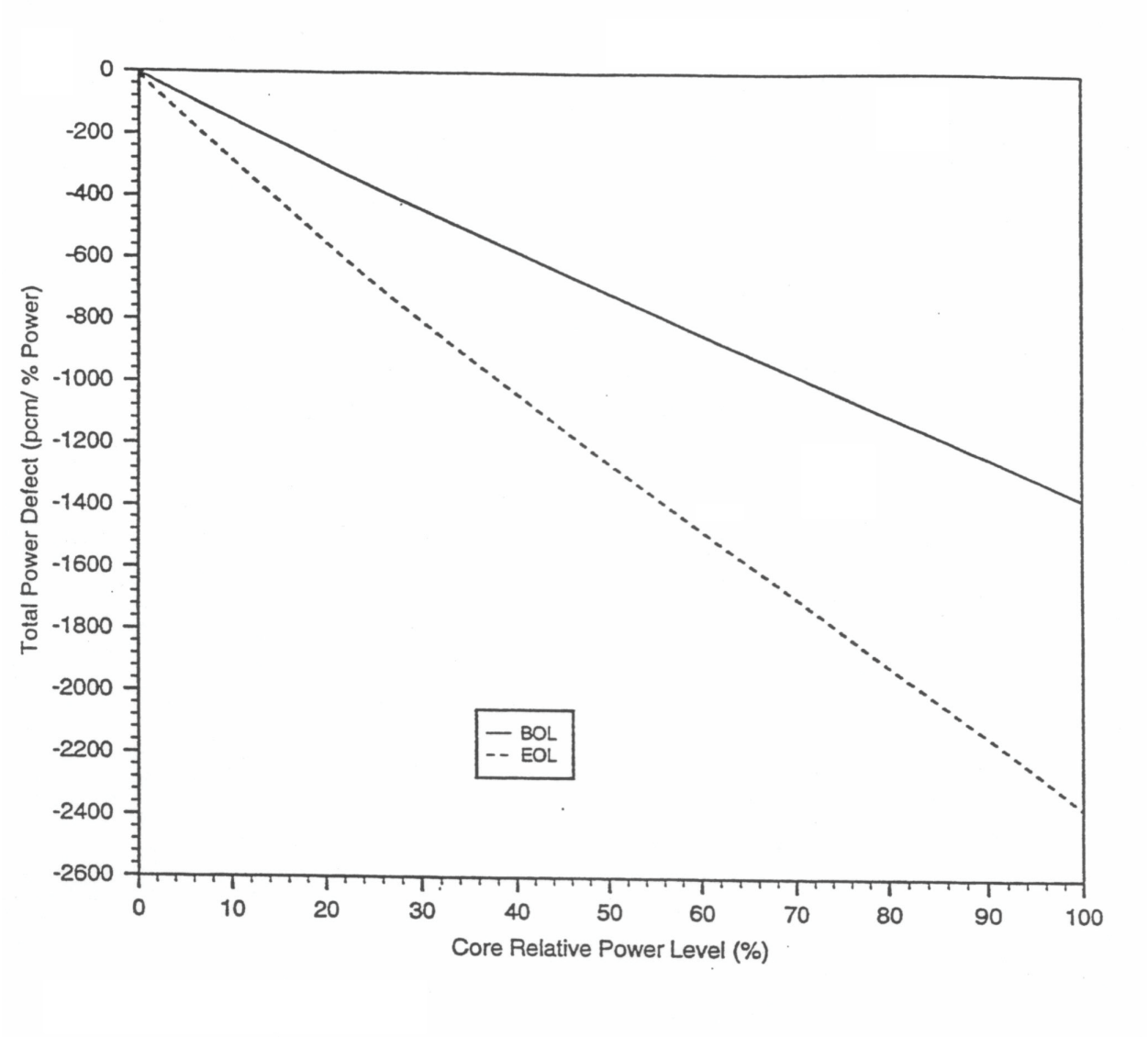

SEABROOK STATION UPDATED FINAL SAFETY ANALYSIS REPORT	Typical Low Leakage Core Design Total Power Defect at BOL & EOL	
		Figure 4.3-35

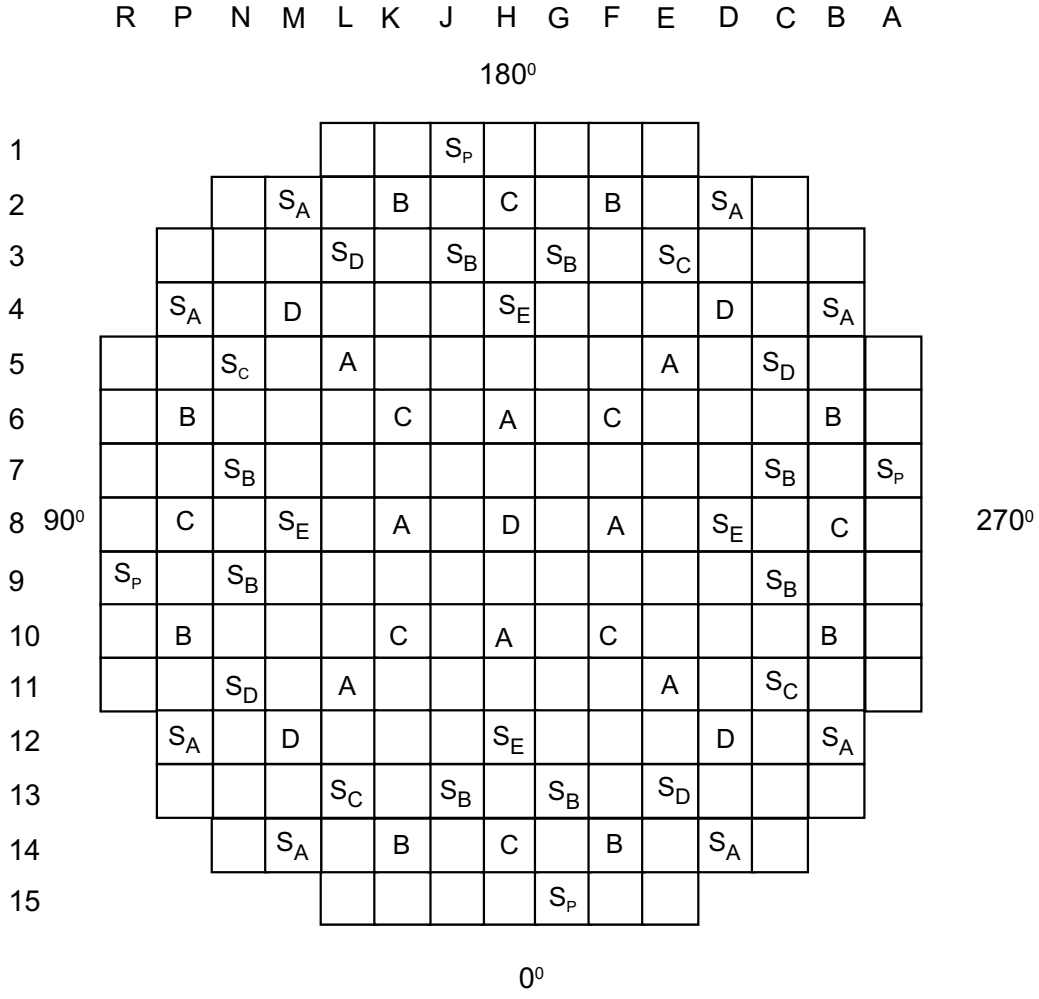

Control Bank	Number of Rods
A	8
B	8
C	8
D	5
Total	29

S_P - Spare Locations

Shutdown Bank	Number of Rods
SA	8
SB	8
SC	4
SD	4
SE	4
Total	28

G:\Word\Images_P\UFSAR\4336.ds4

SEABROOK STATION UPDATED FINAL SAFETY ANALYSIS REPORT	Rod Cluster Control Assembly Pattern	
		Figure 4.3-36

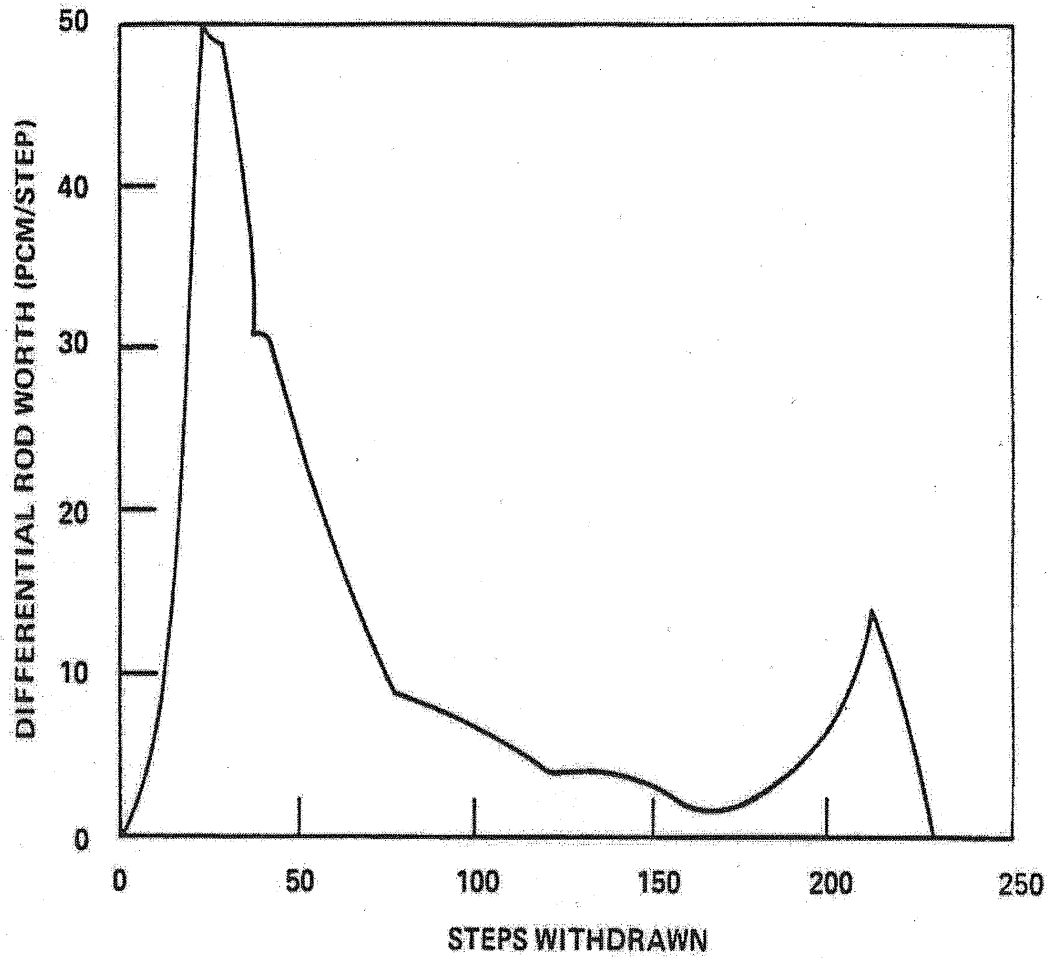

SEABROOK STATION UPDATED FINAL SAFETY ANALYSIS REPORT	Accident Simulated Withdrawal of Two Control Banks - EOL, HZP, Banks C and B Moving in Same Plane	
		Figure 4.3-37

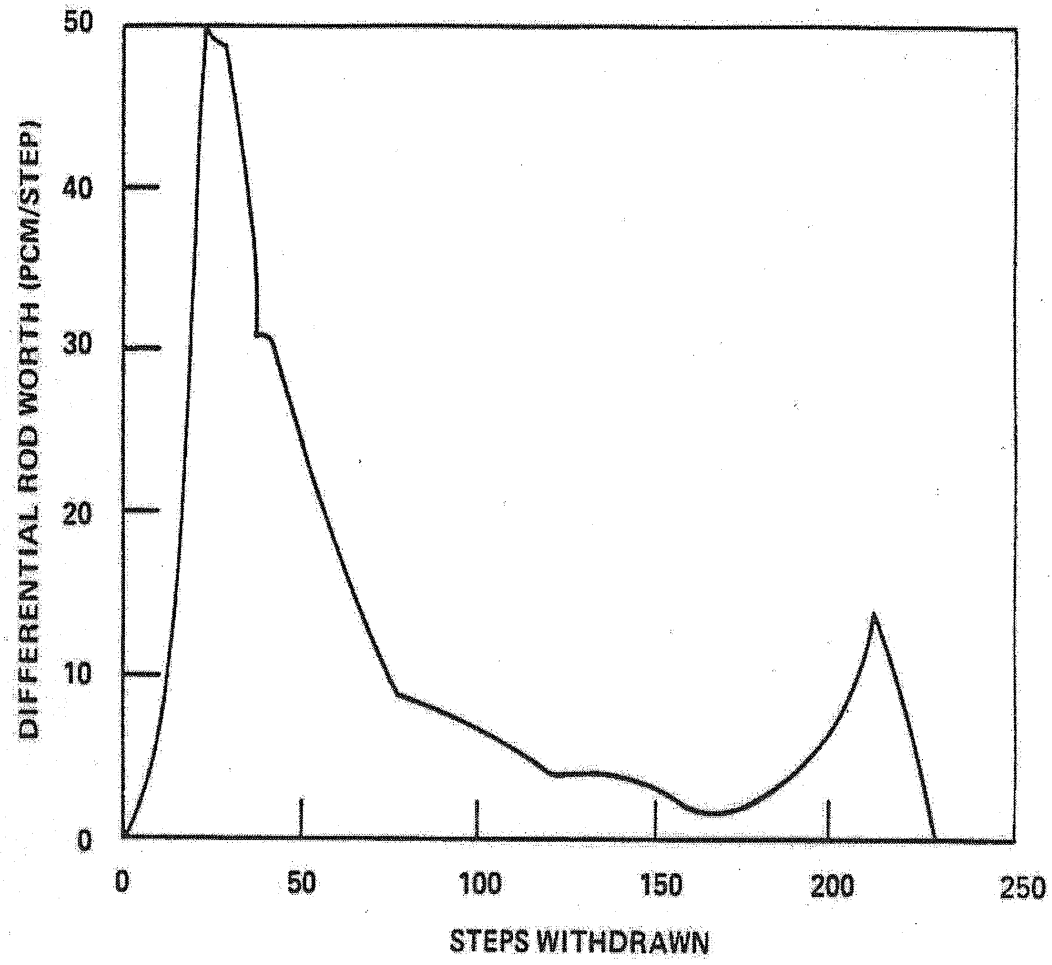

SEABROOK STATION UPDATED FINAL SAFETY ANALYSIS REPORT	Accident Simulated Withdrawal of Two Control Banks - EOL, HZP, Banks C and B Moving in Same Plane	
		Figure 4.3-37

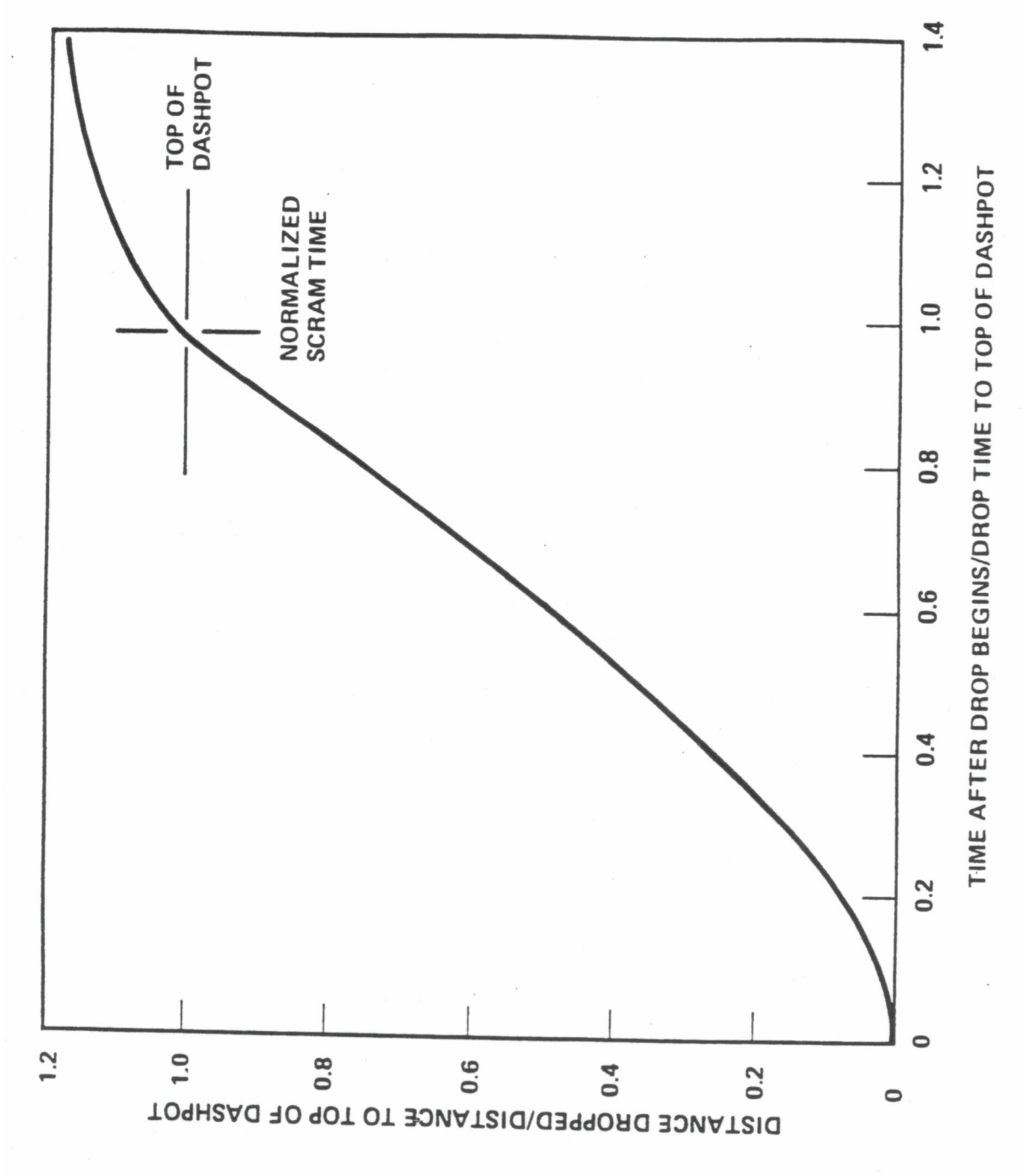

SEABROOK STATION UPDATED FINAL SAFETY ANALYSIS REPORT	Design Trip Curve	
		Figure 4.3-38

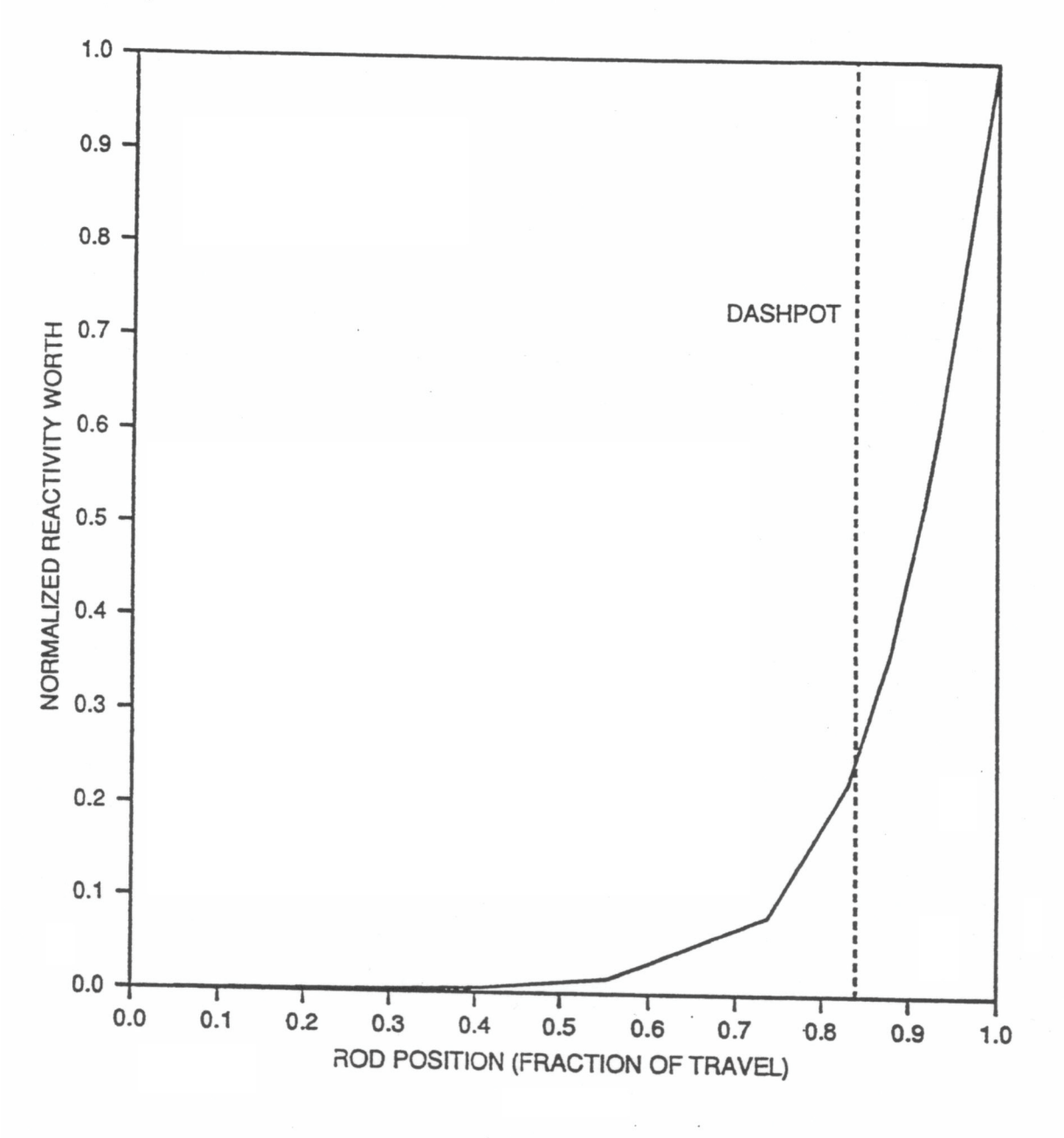

SEABROOK STATION UPDATED FINAL SAFETY ANALYSIS REPORT	Normalized RCCA Reactivity Worth versus Fraction of Travel	
		Figure 4.3-39

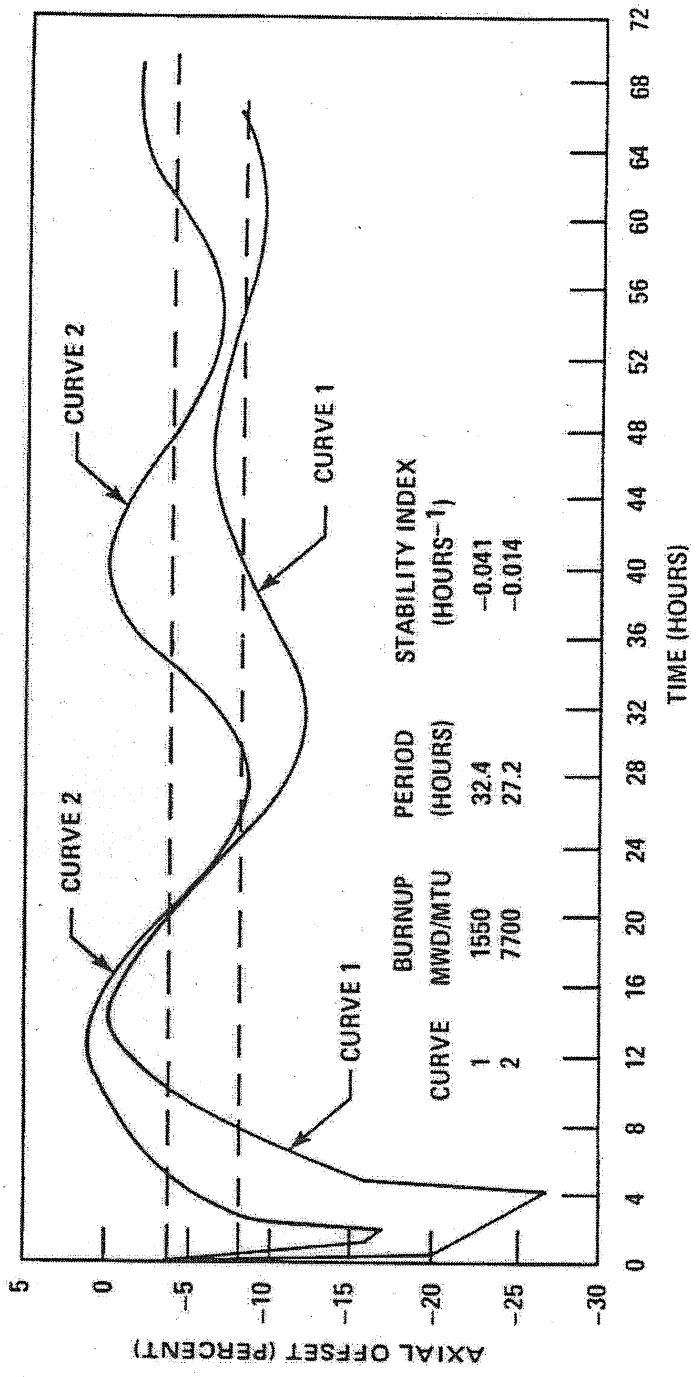

SEABROOK STATION UPDATED FINAL SAFETY ANALYSIS REPORT	Axial Offset vs. Time - PWR Core with a 12-Ft Height and 121 Assemblies	
		Figure 4.3-40

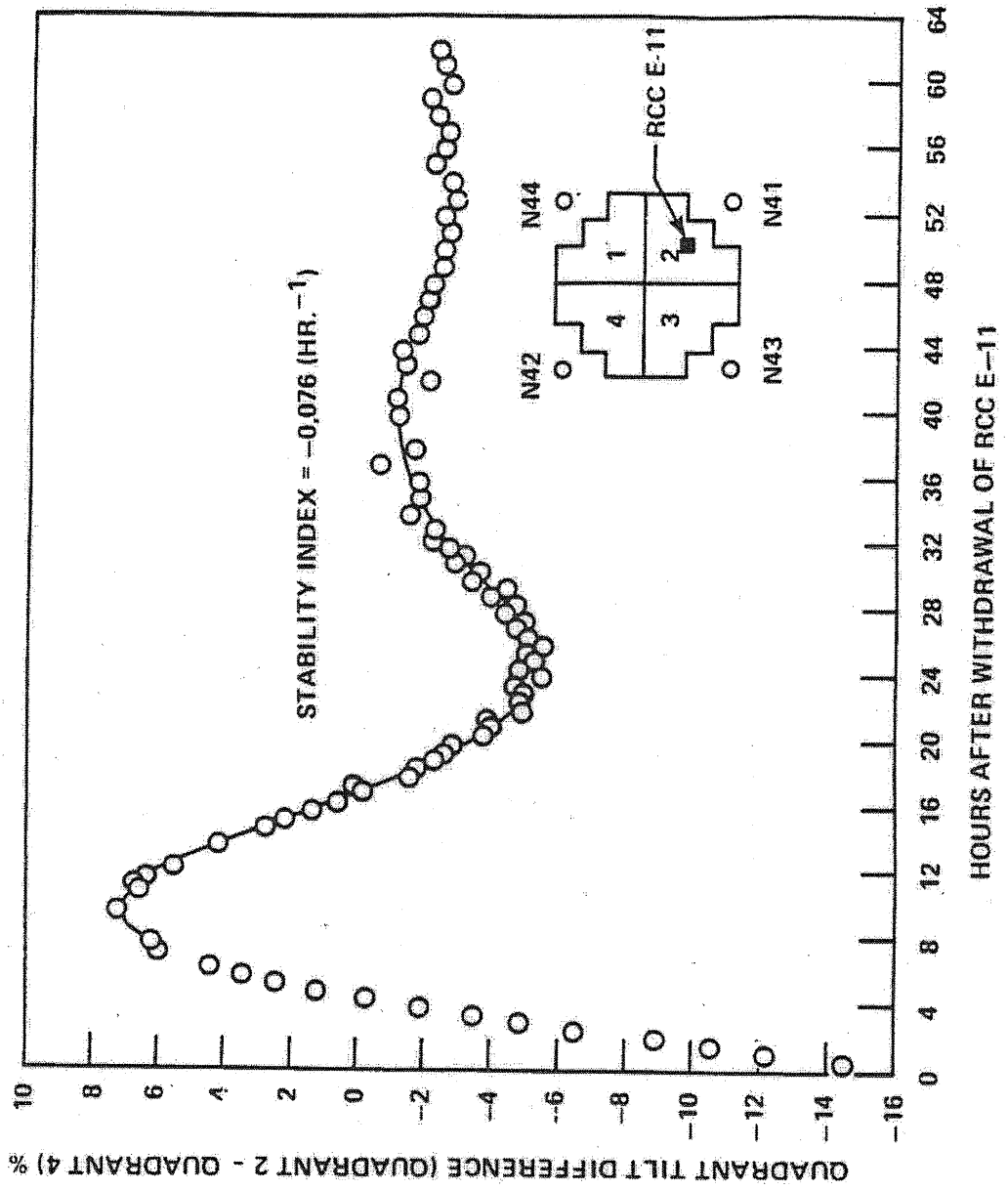

SEABROOK STATION UPDATED FINAL SAFETY ANALYSIS REPORT	XY Xenon Test Thermocouple Response - Quadrant Tilt Difference vs. Time	
		Figure 4.3-41

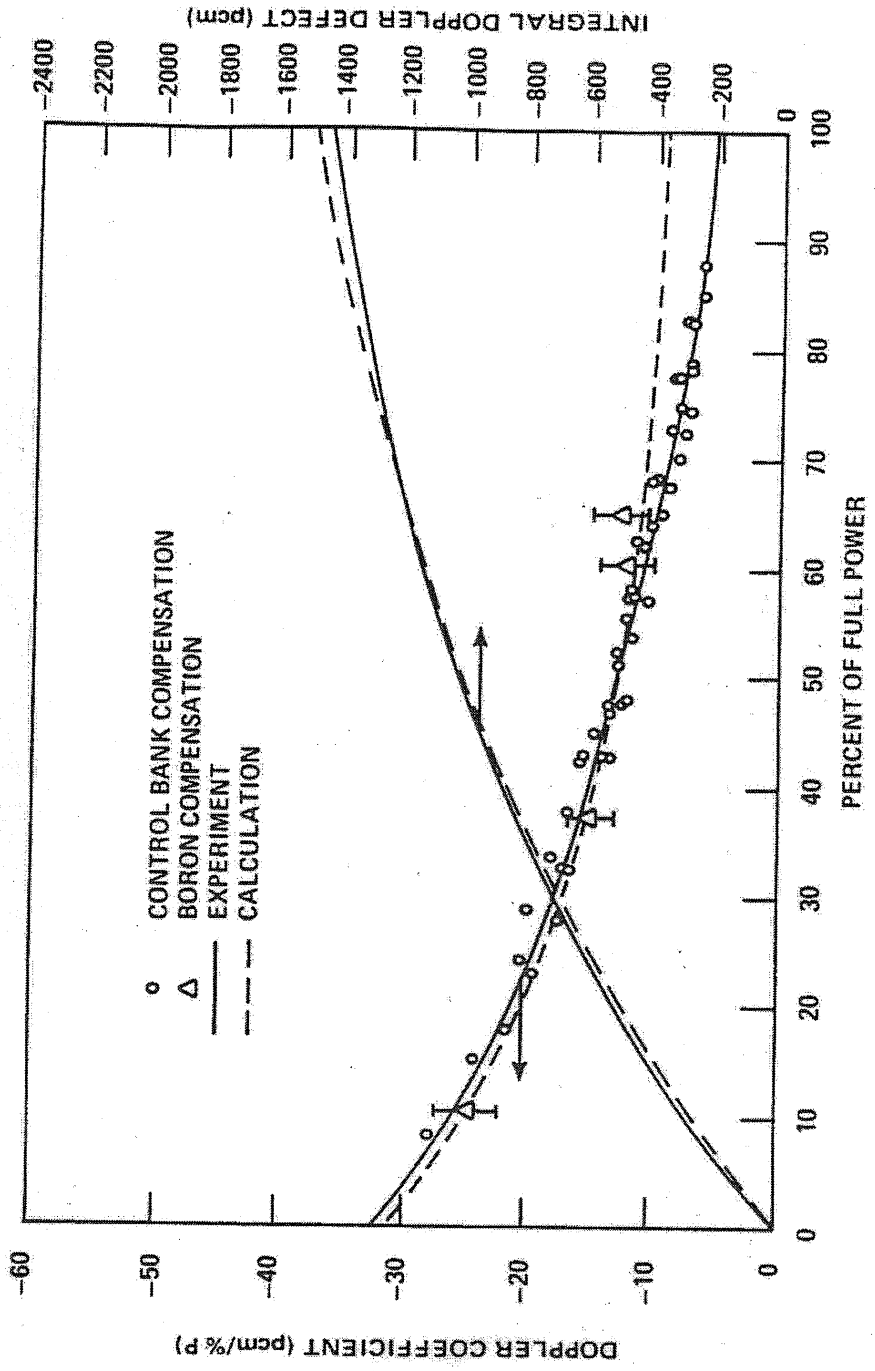

SEABROOK STATION UPDATED FINAL SAFETY ANALYSIS REPORT	Calculated and Measured Doppler Defect and Coefficient at BOL, 2-Loop Plant, 121 Assemblies, 12-Ft Core	
		Figure 4.3-42

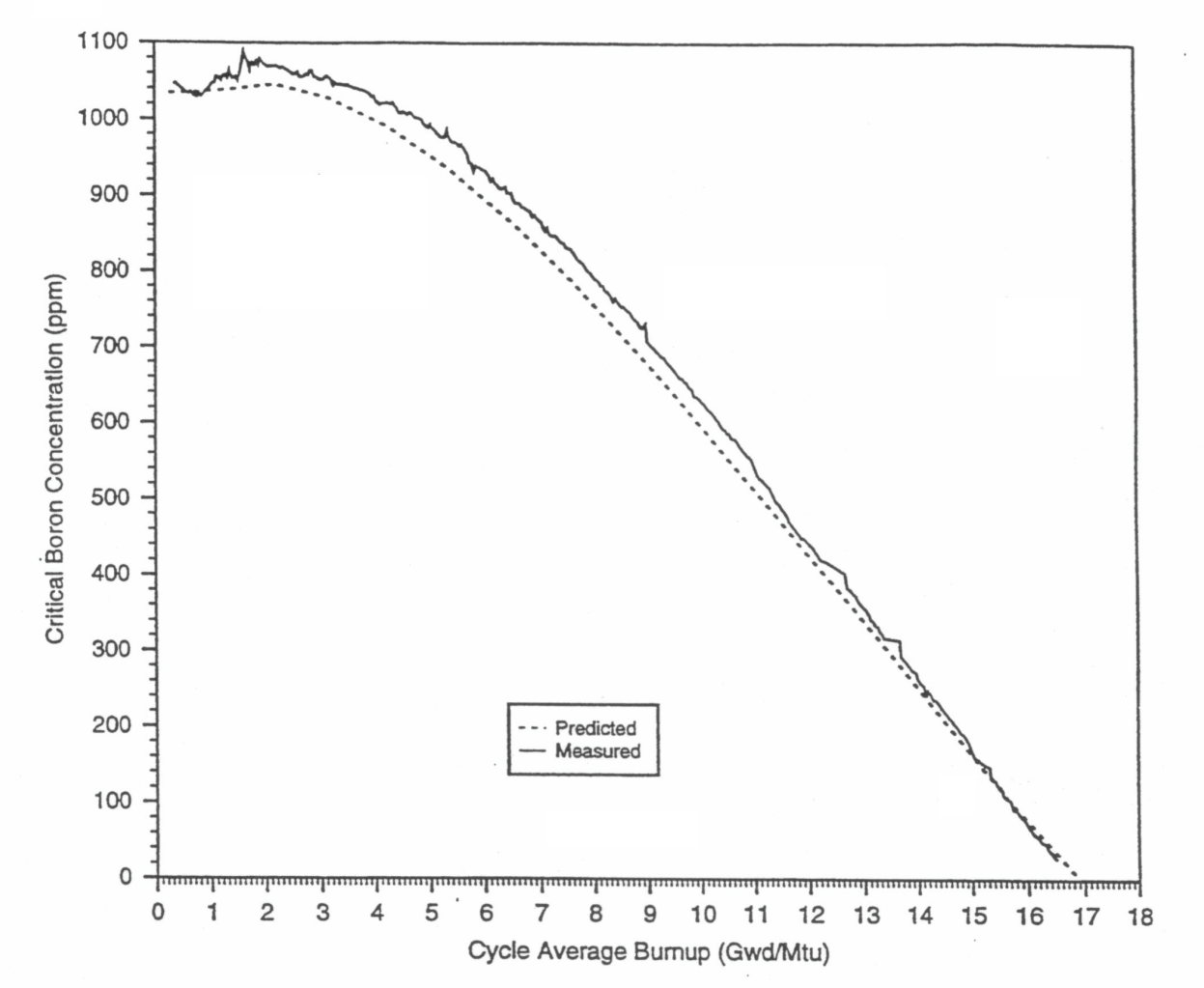

SEABROOK STATION UPDATED FINAL SAFETY ANALYSIS REPORT	Typical Low Leakage Core Design Comparison of Calculated and Measured Boron Concentration	
		Figure 4.3-43

DELETED

DELETED

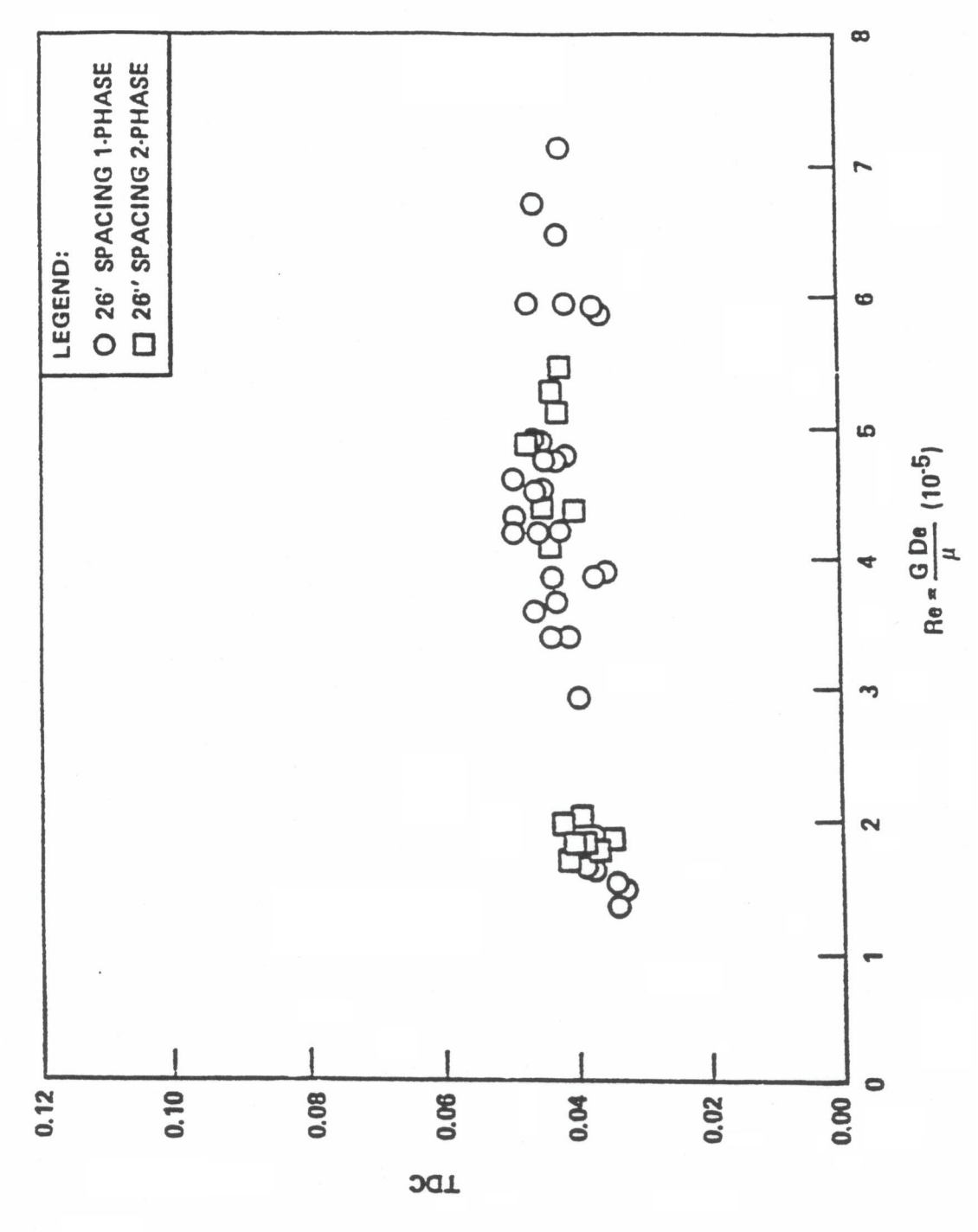

SEABROOK STATION UPDATED FINAL SAFETY ANALYSIS REPORT	TDC vs. Reynolds Number for 26 Inch Grid Spacing	
		Figure 4.4-1

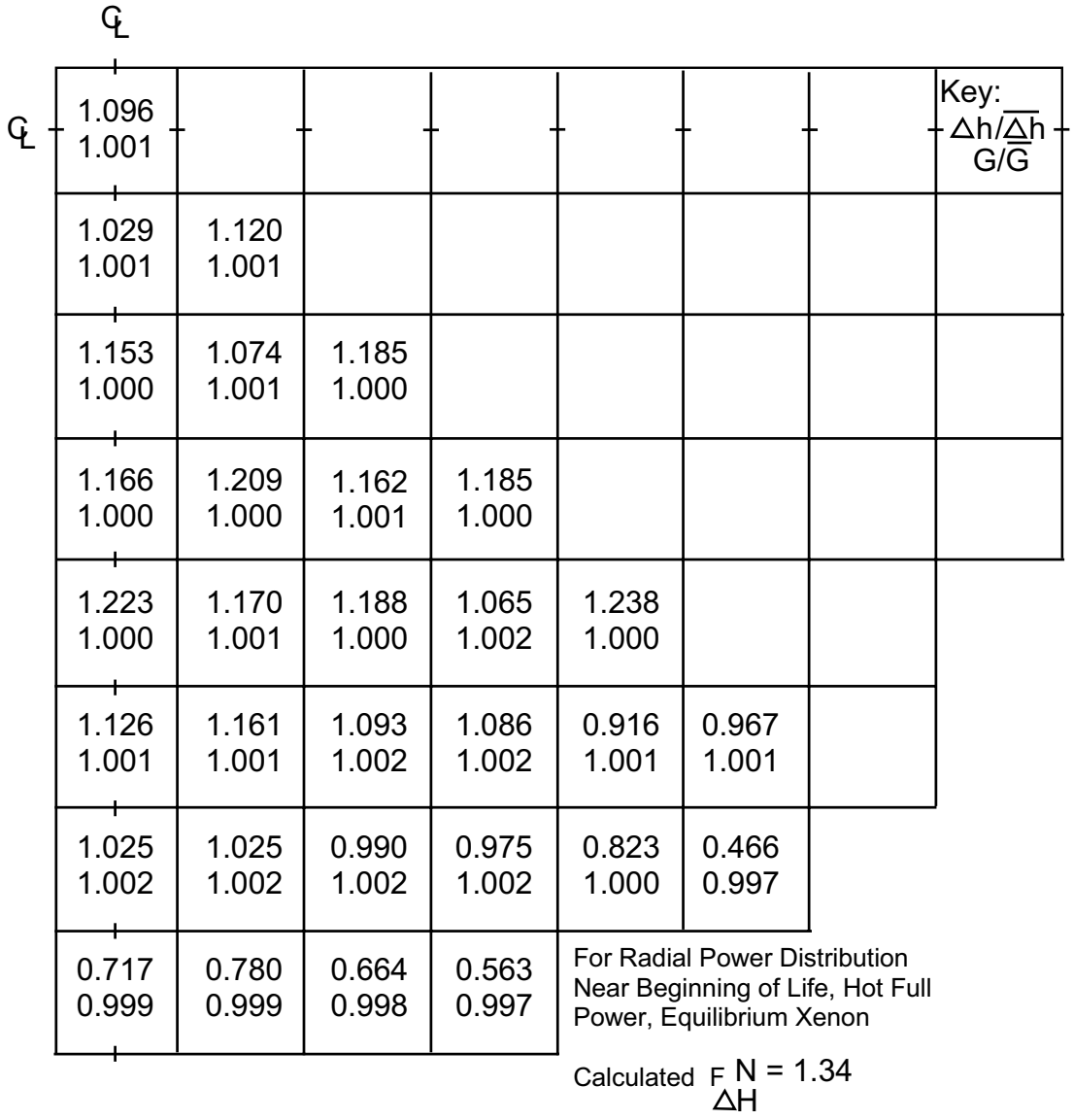

G:\Word\Images_P\UFSAR\442.ds4

SEABROOK STATION UPDATED FINAL SAFETY ANALYSIS REPORT	Normalized Radial Flow and Enthalpy Distribution at 4-Ft Elevation for Cycle 1	
		Figure 4.4-2

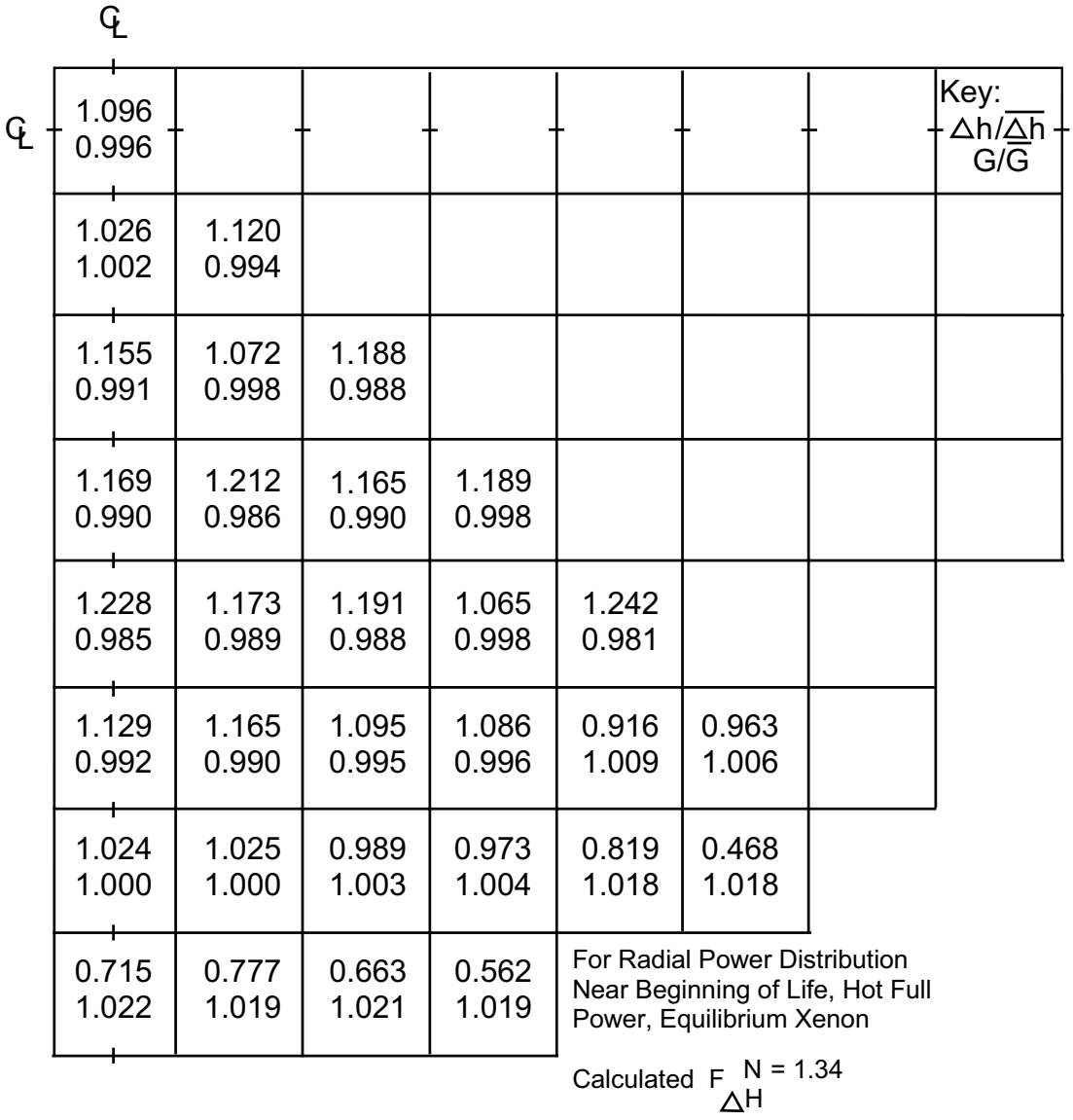

G:\Word\Images_P\UFSAR\443.ds4

SEABROOK STATION UPDATED FINAL SAFETY ANALYSIS REPORT	Normalized Radial Flow and Enthalpy Distribution at 8-Ft Elevation for Cycle 1	
		Figure 4.4-3

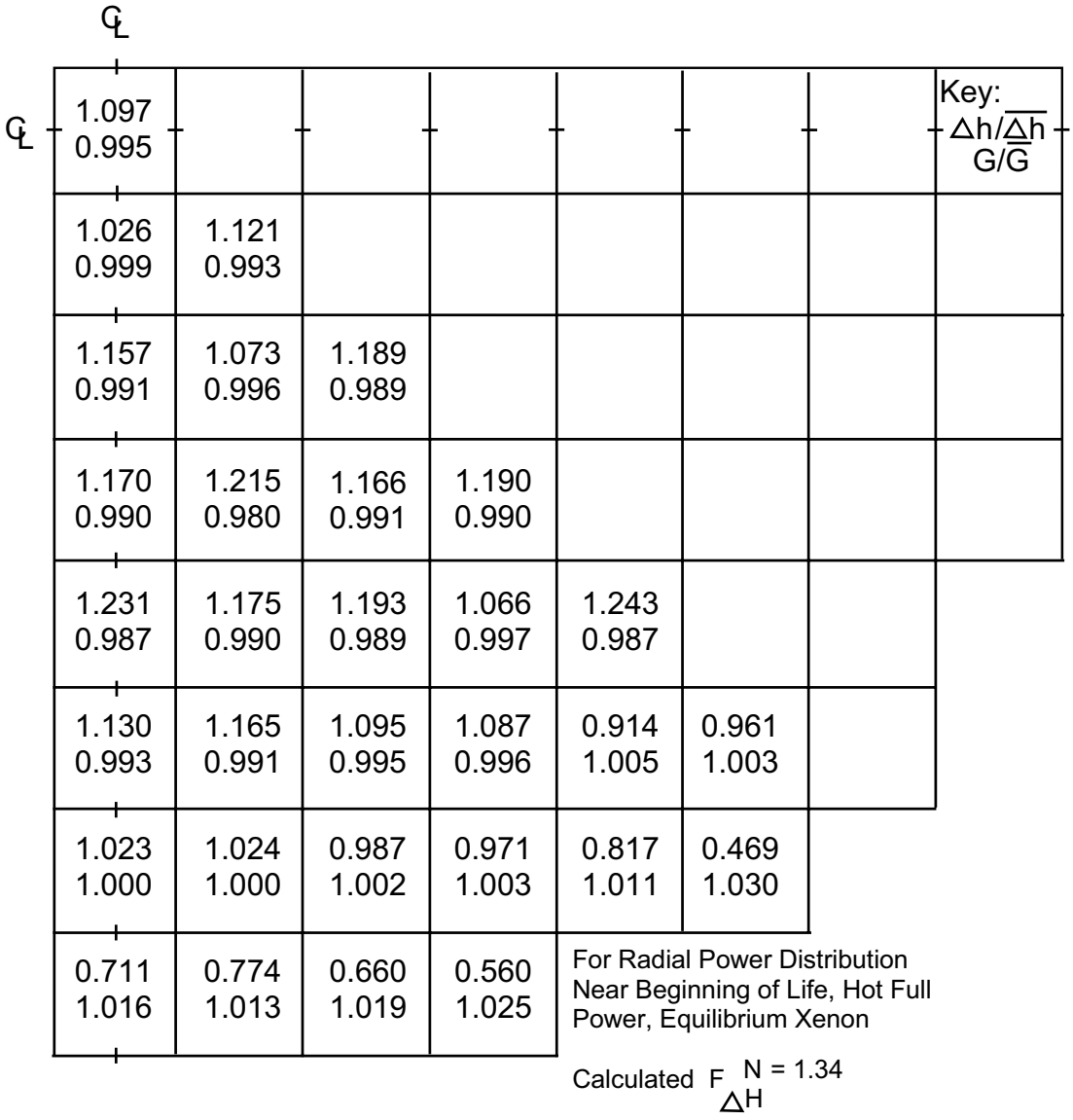

G:\Word\Images_P\UFSAR\444.ds4

SEABROOK STATION UPDATED FINAL SAFETY ANALYSIS REPORT	Normalized Radial Flow and Enthalpy Distribution at 12-Ft Elevation - Core Exit for Cycle 1	
		Figure 4.4-4

DELETED

SEABROOK STATION UPDATED FINAL SAFETY ANALYSIS REPORT	Void Fraction vs. Thermodynamic Quality $H-H_{Sat}/Hg-H_{Sat}$	
		Figure 4.4-5

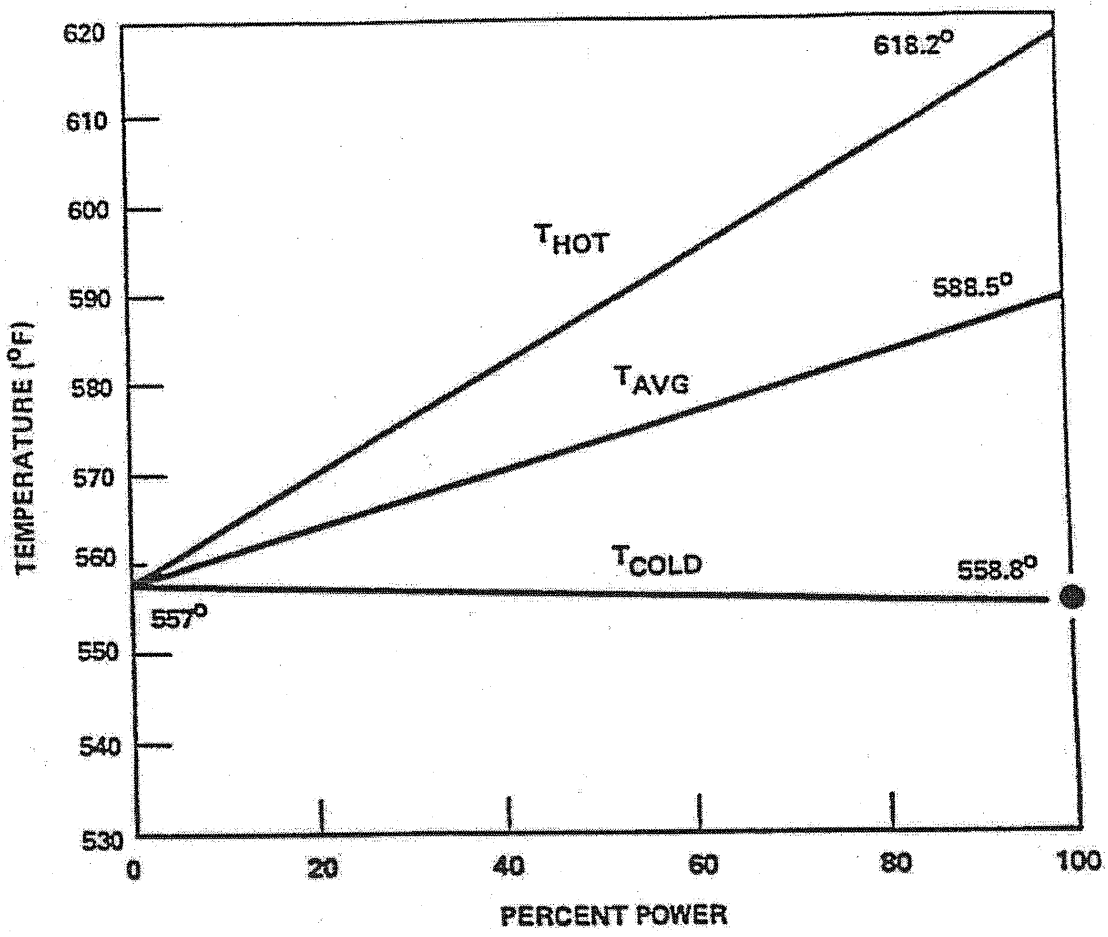

SEABROOK STATION UPDATED FINAL SAFETY ANALYSIS REPORT	Reactor Coolant System Temperature - Percent Power Map	
		Figure 4.4-6

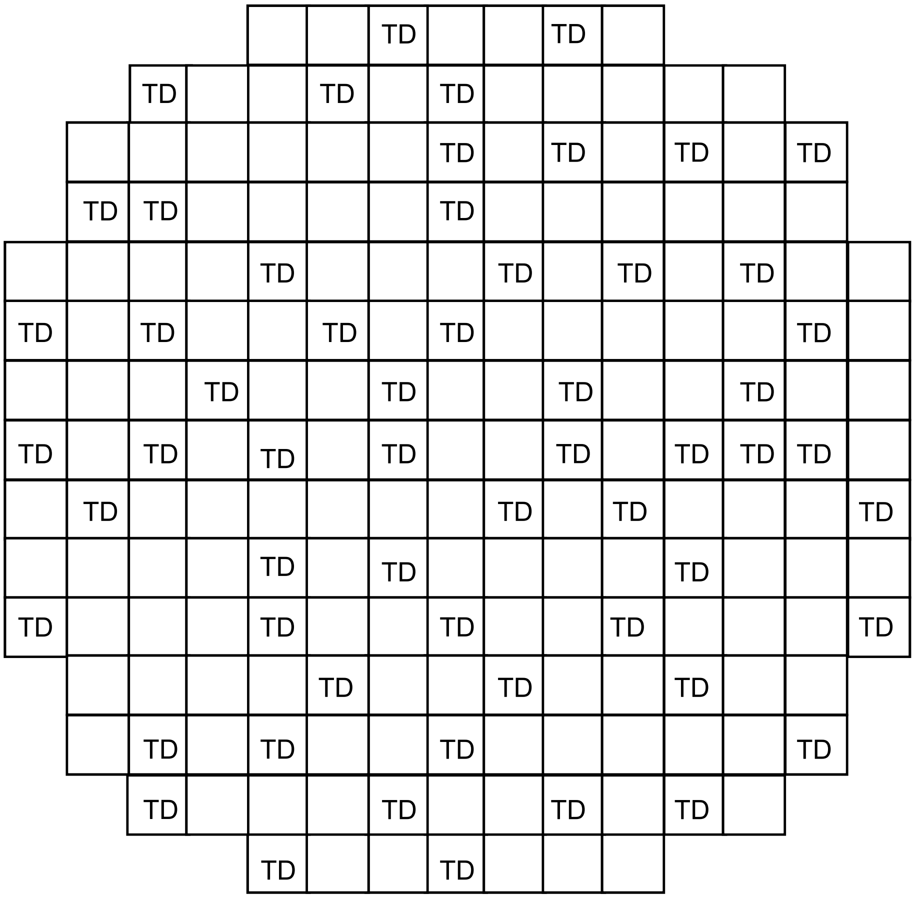

T = Thermocouple (58)
D = Movable Incore Detector (58 Locations)

G:\Word\Images_P\UFSAR\447.ds4

SEABROOK STATION UPDATED FINAL SAFETY ANALYSIS REPORT	Distribution of Incore Instrumentation	
		Figure 4.4-7

DELETED

DELETED

DELETED

DELETED

DELETED